A Prosim Knee Simulator Study of UHMWPE Wear: The Effect of Molecular Architecture and New Generation Radiation Crosslinking

MARTIN JAMES STANLEY

A Prosim Knee Simulator Study of UHMWPE Wear: The Effect of Molecular Architecture and New Generation Radiation Crosslinking

Martin J. Stanley

A thesis submitted for the degree of Doctor of Philosophy

School of Engineering and Computing Sciences

Durham University

July 2011

Contents

List of Figures

List of Tables

Acronyms

AA	Abduction/Adduction
ACL	Anterior Cruciate Ligament
ADC	Analogue to Digital Converter
AF	Axial Force
AP	Anterior/Posterior
ASTM	American Society for Testing and Materials
BMI	Body Mass Index
BS	Bovine Serum
CAD	Computer Aided Design
CISM	Cold Irradiation and Subsequent Melting
CoCr	cobalt chrome
CoCrMo	cobalt chrome molybdenum
CR	Cruciate Retaining
DCM	Direct Compression Moulded
DSC	Differential Scanning Calorimetry
DW	Distilled Water
EAB	Elongation At Break
EDTA	Ethylenediaminetetraacetic acid

EHL Elasto-Hydrodynamic Lubrication

EMG Electromyography

FB Fixed Bearing

FDA Food and Drug Administration

FE Flexion/Extension

FRGC free radical generating chemical

FTIR Fourier Transform Infra-Red

HDPE High-Density Polyethylene

ISM Irradiation in the Molten State

ISO International Standards Organisation

LED Light Emitting Diode

LSC Load Soak Control

LVDT Linear Variable Differential Transformer

MC Million Cycles

ML Medial/Lateral

MoM Metal-on-Metal

NHS National Health Service

NJR National Joint Registry for England and Wales

PCL Posterior Cruciate Ligament

PCR Posterior Cruciate-ligament Retaining

PE Polyethylene

PID Proportional-Integral-Differential

POD Pin-On-Disc

POP Pin-On-Plate

psi pounds per square inch

PTFE polytetrauoroethylene

RP Rotating Platform

RT Room Temperature

RTD Resistance Temperature Detection

SC Soak Control

SD Standard Deviation

SS Stainless Steel

THR Total Hip Replacement

TJR Total Joint Replacement

TKR Total Knee Replacement

TR Tibial Rotation

UHMWPE Ultra-high Molecular Weight Polyethylene

UTS Ultimate Tensile Strength

WIAM Warm Irradiation with Adiabatic heating and subsequent Melting

XL Cross-linked

YS Yield Strength

Acknowledgments

I would like to thank my supervisor Dr. Junjie Wu for her guidance and enthusiasm throughout the duration of the project. Recognition also must go to Imran Kahn at Biomet UK for provision of the testing samples.

Also, thanks go out to my office mates without whom the project would not have been as enjoyable. Qianqian, who has been there from the start, and who can now just about 'get' my sense of humour. Daniel, whose exuberant enthusiasm balances nicely with newcomer Elaine's mellowness. And finally, DJ Lal, breakdancing his way to a stage near you. To you all I leave my mini fridge (that has the wrong transformer, and probably needs another PAT test by now).

My appreciation goes out to other members of the group, both past and present, Tony Unsworth, Susan Scholes, Sarah Williams, and also to the 10:30 coffee club.

Many thanks to Arthur Newman for his technical assistance, and also to Colin and the rest of the technical (football team) staff.

Finally I'd like to thank Mum, Dad, Ros and Stu, and the rest of my family. And especially big love and appreciation to Hayley, you can finally read about my Ummwipe project now!

I had planned on making this far more eloquent, but time is tight and research waits for knee man.

Abstract

Martin J. Stanley

A Prosim Knee Simulator Study on UHMWPE Wear: The Effect of Molecular Architecture and New Generation Radiation Crosslinking

Arthritis is a painful and degenerative condition that affects synovial joints within the human body. Total knee replacement can reduce the pain and increase mobility. Metal on Ultra-high molecular weight polyethylene (UHMWPE) implants have been used successfully for the last 40 years. However, the increasing incidence of implantation in younger patients and the resultant increase in activity has led to higher mechanical demands on the implants. The work in this thesis aims to improve the understanding of UHMWPE with the clinical goal of improved resistance to wear by reducing type 2 fusion defects through improving processing methods and post-processing treatments.

The wear properties of four variants of direct compression moulded (DCM) UHMWPE plates were assessed using statically loaded, multidirectional, pin-on-plate machines. Moulding temperatures and durations were varied between 145°C - 195°C, and 15 min - 30 min, respectively. Mean wear factors for the specific processing conditions were as follows 145°C 30 min - 4.362±0.535, 155°C 30 min - 2.903±0.443, 165°C 15 min - 3.026±0.379, 195°C 15 min - 2.631±0.295 (All wear factors x10^{-6}mm^{3}N^{-1}m^{-1}). Wear properties improved with increased temperature. For cases where moulding temperatures were within 10°C, an increase in moulding duration had a positive effect on wear properties. Surface analysis revealed a link between increased number of type 2 fusion defects and an increase in wear factor. Tests using roughened pins increased wear factors, but the differences between processing conditions became smaller. Molecular weight was also found to affect the wear factor with best performance exhibited by that with a molecular weight of 5,000,000 g/mol, compared to 600,000 g/mol and 9,000,000 g/mol specimens.

A state-of-the-art Prosim knee simulator was used to assess the wear properties of both the current 'gold standard' ArCom® DCM UHMWPE and a new generation of vitamin E infused, highly cross-linked E1™ UHMWPE inserts. Inserts were of geometrically identical designs and were assessed using a high kinematic test profile. A new load soak control (LSC) station was developed and incorporated into the simulator. Volumetric wear results were

6.46±1.80 mm^3/million cycles and 0.853±0.131 mm^3/million cycles for the ArCom® and E1™ inserts respectively. Radiation cross-linking was found to reduce wear by 87%. Both wear rates compared favourably to those obtained in similar tests at other research centres, however care must be taken when comparing results as material, experimental, and geometric design differences may all contribute to variations in wear rates. Identical testing using extremely high femoral surface roughness (R_a=0.295μm) increased wear rates to 100±38.5 mm^3/million cycles and 50.7±17.3 mm^3/million cycles for the ArCom® and E1™ inserts respectively, suggesting that with highly roughened counterfaces, some of the cross-linking advantage is lost. Tests on E1™ inserts using smooth femoral components but increased axial force (4.0kN) revealed no detrimental effects on wear. Accelerated ageing and subsequent wear testing of the E1™ inserts showed no change in wear rate, indicating excellent resistance to oxidative degradation afforded by the infused Vitamin E. Temperature monitoring revealed 6.5°C rises in test cell temperature due to frictional heating between the bearing surfaces. Lubricant uptake for both types of insert was found to increase under dynamic loading, indicating the importance of a LSC.

In conclusion: it is possible to improve the wear properties of DCM UHMWPE with small changes in processing conditions. Cross-linking resulted in substantial decreases in wear, however this was less evident when tested using femoral components with increased surface roughness. Vitamin E proved successful in preventing oxidation of the E1™ inserts.

Chapter 1

Introduction

Total joint replacements have been used for over four decades to alleviate the pain and reduced mobility associated with both osteoarthritis and rheumatoid arthritis. In the most recent survey of the National Joint Registry for England and Wales (NJR) it was recorded that in the 2009/10 financial year, a total of 163,940 hip and knee joint replacement procedures were undertaken. This was more than in any previous year and brought the total number of procedures recorded for the period from 1st April 2003 to 31st March 2010 to 905,384. The total number of knee procedures in the 2009/10 financial year was 77,545 which was an increase of 2.8% on the previous year. It was also noted that the Body Mass Index (BMI) of patients undergoing knee replacement procedures has increased to 30.5 from 29.2 in 2004, thereby increasing the forces imparted on the Total Joint Replacement (TJR). However, it is not known whether this increase in BMI has been accompanied by a reduction in activity. The TJR procedure is currently a very successful one with 75% patient satisfaction (Noble et al., 2006), and only a 3% revision rate of cemented prostheses after 5 years of implantation (NJR for England and Wales, 2010). However, with the ever increasing number of procedures performed, this still amounts to a significant number of revisions.

Ever since the inception of the Total Knee Replacement (TKR) procedure, a metal femoral component articulating on a Ultra-high Molecular Weight Polyethylene (UHMWPE) tibial bearing surface has been the material combination of choice. This seems to have been influenced by the lessons learnt with catastrophic failures of hip prostheses when first introduced five decades ago (Charnley, 1961). UHMWPE is used as it has excellent resistance to wear, and is highly stable within the environment of the body.

The main cause of TKR failure observed during revision procedures is that of excessive Polyethylene (PE) wear, with 25% of revisions caused by this defect (Sharkey et al., 2002). Wear of PE bearings in TKRs generates microscopically small wear debris particles which can have an adverse reaction with the tissue around the joint, and upon a threshold being reached, can cause osteolysis, joint loosening, and subsequent joint failure.

Thereby, PE wear remains an issue in TKR and efforts are currently being made by all medical device manufacturers to reduce it. This has included refinement of the manufacturing processes for UHMWPE (Bellare and Cohen, 1996), and the introduction of new manufacturing methods that significantly enhance the mechanical and wear properties of UHMWPE. An example of this being the ArCom® variant of the Direct Compression Moulded (DCM) process developed by Biomet (Warsaw, IN) which is used to manufacture the current 'gold standard' in conventional UHMWPE. However, slight variances in the conditions in which the DCM process takes place has been shown to introduce fusion defects into the UHMWPE which results in distinct grain boundaries which can negatively affect the material properties (Wu et al., 2002).

In the past decade, much research effort has gone into exploring the concept of cross-linking UHMWPE for use in Total Hip Replacement (THR)s and TKRs. This material has been used successfully *in vivo* in THRs for a number of years, but questions still remain on its suitability in the significantly higher stress environment of the knee joint. Cross-linking can be achieved using a variety of methods, but is usually performed using ionising radiation. This causes the millions of polymer chains in UHMWPE to form covalent bonds between each other which changes the mechanical properties of the material (Grobbelaar et al., 1978). The beneficial effect is that the wear resistance is significantly increased although inevitably there are also downsides associated with the procedure, primarily that the Cross-linked (XL) UHMWPE reacts with oxygen upon implantation, which can ultimately cause catastrophic failure of the implant. Multiple post-processing techniques have been introduced by manufacturers to combat this, all with both positives and negatives. However, recently a new technique of infusing Vitamin E into the XL UHMWPE has been proposed (Oral et al., 2004), and implemented into TKR bearings by Biomet (Warsaw, IN), This material is claimed to have all of the benefits, and none of the drawbacks of other XL UHMWPE components. However this Vitamin E infused UHMWPE (termed E1™) is still largely untested *in vivo*.

The aim of this thesis is to assess the effectiveness of these changes made in both the processing and post-processing techniques, using a combination of both pin-on-plate wear screening, and more complex anatomical wear simulations.

Initially, the effect of variations in processing conditions on wear rates of DCM UHMWPE was assessed using simple, but highly controllable, pin-on-plate rigs which generated contact pressures of approximately 2 MPa. A similar DCM processing technique (termed the 'ArCom®' process) was then used to produce the tibial bearing of a TKR. The wear performance of these 'gold standard' bearings was then assessed in a knee wear simulator using an aggressive loading and displacement regime which generated more representative contact pressures than the pin-on-plate rigs. A standard test duration of 5.0 million cycles was used, with special emphasis placed on the analysis of the articulating surfaces. A more aggressive test than outlined in the International Standards Organisation (ISO) standard was used in order to ensure that the TKRs were being tested under conditions that were consistent with implantation in younger patients. A set of XL, Vitamin E infused UHMWPE TKRs were then tested on the knee wear simulator using the same aggressive profiles, albeit with slight adjustments to improve the response of the simulator to the demand. The wear rate and surface conditions were compared to the ArCom® tibias to establish the effect of crosslinking. An oxygen bomb was used to age the E1™ tibias (ASTM F2003 - 02) and a subsequent wear test was used to assess the resistance to oxidation. To simulate the extensive femoral damage sometimes found on TKRs retrieved from patients, the E1™, ArCom®, and DCM pin-on-plate UHMWPE samples were additionally tested against an artificially scratched metal counter-face under otherwise unchanged conditions.

Aside from the main aims outlined above, several other additional factors regarding experimental methods and the use of UHMWPE in TKRs were investigated. These included: the effect of molecular weight on the wear of UHMWPE; short term changes in wear particle generation areas; the effect of increased axial loading on the wear of E1™ XL UHMWPE; temperatures generated through frictional heating; lubricant uptake rates into the test components; and the recording and presentation of simulator performance.

This thesis is presented as follows: Chapter 2 comprises of a thorough literature review of the research area; Chapter 3 contains details and discussion of the influence of type 2 fusion defects on UHMWPE wear; Chapter 4 introduces the ProSim knee wear simulator and describes the methods used in both calibration and operation; Chapter 5 covers the

testing of ArCom® UHMWPE; Chapter 6 describes testing of the E1™ highly cross-linked UHMWPE; Chapter 7 covers the further testing of both types of previously mentioned UHMWPE under scratched counter-face conditions; Finally, Chapter 8 discusses the clinical relevance of the work, conclusions of the study, and suggestions of future work to enhance the results presented in this thesis.

Chapter 2

Literature Review

Total Knee Arthroplasty has been the subject of intensive research throughout the last five decades. The following chapter analyses and assesses the current thinking relevant to the research presented in this thesis. It will first cover the natural knee, the problems that can affect it, and the need for TKR. The topic of TKR will then be covered, with a brief history followed by limitations of the procedure. Topics relating to the laboratory testing of TKRs and biomaterials will be covered, and finally the gaps in academic knowledge and subsequent topics of research undertaken in this thesis will be outlined.

2.1 The Natural Knee

The knee is the the largest and arguably the most complex joint in the human body, a diagram of which can be seen in Figure 2.1. It is a two joint structure consisting of both the tibio-femoral and patello-femoral joints. It is a synovial joint which allows a large degree of motion when compared to the other two types of joint found in the human body such as cartilaginous and fibrous. In normal joints the bone ends are covered by relatively thin hyaline articular cartilage, which is a highly specialised tissue suited to withstanding the highly loaded environment without failure during a normal person's lifetime. Physiologically, it is an avascular tissue, meaning that it has no blood supply and consequently, repair when damaged requires external intervention. In synovial joints the articular cartilage has two main functions, firstly, to distribute loads over the wider joint area, consequently decreasing stresses (Ateshian et al., 1994), and secondly, to allow relative movement of the

opposing joint surfaces with minimal friction and wear. Between the two cartilage surfaces the menisci can be found. These are two semi-lunar cartilaginous pieces of tissue that act to distribute load, cushion impacts, and aid with joint lubrication. The joint is lubricated with synovial fluid which is contained within the joint capsule which is attached to the margins of the articular surfaces. The knee features two cruciate ligaments, the Anterior Cruciate Ligament (ACL) which resists anterior movement of the tibia with respect to the femur, and the Posterior Cruciate Ligament (PCL) which resists posterior movement of the tibia with respect to the femur. The knee also features medial and lateral collateral ligaments which prevent excessive Abduction/Adduction (AA).

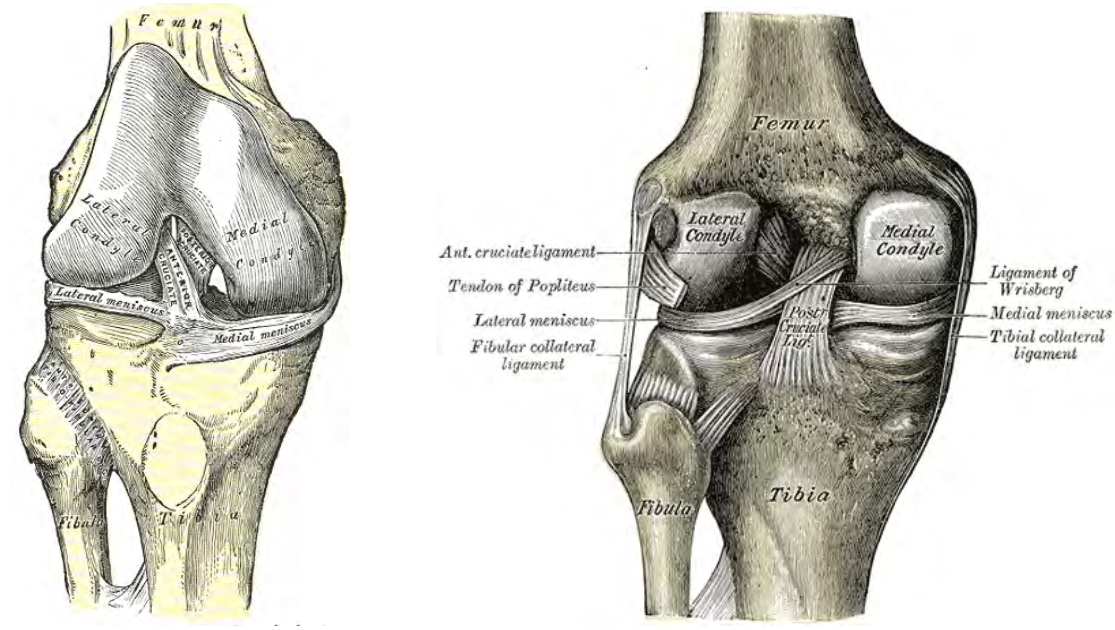

(a) Anterior view of a right knee.

(b) Posterior view of a left knee.

Figure 2.1: Diagram of the knee joint (Gray, 1918).

2.1.1 Natural Knee Kinematics

The kinematics of the natural knee are notoriously difficult to measure and much research effort has gone into the topic over the years. Several methods have been used, including bone markers (Lafortune et al., 1992) in a highly cited study which used triad markers that were temporarily affixed to both the femur and tibia of five healthy male subjects. Four high-speed cameras were used to track the position of the markers as the subjects walked normally. Direct linear transformation calculations were performed to translate the optical data into numerical plots, the relevant ones of which are shown in Figure 2.2. The most

consistent kinematic between the 5 patients was that of Flexion/Extension (FE); the knee was shown to flex to approximately 20° before extending back to a flexion of 1.3°. Thereafter the joint flexed again reaching 35° by toe-off and reached a maximum of 60° before extending back to 0° ready for heel strike. AA of the tibiofemoral joint had a maximum mean value of 5.0°. In the stance phase, little AA movement took place, although it remained constant at around 1.2°. In four of the subjects, shortly before toe-off the joint began to abduct and reached a mean maximum value of 6.4°. However in one subject adduction was noted in the swing phase, contrary to all other subjects. Internal/external rotation of the tibia with respect to the femur is shown in Figure 2.2(c). Twice during gait did the tibia rotate internally, once at heel-strike and again just prior to toe-off. At both these times, the internal rotation measured just less than 5°. During the middle part of the stance phase, the tibia remained close to the neutral position. From toe-off to just prior to heel strike the tibia rotated externally for a total of 9.4°. Anterior/Posterior (AP) translation of the tibia with respect to the femur is shown in Figure 2.2(b), this showed a similarity with the FE axis in that when the knee flexed, the tibia moved posteriorly, and when the knee extended, the tibia moved anteriorly. The size of the posterior translation during stance phase was 3.6mm and during the swing phase it was 14.3mm. There was a slight anterior translation during the stance phase and the maximum was 1.3mm. No loads on the knee were measured during this study.

When a natural knee flexes under load-bearing conditions the contact point between the femur and tibia translates 2±1 mm to the posterior from an original position of 6±1 mm anterior to the mid-line in the sagittal plane of the tibia joint (Stiehl et al., 1995). An illustration of the contact points on both the medial and lateral sides of the tibia at various flexion angles can be seen in Figure 2.3. The roll-back is believed to prevent impingement of the femur on the posterior region of the tibia, hence increasing the range of flexion.

Loading on the knee joint during gait can be characterised as internal and external forces. External forces are the combination of the weight of the body, and subsequent ground reaction forces, and the forces generated by acceleration and deceleration of the limb segments. Internal forces act to balance the external forces and can be defined as muscle, ligament, and joint contacts (Andriacchi et al., 1986). External forces can easily be measured in the laboratory using motion analysis and force plates, however it is far more difficult to measure the internal forces, except with instrumented implants (Heinlein et al., 2007), but the ques-

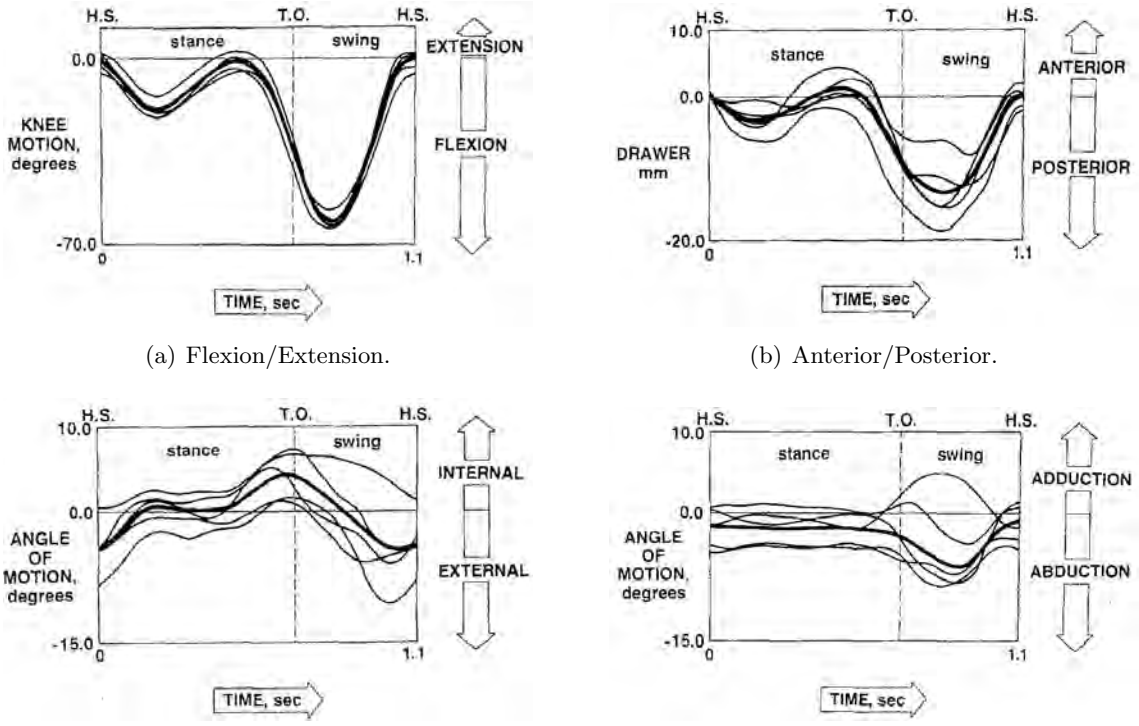

(a) Flexion/Extension.

(b) Anterior/Posterior.

(c) Tibial rotation.

(d) Abduction/Adduction.

Figure 2.2: Displacements of the natural knee (Lafortune et al., 1992). Thin black lines indicate recorded traces from the five individual subjects. The thicker black line indicates the mean response of the five subjects.

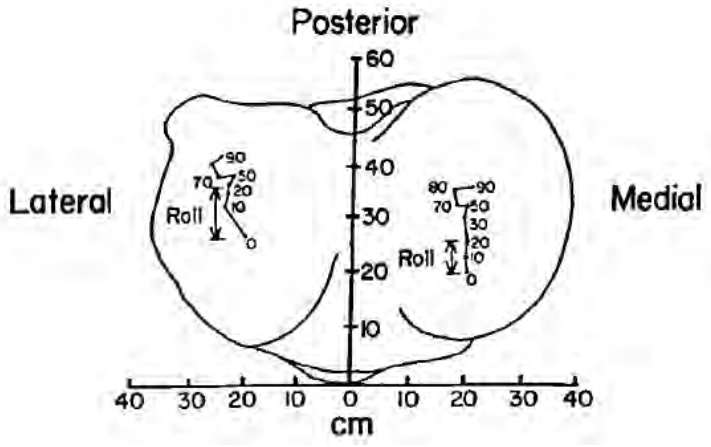

Figure 2.3: Location of the typical contact point on the natural tibial plateau during flexion. Numbers on diagram indicate degree of flexion. Note that the contact on the lateral side moves to the posterior a greater amount than on the the medial side throughout 0-20° of flexion. This is due to a larger rolling radius than on the medial side. At flexion angles greater than 20° the contact point changes due to sliding rather than rolling. (Andriacchi et al., 1986).

tion then arises as to whether the implant has altered the geometry and tribology of the joint, therefore affecting the forces and motions within the joint. Therefore, internal forces are most often calculated using mathematical models, or cadaver experiments (Fukubayashi et al., 1982). Due to the medial offset of the centre of mass of the body from the knee, asymmetric loading of the medial and lateral compartments occurs. An experiment combining mathematical models with recorded gait, force plates, and Electromyography (EMG) revealed maximum forces on the knee during walking of between 2-4 times bodyweight with the average value of the 12 subjects being 3.03 times bodyweight. Additionally, when the joint was highly loaded, a greater proportion of the load was transmitted through the medial condyles, although no numerical value was stated (Morrison, 1970)

2.1.2 Natural Joint Lubrication

Lubrication between the cartilage surfaces within the natural knee joint is provided by synovial fluid. This is a highly viscous, clear, with an often yellowish tint liquid that is secreted by the synovium. Between 1 and 5ml of this fluid is contained within the joint cavity of a healthy human knee joint. Synovial fluid is a dialysate of blood plasma, and does not contain clotting factors, erythrocytes, or hemoglobin, but does contain halyuronate, an extended glycosaminoglycan chain, and lubricating glycoproteins and wear retarding phospholipids. Experiments using a Weissenberg rheogonomiter have shown healthy synovial fluid to be markedly non-Newtonian (Newtonian fluids have by definition a viscosity independent of applied shear rate). Osteoarthritic synovial fluid was found to have a markedly diminished viscosity, and exhibited less non-Newtonian features, and rheumatoid arthritic synovial fluid saw a further decrease in shear properties as seen in Figure 2.4 (Cooke et al., 1978). Synovial fluid also provides the nutrients for the articular cartilage and the menisci and also takes waste products away from the joint.

There has been significant debate about the mode of lubrication that exists in a synovial joint. The anatomical features of animal joints were first compared to those of engineering bearings and the concept of hydrodynamic lubrication proposed for animal joints (Macconaill, 1932). Experiments conducted using interphalangeal joints as the fulcrum of a pendulum, revealed an exponential decay in the amplitude. This led to the conclusion that the lubrication must be viscous in nature, and therefore full fluid film must be present (Jones, 1936). These fulcrum experiments were repeated using ankle joints, however the

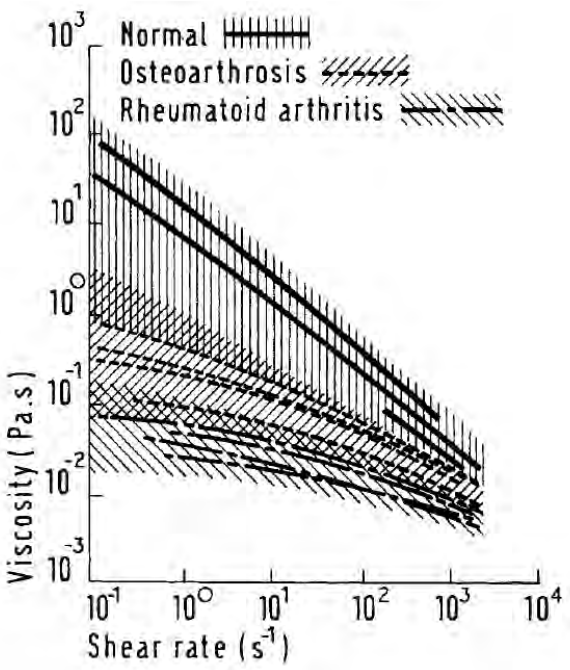

Figure 2.4: Plot demonstrating change in viscosity of human synovial fluid at differing rates of shear. Both normal and pathological conditions are shown. Viscosity was measured using a Weissenberg rheogoniometer (Cooke et al., 1978).

opposite result was found, with a linear attenuation of the pendulum amplitude, leading to the conclusion that the mixed lubrication was responsible and the warning that, "attempts to reconstruct artificial joints on the hydrodynamic theory of lubrication are doomed to failure" (Charnley, 1960). It was at a similar time that the theory of 'weeping' lubrication was proposed, whereby the cartilage when loaded 'weeps' fluid out of the solid matrix into the bearing space, which results in a pressurised fluid between the bearing surfaces (McCutchen, 1962). However, this theory was placed into doubt when it was demonstrated that the flow rate in and out of cartilage was tiny (Maroudas, 1967). An alternative to the 'weeping lubrication' theory was proposed by Dowson *et al* , who in 1970, described an increase in hyaluronic acid concentration in synovial fluid during the squeeze-film process. This increase in concentration has a direct link with the effective viscosity of the fluid, and this coupled with the porous nature and surface topography of the cartilage led to the concept of 'boosted lubrication' (DOWSON et al., 1970). More recent theories on joint lubrication however propose changing forms of lubrication over the gait cycle (Unsworth, 1991) as illustrated for the hip joint in Figure 2.5. During the lightly loaded swing phase, a thick fluid film can be entrained between the cartilage layers. At heel strike, transmitted loads through the joint can exceed 2kN and the entraining velocity is low, and consequently

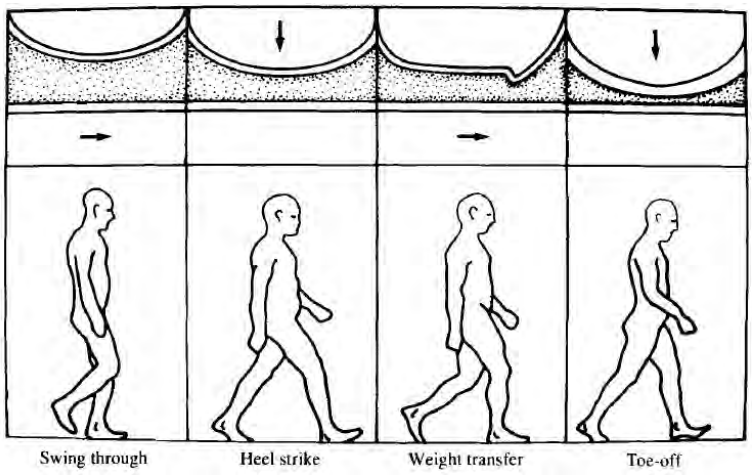

Figure 2.5: Lubrication mechanisms for a right hip joint during a walking cycle (Unsworth, 1991).

the thick film of fluid is 'squeezed' out. During the stance phase, transmitted loads are lower and entraining velocity is higher. These conditions promote Elasto-Hydrodynamic Lubrication (EHL) which retains a synovial fluid layer between the cartilage. At 'toe-off' maximum loading occurs and the entraining velocity is minimal, however 'squeeze film' lubrication is still thought to maintain a fluid film.

Studies on the lubrication in the natural knee joint are far more sparse, and the lubrication situation is complicated by the addition of the meniscus-cartilage contact, rather than the pure cartilage-cartilage articulation in the hip. However, recent efforts into the tribology and lubrication of the natural knee have intensified due to an increase in tissue engineered solutions for knee repair (Stapleton et al., 2008).

2.1.3 Degeneration of the Natural Knee

Arthritis is by far the most common cause for TJR. In a study of 235 consecutive TKRs between 1984 and 1986, the reasons for replacement were as follows; 62% had primary osteoarthritis, 33% with rheumatoid arthritis, 3% with junior rheumatoid disease, 2% with post traumatic arthritis (Schai et al., 1998). The onset of osteoarthritis in the knee joint can be accelerated due to trauma which causes damage to either the hyaline cartilage, or the menisci. This can result in less than ideal lubrication conditions and result in accelerated wear of the cartilage. When the articular cartilage wears away, the bone ends are exposed which further adversely affects the frictional properties of the joint, and also exposes the nerve endings, increasing the sensation of pain.

2.2 Total Knee Replacement

The surgical process of TKR is relatively new when compared to the established procedure of THR, of which the first procedure was performed in 1962 (Charnley, 1979). TKR is now an established surgical procedure and in England and Wales in 2010 there were 58,870 recorded knee replacement procedures completed by the National Health Service (NHS) and 24,958 recorded procedures completed in independent hospitals (NJR for England and Wales, 2010). Both these figures were higher than the number of hip procedures performed in the same period. There is a significant challenge in designing knee replacements in that the operating conditions are severe, due to a combination of high loads, low velocities, and an environment that is hostile in terms of corrosion and biological attack. Consequently, the design of TKRs has changed markedly over the years. The knee is particularly challenging as computer models have shown that the contact stresses are significantly higher than in the hip (Bartel et al., 1986). Early designs used the methodology that the knee was a simple hinge, and as such, replaced it with one. However follow up results were not good, with limited range of motion and complications including deep sepsis (Deburge, 1976).

Failures of TKRs most commonly occur at the junction between the tibial component and the underlying tibial bone. Metal backed tibia components are used in an attempt to better distribute stresses on cancellous bone. Component size is an important consideration in knee replacement and an undersized component that has penetrated into the bone has been reported (Harris and Sledge, 1990). All-plastic tibial components were found to cause stress concentrations on the bone and cement (Walker et al., 1976) and all known modern designs feature a metal backed tibia component. One piece metal tray components have been shown to deflect less under loading when compared to compartmental designs (Walker et al., 1981).

2.2.1 Effect of Total Knee Replacement on Kinematics

Posterior Cruciate-ligament Retaining (PCR) designs of bearings have been advocated in the literature as a way of preserving the anatomical femoral rollback and therefore potentially increasing the patients range of motion, and there is significant evidence that this is the case. Patients with PCR designs have been shown to perform better in tasks such as stair climbing than those without cruciates. In a study using Light Emitting Diode (LED)s placed on the

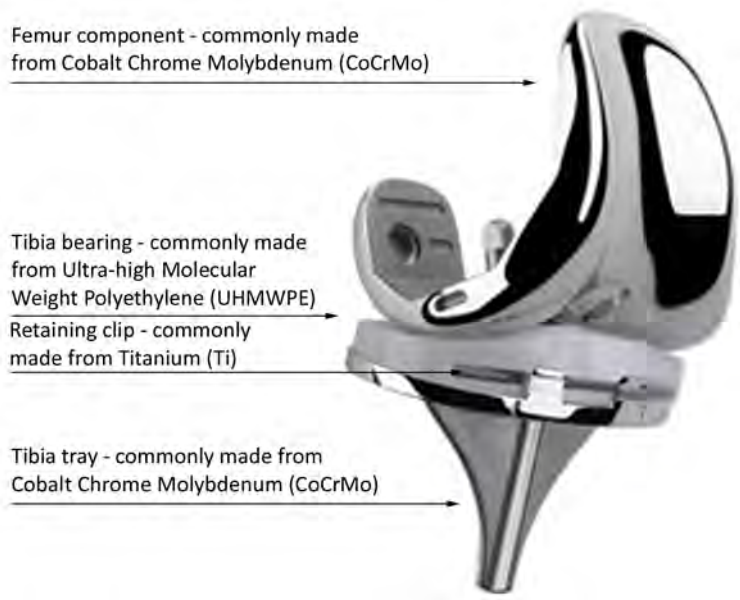

Figure 2.6: Illustration showing a Total Knee Replacement (Modified from original source image at www.biomet.co.uk).

skin surface to track limb movement, stride length was shown to be shorter than that of a person with a normal knee. Both reduced and abnormal flexion during the stance phase was also noted for TKR patients when compared to subjects with normal knees and a similar walking speed. There was little observed differences in gait between patients with different TKR designs, however in a more stressful stair-climbing exercise, only the least constrained PCR design allowed a similar range of motion to that of the natural knee (Andriacchi et al., 1982).

Fluoroscopic analysis of 47 patients with PCR TKR versus 4 control patients with normal knees revealed that the cruciate retaining knee did not produce normal kinematics, and showed a start point 10±5 mm posterior to the tibia mid-line which translated anteriorly with flexion to a point 5±3 mm anterior to the mid-sagittal point of the tibia. This was in contrast to normal knees that start anteriorly, then translate slightly posteriorly. Also, the motion of the knee replacements had a 'jerky' tendency in contrast to the normal knees which produced a smooth motion (Stiehl et al., 1995). It should be noted that this was in loaded flexion, rather than normal gait, in which the majority of the flexion occurs in the unloaded swing phase. It is thought that the loss of the ACL could contribute to the lack of anterior stability. Another radiographic study of 49 patients with identical PCR TKRs (Genesis Total Knee System, Smith & Nephew Orthopaedics, Memphis, TN) revealed no demonstrable rollback of the femoral component on the tibial during unloaded flexion (Kim

et al., 1997).

2.3 The Current Causes of Total Knee Replacement Failure

Statistically, knee replacement arthroplasty is a largely successful procedure with 75% of patients either satisfied or very satisfied with the procedure (Noble et al., 2006) and less than 3% of operations performed in the USA between 1985 and 1995 required revision surgery within the first 2 years post operation (Heck et al., 1998). However, with over 200,000 procedures performed in this time period, this still equates to a significant number of revisions. An additional observation of this study was that patient age at the time of initial operation had a significant effect on the likelihood of revision within 2 years, indicating younger patients place greater demands on their artificial joints. A review of 212 consecutive knee arthroplasty revisions (Sharkey et al., 2002) revealed polyethylene wear was a cause of failure in 25% of all cases, and in revisions conducted over 2 years post the initial surgery, accelerated polyethylene wear was found in 44.4% of revisions. Early failure (less than 2 years) was primarily due to instability or misalignment, although significant polyethylene damage was found in 11.8% of cases. The average interval that the polyethylene components had been in place before failure was 7 years, and certain designs of knee replacement have been associated with accelerated polyethylene wear with a flat polyethylene tibia bearing producing high failure rates (Feng et al., 1994). A relatively flat design of the tibia bearing surface is also thought to contribute failures of the polyethylene bearing surface with excessive wear in the posteromedial region and subsequent subluxation. (Lewis et al., 1994).

A secondary effect of polyethylene wear is the release of wear particles into the joint environment, causing aseptic loosening of the joint. Aseptic loosening was originally blamed on acrylic bone cement and as such the term ‘cement disease’ was coined (Jones and Hungerford, 1987). However, more recent studies have attributed the activation of tissue resident macrophages to polyethylene particles generated because of wear. This ultimately leads to osteolysis and implant loosening (Amstutz et al., 1992) which has been found in 16.9% of revisions performed less than 2 years from operation date, and in 34.4% of revision performed after 2 years from operation date (Sharkey et al., 2002). Both the total volume and individual size of debris particles are critical factors in determining the reactivity of

Property	FDA (range)	ASTM F-648 (min)	ISO 5834-2 (min)
Yield strength (MPa)	19-26	19	19
Ultimate tensile strength (MPa)	27-60	27	27
Elongation at break (%)	200-400	250	250
Melting point (°C)	125-145	NA	NA
Crystallinity (%)	45-75	NA	NA
Izod value (kJ/m^2)	Na	30	25

Table 2.1: Standard mechanical properties for UHMWPE (Adapted from Muratoglu et al. (2001)).

polyethylene particles in vitro (Green et al., 1998). Polyethylene wear particles from cross-linked polyethylene when worn with a scratched counterface have been found to be more biologically active than those from a non-crosslinked polyethylene with similar molecular weight when worn under the same conditions. The reactivity of both sets of particles are the same though when worn with a smooth counterface (Ingram et al., 2004). The same study also compared the reactivity of wear particles from GUR1150 and GUR1120 polyethylenes. The GUR1150 polyethylene has a higher molecular weight and was found to produce a greater percentage of particles in the biologically active range.

2.4 Ultra-high molecular weight polyethylene

Polyethylene (PE) is a polymer formed from the monomer ethylene (C_2H_4), which is a gas at room temperature with a molecular weight of 28.

Ultrahigh Molecular Weight Polyethylene (UHMWPE) is a form of polyethylene that has extremely long chains consisting of up to 200,000 ethylene repeat units which consequently can contain up to 400,000 carbon atoms. It is a semi-crystalline solid that can be visualised as a set of ordered crystalline lamellae embedded in a disordered amorphous phase (Bellare et al., 1995). The mechanical properties of UHMWPE are linked to its chemical structure, molecular weight, crystalline organisation, and thermal history (Turell and Bellare, 2004), and as a result can vary significantly based on processing and manufacturing methods used. To ensure consistency of the material when used in bio-medical applications, there are minimum values for mechanical properties specified by standards organisations and these are shown in Table 2.1.

The degree of crystallinity is an important parameter, with higher crystallinity resulting in increases in Elastic modulus, yield strength, resistance to creep deformation, and fatigue strength.

Sterilisation and packaging of UHMWPE for use in orthopaedic applications has also developed over time. Historically, components were sterilised using low doses of gamma radiation and stored in air, however these were found to show increasing amounts of oxidation over time. This increased level of oxidation led to significantly poorer wear performance in pin-on-disc tests when compared to geometrically identical shelf aged non-irradiated components (Besong et al., 1997). Oxidation occurs mostly in the region 1cm below the surface of the UHMWPE and this peak oxidation layer follows both the convex and concave contours of the articular surfaces. The regions showing increasing density and crystallinity correspond to the regions showing an increase in oxidation. In these high areas of oxidation the UHMWPE becomes brittle, as a result of the chain scission that occurs.

2.4.1 Types of UHMWPE resin

In a review published in 1994, the three main grades of polyethylene resin used in the manufacture of orthopaedic devices were listed as 1900, manufactured by Himont, GUR 412, and GUR 415, both manufactured by Hoechst/Celanese (Li and Burstein, 1994) (these two Hoechst grades were also known as CHIRULEN P in Europe) (Kurtz et al., 1999). The nomenclature used by Hoechst for their UHMWPE resins has changed several times. GUR is an acronym of Granular UHMWPE and Ruhrchemie, the latter is the manufacturing facility in which the resin was made.

In 1992 a fourth digit was added to the previously mentioned examples to allow additional product lines. Therefore GUR 415 became GUR 4150, and GUR 412 became GUR 4120. The CHIRULEN trade name was sold by Hoechst in 1994, and as a result Hoechst in Europe designated all resins for the surgical market with a 1. GUR 4120 became GUR 1120, and GUR 4150 became GUR 1150, although in North America an HP was added as a suffix to the original name to denote 'High Purity' (GUR 4150 became GUR 4150 HP). In 1998, sense prevailed and the names were consolidated for the worldwide orthopaedic market, and four grades were available: GUR 1150, 1050, 1120, and 1020. The first digit originally referred to the loose bulk density of the resin, remember initially this was a '4' which equates to a bulk density of over 400g/l. The second digit refers to the addition (1)

or non-addition (0) of Calcium Stearate. The third digit refers to the average molecular weight of the resin, calculated using the intrinsic viscosity. The fourth digit is used as an internal code designation. In 1998 all UHMWPE dealings of Hoechst were handled by a spin out company, known as Ticona (Kurtz et al., 1999).

The 1900 resin has also undergone several name changes. In the 1960s it was known as Hi-Fax 1900 produced by Hercules Powder Company (Wilmington, Delaware, USA), and in 1983 in a joint venture with Montedison (Italy), the resin became known as Himont 1900. In 1995 Montedison and Shell Oil (Netherlands) formed Montell Polyolefins, and in 2001 the company was merged into BASF and Shell to form Basell Polyolefins. However in 2002, Basell stopped production of the 1900 resin and the production technology was sold to Polialden (Brazil) who are yet to announce whether they will resume production for orthopaedic use. (Kurtz, 2004). It should be noted that Basell retained the 1900 trade name in this sale, so any resin manufactured by Polialden will be marketed under a new name.

Experimental comparisons between the resin types has been conducted with no significant differences found between the H1900 and GUR1050 resins when used in ArCom® DCM tibia bearings (Tsukamoto et al., 2008). A retrieval study compared DCM 1900H (type 1), ram extruded and machined GUR4120 (type 2), and ram extruded and machined GUR4150 (type 3) acetabular liners of the same geometric design. Wear measurement was conducted by filling the acetabular cup with oil using a known drop size. The 1900H (type 1) cups experienced statistically significant lower clinical wear than both the machined conditions, however, it is possible that either the processing method, the addition or absence of Calcium Stearate, or both, also contributed to the difference in wear (James et al., 1999).

2.4.2 Direct Compression Moulding (DCM) of UHMWPE

DCM effectively converts the UHMWPE resin directly into finished, or semi-finished components using individual moulds. The main advantage of DCM is that an extremely smooth surface finish can be obtained as there is no subsequent machining of the component, except possibly for tibia tray fixation. Additionally, higher processing pressures can be obtained in these individual moulds, as the moulded area is much smaller than that of the compression moulded sheets that would otherwise be manufactured using the press.

The compression moulding process usually features four distinct stages as outlined below

(Wu et al., 2002). It is usually performed in air, although there are other cases where inert gases are used instead, an example of which is the ArCom® process developed by Biomet, which is explained in further detail in Section 2.4.2.1.

- Compaction of the powder in a solid state.
- Elevation of the mould temperature to a value above the melting temperature of the polymer.
- A constant temperature dwell of a certain time at this mould temperature.
- Cooling of the mould at a constant rate of 7K/min to ambient temperature.

In retrieval studies of UHMWPE liners, DCM has been shown to be better consolidated (or have less fusion defects) than their ram extruded counterparts (James et al., 1999). However, it is important that the conditions used in DCM are highly controlled, as it has been shown that relatively small variations in moulding temperature and pressure can have a marked effect on the mechanical properties of the resultant moulded specimen. A study using the 1900H resin varied both the time (10 - 90 min) and temperature (145 - 200 °C) during the melt state of the compression moulding process. Differential Scanning Calorimetry (DSC) showed no variance in crystallinity between the processing conditions. In tensile testing experiments using dumbbell specimens machined from the DCM samples there was little difference in the stress-strain relationship and ultimate yield stress of the different conditions. The nominal strain at failure was much more dependent on the processing conditions with weak evidence for peak elongation to break ratio of greater than 450% at 175°C. A low dwell temperature of 145°C, which is just marginally greater than the crystal melt temperature of UHMWPE (141°C), gave very poor elongation to break ratios of between 10 and 200% (Wu et al., 2002).

Varying the moulding pressure at which DCM takes place has also been shown to have a significant influence on the mechanical properties of the resultant UHMWPE. A comparison of UHMWPE discs moulded at 10, 15, and 20 MPa exhibited different properties during hardness, punch, scratching, friction, and wear tests. With the 15 MPa samples obtaining the best mechanical properties and highest wear resistance. Wear particle size distribution was not affected. These differences in mechanical properties can be explained by variations in the UHMWPE microstructure. At lower compression pressures (10 MPa),

grain defects arise, which reduce the bonding strength at the grain boundaries, however at higher pressures (15 MPa), self diffusion occurs, which is sufficient for the molecular chains to migrate across the grain boundaries. However, raising the pressure too high (20 MPa) introduces stress induced orientation microstructures, which result in lower mechanical properties (Wang and Ge, 2007).

2.4.2.1 Conventional 'Gold-Standard' ArCom® UHMWPE

ArCom® is the trade name for a proprietary conversion process used by Biomet. It signifies that the UHMWPE resin has been compression moulded in the prescence of argon gas. Both 1900 and GUR resins have been used with this process. Pre 2002 all isomoulded ArCom® was produced using 1900H resin. Post 2002 GUR1050 is used for isostatic moulding, while 1900H continued to be used in the direct compression moulding process. However, it is thought that currently all ArCom®components are manufactured using the GUR1050 resin. There is little published data on the performance of ArCom® manufactured UHMWPE.

Tsukamoto *et al* performed a wear test on the Vanguard (PCL sacrificing) design (Biomet, Warsaw, IN) TKR to assess whether there were any differences in the two UHMWPE resins used in the ArCom® DCM process. Wear rates of 3.6 and 3.4 mm^3 per $1x10^6$ cycles were obtained for the H1900 and GUR1050 inserts respectively, with the conclusion that there was no significant difference between the two, and both rates were some of the lowest seen in literature for conventional UHMWPE (Tsukamoto et al., 2008).

2.4.3 Crosslinked UHMWPE

Cross-linking of UHMWPE is a process whereby through a variety of means, the long polymer chains found in UHMWPE become linked together, with a favourable increase in wear properties. As a result there has been much research into whether this crosslinked UHMWPE would offer improvements over standard UHMWPE. There are three main methods of cross-linking found in the literature, these are:

- **Radiation induced cross-linking** which uses ionising radiation.
- **Chemical induced cross-linking** which uses a free-radical generating chemical.

- **Silane compound induced cross-linking** which grafts a silane compound onto the polymer.

Cross-linked UHMWPE has been used successfully in THR for a number of years, however, there is still significant debate on the benefits of using it in TKR with opposition (Ries, 2005) and endorsement (Jasty et al., 2005). All three methods will be described, however, the focus will be on radiation induced crosslinking as this is currently the most commonly used method.

2.4.3.1 Radiation induced cross-linking

In the following section radiation doses are specified in both Mrad and kGy (1 Mrad = 10 kGy).

When a polymer is exposed to ionising radiation, two structural changes occur. Firstly, chain scission of the C-C tie molecules in the polyethylene chains as seen in Figure 2.7a, and then the subsequent reaction of the free-radicals, that have been produced due to breakage of the C-H bonds, with each other to form cross-links between the polymer chains, as seen in Figure 2.7b. UHMWPE implants are typically exposed to doses of radiation (2-4 Mrad) for sterilisation purposes. At these low exposure doses, only chain scission occurs, and there is very little cross linking. However, free radicals are produced and these remain trapped in the material. They are long-lived and as a result can diffuse or dissolve into the bulk material over time and then react with available oxygen species either in storage or *in vivo*. When the radiation dose is increased (5-1000 Mrad), the majority of the free radicals combine to form cross-links.

There are two main problems with radiation induced crosslinking. Firstly, when performed on solid UHMWPE the resultant crosslinked material is highly inhomogeneous with cross-linking mainly occurring in the amorphous region of the polymer and not the crystalline. Secondly, the process is not 100% efficient and therefore residual free radicals are left in the polymer, so oxidation of the polymer is a problem as in with gamma irradiated sterilisation methods. Several post irradiation thermal treatments have been devised to counteract this problem and these are discussed later in the section.

Radiation cross-linking of High-Density Polyethylene (HDPE) was first proposed in 1978 using 15Mrad gamma radiation in the presence of nitrogen, acetylene and chlorotrifluoroethylene. It was found to increase the surface hardness, but reduce the impact strength.

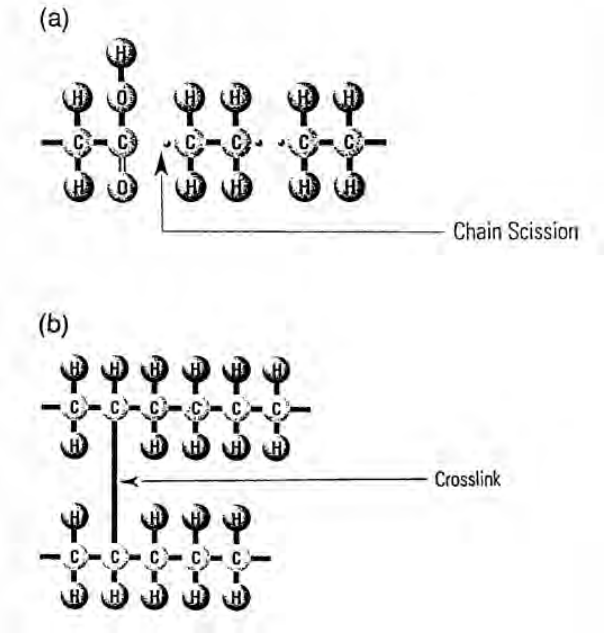

Figure 2.7: The process of chain scission in UHMWPE (a) and the subsequent cross-linking reaction (b) with the formation of covalent C-C bonds between adjacent molecular chains (Lewis, 2001).

It also showed a 30% improvement in abrasion resistance over unirradiated controls and the conclusions drawn were that radiation crosslinking could be used routinely in hip and knee prostheses to add life to the component (Grobbelaar et al., 1978).

Irradiation of the UHMWPE can be carried out at different temperatures with irradiation occurring at Room Temperature (RT) in the Cold Irradiation and Subsequent Melting (CISM) process or between 90 - 125°C in the Warm Irradiation with Adiabatic heating and subsequent Melting (WIAM) process (Muratoglu et al., 2001). A third method is termed Irradiation in the Molten State (ISM) which involves exposing the polymer to electron beam radiation while it is molten, typically at a temperature of 150°C.

In 2001, there were five fully cross-linked commercially available forms of UHMWPE (Lewis, 2001) and by 2005 this had risen to six (Harris and Muratoglu, 2005)

The radiation dose and technique varies among manufacturer but as of 2005, six modern types of cross-linked polyethylenes were available and all six were irradiated to above the normal sterilisation dose of 25-45 kGy either by Gamma irradiation or electron beam methods, with a maximum total dose of 105 kGy and a minimum total dose of 50 kGy (Harris and Muratoglu, 2005).

The magnitude of irradiation dose applied can greatly affect the mechanical and wear

properties of the polyethylene. Elastic modulus, ultimate true stress, and ultimate true strain were all found to decrease monotonically with increasing radiation dose (Gomoll et al., 2002). Crystallinity was not found to be affected by the various cross-linking doses. The reduction in elastic modulus is attributed to a higher number of smaller fragmented lamellae in the cross-linked polymer, which is thought to reduce the tensile modulus of UHMWPE. Additionally it has been shown that an increase in cross link density results in a decreased resistance to crack propagation due a reduction in the possible plastic deformation ahead of the crack tip. Stress life tests revealed a slight increase in cycles to yield for a given stress range as crosslink density increased, indicating that while cracks may propagate at a faster rate, they will also take longer to initialise (Baker et al., 2003).

However, some free radicals remain in the UHMWPE which can then react with oxygen, causing oxidative degradation which reduces both the wear and mechanical properties of UHMWPE. To eradicate these remaining free radicals a post-irradiation heat treatment or annealing phase is required. Annealing above the melt transition temperature, the residual free radicals produced by irradiation are neutralised. Annealing above the melt transition temperature (135°C) also changes the crystalline phase of UHMWPE into mobile polymer chains. When the UHMWPE is cooled to room temperature the polymer chains may not fully crystallise and consequently the crystallinity of highly-cross linked melt annealed UHMWPE is lower than that of conventional UHMWPE. Decreased crystallinity is associated with decreased elastic modulus and while it may be beneficial for wear as it reduces contact stress, it has a negative effect on mechanical properties. Alternatively annealing to below the melt transition temperature does not alter the crystallinity but is less effective in reducing the number of residual free radicals. Additional re-melting at a temperature of 240°C at a pressure of 500 MPa for a period of one hour has been shown to increase the crystallinity of cross-linked polyethylene from 50% to 75% (Simis et al., 2006), hence improving the mechanical properties whilst retaining the same level of cross-linking.

Contemporary cross linked Polyethylenes were first used clinically in 1998 and as a result there is still little *in vivo* information available. However, early failures in highly cross-linked acetabular cups have been attributed to fatigue crack fracture caused by impingement of the femoral head or stem on the liner rim (Furmanski et al., 2009).

Galvin *et al* showed that in multidirectional Pin-On-Plate (POP) tests, a 73% reduction in wear of ram extruded GUR 1050 UHMWPE is seen with an increase in radiation cross-

linking from 0 to 10 MRad (Galvin et al., 2006). Increased radiation dose has been shown to improve the wear resistance of GUR 1050 tibia components. Eight rods were machined from compression moulded UHMWPE and were gamma irradiated in air at 0, 25, 35, 50, 75. 100, 150, and 200 kGy, followed by annealing at 110°C for 12h in Nitrogen. They were then machined into experimental KOM tibial inserts. A six station displacement controlled simulator (Shore-Western Manufacturing Inc., Monrovia, CA) was run for $4.0x10^6$ cycles and the wear of components gravimetrically assessed. As the radiation dose increased from 0 to 200 kGy the wear rate decreased exponentially, however from 100 to 200 kGy no significant differences were noted. Small punch testing of discs machined from the tested tibias, versus discs machined from irradiated untested tibias revealed lower toughness' for the tested tibias at all radiation doses, indicating fatigue damage due to multi-directional sliding and cyclic loading. The difference in toughness between the simulator tested and non tested UHMWPE was smallest at 50 kGy, suggesting that this dose imparts the best fatigue resistance in crosslinked UHMWPE (Akagi et al., 2006). Similar conclusions on a decrease in plastic properties (Ultimate Tensile Strength (UTS), and Elongation At Break (EAB)) with an increase in radiation dose has been shown in other studies (Oral et al., 2006a). Fatigue crack propagation resistance has been shown to reduce with increasing radiation dose (Oral et al., 2006a).

2.4.3.2 Chemically induced cross-linking

A free radical generating chemical (FRGC) is mixed with the resin before consolidation. At the elevated temperatures used during moulding, the FRGC decomposes and produces free radicals. This process leaves reactive sites on the molecules, and these react with similar sites on neighbouring molecules and these link to form the cross-links. Examples of FRGC are organic peroxides, azo compounds, peresters, tetrazenes, and silanes, however with UHMWPE, organic peroxides are the preferred compound. There are three main drawbacks in this chemically induced process. Firstly, imperfections in the crystal structure of the consolidated polymer can arise. Secondly, as the cross-linking process takes place in the molten state, there can be limited FRGC diffusion, therefore cross-links can group in areas adjacent to the polymer flake surface. Finally, there are undesirable by-products, which if not eliminated, can affect the long-term stability of the polymer (Lewis, 2001).

2.4.3.3 Silane compound induced cross-linking

A silane compound that contains both a vinyl group and hydrolyzable group is grafted onto the polymer chain. This is achieved by using a suitable peroxide. The main difference in this process is that it is the peroxide that forms the links rather than just facilitating the crosslinking process as in the previous two methods. There is limited literature on this type of crosslinked UHMWPE although it has been tested using pin-on-plate and finger simulator studies (Joyce and Unsworth, 1996; Sibly and Unsworth, 1991)

2.4.4 Preventing Oxidation of Cross-linked UHMWPE

As stated previously, although cross-linking improves the wear resistance, there are problems associated due to the increase in residual free radicals left in the polymer. These free radicals then react with oxygen either in air or after implantation, leading to oxidation which in turn causes chain scission. This causes a drop in molecular weight which leads to increased chain mobility. This then leads to recrystallisation of and an increase in crystallinity of the polymer.

Various post crosslinking processes can be applied in order to reduce the number of free radicals left in the polymer. Two thermal treatments are commonly used, these are termed re-melting and annealing. Annealing involves heating the irradiated UHMWPE to a temperature lower than its melting point while re-melting involves heating to above the melting point. Post-irradiation annealing is less effective than melting in reducing post-irradiation free radicals. If the material is fully re-melted after irradiation, the concentration of free radicals is lower than can be detected using electron spin resonance images. This reduction in free radicals led to mechanical properties that were still within Food and Drug Administration (FDA), American Society for Testing and Materials (ASTM), and ISO standards, and a significant reduction in wear of acetabular liners (Muratoglu et al., 2001). However, remelting causes a reduction in fatigue crack propagation resistance when compared to irradiated UHMWPE with no thermal treatments (Oral et al., 2006b).

Addition of α-tocopherol (Vitamin E) shown in Figure 2.8 to XL UHMWPE was first proposed in 2004 as a way of reducing the undesirable residual free radicals without post irradiation re-melting (Oral et al., 2004). As previously stated, the re-melting process reduces the fatigue resistance of the polymer and thereby limits the use of highly XL UHMWPE to low stress applications. The α-tocopherol acts as an anti-oxidant and hence limits the

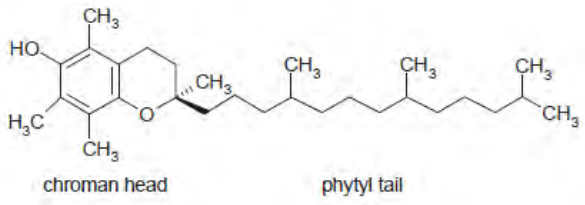

Figure 2.8: The chemical structure of α-tocopherol. The chroman head is responsible for abstracting free radicals and stabilising them within the structure. The lipophilic chain termed the 'phytyl tail' provides compatibility with UHMWPE (Oral et al., 2004).

oxidation of the UHMWPE.

The hydrophobic nature of Vitamin E means it blends easily with UHMWPE and can therefore be added before consolidation (Vaidya et al., 2011), however most published methods involve doping by diffusion, as blending before consolidation reduces the cross-link density of the UHMWPE due to the α-tocopherol reacting with the free radicals during consolidation that would otherwise go on to form cross-links (Oral et al., 2005).

The process of Vitamin-E diffusion into UHMWPE involved several steps. Standard UHMWPE bar stock is used, then γ-irradiated to achieve the desired level of cross-linking. The bar stock is then machined into the desired geometry and then doped with α-Tocopherol. This process can take place at a variety of temperatures (RT or 100°C) and gaseous environments (air or nitrogen) (Oral et al., 2004).

In early diffusion tests carried out at 100°C, α-tocopherol was shown only to diffuse into the first 0.5mm of the material while the bulk material was unaffected (Oral et al., 2004). The effect of ageing has also been shown to reduce with the addition of Vitamin E. After 5 weeks of accelerated ageing in air the 65-kGy and 100-kGy α-T doped irradiated UHMWPE showed significantly lower oxidation indices (0.48 ± 0.25 and 0.44 ± 0.06) compared to the undoped 100-kGy controls (3.74 ± 0.16). In bidirectional Pin-On-Disc (POD) tests the process of accelerated ageing was not found to cause a significant increase in wear, a similar finding to crosslinked and remelted UHMWPE. However, highly crosslinked UHMWPE with annealing exhibited a highly significant increase in wear rate from approximately 2mg/million cycles to 27 mg/Million Cycles (MC) after ageing (Oral et al., 2004).

In physiological hip simulations using radiation XL UHMWPE acetabular cups infused with α-tocopherol, a 4-fold decrease in wear rate (1mg/MC) compared to conventional UHMWPE was found when using clean serum lubricant, and a 10-fold decrease (6mg/MC)

in wear rate was found when using serum lubricant containing third body particles. The mechanical properties, such as UTS, Yield Strength (YS), EAB, and fatigue strength, of similarly doped samples were all found to be significantly higher than irradiated and re-melted control samples. Accelerated ageing also had no effect on the Vitamin E doped samples, whereas for the irradiated and remelted samples, the crystallinity significantly increased, resulting in a decrease in UTS (Oral et al., 2006a).

Current second-generation cross-linked UHMWPE infused with Vitamin-E has better mechanical properties than first-generation irradiated and re-melted UHMWPE and better bending and fatigue resistance than that of aged conventional UHMWPE. Oxidation resistance and wear resistance of the second-generation vitamin-E doped crosslinked UHMWPE is comparable to first generation, cross-linked and remelted UHMWPE (Oral et al., 2008).

2.5 Pre-clinical assessment of knee replacement solutions

Ethically, it is essential that maximum effort is put into assessing the potential performance of a knee replacement solution in an *in vitro* environment before progressing to clinical trials, as with any new medical technology there are inherent risks. This is especially important now, as there have been publicly high profile failures such as the ASR® Hip resurfacing, which has now been recalled worldwide by the manufactures DePuy. Metal-on-Metal (MoM) resurfacing hips had good outcomes in early studies (McMinn et al., 1996; Treacy et al., 2005) and the ASR® hip had low revision rates of 2.7%, although only after an admittedly short mean followup period of 202 days (Siebel et al., 2006). However, more long term clinical studies have revealed pseudo-tumors occurring in patients (Pandit et al., 2008) possibly due to increased levels of metal ions in the body (Clarke et al., 2003). This clearly indicates the importance of strenuous pre-clinical testing as revision operations are generally less successful than primary interventions.

Preliminary wear screening often uses simple wear testers, such as POP, or POD machines. These involve geometrically simple specimen shapes, and simple motions and loads. These tests are primarily run in order to obtain the tribological properties and wear performance characteristics of material combinations. Early testing at Durham featured statically loaded pins, articulating against sinusoidally reciprocating plates (Sibly and Unsworth, 1991), however it was soon realised amongst the academic community that this linear mo-

tion could be the cause of reduced wear rates. *In vivo* there is a certain amount of cross shear between the two articulating surfaces, consequently the Durham pin-on-plate rigs were modified to incorporate cross shear (Joyce et al., 2000). However, for a new type of biomaterial or joint replacement to be clinically trialled, it first needs to be tested in an physiologically relevant wear simulator.

Examples of several kinds of knee simulator can be found in the literature from manufacturers including Stanmore, AMTI, Prosim and MTS. However these fall broadly into two categories, force controlled or displacement controlled (Burgess et al., 1997), and some simulators can do both (Barnett et al., 2002). The overall aim of these simulators is to accurately simulate the *in vivo* loads and displacements of the knee joint in order to produce wear rates on TKRs that are comparable to *in vivo* performance. However, this in itself presents several challenges for researchers. One problem regards the loads and displacements within the knee. This has been addressed with the introduction of test standards from ISO, however there is significant debate about whether these are aggressive enough, and whether they produce the right contact areas. A choice also has to be made whether to use the profiles for force or displacement control, although this is usually determined by the geometry of the test implant, as non-conforming implants such as the Cruciate Retaining (CR) designs are impossible to test using force control as it results in dislocation of the femur from the tibia. Similarly, constrained designs such as Rotating Platform (RP) knee replacements cannot be tested using the displacement profiles as they can cause articulations at a greater magnitude for than that which the knee replacement was designed, therefore force control is often used (McEwen et al., 2001). It should also be noted that wear results from force and displacement controlled simulators cannot be directly compared as the force control method has been shown to produce wear rates 50% higher than the displacement control on the same simulator with the same knee design (Schwenke et al., 2009)

2.6 Relating Pre-Clinical Assessment to Clinical Findings

The challenge in simulator studies is to achieve the same amount and type of damage to that seen *in vivo*. The following section outlines some existing methods in order to simulate damage to the otherwise smooth femoral component and oxidative degradation of the UHMWPE components.

2.6.1 Scratching of the Counterface

Scratching of the smooth counterface is thought to account for discrepancies between in vivo and in vitro wear factors of UHMWPE. Retrieval analysis of TKRs has suggested that roughness of the femoral component can increase by an order of magnitude over the life of the component with the predominant damage mode being scratches parallel to articulation (Que et al., 2000). Other investigators have suggested that there was no change in surface roughness, although analysis of their methods reveals that the profiles used to calculate the R_a ran parallel to the majority of scratching, and therefore could potentially miss these features (Lakdawala et al., 2005).

Early pin on plate tests using surgical grade stainless steel plates (EN58J) and surgical grade UHMWPE (Hoechst RCH 1000) showed that transverse scratches on the counterface can increase the wear factor by an order of magnitude. It was concluded that the piled up material flanking each transverse scratch was primarily responsible for the increased wear rate (Dowson et al., 1987). Later pin-on-plate tests using UHMWPE pins reciprocating against scratched 316L stainless steel counterfaces also produced a 70-fold increase in wear factor than that of an unscratched counterface (Fisher et al., 1995). Similarly, the wear factors of various grades of cross-linked UHMWPE were all found to increase when worn with perpendicularly scratched stainless steel plates verses smooth plates (Galvin et al., 2006).

Other studies went on to assess the effect of a scratched counterface in the more complex motion in knee and hip simulator testing. In hip testing, the roughening of the femoral head was found to increase the rate of debris production and additionally, rougher heads produced much larger wear particles (Elfick et al., 2001). An increase in the R_a of CoCrMo heads form 0.016 to 0.38μm was found to increase the wear of crosslinked UHMWPE sockets by 800% during normal walking (Bowsher and Shelton, 2001). Jedenmalm *et al* demonstrated a 2-fold increase in wear of compression moulded GUR1020 UHMWPE cups when the femoral head roughness was increased from 15nm to 400nm. In the same study moderately crosslinked (3MRad in nitrogen) cups were articulated against the roughened heads and were found to have a wear rate over two times that of the non-crosslinked UHMWPE (Jedenmalm et al., 2009).

Comparing artificially roughened oxidized zirconium and CoCr femoral components articulating against UHMWPE in a knee simulator, the OxZr was found be more resistant

to scratching by alumina powder than the CoCr components. The mean R_a for two OxZr components after scratching was 58±16nm compared to 172±29nm for CoCr. This lower R_a for OxZr resulted in a mass loss of 16.6±7.6mg per million cycles compared to 92.0±24.4mg per million cycles for CoCr (DesJardins et al., 2008).

One method for obtaining scratches on the femoral components is that of tumbling the components along with 25μm alumina powder and plastic cone media in a centrifugal finishing barrel for 30 seconds (DesJardins et al., 2008). Using this method the R_a (measured at four discrete locations on each condyle of 2 femoral components) of CoCrMo femoral components was found to increase from 38±11nm by 4.6 times to 172±29nm, however due to two different counterface materials being used, this may have an effect.

2.6.2 Oxidative Degradation

With conventional UHMWPE the problem of oxidative degradation appeared to have been solved with the discovery that gamma irradiation in air led to a reduction in the mechanical and wear properties of the UHMWPE. However, with the advent of highly cross-linked UHMWPE and the inherent free radicals introduced in the cross-linking process, the problem of oxidative degradation has once again emerged. There are several methods for reducing this oxidation such as post-irradiation re-melting or the infusion of anti-oxidants and these have been described in detail previously. This section describes some of the published methods that have been used to test the effectiveness of the anti-oxidation techniques.

Ageing components can be achieved in several ways. Shelf ageing is the act of simply letting the components remain in their packaging for a prescribed time after manufacture (Besong et al., 1997; McEwen et al., 2005). However, while easy to do, this is obviously a lengthy process. Also, it is not relevant for today's modern inserts, as they are either vacuum packed or packed in an inert atmosphere. Ageing at 120°C in air has been used for small materials test, as has placing the test samples in an oxidising solution of 10% aqueous H_2O_2 (Wolf et al., 2006). Conventional and cross-linked UHMWPE tibia inserts have been aged for 35 days at 80°C, and this succeeded in causing de-laminations in the conventional UHMWPE tibias when subjected to a standard knee wear test. However, only a slight change in volumetric wear rate was seen. The highly cross-linked UHMWPE did not demonstrate any oxidation, however this had been fully re-melted post irradiation, so this was to be expected (Muratoglu et al., 2004a). The most common process for oxidising

UHMWPE is that which is outlined in the ASTM standard F2003. This involves holding the test components at 70°C at 5 Bar (73 pounds per square inch (psi)) in an oxygen rich atmosphere for a total of 14 days. This process has been shown to increase the wear, reduce the tensile strength and severely reduced the fatigue life of GUR 415 UHMWPE which was γ-irradiated (25 kGy) (Bell et al., 1998). A study on this ageing method however has shown interlaboratory reproducibility errors of 129.1%, measured using an oxidation index, so care must be taken when interpreting from other laboratories.

2.7 Summary

TKR is currently a very successful procedure with low revision rates and high patient satisfaction, although wear of the UHMWPE is still a contributing factor in most TKR failures. The traditional cohort of patients is changing, and in the future the procedure will be available to younger, bigger, and more physically active patients. This increasing demand requires implant manufacturers to constantly improve and refine their designs and processes in order to ensure the TKRs have the best chance of surviving without painful revision. In the next 10 years, there is no question that metal on UHMWPE will remain the material combination of choice, so therefore efforts should be focused on this. Changes that improve performance, whilst requiring minimal changes to the manufacturing process would be easy to implement. The human knee is a very hostile environment and so conditions for the testing of new designs, materials, and processes must reflect this. Hence, with respect to the performance of UHMWPE in TKRs, the main aims of this thesis are:

- Assess the effect of varying DCM processing conditions (fusion defects) on the wear properties of UHMWPE, in both standard and more clinically relevant conditions.
- Assess the effect of polymer chain entanglement on the wear properties of UHMWPE.
- Assess the potential performance of DCM UHMWPE tibia components in more active patients.
- Assess the potential performance of Vitamin E infused XL UHMWPE tibia components in more active patients.
- Assess the potential performance of Vitamin E infused XL UHMWPE tibia components in more active patients for extended time periods.

- Assess the potential performance of DCM UHMWPE tibia components in more active patients under clinically relevant conditions.
- Assess the potential performance of Vitamin E infused XL UHMWPE tibia components in more active patients under clinically relevant conditions.

Ultimately, we are trying to optimise the manufacturing conditions to produce the best material for TKRs.

Chapter 3

Influence of Type 2 Fusion Defects on UHMWPE Wear

Pin-on-plate testing is a method of pre-clinical wear testing that seeks to replicate the sliding speeds and contact stresses encountered in the hip joint of the human body. It is not however, designed to replicate the complex kinematics and dynamic loading found *in vivo*. For this, more complex, and consequently more expensive, simulators are required. The advantage of POP machines over these more complex simulators is that the test samples are easier to manufacture due to their simple cuboid and cylindrical geometry and previous studies have shown that multi-directional pin-on-plate machines can give a good indication of the wear properties of material couples and hence their projected performance *in vivo* (Saikko, 1998; Tipper et al., 1999; Wang et al., 1996). The machines used in this study were four station machines that applied both reciprocation and rotational motion and can be seen in Figure 3.1 and in schematic form in Figure 3.2. They have been described in detail previously (Joyce et al., 2000; Scholes and Unsworth, 2001, 2007). Three independently controlled machines were used during testing and the loads and displacements on each were all individually calibrated using an externally calibrated load-cell and vernier calipers. The calibration data and the maximum errors can be seen in table 3.1.

Sample pins were held in the stainless steel pin-holder using a grub screw, which contacted a machined flat on each of the sample pins. Care was taken not to over tighten the screw so that damage to the pin was minimised. The rotational motion was provided by four individual DC motors and transferred to the pin holder by the of a pair of fixed gears.

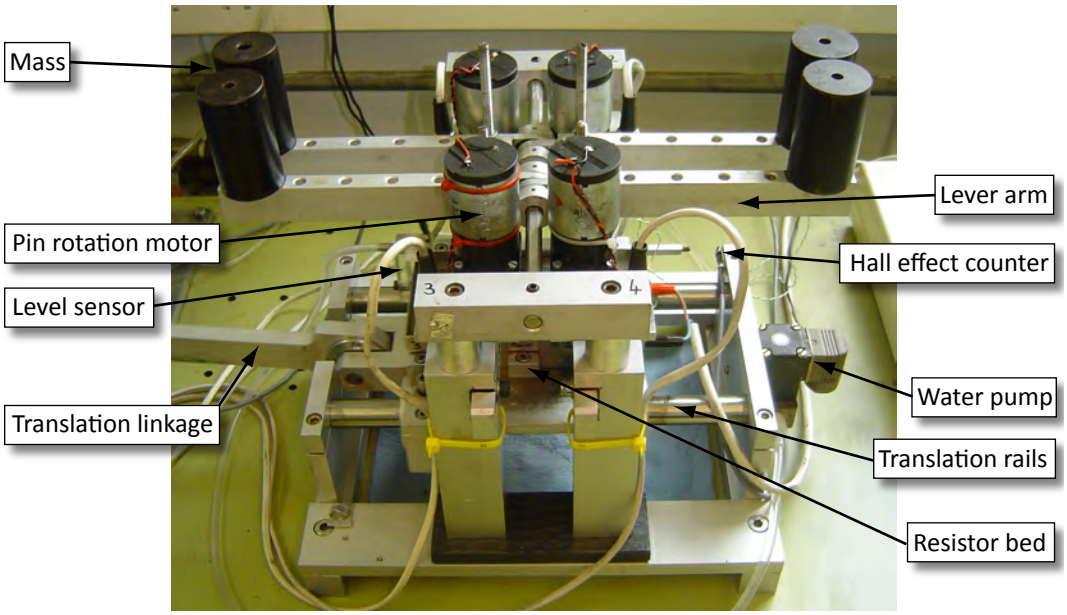

Figure 3.1: The Durham pin-on-plate rig.

Rig	Station	Date	Readout (mV)	Load (N)	Error (%)	Pin Rotation
1	1	21/07/2009	336.8	39.24	-1.9	Clockwise
	2		345.0	39.95	-0.1	
	3		343.6	39.83	-0.4	
	4		347.6	40.17	+0.4	
2	1	10/08/2009	339.2	39.45	-1.4	Anti-Clockwise
	2		346.0	40.04	+0.1	
	3		347.3	40.15	+0.4	
	4		340.0	39.52	-1.2	
3	1	14/07/2010	325.9	39.95	-0.1	Clockwise
	2		319.7	39.41	-1.5	
	3		324.8	39.86	-0.4	
	4		327.5	40.09	+0.2	

Table 3.1: Calibration data of the three pin-on-plate rigs used in this study.

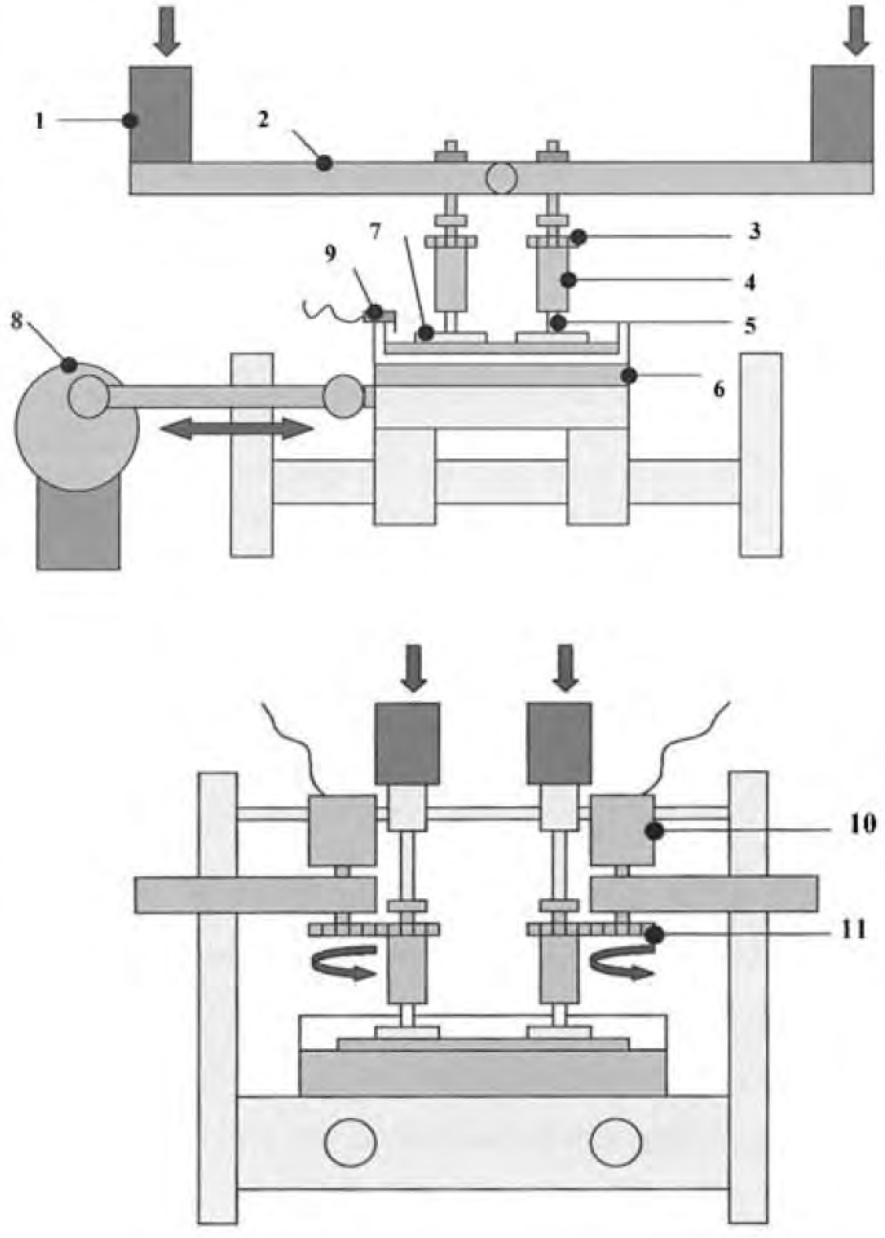

Figure 3.2: Schematic diagram of the Durham pin-on-plate rig. 1: Mass to provide load; 2: Lever arm; 3: Pin holder gear; 4: Pin holder; 5: Pin; 6: Heater bed; 7: Plate; 8: Motor to provide reciprocation; 9: Lubricant level sensor; 10: Motor to provide pin rotation; 11: Pin motor gear (Scholes and Unsworth, 2007).

The pin holder was held in place using a nylon bush which was lubricated with olive oil. For all tests the pins rotated at 1.000 ± 0.008 Hz which was monitored daily and adjusted manually if outside of the limits.

The test plates were located in a polyethylene insert that was machined exactly to size so that no movement of the plate was allowed. The polyethylene insert and the test plate were then clamped into a stainless steel tray into which the lubricant was later poured. This stainless steel tray was clamped to a sledge linked to a 200V DC motor which provided the reciprocating motion. The stroke length was set at 20mm. A static load of 40N was applied to the top of each pin holder using a lever arm and mass arrangement.

Five different pin-on-plate tests were conducted throughout this research. In this chapter the materials, methods, and results from each test are presented. All tests were conducted using the pin as the harder part of the bearing couple. It was felt this configuration would more accurately mimic the *in vivo* conditions of a TKR.

The lubricant used in all tests was new born calf serum (Harlan UK Ltd., Loughborough, UK) diluted with deionised water to a concentration of 25%. 0.2% w/w Sodium Azide (NaN_3) was also added to retard bacterial growth and 20mM/l of Ethylenediaminetetraacetic acid (EDTA) was also added to prevent calcification. The lubricant was heated to a constant 37°C using a resistor bed and monitored using a thermocouple. 65ml of lubricant was used for each rig and the lubricant level was monitored using a platinum wire sensor. Any drop in the level was assumed to be evaporation of distilled water so was automatically topped up from a reservoir. The number of reciprocating cycles was recorded using a hall effect probe.

All mass changes of both the pins and plates were assessed gravimetrically. Initially the samples were cleaned using a consistent protocol which was designed to completely remove any contaminants without damaging any of the surfaces. This is outlined in Appendix A.2.1.1. After cleaning both the pins and plates were weighed on a Mettler Toledo AX205 balance which was accurate to 0.01mg. The ISO standard 14243-2 outlines a method for gravimetric assessment of specimens used in wear testing, which involves the following steps:

- Weigh the test specimen and control specimen on the balance twice in rotation within 90 minutes of the end of the cleaning process.
- If the two readings are not identical within 100 μg, continue taking readings in rotation

until at least two readings per specimen are identical within 100 μg.

- Store the specimen in a sealed dust-free container between weighings.
- Repeat the cleaning and weighing process at intervals until the incremental mass change of the specimen over 24h is less than 10% of the previous cumulative mass change.

The weighing process defined in the standard therefore had a minimum duration of 24hrs which was felt to be less than ideal for the purposes of this test, as it was more important to maximise simulator time. Instead, a similar protocol was used with the additional requirement that three (instead of two) readings per specimen were identical within 100 μg, and the removal of the requirement of additional weighing steps, as it was felt this would be compensated for by the use of the control specimen. It should be noted that even if just one specimen did not have the three values within the specified range, all specimens would be re-weighed in turn until the three readings within the specified range had been obtained. When calculating the mean values for each specimen, priority was placed with the most recent readings i.e. if seven readings had been taken for a sample and the both the first and last three readings were within 100 μg, then the last three readings would be used to calculate an average.

Volumetric wear rates were assumed to be linear as suggested in the ISO standard. This is based on findings by Archard which demonstrated a proportional relationship between wear volume and sliding distance, as shown in Archard's wear law below:

$$Q = \frac{KWL}{H} \tag{3.1}$$

Where Q is the the total volume of wear debris produced, K is a dimensionless constant, W is the total normal load, H is the hardness of the softest contacting surfaces, and L is the total sliding distance.

At various stages throughout the test, the surfaces of the samples were imaged optically using an optical microscope and firewire camera, and morphologically using a Zygo white light interferometer. The locations imaged varied between tests but were always at one of the locations shown in figures 3.3 and 3.4.

Figure 3.3: Approximate locations of R_a readings.

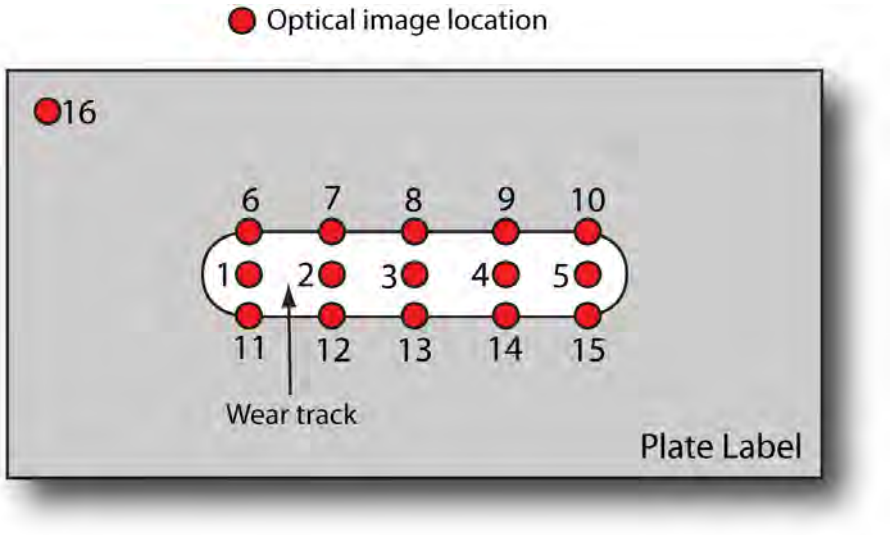

Figure 3.4: Plate optical and Zygo locations.

3.1 Reproducibility Test

An initial test using commercial UHMWPE plates and Stainless Steel (SS) pins was conducted in order to asses the reliability and repeatability of the POP rigs.

3.1.1 Materials and methods

Twelve plates of dimensions 24mm x 44mm x 3mm were machined from stock UHMWPE PE 1000 rod (Bay Plastics, North Shields, UK). The average R_a of each plate was calculated from 5 random locations on the surface and the smoothest 8 plates were used for test samples and the remaining 4 were used as soak controls, 2 at RT and 2 at 37°C.

14 stainless steel pins of 5mm diameter were manufactured from 5mm diameter stock rod. The contacting end surface was polished using both increasing grades of grinding paper and polishing fabric. The roughness of the surface was measured in five locations using the Zygo surface profiler. These five locations can be seen in Figure 3.3. The 8 pins with the lowest mean R_a were used in the test. A chamfer of approximately 45° was ground onto the circumference of the pins in order to minimise edge effects. The size of this chamfer was measured on the optical microscope at four locations on each pin 90° apart. From this measurement the contact area between the each pin and plate could be calculated by subtracting twice the average chamfer radius from the measured diameter of the pins. As the loading was constant, the contact pressure between the pins and plates could then be calculated.

The 8 commercial UHMWPE plates were immersed in lubricant for approximately 15 days to equalise fluid content. The 4 soak controls were immersed for approximately 7 days, two plates were soaked at 37°C and the remaining two were soaked at RT. These two soaking conditions were maintained throughout the duration of the wear test.

Throughout the wear test, pins and plates were removed from the rig at approximately 0.25 MC intervals for cleaning and gravimetric assessment. Upon completion of weighing, the pins and plates were then returned to the rig and the lubricant renewed. Great care was taken to correctly align the pins and plates so that the wear area was the same every time. The wear test was conducted for 3.0 MC which equates to a total sliding distance of approximately 125km. Two independent rigs were used.

Due to the combined reciprocation and rotation of the pin, the sliding distance could not

Rig	Station	Pin	Mean Initial R_a (μm)	Plate	Mean Initial R_a (μm)
1	1	12	0.021	5	0.902
	2	3	0.019	8	0.918
	3	8	0.022	7	1.123
	4	6	0.022	9	1.174
	37°C			3	
	RT			2	
2	1	2	0.022	11	0.916
	2	5	0.019	12	1.081
	3	11	0.022	1	1.141
	4	7	0.017	4	1.179
	37°C			10	
	RT			6	
Mean			0.021		1.054

Table 3.2: Pin and Plate sample location and mean initial R_a of the surface of each test component.

be assumed to be double the translation distance as the total sliding distance of a point on the surface is dependent on the polar coordinates of the particular point, as is illustrated in Figure 3.5. If the sliding distance of point 5 (pin centre) in one full reciprocation was 40.00 mm, then the sliding distance of point 4 would be 52.52 mm, point 2 would be 33.41 mm, and points 1 and 3 would be 42.61 mm. Scholes (Scholes, 1999) developed a computer algorithm to calculate the average sliding distance of a point on the surface of a pin undergoing both reciprocation and rotation at the same frequency. Using this program to calculate the sliding distances of 20 radial points at 1° intervals (20 x 360=7200 points) gave an average sliding distance for a 20 mm stroke of 41.02 mm. This figure was used in all future calculations of sliding distance.

3.1.2 Results

The results of the commercial UHMWPE reproducibility test are presented in the following section. Just gravimetric data is presented as the focus of the test was to establish any inter station variability.

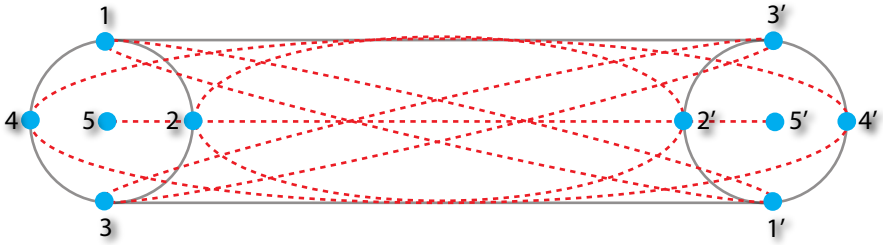

Figure 3.5: Paths taken by five points on the pin surface during one full reciprocation and rotation.

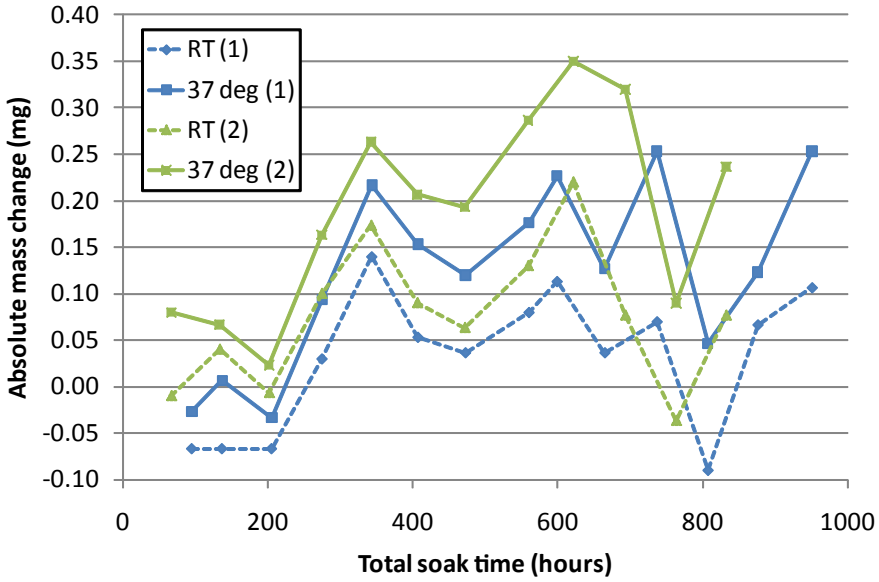

Figure 3.6: Absolute mass change of the four commercial UHMWPE control plates.

3.1.2.1 UHMWPE Plate Fluid uptake

Four control plates were used during the wear test in order to account for fluid uptake in the eight test plates. The absolute mass change of the 4 plates during the wear test is shown in Figure 3.6. Here it can be seen that all four plates experienced a mass increase from the initial value at the start of the test. However a quantifiable relationship between mass increase and soak time is not obvious, mainly due to the mass fluctuations caused by varying environmental conditions at the time of gravimetric assessment.

However, if the relative differences between the UHMWPE plates soaked at RT and 37°C are compared the result is shown in Figure 3.7. Due to differences in the timing of gravimetric assessment, the two rigs were plotted independently, but it is clear that a similar trend exists for both rigs. The plates soaked at 37°C experienced a greater mass increase than those at RT and this rate of increase was approximately linear. The rates and R^2

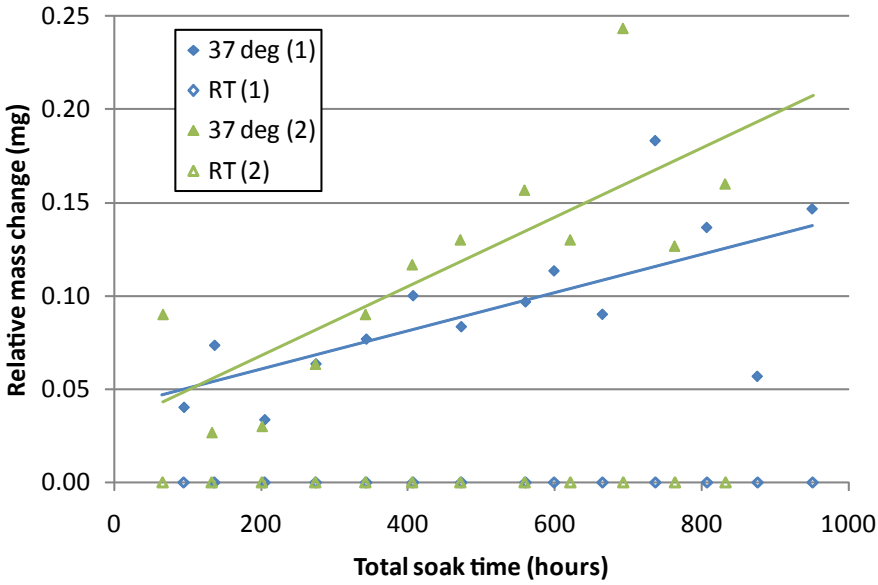

Figure 3.7: Relative mass increase of the two control plates immersed in test lubricant at 37°C with respect to the two control plates immersed in test lubricant at RT.

	Test 1	Test 2	Mean
mg/hour	0.00010	0.00019	0.00014
R^2	0.459	0.607	0.533

Table 3.3: Fluid uptake rates for commercial UHMWPE soaked at 37°C with respect to commercial UHMWPE soaked at RT.

values ares shown in Table 3.3.

3.1.2.2 Pin and Plate Wear

For the purposes of volumetric wear calculations. The mean density of the 12 commercial polyethylene plates used in the test was 0.9316±0.0007 g/cm^3. This was calculated experimentally using a Mettler Toledo AX205 balance and density kit.

The wear results for the four individual commercial PE plates on rig one can be seen in Figure 3.8. The mean wear factor of the four plates, using the previously obtained density value was 2.316±0.252 x10^{-6} mm^{3}N^{-1}m^{-1}

The absolute mass change of the four SS pins used on rig 1 can be seen in Figure 3.9. Pins 12, 3, and 8, all exhibited a similar trend and the mass change was very small and was therefore considered negligible. Sometime between 42 and 49 km of sliding, pin 12 started to experience a comparatively drastic mass loss, which continued all the way to the conclusion of the test. The contacting, polished surface of the pin was examined using

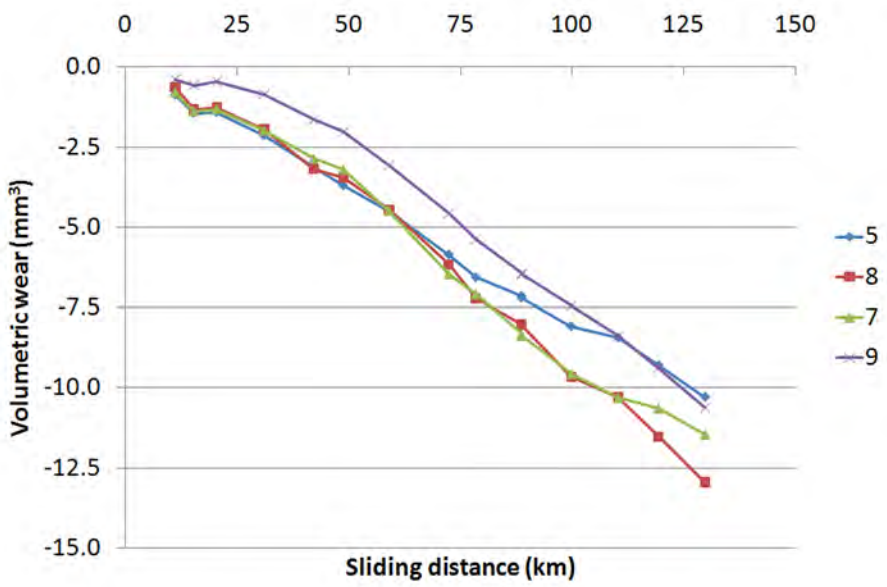

Figure 3.8: Volumetric wear plots of individual commercial UHMWPE plates 5, 8, 7, and 9, on stations 1, 2, 3, and 4, respectively on rig 1.

the optical microscope, but no uncharacteristic damage was found and therefore the mass loss was assumed to come from the part of the pin in contact with the pin holder. It was therefore not considered significant. Observation of plate 4 in Figure 3.8 shows no change to the trend of UHMWPE plate wear, reinforcing the assumption that the mass loss was not due to damage at the polished surface.

The wear results for the four commercial PE plates on rig two can be seen in Figure 3.10. The mean wear factor of the four plates, using the previously obtained density value was 2.608±0.441 x10^{-6} $mm^3N^{-1}m^{-1}$. Similarly to rig 1, all four plates followed a highly linear trend.

The mass change of the four SS pins used on rig 2 can be seen in Figure 3.11. The mass fluctuations were very small and was therefore considered negligible. All four pins followed the same fluctuation trend, indicating that this was caused by the local environmental conditions at the time of gravimetric assessment.

The mean results for both rigs, with ± standard deviation, can be seen in figure 3.12.

The mean wear factor for all 8 plates was 2.462±0.367 x10^{-6} $mm^3N^{-1}m^{-1}$. The individual wear factors for each plate can be seen in Table 3.4.

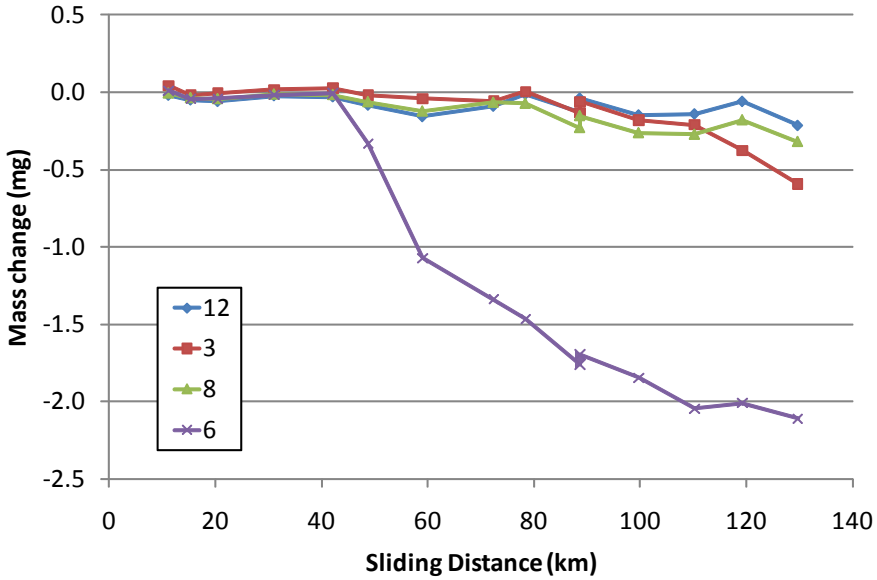

Figure 3.9: Absolute mass change of the four SS pins on stations 1, 2, 3, and 4, respectively on rig 1.

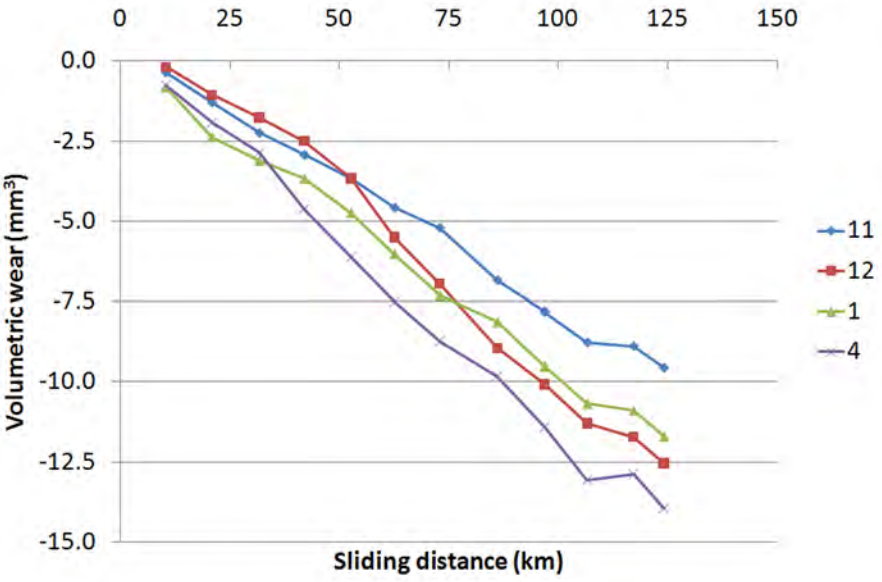

Figure 3.10: Volumetric wear plots of individual commercial PE plates 11, 12, 1, and 4, on stations 1, 2, 3, and 4, respectively on rig 2.

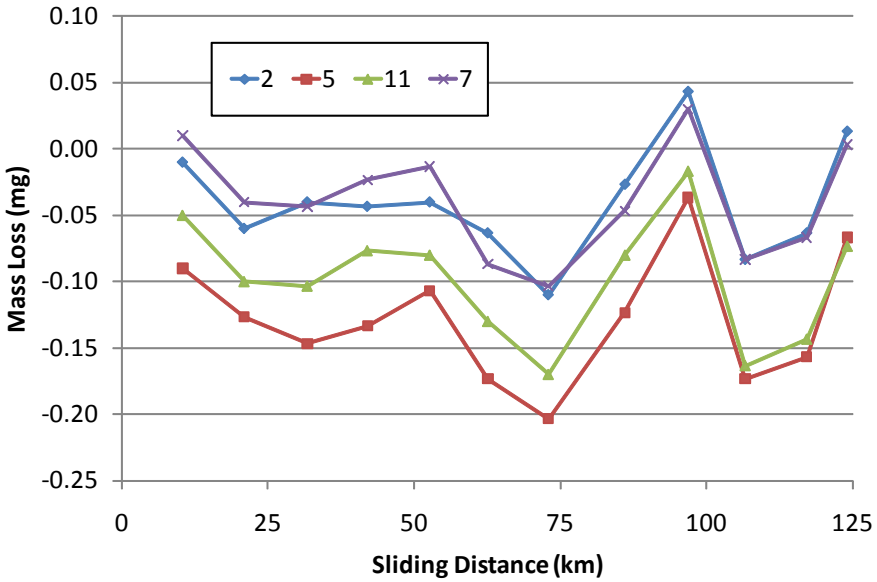

Figure 3.11: Absolute mass change of the SS pins on stations 1, 2, 3, and 4, respectively on rig 2.

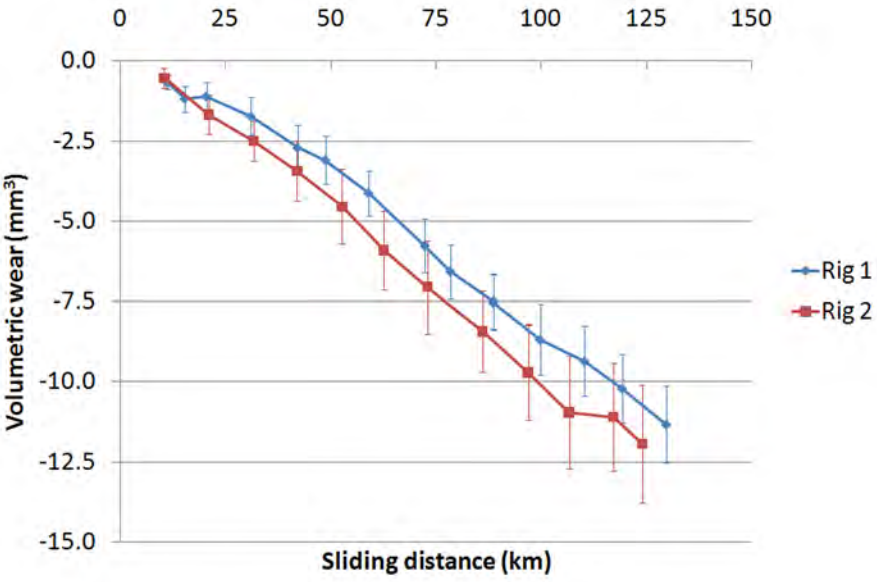

Figure 3.12: Mean volumetric wear plots (± 1 SD) of commercial PE plates on rigs 1 and 2.

Rig	Station	Plate	Wear Factor	Rig Mean	Test Mean
1	1	5	2.004	2.316±0.252	2.462±0.367
	2	8	2.589		
	3	7	2.430		
	4	9	2.242		
2	1	11	2.081	2.608±0.441	
	2	12	2.945		
	3	1	2.408		
	4	4	2.999		

Table 3.4: Wear factors (x10^{-6} $mm^3N^{-1}m^{-1}$) of the eight commercial UHMWPE plates.

3.2 Effect of molecular weight

3.2.1 Materials & Methods

Three different molecular weights of UHMWPE were tested. Two plates had an average molecular weight of 5,000,000 g/mol, one plate had an average molecular weight of 9,000,000 g/mol, and the remaining plate had an average molecular weight of 600,000 g/mol.

The POP test was run for a total of 3.0 MC with a stroke length of 20mm. This equates to approximately 124 km total sliding distance. The test components were assessed gravimetrically at 0.25 MC intervals. The UHMWPE plates were assessed optically prior to testing, then at approximately 0.5 MC intervals until the test conclusion at approximately 3.0 MC. The central area of the wear track (locations 1-5) on the plates were also assessed with the Zygo at the conclusion of the test after 3.0 MC. The SS pins were assessed gravimetrically at the same intervals as the UHMWPE plates and were assessed optically prior to testing, then after 0.5, 1.0, 2.0 and 3.0 MC. The pins were assessed on the Zygo prior to testing, then at 0.5 MC and at the conclusion of the test at 3.0 MC. The wear test was conducted on POP rig 3, the calibration data for which can be found in Table 3.1.

To assess the density of the various molecular weights, the Mettler Toledo AX205 balance with density kit was used.

During the wear test a plate of each molecular weight was used as a soak control to account for any fluid uptake by the wear samples. Based on the findings from the test conducted in Section 3.1 the control pates were placed in test lubricant held at 37°C as this

Station	Plate	Pin
1	PE5 P2	D9
2	PE6 P2	D10
3	PE5 P3	1
4	PE9 P3	10
	PE5 P4	
Control	PE6 P3	15
	PE9 P4	

Table 3.5: Station locations and combinations for SS pins and UHMWPE plates of varying molecular weights.

increased temperature was found to have a positive effect on lubricant uptake.

Both the pins and plates were assessed gravimetrically using the cleaning and weighing protocols outlined in Appendices A.2.1.1 and A.2.2 respectively.

3.2.2 Results

The results for the effect of molecular weight on the wear of UHMWPE are presented in the following section. Here, density, wear, lubricant uptake, and optical analysis results are shown.

3.2.2.1 Density Results

The mean density of the UHMWPE plates can be seen in Figure 3.13. There were two sample plates for 600,000 g/mol, three sample plates for 5,000,000 g/mol and two sample plates for 9,000,000 g/mol. It can be seen that as molecular weight increases, the density of the UHMWPE decreases. The mean of measured densities for each condition were used for volumetric wear and wear factor calculations.

3.2.2.2 Lubricant uptake

Three control UHMWPE plates were used to adjust the wear results to account for mass changes caused by lubricant uptake into the samples. The absolute mass change of the three plates can be seen in Figure 3.14. Both the 9,000,000 g/mol plate and 5,000,000 g/mol plate exhibited a sharp increase in mass at the start of the wear test, which then levelled off and

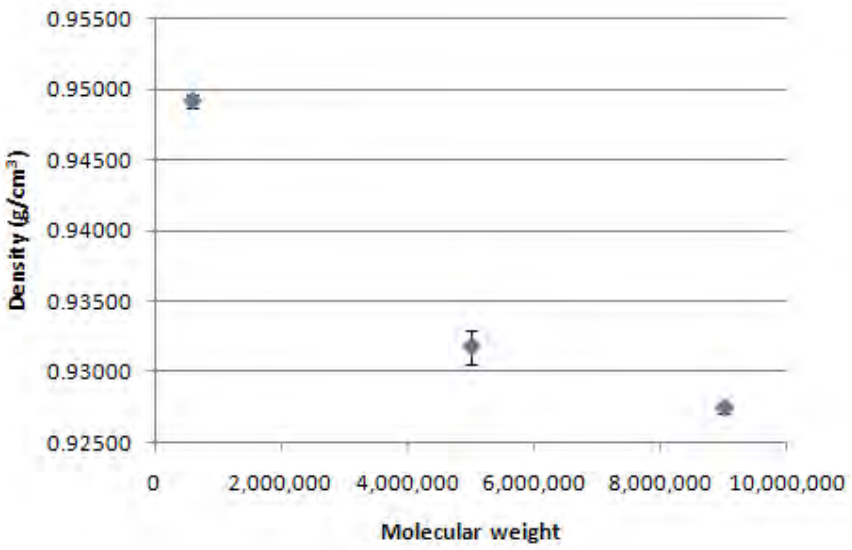

Figure 3.13: Plot of mean density (± 1 SD) vs molecular weight.

Molecular weight (g/mol)	Rate of Mass increase (mg/hour)	R^2
9,000,000	0.00028	0.919
5,000,000	0.00037	0.971

Table 3.6: Mass increase rates of control plates relative to 600,000 g/mol control plate (N.B. Rate of mass increase is from 260 to 1070 hours test duration).

fluctuated around 0.6 mg. In contrast, the control plate with a molecular weight of 600,000 g/mol did not experience a sharp increase and fluctuated around 0.15mg.

Plotting the mass change of the 9,000,000 g/mol and 5,000,000 g/mol control plates relative to the 600,000 g/mol control plate is shown in Figure 3.15. Interestingly there is little difference in the fluid uptake trends between the three control plates up to 160 hours of soaking. After this however a clear difference is apparent. Between 160 and 260 hours both the 9,000,000 g/mol and 5,000,000 g/mol control plates experience a mass increase approximately 0.25mg greater than that of the 600,000 g/mol control plate. From then on until the conclusion of the test after 1070 hours the same two plates experienced a linear mass increase of another 0.3mg over the 600,000 g/mol control plate. The rate of increase of the two plates during this linear region is shown in Table 3.6.

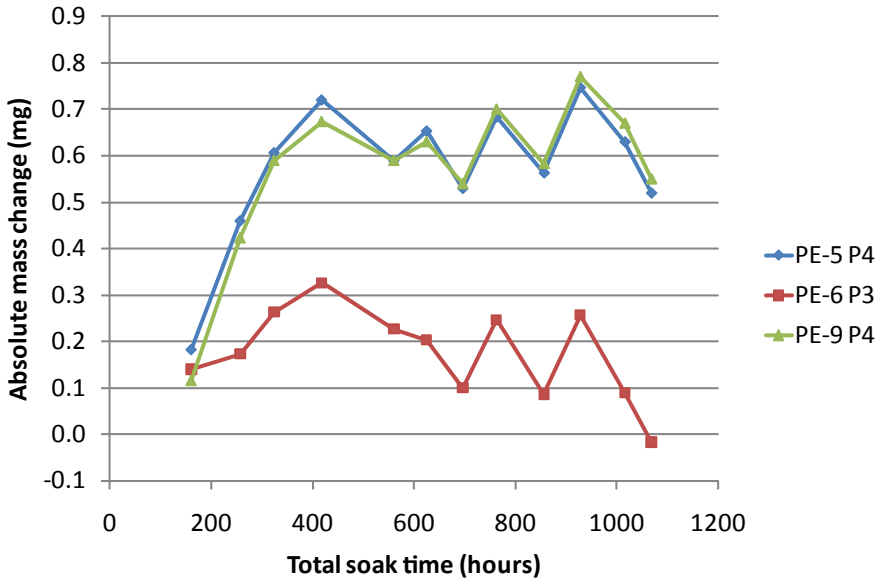

Figure 3.14: Plot showing absolute mass change of the 3 control plates of varying molecular weights. PE-5 refers to the 5,000,000 g/mol control plate, PE-9 refers to the 9,000,000 g/mol plate, and PE-6 refers to the 600,000 g/mol control plate.

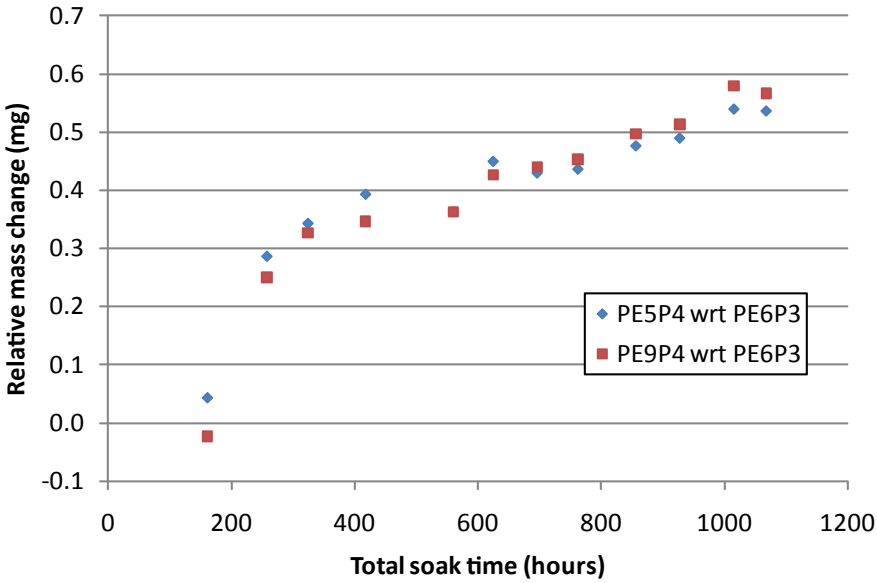

Figure 3.15: Plot showing the differential mass change during soaking of the 5,000,000 g/mol and 9,000,000 g/mol control plates relative to the 600,000 g/mol control plate.

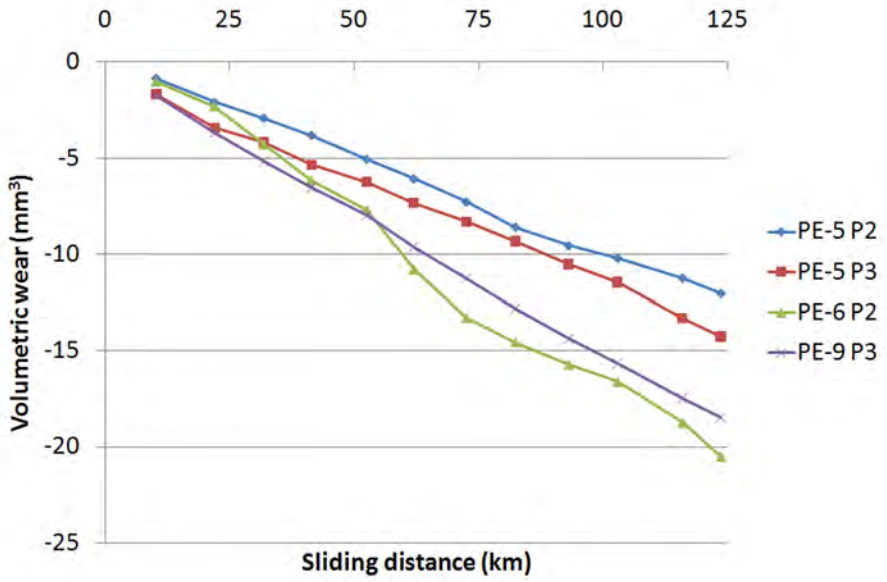

Figure 3.16: Individual volumetric wear plots of UHMWPE plates with differing molecular weights. PE-5 P2 and PE-5 P3 had an average molecular weight of 5,000,000 g/mol. PE-6 P2 had an average molecular weight of 600,000 g/mol. PE-9 P3 had an average molecular weight of 9,000,000 g/mol. The plates were in stations 1,3,2,and 4, respectively on rig 3.

Molecular weight (g/mol)	Plate	Wear Factor (x10^{-6} $mm^3N^{-1}m^{-1}$)	R^2
600,000	2	4.404	0.988
5,000,000	2	2.516	0.996
5,000,000	3	2.668	0.997
9,000,000	3	3.707	0.999

Table 3.7: Wear factors of UHMWPE plates with differing molecular weights

3.2.2.3 Wear Results

The individual volumetric wear plots of the four tested plates can be seen in Figure 3.16. The calculated wear factors are shown in Table 3.7. The UHMWPE plate with a molecular weight of 600,000 g/mol had the highest wear factor of 4.404 x10^{-6} $mm^3N^{-1}m^{-1}$, additionally it showed the greatest non-linearity with a R^2 value of 0.988, however this still indicates a high degree of linearity. The plate with a molecular weight of 9,000,000 g/mol had a wear factor of 3.707 x10^{-6} $mm^3N^{-1}m^{-1}$ and showed the greatest linearity with a R^2 value of 0.999. The lowest wear factor was shown by the two plates with a molecular weight of 5,000,000 g/mol, with wear factors of 2.516x10^{-6} $mm^3N^{-1}m^{-1}$ and 2.668x10^{-6} $mm^3N^{-1}m^{-1}$. Both showed high linearity with R^2 values of 0.996 and 0.997 respectively.

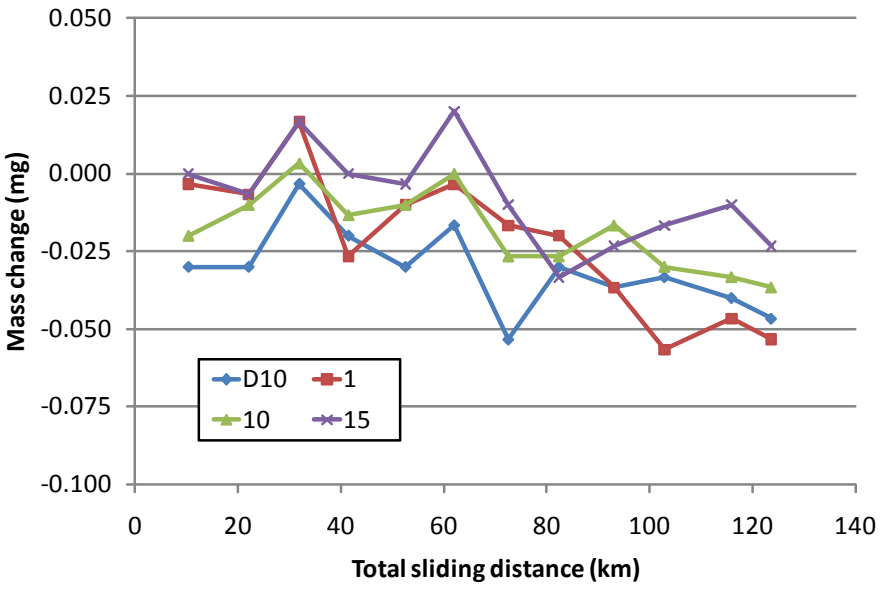

Figure 3.17: Mass change of the four test pins (soak control adjusted).

The mass change of the four pins used in the test is shown in Figure 3.17. A slight mass loss trend over the course of the test is visible for all pins. Although the plot is soak control adjusted, there was no measurable fluid uptake into the stainless steel pin, and the control is really there to account for varying environmental conditions during gravimetric assessment. The total mass loss of pin 1 is approximately 0.05mg. Converting this to a volumetric loss using a density of 7.99g/cm^3 gives a maximum volume loss of 0.00626 mm^3. This is approximately 0.05% of the lowest wearing UHMWPE plate in the test and 0.03% of the highest wearing UHMWPE plate in the test. This is expected as the Rockwell hardness of stainless steel is B79 compared to the UHMWPE which normally falls within the R50-R66 range.

3.2.2.4 Surface Analysis

The surface of the UHMWPE plates was observed prior to the test start and at 0.5 MC intervals thereafter until the conclusion of the test at 3.0 MC. The plates were imaged at 16 locations, both in and on the edge of the wear track. An additional point well away from the wear track was used as a control location. The exact locations are illustrated by numbers 1 - 16 in Figure 3.4. Over 400 optical micrographs were collected, and while it is not practical to present them all, the most interesting are shown in the following section.

Initial observations of the all test plates prior to the test start showed fine scratches in random directions and fine black pitting. There were no observed differences of the surface

between the molecular weights as can be seen in Figure 3.18. At the control location on the plates (location 16 on Figure 3.4) there was no observed changes throughout the whole duration of the test indicating that soaking in lubricant has no visible adverse effects on the plate surface.

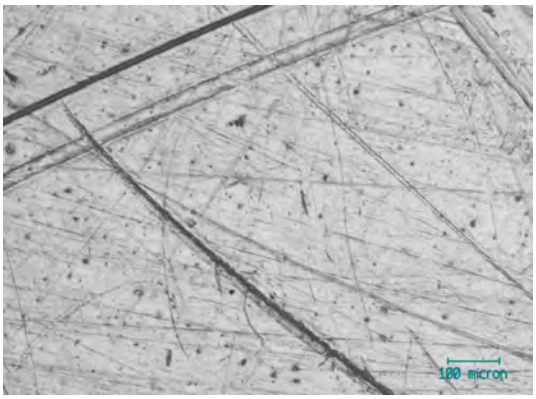

(a) Molecular weight 5,000,000 g/mol - Plate 2.

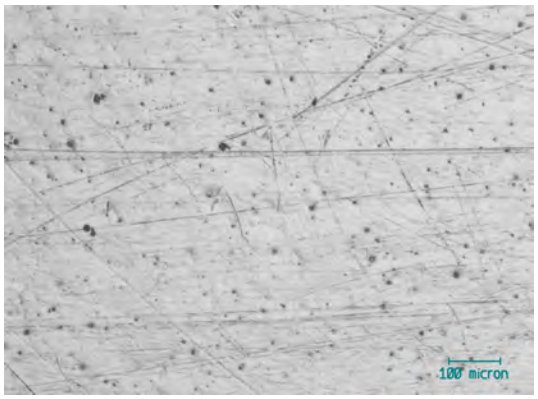

(b) Molecular weight 5,000,000 g/mol - Plate 3.

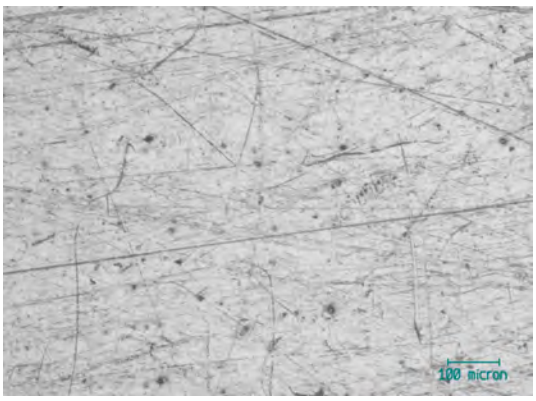

(c) Molecular weight 600,000 g/mol - Plate 2.

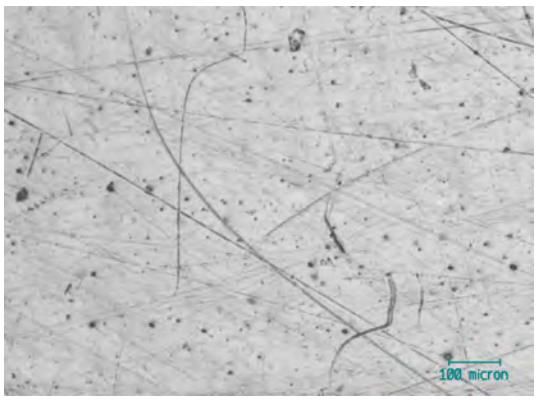

(d) Molecular weight 9,000,000 g/mol - Plate 3.

Figure 3.18: Pre-test optical micrographs of UHMWPE plates of different molecular weights. No differences in the initial surface condition between molecular weights was observed.

Observing the 600,000 g/mol plate at the centre of the wear track (locations 1 - 5) the surface became highly polished with a generally homogeneous appearance as seen in Figure 3.19(a). Light scratching in the translation direction was observed at locations 2-4 as seen in Figure 3.19(d), coinciding with where the translation velocity of the plate was greatest compared to the rotational velocity of the pin. Striking features were observed around the edge of the wear track. Adhesive wear was observed at the centre of the wear track at location 3 as seen in Figure 3.19(f) and more commonly at the ends of the wear track at locations 1 and 5 shown in Figures 3.19(e) and 3.19(c) respectively. Fine rippling, perpendicular to the translation direction was also observed as shown in Figure 3.19(c).

Although this was observed far more frequently at the extreme edges of the wear track as shown later.

The central area of the wear track of the 9,000,000 g/mol sample was far more homogeneous than that of the 600,000 g/mol plate. The majority of the surface at locations 1-5 at all time intervals was similar to Figure 3.20(a) in which a highly burnished surface is visible. Interestingly after 2.0 MC, grain boundaries were visible at location 5 as seen in Figure 3.20(b). Rippling perpendicular to the translation direction was again seen, as shown in Figure 3.20(c). Contrasting dark and light patches were also observed as can be seen in Figure 3.20(d).

Analysis of the first UHMWPE plate with an average molecular weight of 5,000,000 g/mol revealed a mixture of features both previously observed on the plates with higher and lower molecular weights. The most common observed feature was fine rippling in the direction perpendicular to the translation direction, an example of which can be observed in Figure 3.21(a). Grain boundaries were again observed, clearly visible in Figure 3.21(d), and to a lesser extent in Figure 3.21(f). Burnishing was a common feature, as evidenced in Figure 3.21(e). Scratching was observed as seen in Figure 3.21(c), the scratches were in a direction that correlated between the combined rotational and translational direction of contact between the pins and plates. Dark and light linear regions in the same direction were observed in Figure 3.21(b), also in this micrograph, adhesive deposits can be seen surrounded by fine ripples in a direction perpendicular to the translational motion. Figure 3.21 is very interesting in the fact it combines several different surface features in one image. The darkened area covers the majority of the micrograph and features clearly defined ripples in a direction perpendicular to the translation. Grain boundaries are also visible in this darkened area. Below this is a highly burnished area, and below that is a seemingly raised area.

Analysis of the second plate with an average molecular weight of 5,000,000 g/mol confirmed the correlation between darkened areas and the rippling, with all four examples shown in Figure 3.22 showing rippling in the dark areas. Both Figures 3.22(c) and 3.22(d) showed the ripples surround raised areas, indicating they were either the cause of, or the result of adhesive deposits.

Optical micrographs taken around the edge of the wear tracks at locations 6 - 15 showed far more extreme forms of surface changes. For the plate with an average molecular weight

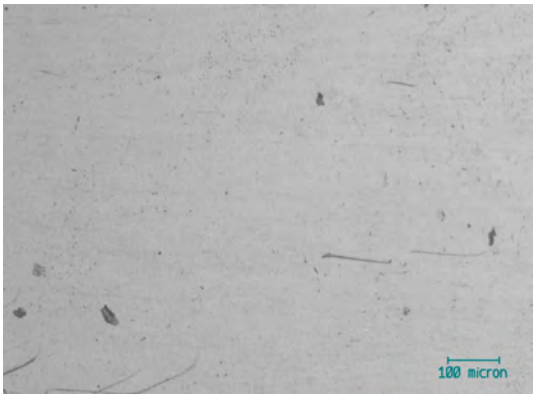

(a) 600,000 g/mol UHMWPE plate at location 2 after 1.0x10^6 cycles. Note the smooth, burnished like appearance.

(b) 600,000 g/mol UHMWPE plate at location 5 after 1.0 MC. Note the smooth burnished appearance with material deposition.

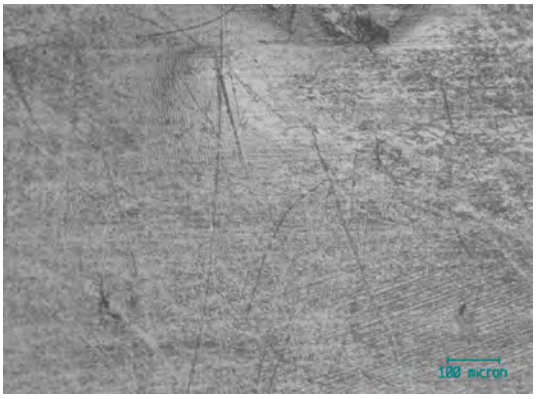

(c) 600,000 g/mol UHMWPE plate at location 5 after 1.5 MC. Note the fine ripples beginning to form in a perpendicular direction to the translation.

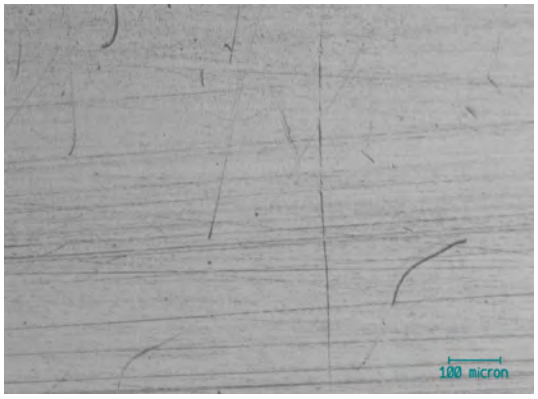

(d) 600,000 g/mol UHMWPE plate at location 4 after 2.0 MC. Note the smooth burnished appearance with fine scratches running in the translation direction.

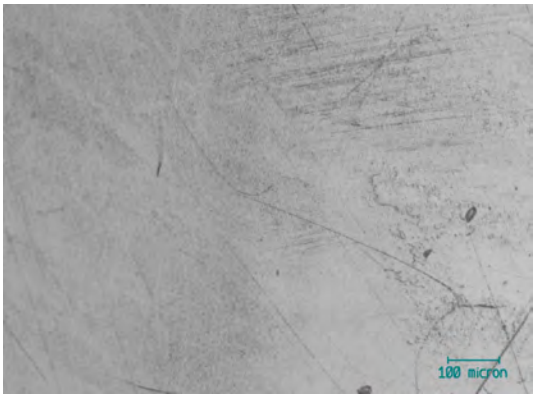

(e) 600,000 g/mol UHMWPE plate at location 1 after 2.5 MC. Note the burnishing with material deposits.

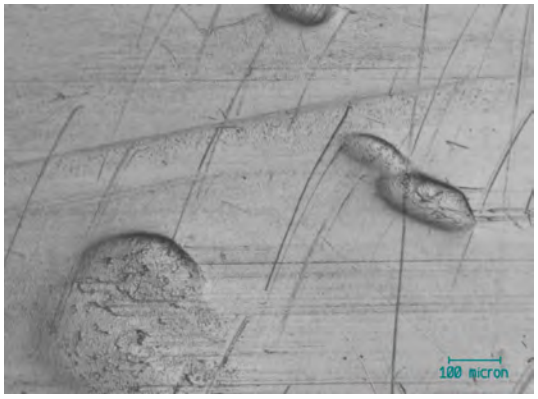

(f) 600,000 g/mol UHMWPE plate at location 3 after 3.0 MC. Note the smooth burnished appearance with larger material deposits.

Figure 3.19: Optical micrographs of the central wear track of the 600,000 g/mol plate at various test durations.

(a) 9,000,000 g/mol UHMWPE plate at location 2 after 0.5 MC. Note the smooth, burnished like appearance.

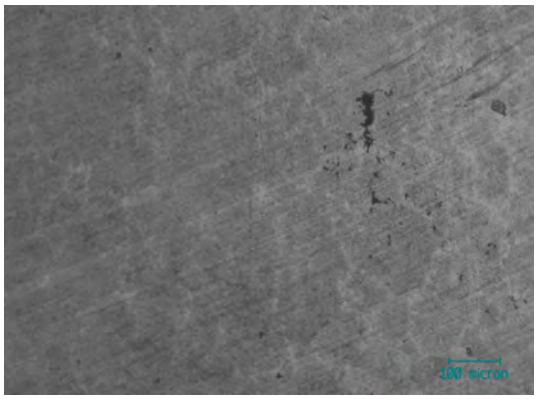

(b) 9,000,000 g/mol UHMWPE plate at location 5 after 2.0 MC. Note the visible grain boundaries.

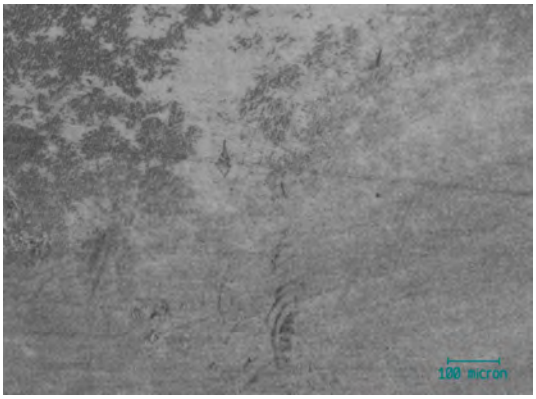

(c) 9,000,000 g/mol UHMWPE plate at location 2 after 2.5 MC. Note the fine ripples beginning to form in a perpendicular direction to the translation.

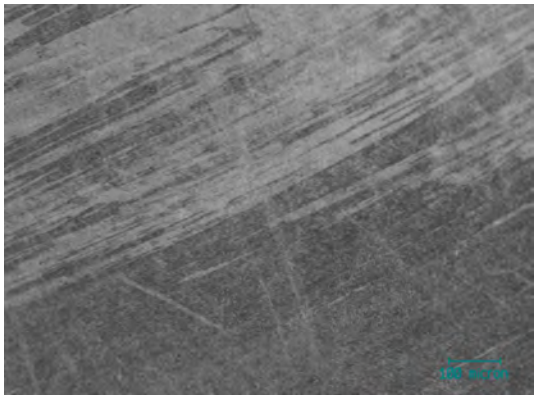

(d) 9,000,000 g/mol UHMWPE plate at location 5 after 3.0 MC. Note the dark and light areas.

Figure 3.20: Optical micrographs of the wear track of the 9,000,000 g/mol plate at various test durations.

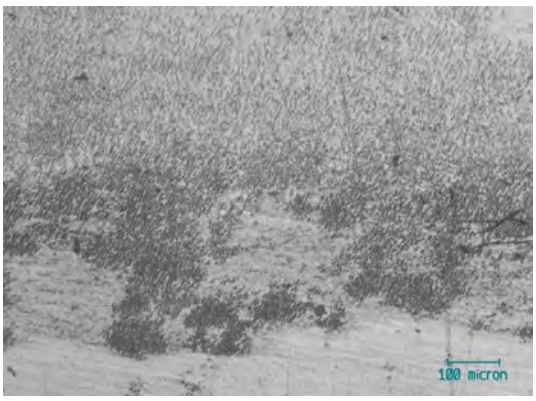

(a) 5,000,000 g/mol UHMWPE plate 2 at location 3 after 0.5 MC. Note the fine rippling.

(b) 5,000,000 g/mol UHMWPE plate 2 at location 5 after 0.5 MC. Note the material deposit and rippling.

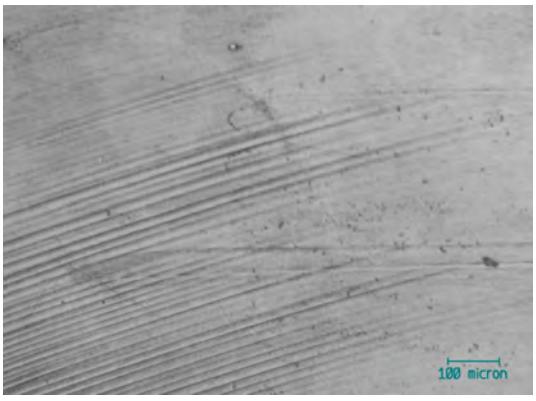

(c) 5,000,000 g/mol UHMWPE plate 2 at location 1 after 1.0 MC. Note the gouges in the rotational direction.

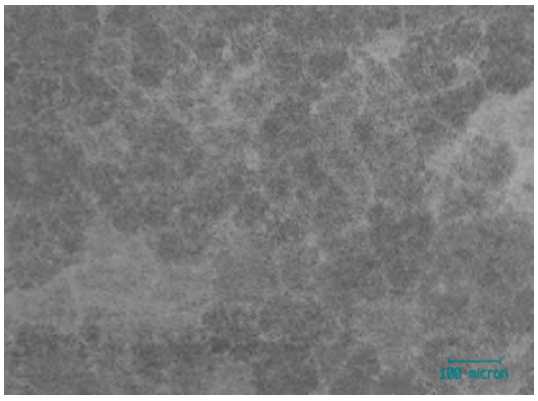

(d) 5,000,000 g/mol UHMWPE plate 2 at location 3 after 1.0 MC. Note the visible grain boundaries.

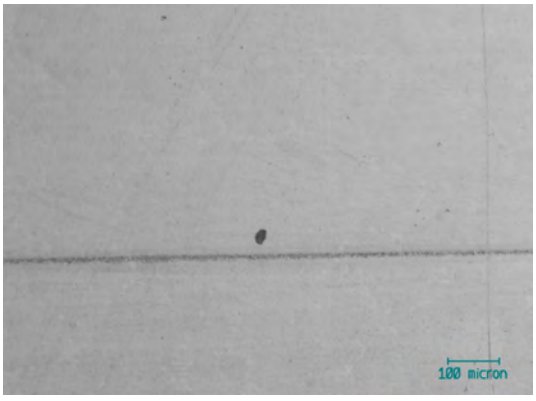

(e) 5,000,000 g/mol UHMWPE plate 2 at location 4 after 1.0 MC. Note the highly burnished surface.

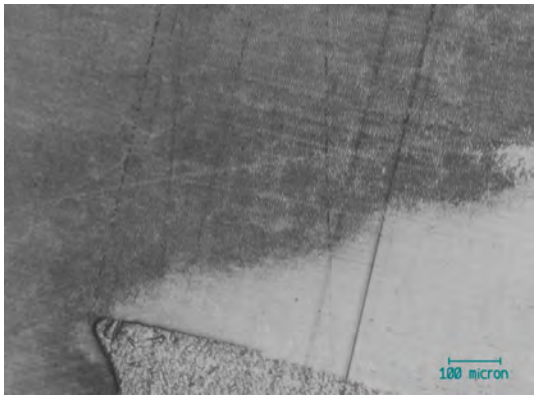

(f) 5,000,000 g/mol UHMWPE plate 2 at location 4 after 3.0 MC. Note the raised areas, fine ripples and burnished areas.

Figure 3.21: Optical micrographs of the wear track of the 5,000,000 g/mol plate 2 at various test durations.

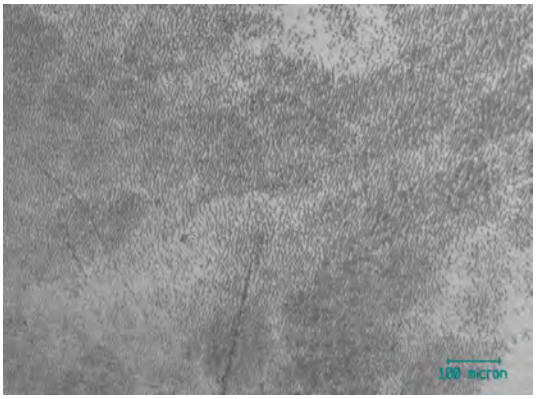

(a) 5,000,000 g/mol UHMWPE plate 3 at location 2 after 0.5 MC. Note the fine rippling covering the whole area.

(b) 5,000,000 g/mol UHMWPE plate 3 at location 3 after 0.5 MC. Note the burnishing with sporadic areas of rippling.

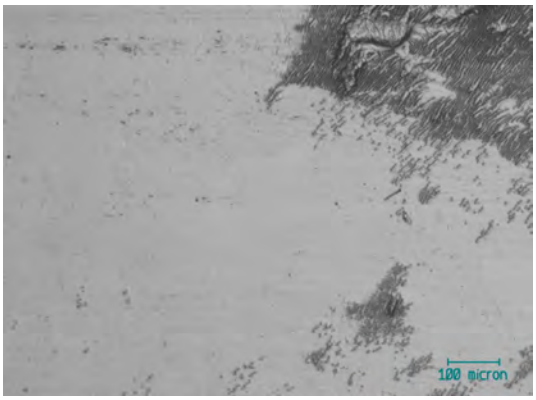

(c) 5,000,000 g/mol UHMWPE plate 3 at location 4 after 1.0 MC. Note the burnishing ripples and material deposits.

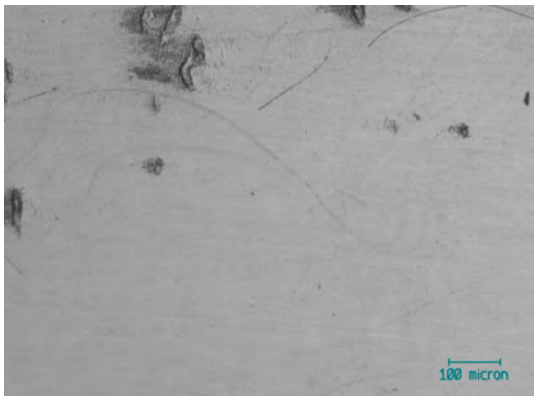

(d) 5,000,000 g/mol UHMWPE plate 3 at location 4 after 2.0 MC. Note the material deposits and ripples.

Figure 3.22: Optical micrographs of the wear track of the 5,000,000 g/mol plate 3 at various test durations.

of 600,000 g/mol. Adhesive material deposits were a common feature and were observed mainly at the ends of the wear track as evidenced in Figures 3.23(a) and 3.23(c), although some raised areas were observed in the mid region as seen in Figure 3.23(f). A common feature of the three previously mentioned images is that the raised areas seem to occur in a smooth burnished region, and that small ripples can be observed in the immediate vicinity around the raised areas. Other highly burnished areas were observed as evidenced in Figure 3.23(e), although these were less common at the edge of the wear scar than they were in the centre. Figures 3.23(b) and 3.23(d) show ripples observed close to the edges of the wear track. The angle of the ripples seems to coincide with the clockwise rotation of the SS pin.

Optical micrographs of the edge of the wear track of the plate with a molecular weight of 9,000,000 g/mol can be seen in Figure 3.24. Compared to the centre of the wear track, there was much less burnishing, with fine ripples that give a dark appearance visible in all figures except for Figure 3.24(e). Figures 3.24(a) and 3.24(b) show the exact same location on the plate after 0.5 MC and 1.0 MC respectively. It is interesting to note that the fine ripples observed at 0.5 MC develop into larger, more defined ridges at 1.0 MC. Figures 3.24(c) and 3.24(f) show the increasing size of the ripples from the centre to the edge of the plate. Adhesive wear deposits were observed, although very sporadically and are evidenced by Figure 3.24(d). The opposite location on the plate (Figure 3.24(e)) had a homogeneous appearance.

Analysis of the 5,000,000 g/mol plate 2 at the edge of the wear track is shown in Figure 3.25. Microcracks on the surface were observed as early as 0.5 MC as evidenced by Figure 3.25(a). There was also evidence of deposited material. Figure 3.25(b) shows both rippling and burnishing occurring in the same slide area. The burnished area seems to be protected from damage, or rippling by the praised material. Rippling was highly prevalent on the 5,000,000 g/mol plate. Both fine ripples and larger ripples were observed in the same location as evidenced by Figure 3.25(c) with the larger ripples towards the wear track edge and the finer ripples occurring alongside burnishing more centrally in the wear track. A similar picture is apparent in Figure 3.25(d) with larger ripples occurring towards he wear scar edge and burnishing with very faint grain boundaries visible more centrally. At the ends of the wear track in location 6 a burnished area with darkened ripples is visible as seen in Figure 3.25(e). Additionally, faint scratches are visible in a criss-cross direction that coincides with the rotation of the pin. Finally, figure 3.25(f) shows the darkened ripples and

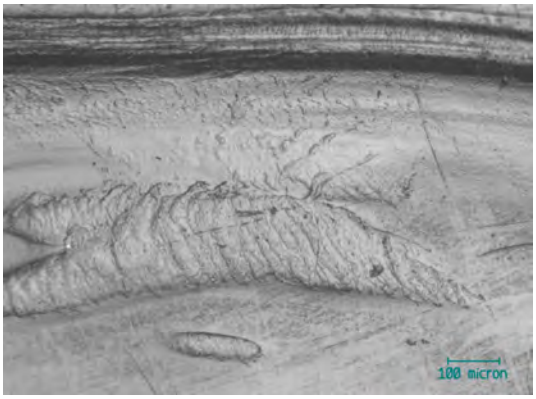

(a) 600,000 g/mol UHMWPE plate 2 at location 10 after $0.5x10^6$ cycles. Note the buildup of material at the ends of the wear track.

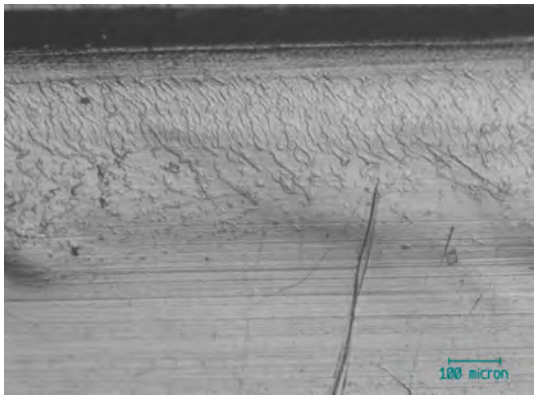

(b) 600,000 g/mol UHMWPE plate 2 at location 9 after $1.0x10^6$ cycles. Note the large cracks perpendicular to the translation direction at the edge of the wear track.

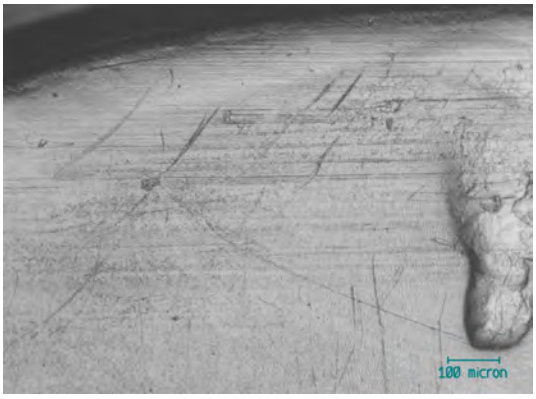

(c) 600,000 g/mol UHMWPE plate 2 at location 6 after $1.5x10^6$ cycles. Note the material deposits surrounded by fine ripples.

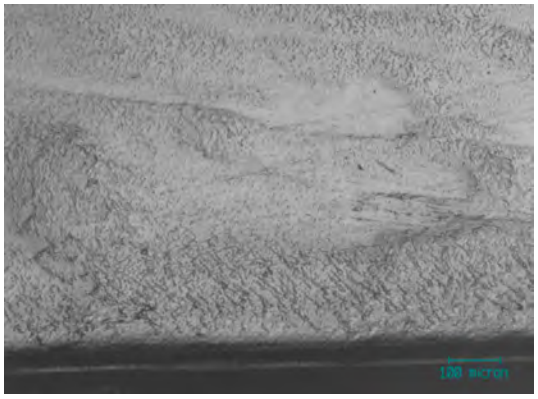

(d) 600,000 g/mol UHMWPE plate 2 at location 12 after $2.0x10^6$ cycles. Note the microcracks across the full slide.

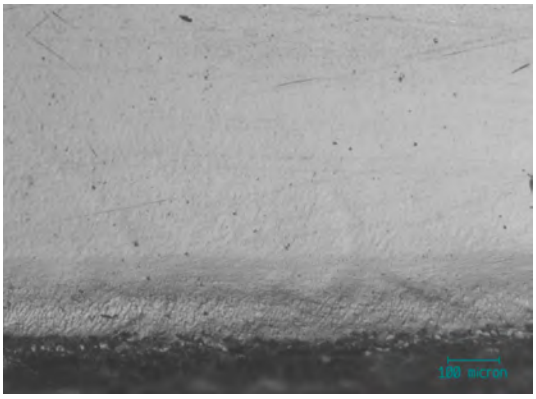

(e) 600,000 g/mol UHMWPE plate 2 at location 14 after $2.5x10^6$ cycles. Note the smooth burnished surface with small ripples at the edge.

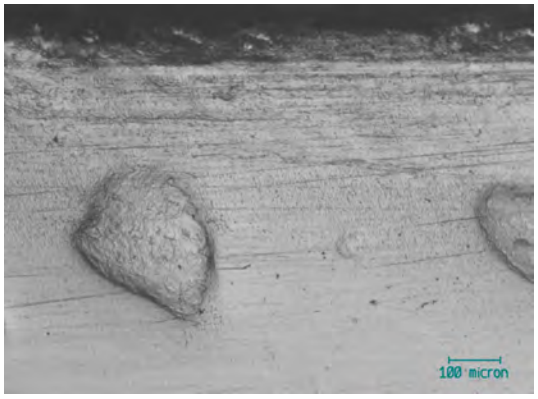

(f) 600,000 g/mol UHMWPE plate 2 at location 9 after $3.0x10^6$ cycles. Note the large adhesive deposits.

Figure 3.23: Optical micrographs of the edge of the wear track of the 600,000 g/mol plate 2 at various test durations.

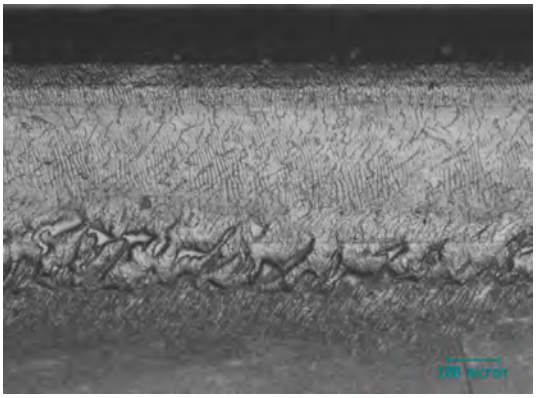

(a) 9,000,000 g/mol UHMWPE plate 3 at location 9 after $0.5x10^6$ cycles. Note the raised area with ripples.

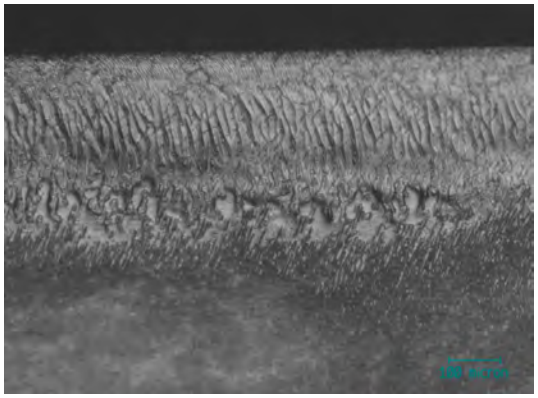

(b) 9,000,000 g/mol UHMWPE plate 3 at location 9 after $1.0x10^6$ cycles. Note that the small ripples have now developed into larger ones.

(c) 9,000,000 g/mol UHMWPE plate 3 at location 13 after $1.5x10^6$ cycles. Note the fine ripples and the larger ones towards the edge.

(d) 9,000,000 g/mol UHMWPE plate 3 at location 6 after $2.0x10^6$ cycles. Note the material deposit at the wear track end.

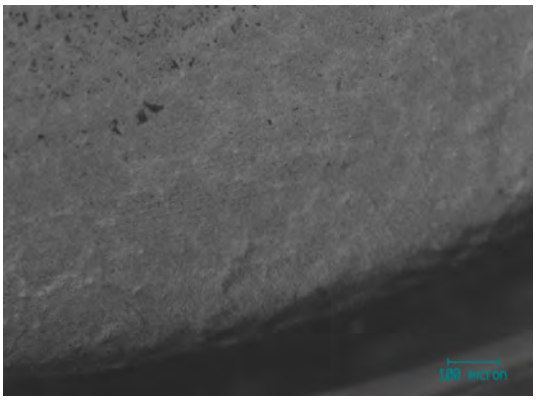

(e) 9,000,000 g/mol UHMWPE plate 3 at location 15 after $2.5x10^6$ cycles. Note the burnished area at the location opposite to the previous subfigure.

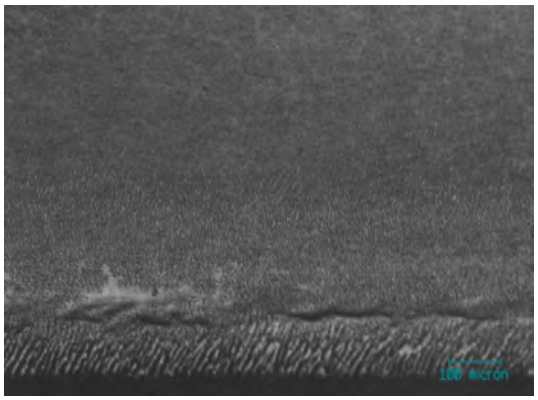

(f) 9,000,000 g/mol UHMWPE plate 3 at location 14 after $3.0x10^6$ cycles. Note the fine ripples getting larger towards the edge.

Figure 3.24: Optical micrographs of the edge of the wear track of the 9,000,000 g/mol plate 3 at various test durations.

Molecular Weight	Wear track location	
	Edge	Centre
600,000 g/mol	Adhesive deposits	Adhesive deposits
	Burnishing	Burnishing
	Fine rippling	Fine rippling
	Translational scratching	Translational scratching
5,000,000 g/mol	Adhesive deposits	Adhesive deposits
	Burnishing	Burnishing
	Grain boundaries	Grain boundaries
	Larger rippling	Fine rippling
	Micro cracking	Dark and light areas
9,000,000 g/mol	Adhesive deposits	Grain boundaries
	Larger rippling	Fine rippling
	Fine rippling	Burnishing
		Dark and light areas

Table 3.8: Summary table categorising the types of wear observed on the UHMWPE plates with differing molecular weights

clear grain boundaries.

Analysis of the second plate with a molecular weight of 5,000,000 g/mol showed some more interesting effects. Burnishing, leading to fine ripples and deposited material was seen in Figure 3.26(b). Large cracks perpendicular to the translation direction were observed at at location 12, as seen in Figure 3.26(b), within $5x10^5$ cycles at the same location these had mostly been removed, and due to this the burnished area towards the top of the image was now in contact with the pin surface and had started to wear. The image shown in Figure 3.26(d) is interesting as these do not appear to be cracks, more adhered material, brought towards the centre of the wear track by the pin rotation.

A summary of all these observed types of wear can be seen in Table 3.8.

Morphologic analysis of the plate surfaces was carried out at the conclusion of the test. The control plates were also analysed to allow a comparison of the pre wear and post wear conditions. All readings were taken at locations 1 - 5 on Figure 3.4. A comparison of the surface roughness at each imaging location is shown in Figure 3.27. There is little difference

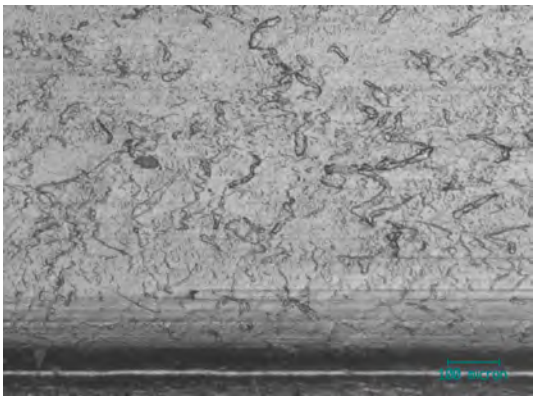

(a) 5,000,000 g/mol UHMWPE plate 2 at location 12 after 0.5x10^6 cycles. Note the microcracks and deposited material.

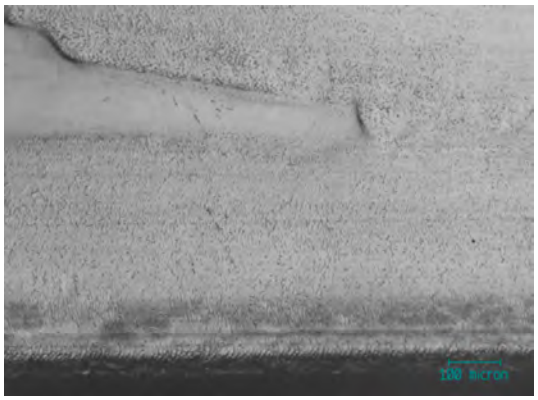

(b) 5,000,000 g/mol UHMWPE plate 2 at location 13 after 1.0x10^6 cycles. Note the rippled area and burnished area.

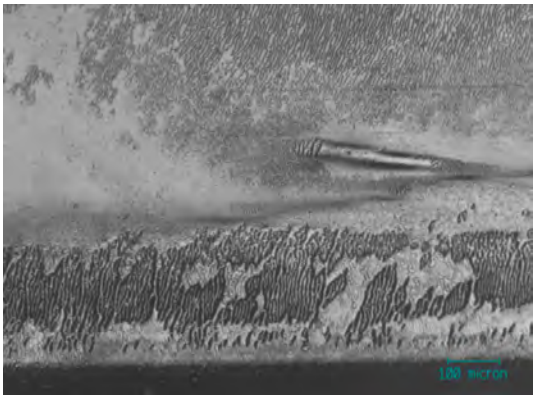

(c) 5,000,000 g/mol UHMWPE plate 2 at location 13 after 1.5x10^6 cycles. Note the burnishing, fine ripples, and larger ripples.

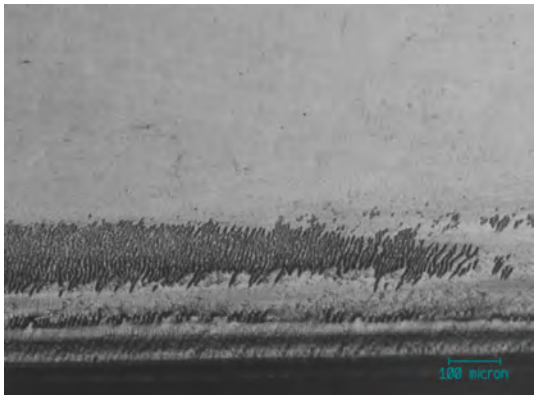

(d) 5,000,000 g/mol UHMWPE plate 2 at location 14 after 2.0x10^6 cycles. Note the burnishing and the darker ripples towards the edge.

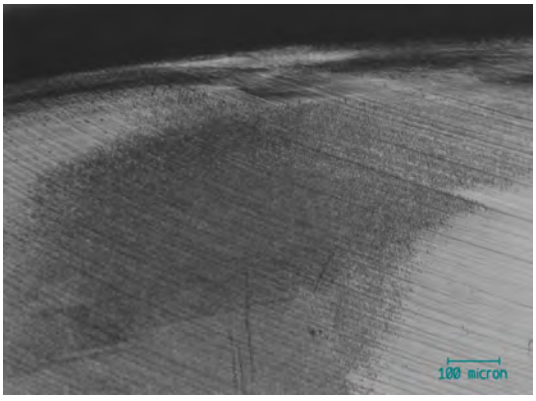

(e) 5,000,000 g/mol UHMWPE plate 2 at location 6 after 2.5x10^6 cycles. Note the fine ripples and directional scratching.

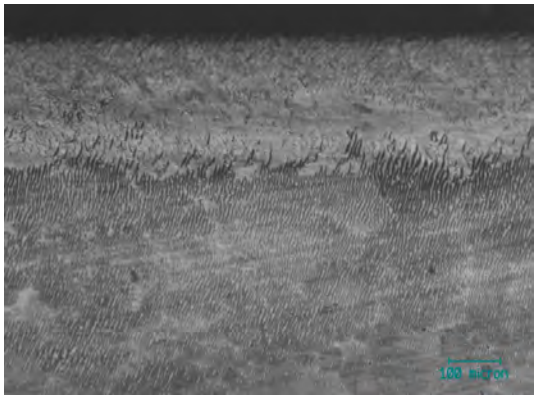

(f) 5,000,000 g/mol UHMWPE plate 2 at location 8 after 3.0x10^6 cycles. Note the fine dark ripples and grain boundaries that are visible.

Figure 3.25: Optical micrographs of the edge of the wear track of the 5,000,000 g/mol plate 2 at various test durations.

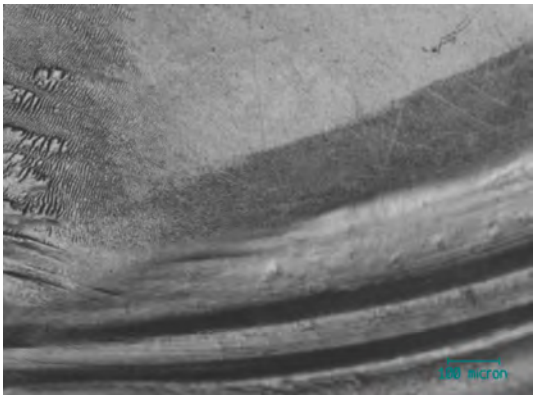

(a) 5,000,000 g/mol UHMWPE plate 3 at location 15 after $0.5x10^6$ cycles. Note the burnishing leading into ripples and deposited material.

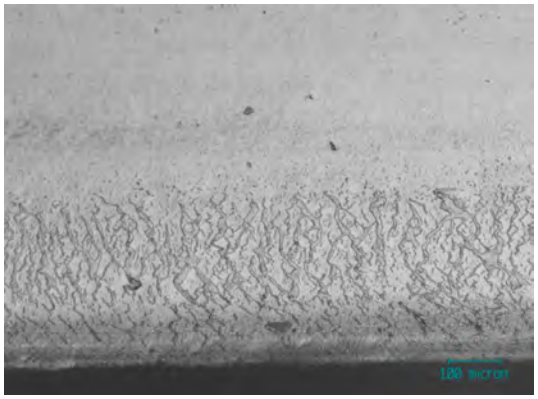

(b) 5,000,000 g/mol UHMWPE plate 3 at location 12 after $1.5x10^6$ cycles. Note the burnishing and cracking at the edge.

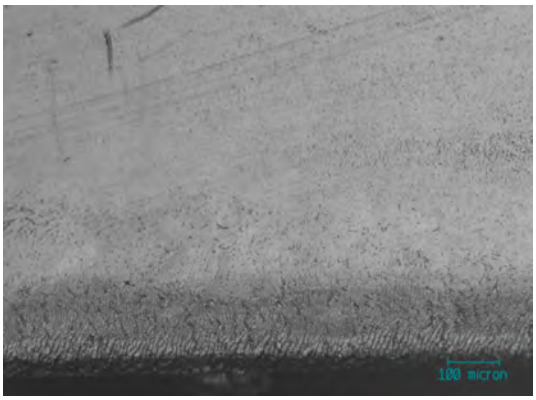

(c) 5,000,000 g/mol UHMWPE plate 3 at location 12 after $2.0x10^6$ cycles. Note the burnishing and darker cracks.

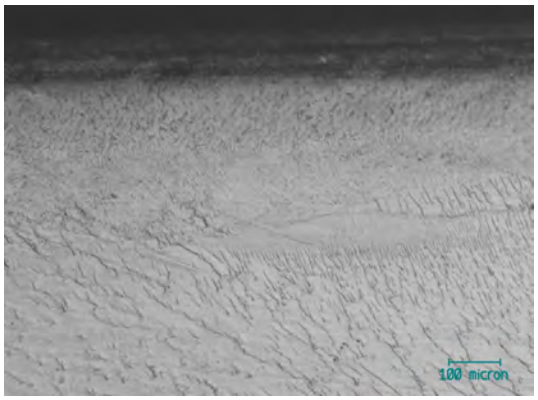

(d) 5,000,000 g/mol UHMWPE plate 3 at location 9 after $2.5x10^6$ cycles. Note the material drawn down into the wear track due to pin rotation.

Figure 3.26: Optical micrographs of the edge of the wear track of the 5,000,000 g/mol plate 3 at various test durations.

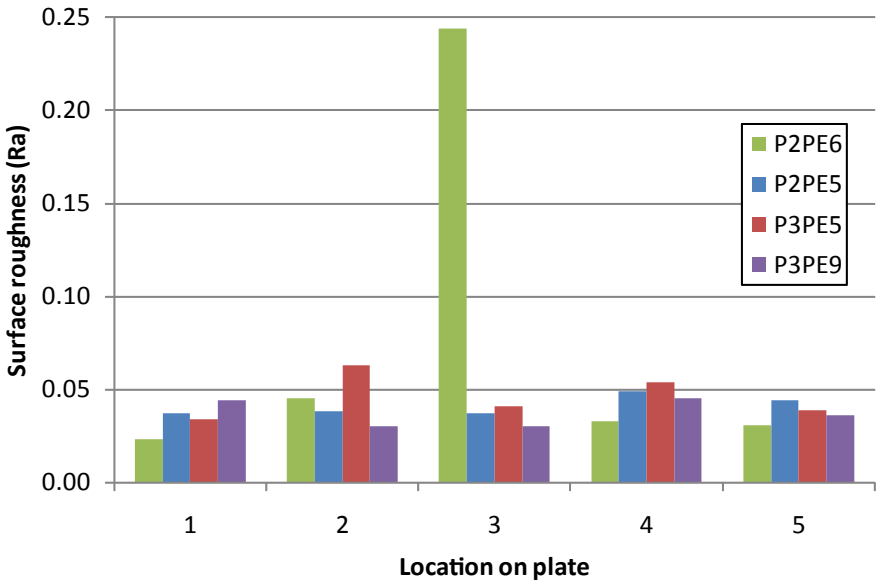

Figure 3.27: Plot comparing the R_a of each test plate at the 5 recorded locations at the conclusion of the test after 3.0 MC.

between each plate except for the 600,000 g/mol plate at location 3 in the exact centre of the wear track which had a far higher R_a value of 0.244μm when compared to all locations on all plates. This is attributed to a large gouge which can be seen in the scan shown in Figure 3.29(a). No significant difference in the R_a at different plate locations was observed. The centre of the wear track was significantly smoother than the surface at the test start. Figure 3.28 shows a comparison of mean R_a of the 4 test plates and the 3 control plates. Taking the mean of all 5 locations the R_a of the test plates was 0.050$\pm$0.04μm compared to the mean R_a of the 3 control plates which was 0.139$\pm$0.037μm, a 64% reduction in surface roughness, excluding the recorded gouge the average R_a drops to 0.039$\pm$0.009μm, a 71% reduction in surface roughness.

Zygo analysis revealed topographical data that was ambiguous when viewed with just the optical microscope. Figure 3.29(b) confirms that the material observed in figure 3.19(f) is indeed raised above the burnished surface. Figures 3.29(d) and 3.29(f) show clear evidence of raised grains in the 9,000,000 g/mol and 5,000,000 g/mol plates respectively. No evidence of this was observed in the 600,000 g/mol plate. The R_a of the surface seen in figure 3.29(d) is 0.030μm and is visibly smoother than the original starting roughness of approximately 0.130μm shown in Figure 3.29(c). The ripples observed in many of the optical images were found to be raised above the burnished surface as evidenced in Figure 3.29(e).

The change in surface roughness (R_a) of the four test pins over the duration of the

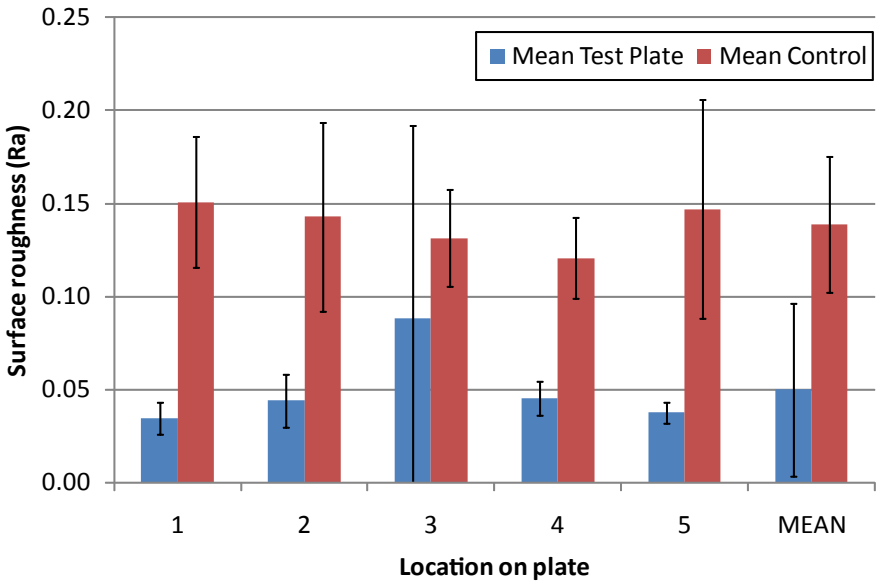

Figure 3.28: Comparison of R_a of the 4 test plates to the 3 control plates. Error bars are ± 1SD.

test can be seen in Figure 3.30. Analysis of the pin surface prior to testing using both the Zygo and optical microscope showed aa highly polished surface with an average R_a of 0.013±0.001μm. All 4 pins experienced a roughening of the surface, both after 0.5MC and upon conclusion of the test at 3.0MC where the mean surface roughness had risen to 0.018±0.010μm.

Optical analysis of the pins was carried out prior to testing and at intervals during testing. Location numbers in the captions relate to the locations shown in Figure 3.3. After polishing, all pins exhibited a similar appearance to that shown in Figure 3.31(a). Faint multi-directional scratches were visible and faint black pits were also observed. The R_a of this type of surface was typically less than 0.015μm as seen in Figure 3.32(a). Circumferential scratching was also observed, as seen in Figure 3.31(b). This was found to increase the surface roughness to around 0.020μm as evidenced by the Zygo scan in Figure 3.32(c). The most common feature observed was deeper multidirectional scratching on an otherwise still polished surface as seen in Figure 3.31(e). This scratching was also found to increase the roughness of the surface to around 0.020μm as evidenced by Figure 3.32(b). The pitting first observed during polishing became more severe during the test and was observed on all pins. Typical examples of this can be observed in Figures 3.31(b) and 3.31(c). The holes are confirmed as being below the bulk surface by the Zygo scan in Figure 3.32(d). This feature also increased the measured surface roughness to 0.023μm. In some areas such as those

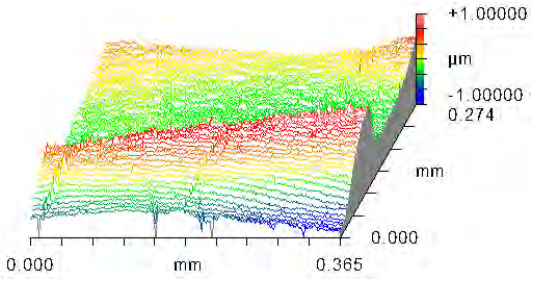

(a) 3D Zygo scan of 600,000 g/mol at location 3 after 3.0 MC with a R_a value of 0.244 μm.

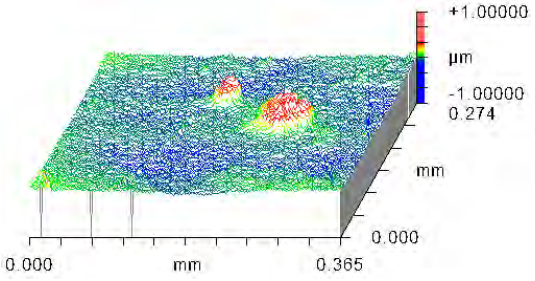

(b) 3D Zygo scan of 600,000 g/mol plate at location 2 after 3.0 MC with an R_a of 0.045 μm. Note here the raised areas of material.

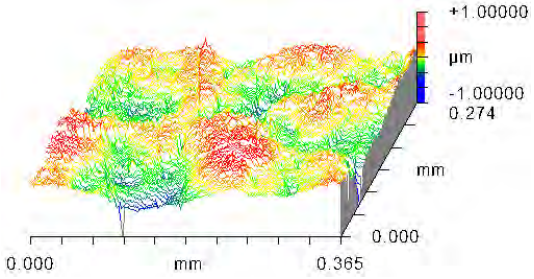

(c) 3D Zygo scan of the 5,000,000 g/mol control plate at location 2, with an R_a of 0.130 μm this is a typical example of the surface of DCM UHMWPE.

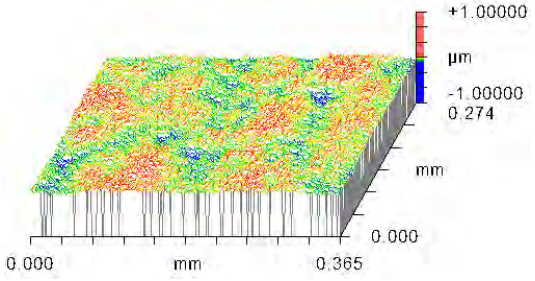

(d) 3D Zygo scan of the 9,000,000 g/mol plate at location 3, with an R_a 0.030 μm. The grain boundaries are clearly visible and exist at a lower level than the grains themselves.

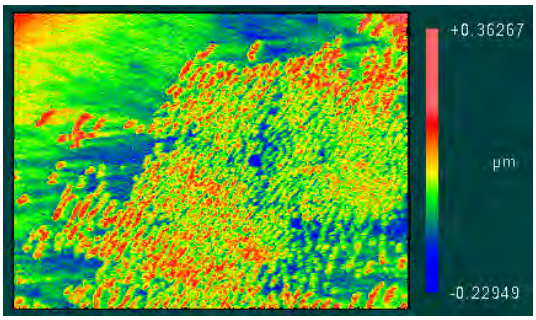

(e) 2D Zygo scan of the 5,000,000 g/mol plate 3 at location 4, with an R_a of 0.054 μm the ripples can clearly be seen to be raised above the burnished surface.

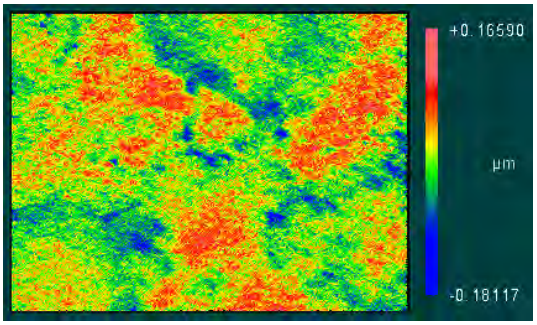

(f) 2D Zygo scan of the 5,000,000 g/mol plate 3 at location 1, with an R_a 0.034 μm. The grain boundaries are clearly visible and exist at a lower level than the grains themselves.

Figure 3.29: Zygo scans of UHMWPE plates of varying molecular weights.

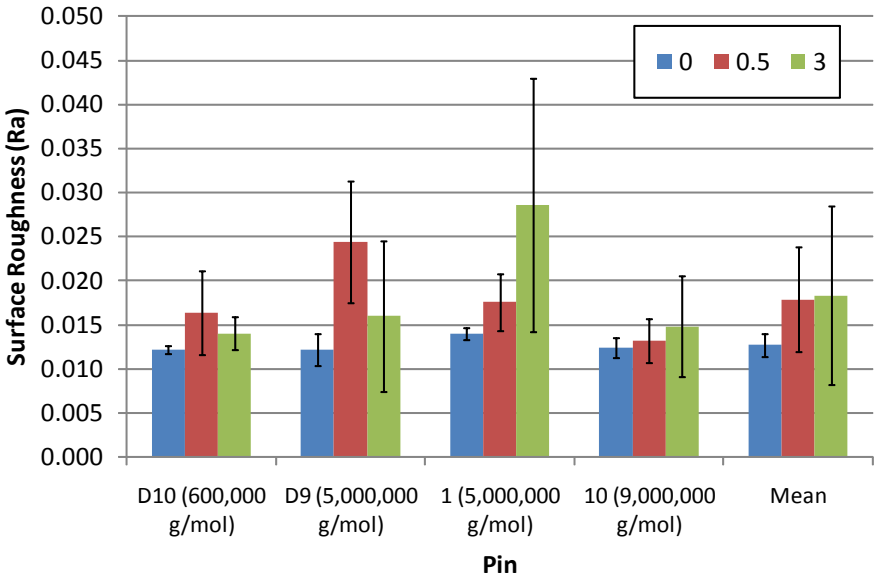

Figure 3.30: Surface roughness of the stainless steel pins throughout the wear test. Numbers in legend are cumulative test duration (MC).

shown in Figures 3.31(c) and 3.32, pitting and scratching occurred in the same location. This raised the surface roughness to a peak measured value of approximately 0.050μm.

3.3 Effect of varying processing conditions

In these pin-on-plate tests the effect of processing conditions on the wear performance of UHMWPE was investigated. Initially two tests of 8 plates were conducted under the standard conditions described previously. A subsequent test using scratched counterface pins was also conducted.

3.3.1 Materials & Methods

Four different processing conditions were tested. All plates were compression moulded and the heat cycle temperature and sintering time that were varied. The four different conditions are outlined in table 3.9.

A total of 16 wear plates and 2 control plates were used for this test. Control plates of the same processing condition as the test plates were not available, instead the two control plates were processed at 150°C and 175°C.

For test 1, the 8 test plates and the two control plates were initially soaked for a total of 21.7 days in the test lubricant in order to equalise the fluid content.

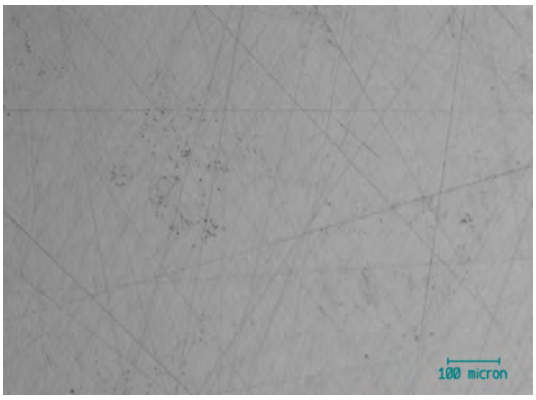

(a) Optical micrograph of Pin 1 prior to test start and post polishing. Note the fine scratches in random directions due to polishing and the slight black pitting.

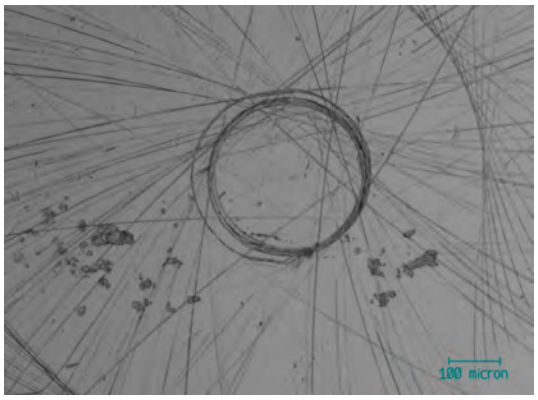

(b) Optical micrograph of pin D9 after 0.5 MC. Note the combination of circumferential and radial scratches.

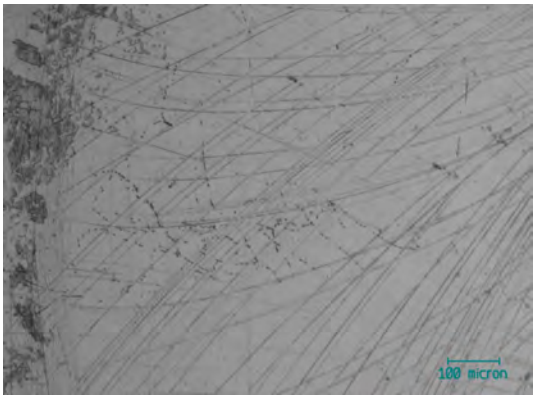

(c) Optical micrograph of pin 1 at location 3 after 1.00 MC. Note the circumferential scratches and the darkened areas that seem to coincide with the scratching.

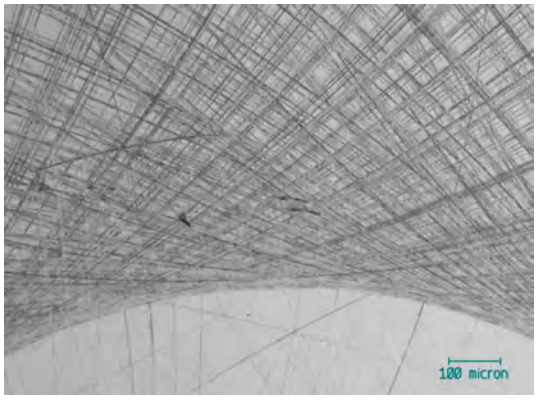

(d) Optical micrograph of Pin 1 at location 4 after 3.00 MC. Note the dense radial scratches.

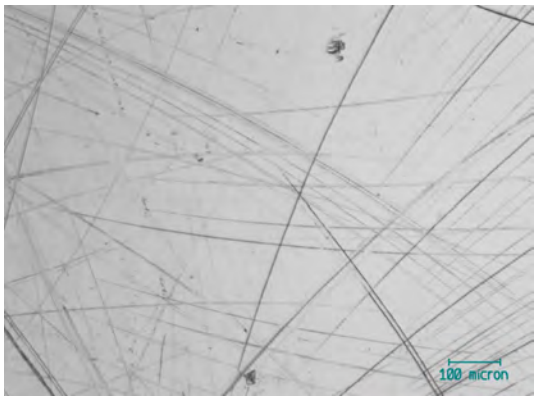

(e) Optical micrograph of pin 10 at location 2 after 3.00 MC. This surface was typical of all the test pins at this stage in the testing.

Figure 3.31: Optical micrographs of the stainless steel pin surfaces, both prior to testing and after various test durations.

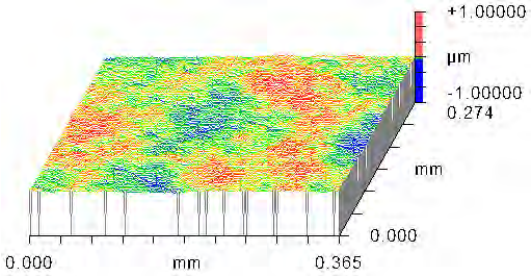

(a) Zygo scan of the surface of pin 1 at location 5 prior to testing and post polishing. This surface had an R_a of 0.014μm.

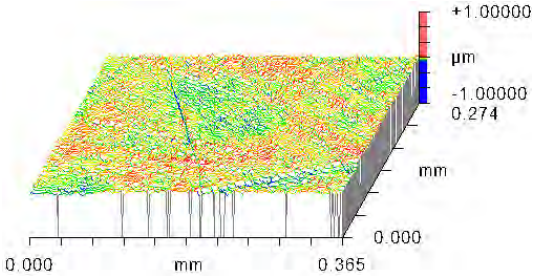

(b) Zygo scan of Pin1 at location 4 after 0.5 MC. Scratches are visible, this surface has an R_a of 0.022μm.

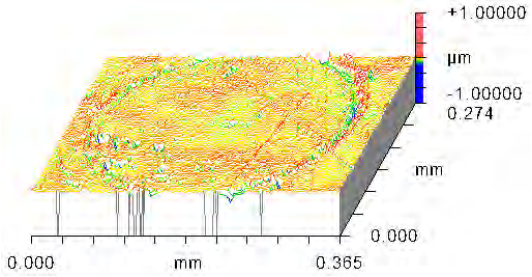

(c) Zygo scan of pin D9 at location 1 after 0.5 MC. This shows circumferential scratching and an R_a of 0.021μm.

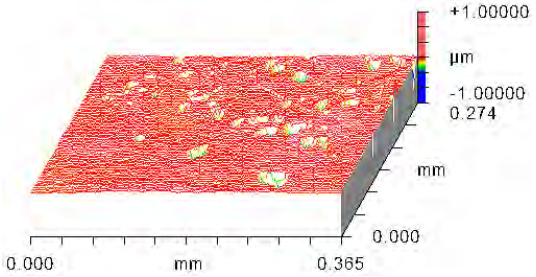

(d) Zygo scan of Pin D10 at location 4 after 0.5 MC showing holes in the surface caused by corrosion. The R_a is 0.023μm.

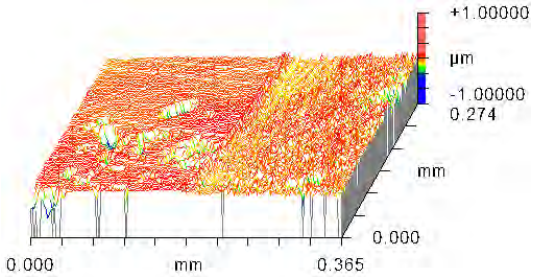

(e) Zygo scan of pin 1 at location 3 after 3.0 MC. Note the holes and circumferential scratches. The R_a is 0.053μm.

Figure 3.32: Zygo scans of the stainless steel pin surfaces prior to testing and after various test durations.

Condition	Max. mould temp. (°C)	Heat cycle dwell time (mins)
1	145	30
2	155	30
3	165	15
4	195	15

Table 3.9: Processing conditions of test samples.

Rig	Station	Test 1				Test 2			
		Temp	Time	Plate	Pin	Temp	Time	Plate	Pin
1	1	155°C	30min	A1	B1	195°C	15min	D8	D8
	2	155°C	30min	A2	B2	195°C	15min	D7	D7
	3	145°C	30min	A3	B3	165°C	15min	D6	D6
	4	145°C	30min	A4	B4	165°C	15min	D5	D5
2	1	165°C	15min	A5	B5	145°C	30min	D4	D4
	2	165°C	15min	A6	B6	145°C	30min	D3	D3
	3	195°C	15min	A7	B7	155°C	30min	D2	D2
	4	195°C	15min	A8	B8	155°C	30min	D1	D1

Table 3.10: Locations of test samples.

Two multi-directional pin on plate rigs were used, and four plates used in each. Upon completion of the first 3.0x10^6 cycle test, a new set of plates was used but the locations swapped so that any rig dependent factors were removed.

In test 1, the UHMWPE plates were examined on the optical microscope pre-testing, then at 2.5x10^5 cycle intervals up to 1.5x10^6 cycles, then at 5.0x10^5 cycle intervals up to the conclusion of the test at 3.0x10^6 cycles. The stainless steel pins were examined on the optical microscope pre-testing, then at 2.5x10^5 cycle intervals up to 1.25x10^6 cycles, and again at the conclusion of the test at 3.0x10^6 cycles. 16 specific locations on each plate were chosen for imaging as shown on Figure 3.4.

In the second test the optical image locations were the same as previously. The plates were examined pre-testing then at 5.0x10^5 cycle intervals up to the conclusion of the test at 3.0x10^6 cycles.

The location of the test samples during both tests is outlined in Table 3.10.

3.3.2 Results

The results from both tests 1 and 2 are presented in this section. Fluid uptake of the control plates is shown, as is the wear of both the pins and plates, and also the surface changes occurring on both the pin and plate samples.

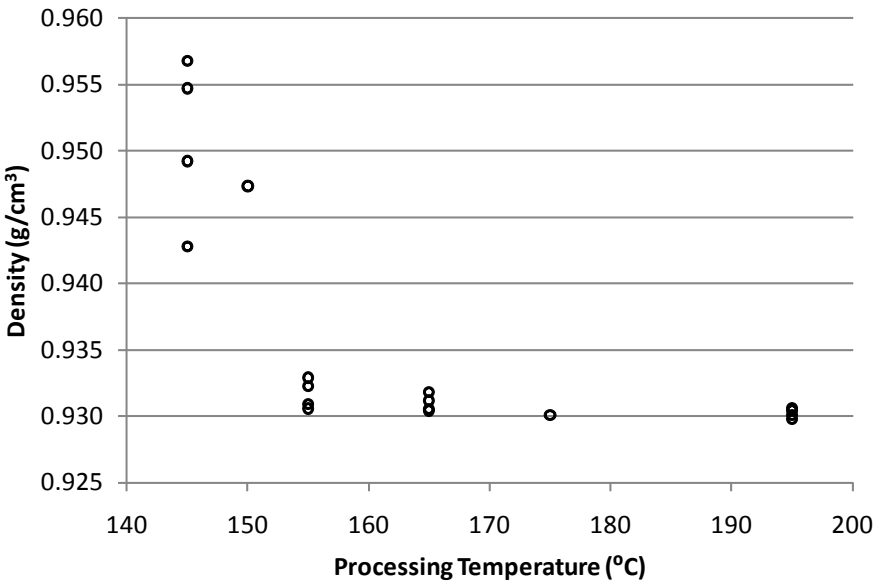

Figure 3.33: Variation in plate density with respect to processing temperature. All 16 test plates and 2 control plates are included in this plot.

3.3.2.1 Density

In order to calculate the volumetric wear rate and hence, wear factor, the density of each plate was required. The density of the plates were found to relate to the processing temperature as can be seen in figure 3.33, with density decreasing as processing temperature increased.

3.3.2.2 Fluid uptake

Similar to previous tests, a set of control plates were used to account for fluid uptake into the UHMWPE test plates. Due to limited plates available, the two plates used were of the same type and molecular weight as the test plates, but had slightly different manufacturing temperatures.

The mass change of the two control plates is shown in figure 3.34. In both tests there was minimal difference in the fluid uptake between the the two plates. However, there was a noticeable difference between the two tests, attributed to different environmental conditions at weighing.

3.3.2.3 Wear

The volumetric wear of the 4 samples in the first test run on rig 1 can be seen in figure 3.35 and the wear of the 4 samples in the first test run on rig 2 can be seen in figure 3.36. The

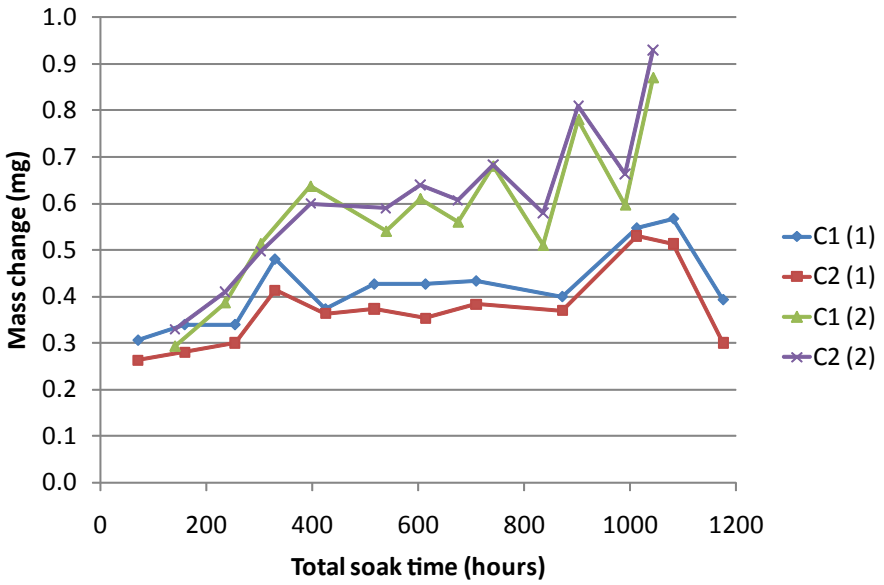

Figure 3.34: Mass change due to lubricant uptake of the two control plates during test 1 and test 2.

mean plots ± the SD are shown in Figure 3.37. All four processing conditions experienced a linear mass loss with the wear of the two plates moulded at 145°C being the greatest. It is also interesting to note that the SD of these two plates was larger than that of the other conditions. Using a least squares linear regression, the wear factor of the 145°C condition was calculated as 4.738±0.532 x10^{-6} $mm^3N^{-1}m^{-1}$. Observing the other three conditions (155°C, 165°C, and 195°C) they are all tightly grouped with wear factors of 2.545±0.245 x10^{-6} $mm^3N^{-1}m^{-1}$, 3.316±0.185 x10^{-6} $mm^3N^{-1}m^{-1}$, and 2.733±0.336 x10^{-6} $mm^3N^{-1}m^{-1}$ respectively. Gravimetric analysis of the eight SS test pins, seen in Figure 3.38 revealed no significant mass loss, although higher wear on the pins paired with the 195°C plates is a possibility.

The gravimetric results from the two rigs used in the second test are shown in Figures 3.39 and 3.40. Many similar trends to the first test were revealed. The mean data for each condition ± the standard deviation is shown in Figure 3.41. It should be noted that the position of the plates was reversed from the first test, such that if a condition was in rig 2 for test 1, in this second test it would be on rig 1. Again the 145°C degree plates are clearly the worst performers in terms of wear, with a wear factor of 3.986±0.109 x10^{-6} $mm^3N^{-1}m^{-1}$. It should be noted that variation between the two plates in this test was minimal, indicated by the low standard deviation. The wear properties of the remaining moulding temperatures increased with temperature with the plates moulded at 155°C, 165°C

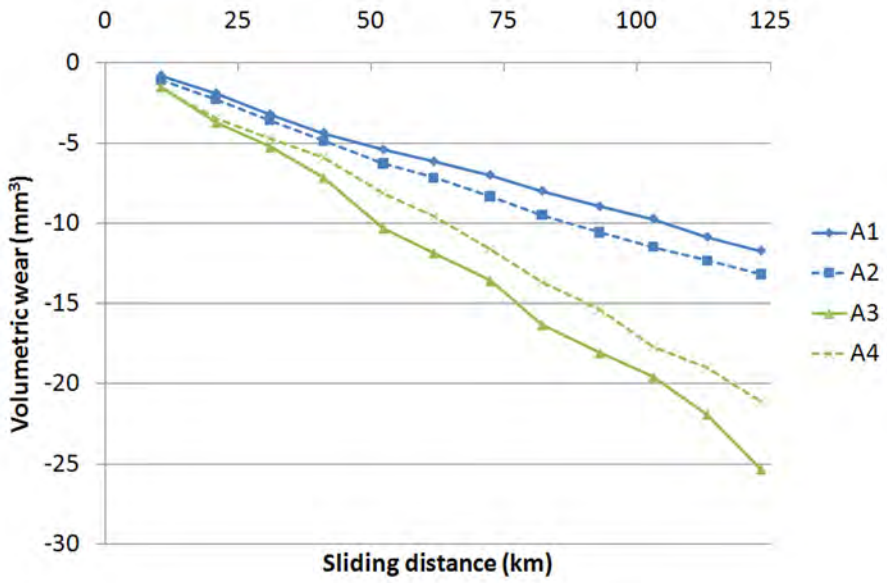

Figure 3.35: Test 1 Rig 1 Volumetric wear plot, A1 & A2 155°C 30min, A3 & A4 145°C 30min.

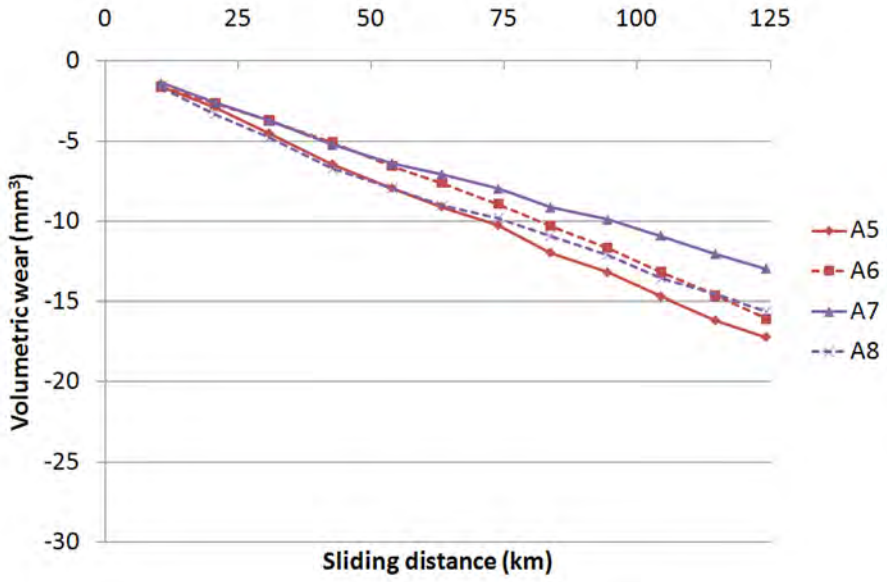

Figure 3.36: Test 1 Rig 2 Volumetric wear plot, A5 & A6 165°C 15min, A7 & A8 195°C 15min.

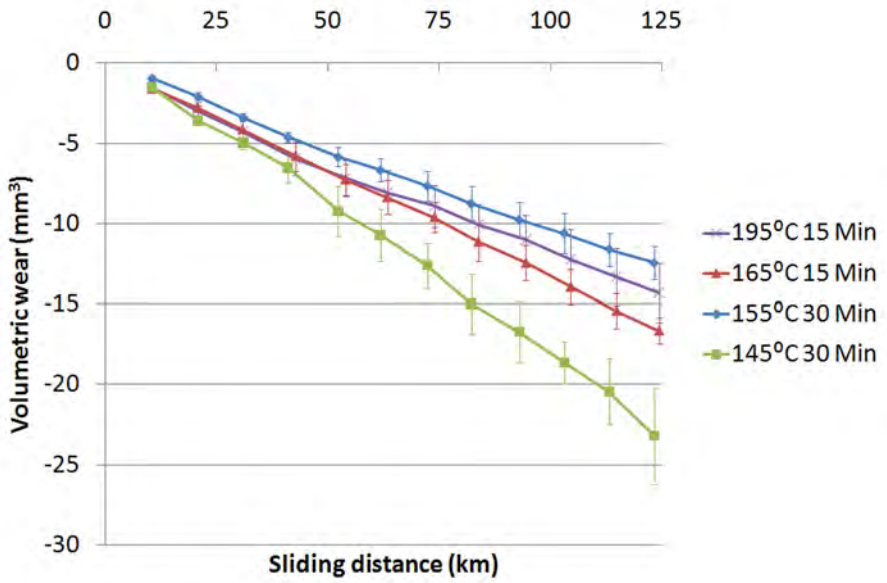

Figure 3.37: Test 1 Average Volumetric wear plot ± 1 SD.

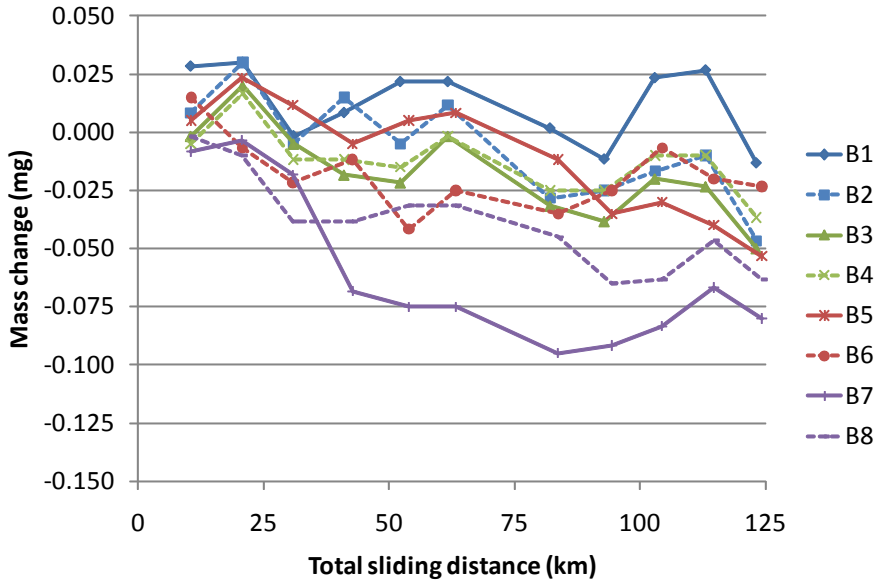

Figure 3.38: Mass change of the stainless steel pins during wear test.

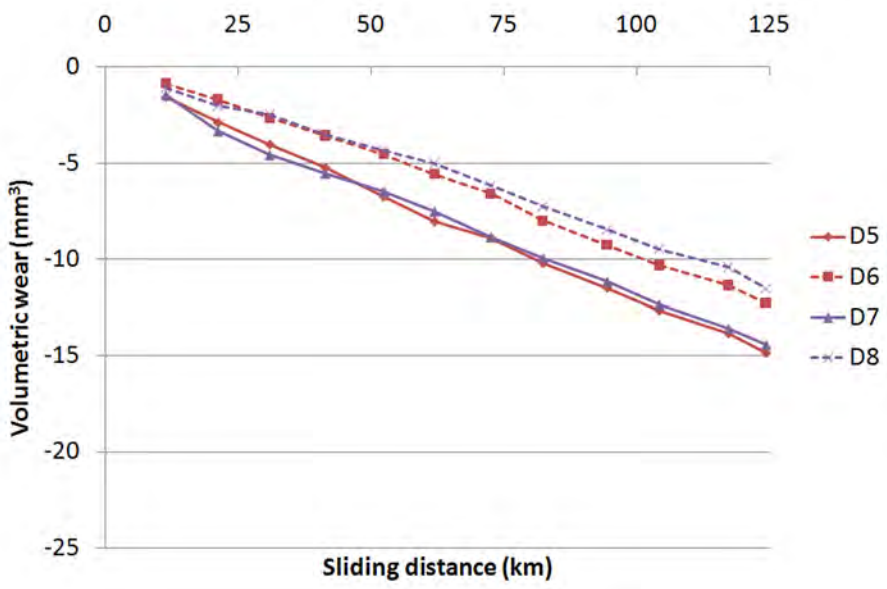

Figure 3.39: Test 2 Rig 1 Volumetric wear plot, D5 & D6 165°C 15min, D7 & D8 195°C 15min.

and 195°C degrees exhibiting wear factors of 3.261±0.124 x10^{-6} $mm^3N^{-1}m^{-1}$, 2.737±0.245 x10^{-6} $mm^3N^{-1}m^{-1}$, and 2.528±0.326 x10^{-6} $mm^3N^{-1}m^{-1}$ respectively. A comparison of these wear factors with those found in the first test is shown in figure 3.43. Analysis of the SS pins used in the second test showed on the most part little mass loss, however two pins, D7 and D1 both exhibited greater mass loss than the remaining six, although this had stabilised by the midpoint of the test and continued on the same trend as the remaining six pins.

A summary of the wear factors obtained for the different processing conditions can be found in table 3.11 and the mean of the individual tests is represented in Figure 3.43. The tabular values indicate a similar variation in individual samples between the two rigs with the range typically being close to 1.000 x10^{-6} $mm^3N^{-1}m^{-1}$, with values of 1.205 x10^{-6} $mm^3N^{-1}m^{-1}$, 0.977 x10^{-6} $mm^3N^{-1}m^{-1}$, 0.884 x10^{-6} $mm^3N^{-1}m^{-1}$, and 0.673 x10^{-6} $mm^3N^{-1}m^{-1}$ for conditions 145°C, 155°C, 165°C, and 195°C respectively.

3.3.2.4 Surface Analysis

Initial optical imaging before the start of the wear test showed darkened areas on the surface of the UHMWPE samples. This was identical for all processing conditions. This surface feature remained at the control location throughout the whole duration of the test. One example can be seen in figure 3.44. The articulating surface of plate D6 (165°C 15min) was

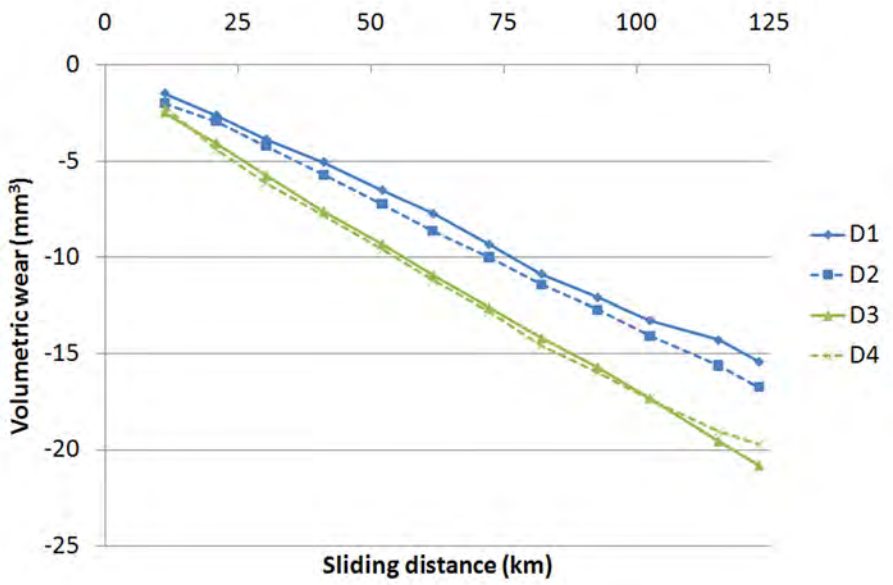

Figure 3.40: Test 2 Rig 2 Volumetric wear plot, D1 & D2 155°C 30min, D3 & D4 145°C 30min.

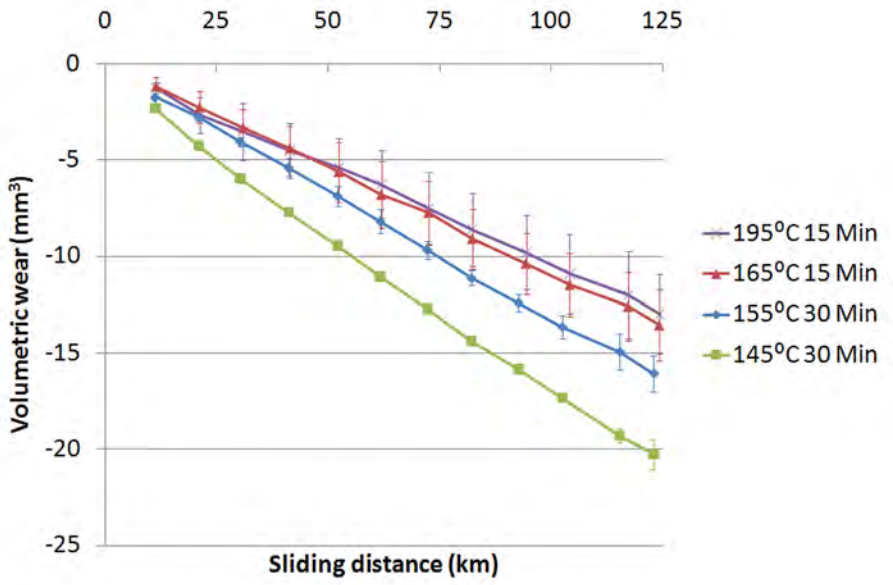

Figure 3.41: Test 2 Average Volumetric wear plot ± 1 SD.

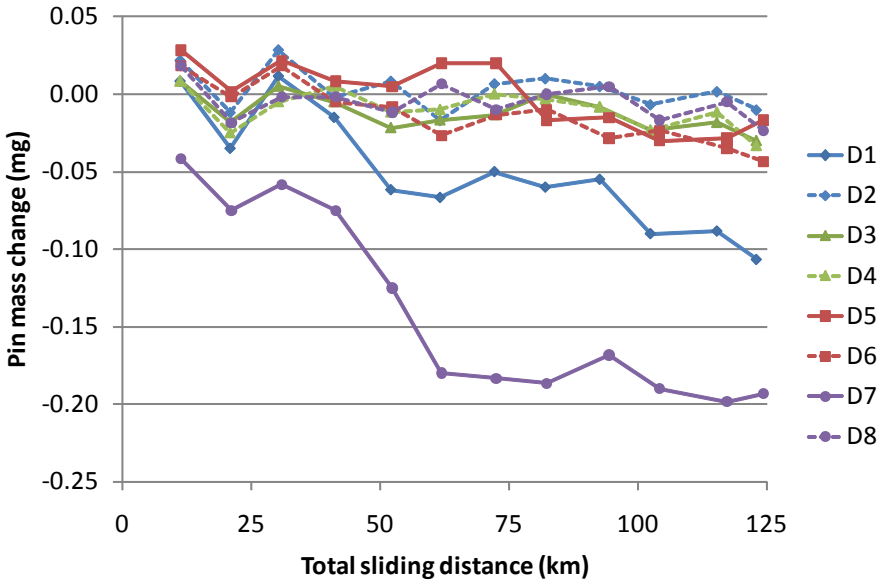

Figure 3.42: Mass change of the stainless steel pins during the second wear test with plates of different processing conditions.

Proc. Cond.	Test	Plate	Wear Factor	Test Mean	Overall Mean
145°C 30min	1	A3	5.114	4.738±0.532	4.362±0.535
		A4	4.362		
	2	D4	3.909	3.986±0.109	
		D3	4.063		
155°C 30min	1	A1	2.371	2.545±0.245	2.903±0.443
		A2	2.718		
	2	D2	3.348	3.261±0.124	
		D1	3.173		
165°C 15min	1	A5	3.447	3.316±0.185	3.026±0.379
		A6	3.185		
	2	D6	2.563	2.737±0.245	
		D5	2.910		
195°C 15min	1	A7	2.496	2.733±0.336	2.631±0.295
		A8	2.971		
	2	D8	2.298	2.528±0.326	
		D7	2.758		

Table 3.11: Individual and mean wear factors (x10^{-6} $mm^3N^{-1}m^{-1}$) of 16 plates tested using 4 different processing conditions.

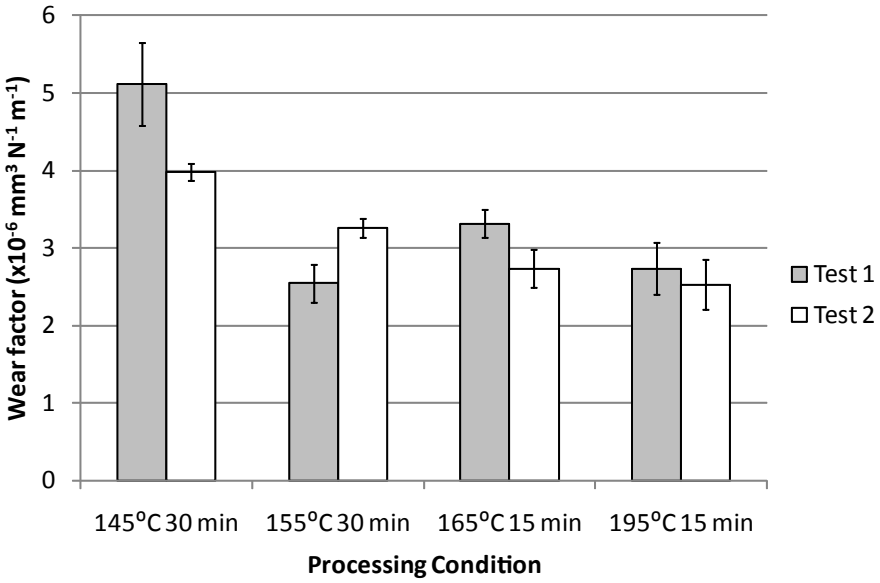

Figure 3.43: Wear factors of the different processing conditions.

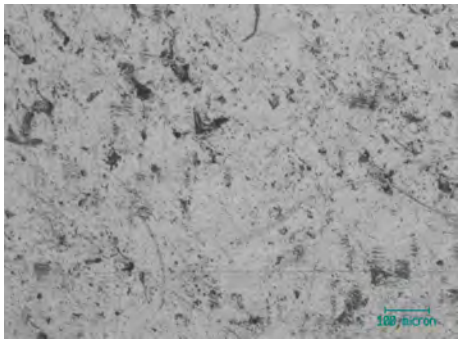

Figure 3.44: Black pitting visible on control location of plate A1.

mistakenly machined during cutting, this can be seen in Figure 3.45.

Observations on the edge of the wear track indicated that on some plates, a full wear track was not observed until 2.00 MC although most achieved a full wear track at significantly lower cycle count. A full list can be seen in table 3.12, the one exception can be seen to be plate D6 which as already mentioned had been machined. However, by 3.0 MC all evidence of the machining had been removed from the wear track. This indicates that either the plates were not perfectly flat after molding, or that they were not positioned perpendicular to the pins. However, observing the wear traces, this did not seem to cause any deviation from a linear wear rate.

Analysis of the centre of the wear track of the 4 plates manufactured using the 145°C 30 min processing condition is shown in Figure 3.46. There seemed to be significant differences in appearance between plates. Figure 3.46(a) appears to show material removed from the

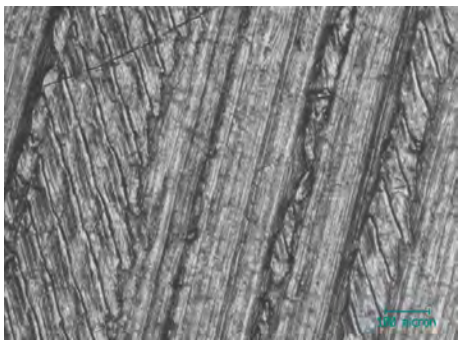

Figure 3.45: Machining marks visible on control location of plate D6.

Plate	Time until full wear track	Plate	Time until full wear track
A1	1.25MC	D1	1.5MC
A2	0.75MC	D2	0.5MC
A3	1.25MC	D3	1.0MC
A4	2.00MC	D4	0.5MC
A5	0.75MC	D5	2.0MC
A6	0.25MC	D6	3.0MC
A7	1.00MC	D7	0.5MC
A8	0.50MC	D8	1.5MC

Table 3.12: Time until full wear track.

edge of the grain boundaries. This material is then dragged along by the pin, thus creating gouges visible in the micrograph. A similar observation can be seen in Figure 3.46(c) with grain boundaries clearly visible and gouges emanating from these. Also of note is that this primarily occurs when the rest of the surface is burnished. Similar features are again seen in Figure 3.46(b). Once the majority of the material has been removed in this fashion, the surface appears like in Figure 3.46(d). The plates used in the second test had a significantly different appearance both between themselves and compared to the plates from test 1. In general the wear area had a more homogeneous appearance. Plate D3 can be seen in Figure 3.46(e), where the grains are visible, but the grain boundaries appear raised. Plate D4 can be seen in Figure 3.46(f), where again the grains are visible but in this case the whole surface seems flatter, with the grains appearing darker than the boundaries because of the occurrence of small ripples on the grain surface, occurring approximately perpendicular to the plate translation direction.

Optical analysis of the 4 plates processed at 155°C and 30 mins is presented in Figure 3.47. Here there was greater consistency between the four plates with similar surface features observed on all. Figure 3.47(c) shows a homogeneous surface of tiny ripples. In Figure 3.47(d), the ripples have become larger and grain boundaries are visible. Figure 3.47(f) shows larger ripples still, and the surface around the grain boundaries has become more burnished and therefore lighter in colour. This continues until there are few ripples left as seen in Figure 3.47(a). Finally all the ripples are removed and the surface appears totally burnished as observed in Figure 3.47(b). Scratching caused by rotation of the pin was also observed in FIgure 3.47(e), this occurred primarily at the ends of the wear track at locations 1 and 5.

Optical analysis of 4 plates processed at 165°C again showed a more homogeneous appearance, as can be seen in Figure 3.48. The centre of the wear track had a largely smooth appearance. Faint scratching due to the rotational motion of the pin was observed and can be seen in Figure 3.48(d). Deeper scratching in a similar direction was also observed as shown in Figure 3.48(a). Closer inspection of this figure also reveals the scratches also coincide with rippling. Grain boundaries were again observed, both distinct in nature as seen in Figure 3.48(c) and fainter in nature as observed in Figure 3.48(b). Also in this figure, a connected grain boundary can also be seen across the whole surface. Gouges were also seen emanating from the larger ripples on an otherwise burnished surface as seen in

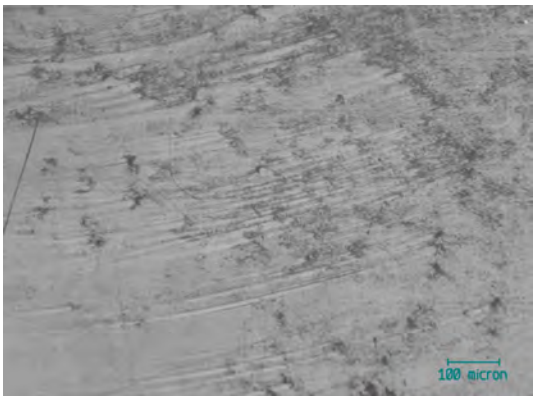

(a) Optical micrograph of Plate A3 from test 1 at location 5 after 1.25 MC. Note the rotational scratches and dark material.

(b) Plate A4 from test 1 at location 2 after 1.25 MC. Note the initiation of surface breakup.

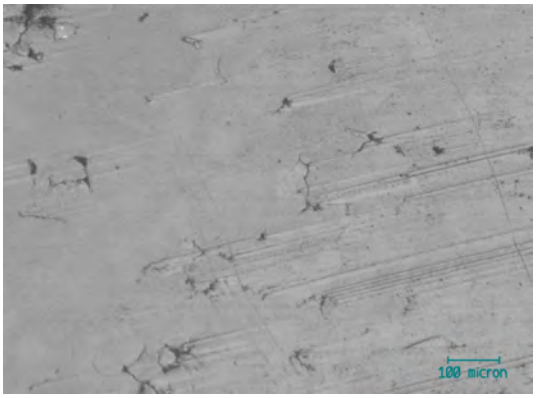

(c) Plate A4 from test 1 at location 2 after 2.00MC. Note the continued breakup of the surface and scratches caused by trapped material.

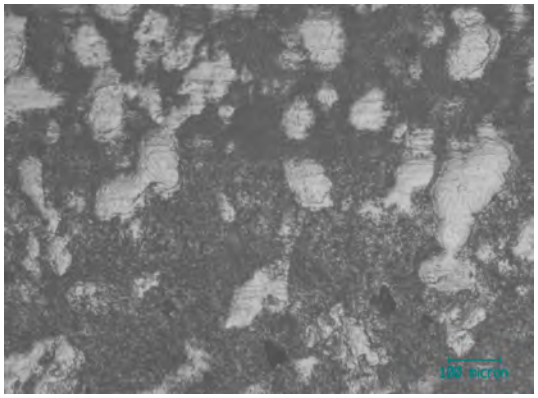

(d) Plate A3 from test 1 at location 4 after 3.0MC. Note the dark areas and light deposits.

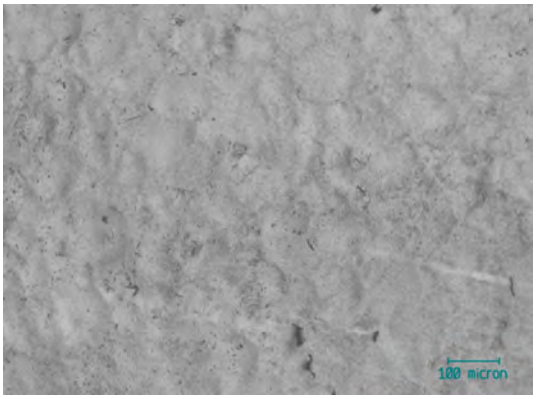

(e) Plate D3 from test 2 at location 3 after 0.5 MC. Note the grains are visible.

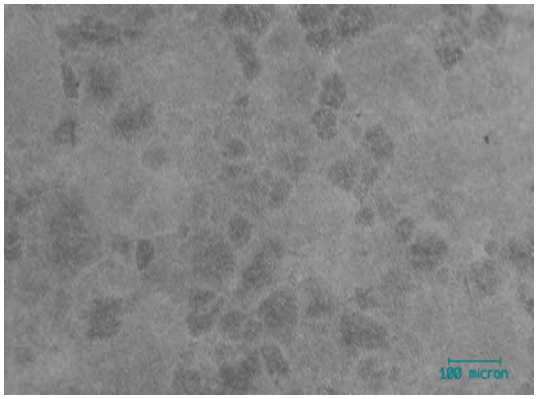

(f) Plate D4 from test 2 a location 2 after 2.50MC. Note the grains are visible and dark ripples on grains.

Figure 3.46: Optical analysis of the centre of the wear track of the UHMWPE plates molded at 145°C 30 mins.

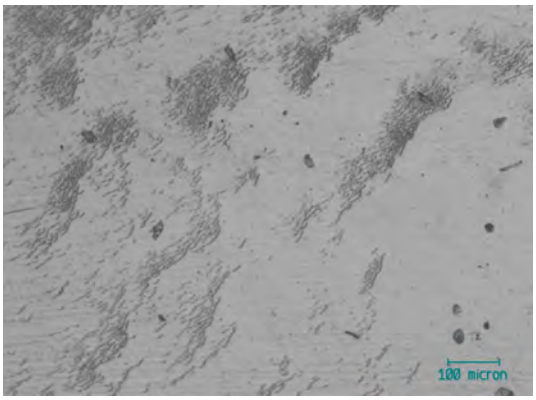

(a) Optical micrograph of plate A1 at location 3 after 0.5 MC. Note the ripples on the burnished area.

(b) Optical micrograph of plate A1 at location 4 after 0.5 MC. Note the burnished appearance of the plate.

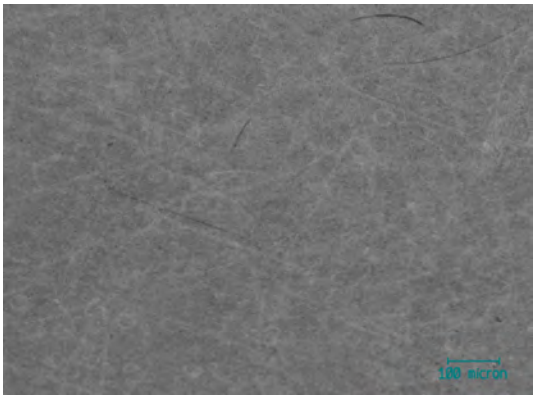

(c) optical micrograph of plate A2 at location 4 after 0.5 MC, Note the darkened area that appears smooth.

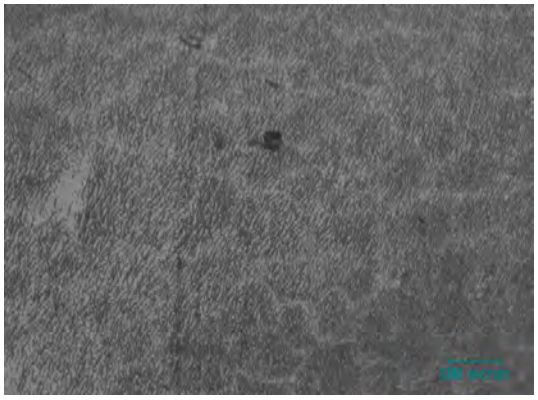

(d) optical micrograph of plate A1 at location 3 after 0.75 MC. Note the large ripples and the grains and grain boundaries visible.

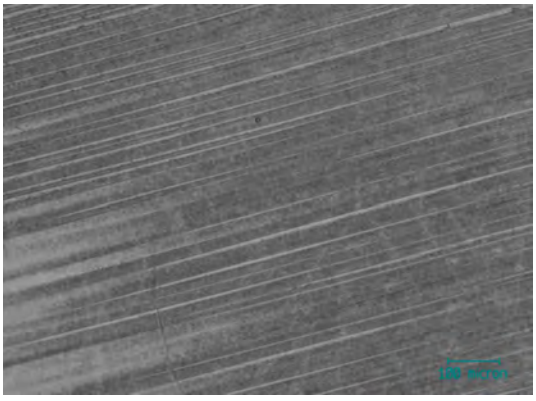

(e) Optical micrograph of plate A2 at location 2 after 0.75 MC. Note the scratches caused by pin rotation.

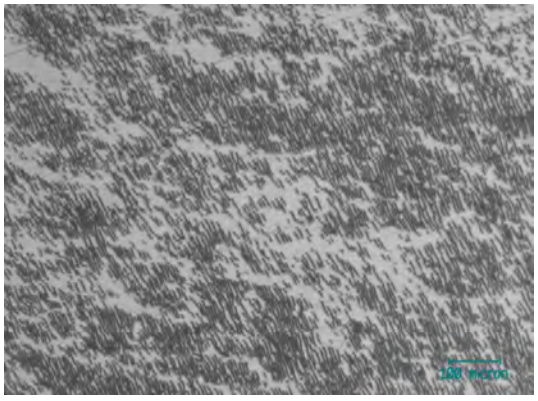

(f) Optical micrograph of plate D1 at location 2 after 1.00 MC cycles. Note the large ripples and burnishing.

Figure 3.47: Optical analysis of the centre of the wear track of the UHMWPE plates molded at 155°C 30 mins.

Figure 3.48(f) and ripples were seen in an interesting formation in Figure 3.48(e). It should be remembered that plate D6 was machined in error prior to the test start, so some surface features may arise from this.

Optical analysis of the four plates process at the 195°C condition can be seen in Figure 3.49. Burnishing was prevalent as observed in Figure 3.49(b), and in areas this was combined with fine rippling as seen in Figure 3.49(a). The size of ripples also coincided with whether grain boundaries were visible as seen in Figure 3.49(c). In the central area of the micrograph, fine ripples are visible, as are the grain boundaries. Towards the top and bottom of the micrograph, the ripples become larger and the evidence of grain boundaries disappears. Grain boundaries and fine ripples are also evidenced in Figure 3.49(e). Rotational scratches were also observed in Figure 3.49(d) and these were also combined with the rippling feature as can be seen in Figure 3.49(f).

Observations of the edge of the wear track revealed large differences between the processing conditions. Analysis of the plates processed at 145°C can be seen in Figure 3.50. For the two plates used in the first test, grains were clearly visible and in some cases, such as Figure 3.50(a) whole grains had been removed. Rippling was also observed on raised grains as can be seen in Figure 3.50(b). The two plates used in the second test differed quite significantly in appearance. Grains were clearly visible, as seen in Figure 3.50(b), however there were no grains removed and the general integrity of the surface was improved. Ripples were also observed on the grain surface, and larger ripples were observed towards the wear track edge, as observed in Figure 3.50(d).

Analysis of the edge of the wear track on the plates processed at 155°C can be seen in Figure 3.51. Rippling was more prevalent in these plates, both with fine ripples as observed in Figure 3.51(c) and larger ripples observed in figure 3.51(d). Material also accumulated at the ends of the wear track as seen in Figure 3.51(b). Adhered material was also observed at the edge of the wear track in as seen in Figure 3.51(a).

Analysis of the plates processed at 165°C saw similar features to that of the 155°C plates. Optical micrographs can be seen in Figure 3.52. Raised areas were seen at the wear track edge in Figure 3.52(a), and fine ripples further into the wear track. Figure 3.52(c) shows large ripples towards the edge of the wear track with finer ripples towards the centre. This is repeated on another plate as seen in Figure 3.52(d).

Analysis of the plates processed at the highest temperature condition of 195°C is shown

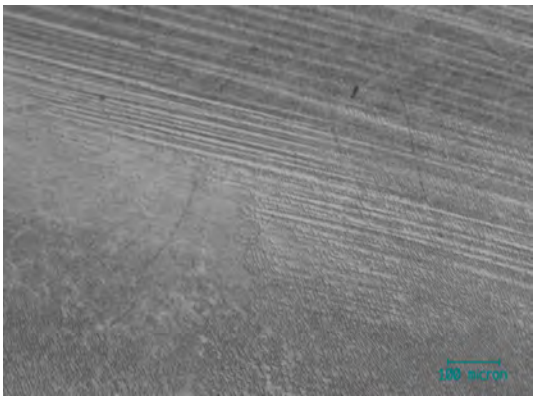

(a) Plate A5 at location 4 after 1.00 MC. Note the burnishing, ripples and scratches.

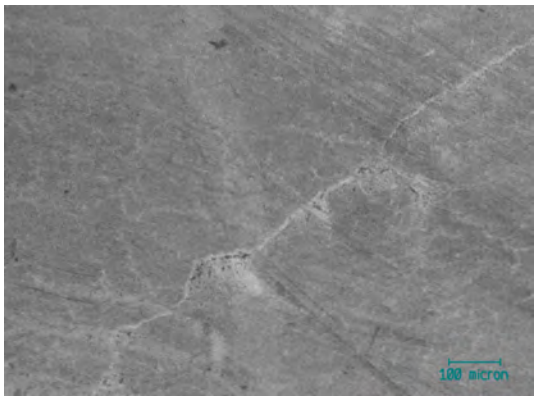

(b) Plate A6 at location 3 after 2.50 MC. Note the grain boundaries and crack running across surface.

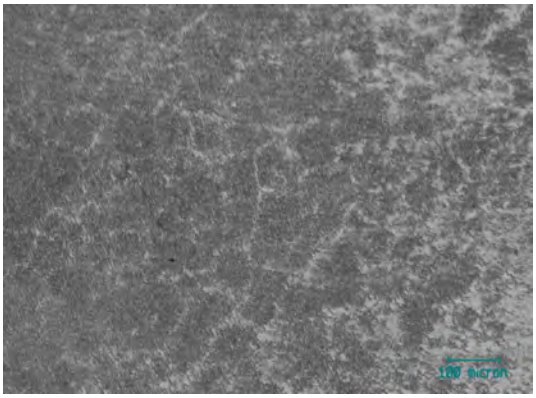

(c) Plate A5 at location 3 after 3.00 MC. Note the ripples and grain boundaries turning to burnishing.

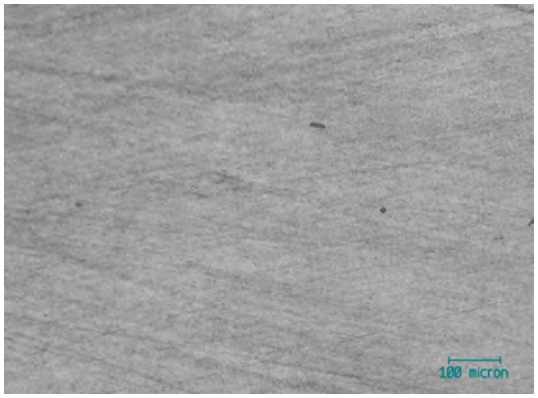

(d) Plate A6 at location 2 after 3.00 MC. Note the burnished surface with fine scratches.

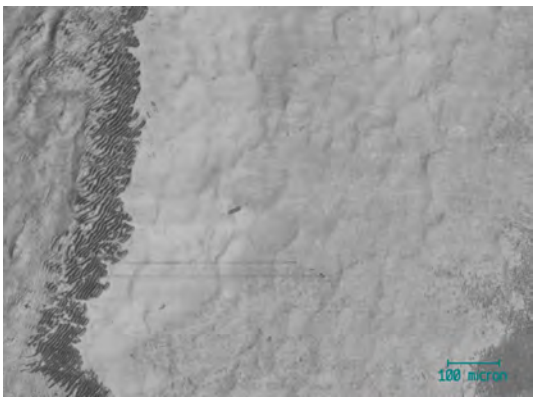

(e) Plate D6 at location 2 after 3.00 MC. Note the grain boundaries and ripples along the ridge.

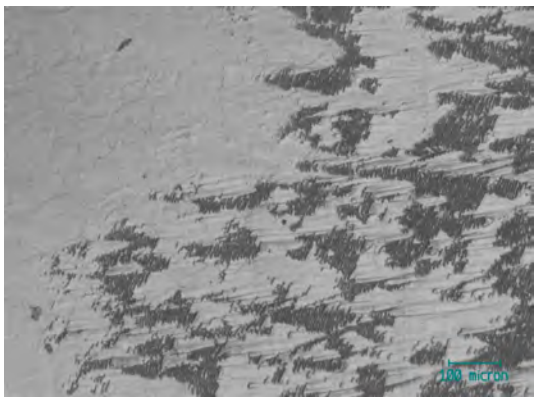

(f) Plate D6 at location 4 after 3.00 MC. Note the burnishing and ripples, and the scratches caused by material removal from the ripples.

Figure 3.48: Optical analysis of the centre of the wear track of the UHMWPE plates moulded at 165°C 15 mins.

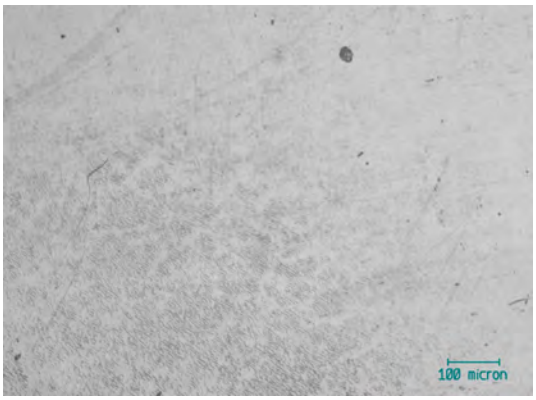

(a) Plate A7 at location 4 after 3.0 MC. Note the ripples on grains leading to burnishing.

(b) Plate D8 at location 2 after 1.5 MC. Note the burnished appearance of the whole surface.

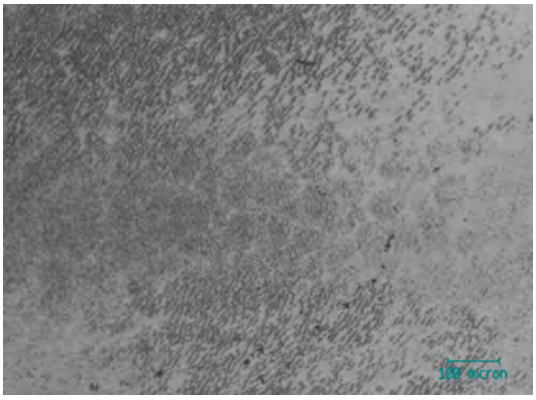

(c) Plate D7 at location 3 after 2.0 MC. Note the smaller ripples on areas where the grains are visible, and larger ripples on areas where there are no grains visible.

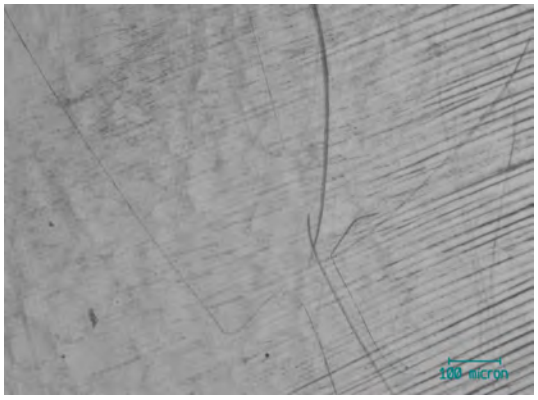

(d) Plate D7 at location 1 after 2.5 MC. Note the scratches caused by rotation.

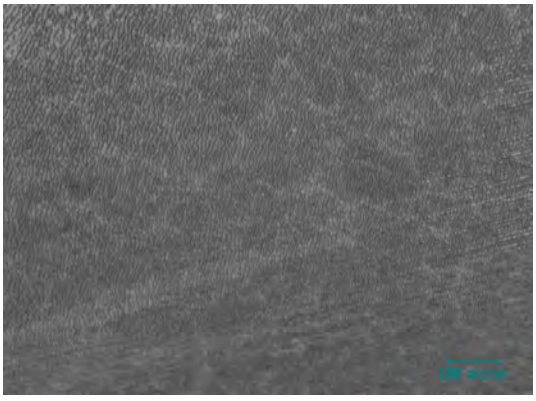

(e) Plate D8 at location 3 after 2.5 MC. Note the ripples and grains visible.

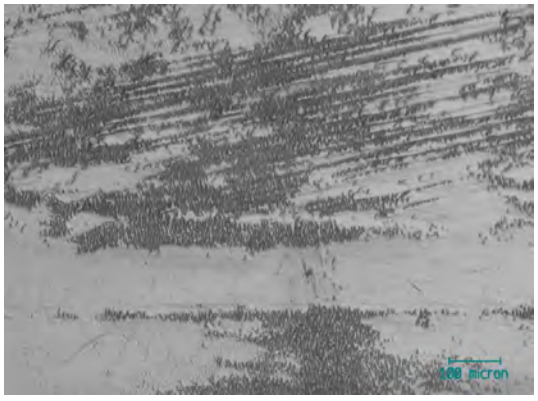

(f) Plate D7 at location 3 after 3.0 MC note the burnishing and ripples, and scratches caused by ripple removal.

Figure 3.49: Optical analysis of the centre of the wear track of the UHMWPE plates moulded at 195°C 15 mins.

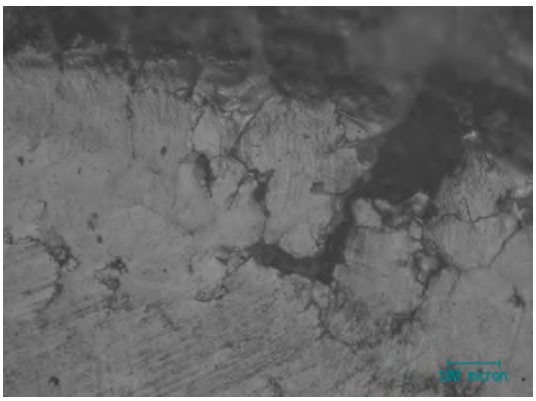

(a) Plate A4 at location 10 after 1.00 MC. Note the visible grain boundaries and grain pullout.

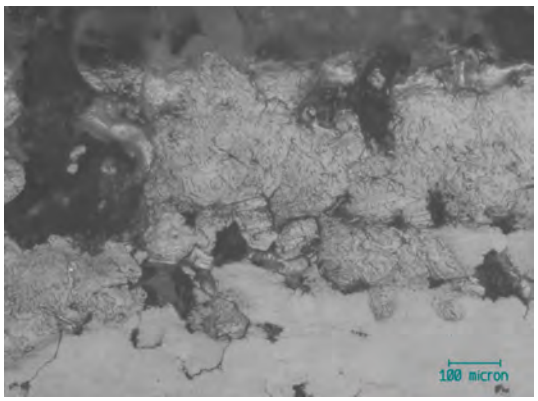

(b) Plate A3 at location 9 after 1.50 MC. Note the grains and ripples on top of raised grains.

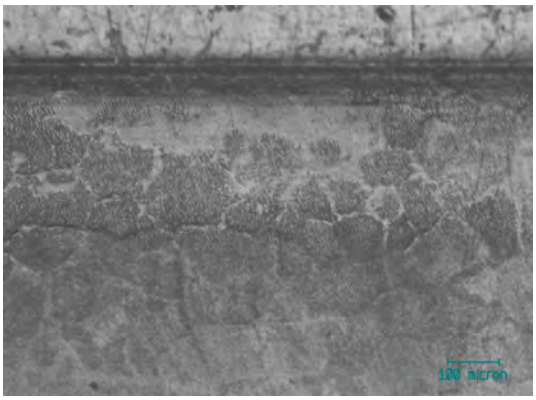

(c) Plate D3 at location 9 after 0.50MC. Note the grains and ripples on grains.

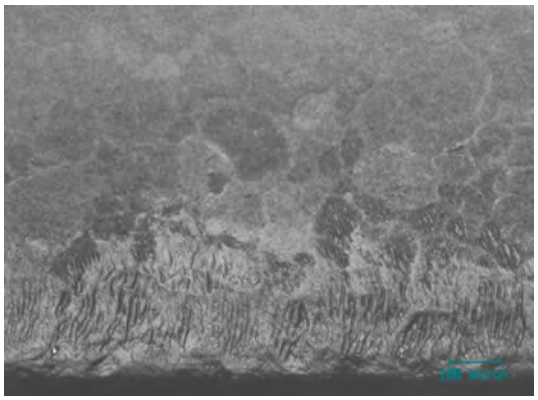

(d) Plate D3 at location 12 after 3.00MC. Note the ripples on top of grains.

Figure 3.50: Optical analysis of the edge of the wear track of the UHMWPE plates molded at 145°C 30 mins.

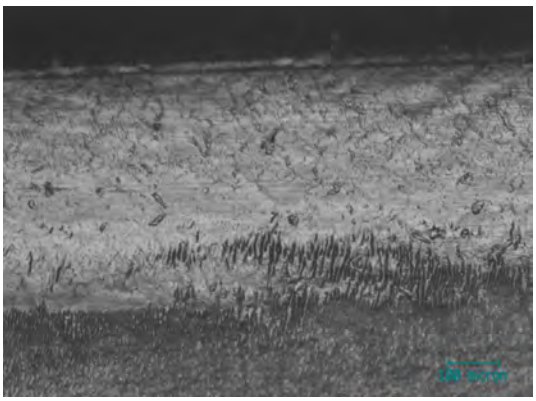

(a) Plate A2 at location 9 after 2.00 MC. Note the dark ripples and cracks towards edge.

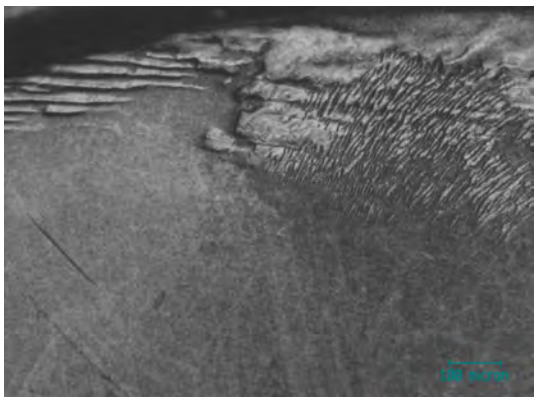

(b) Plate A1 at location 6 after 3.00 MC. Note the material deposit and ripples.

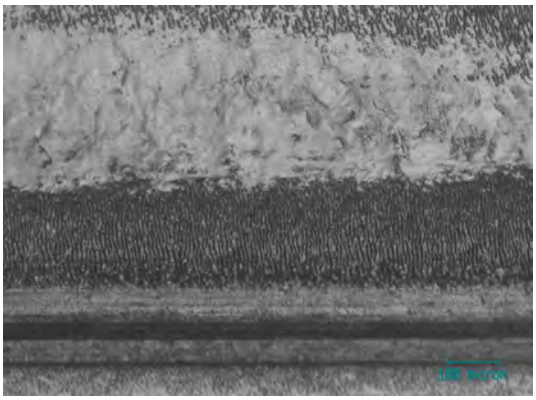

(c) Plate D2 at location 12 after 0.50 MC. Note the dark ripples.

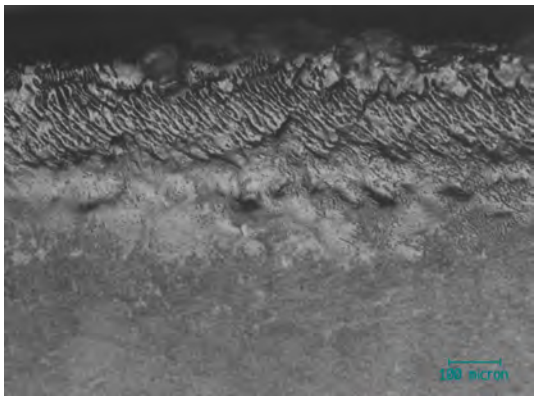

(d) Plate D1 at location 9 after 2.50 MC. Note the ripples on raised material at wear track edge.

Figure 3.51: Optical analysis of the edge of the wear track of the UHMWPE plates moulded at 155°C 30 mins.

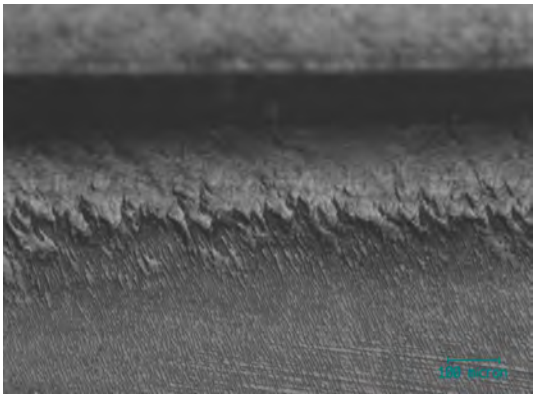

(a) Plate A5 at location 8 after 1.00 MC. Note the raised edge with ripples closer to centre of wear track.

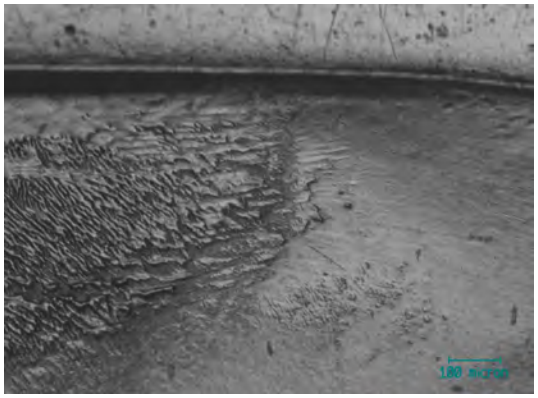

(b) Plate A6 at location 10 after 1.25 MC. Note the raised material and ripples on top.

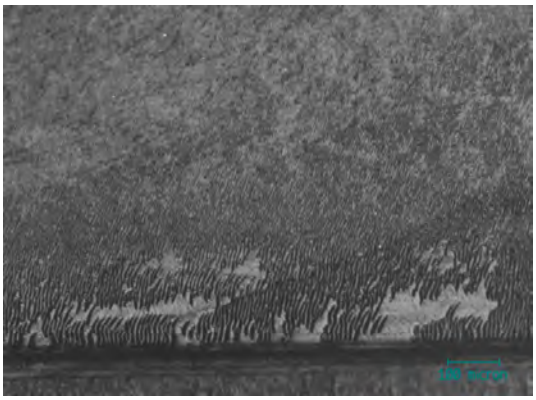

(c) Plate D5 at location 12 after 2.00 MC. Note the large ripples at the edge, and smaller ripples towards the centre.

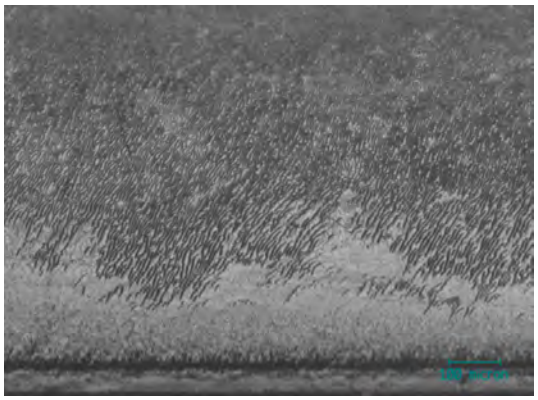

(d) Plate D6 at location 14 after 3.00 MC. Note the cracks at the edge of the war track and ripples closer to the centre.

Figure 3.52: Optical analysis of the edge of the wear track of the UHMWPE plates moulded at 165°C 15 mins.

in Figure 3.53. Fine ripples were observed at the edge of the wear track as seen in Figures 3.53(a) and 3.53(c). Cracks perpendicular to the translation direction were also observed as evidenced in Figure 3.53(b). Adhered material was also observed at the wear track ends as seen in Figure 3.53(d)

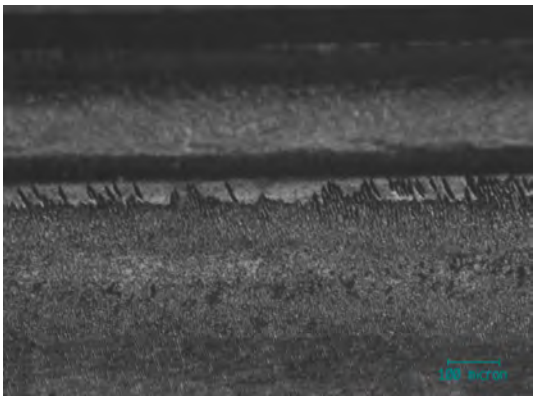

(a) Plate A8 at location 4 after 1.00 MC. Note the large ripples at the edge of the wear track, with smaller ripples towards the centre.

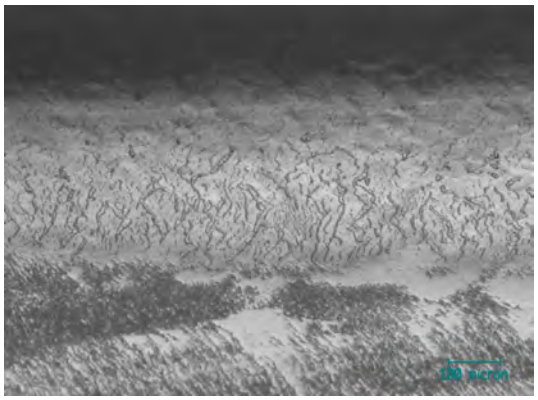

(b) Plate A7 at location 7 after 2.00 MC cycles. Note the large ripples towards the wear track edge.

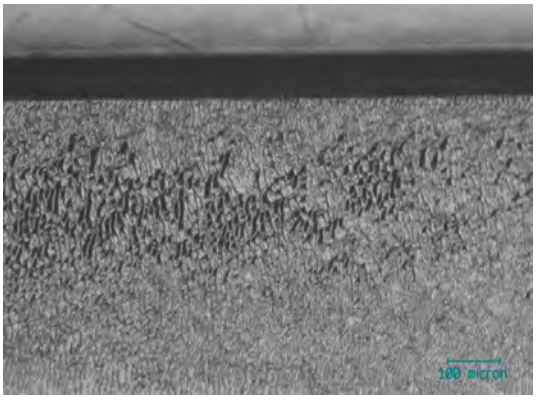

(c) Plate D7 at location 8 after 0.50 MC. Note the large dark ripples at the edge of the wear track.

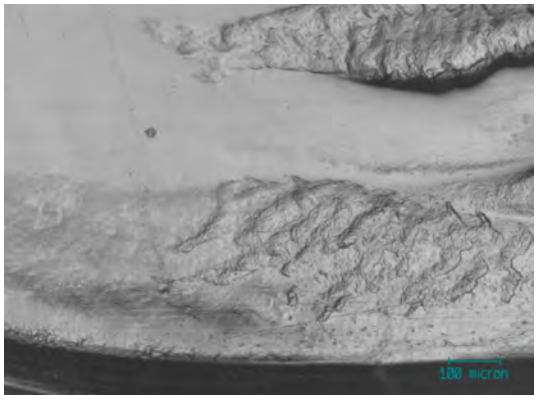

(d) Plate D8 at location 11 after 1.00 MC. Note the large material deposits at the end of the wear track.

Figure 3.53: Optical analysis of the edge of the wear track of the UHMWPE plates moulded at 195°C 15 mins.

A summary of the observed wear types on the UHMWPE plates is shown in Table 3.13

The surface roughness of the plates used in the second test was analysed using the Zygo at the conclusion of the wear test. Five points inside the wear track were analysed, approximately at points 1 - 5 in Figure 3.4. Five points on the surface of each control plate were also analysed so a comparison could be made. The mean surface roughness for the different conditions and the control plates can be seen in Figure 3.54.

The mean surface roughness of the two control plates was found to be $0.125 \pm 0.023 \mu$m. This compares to an average for the eight test plates of $0.063 \pm 0.076 \mu$m. There was no clear

Molecular Weight	Wear track location	
	Edge	Centre
145°C 30 min	Grain boundaries	grain boundary removal
	Grain removal	Grain boundaries
	Fine Rippling	Fine Rippling
	Larger Rippling	Burnishing
155°C 30 min	Adhesive deposits	Fine Rippling
	Fine Rippling	Burnishing
	Larger Rippling	Grain Boundaries
		Larger Rippling
		Rotational Scratching
165°C 15 min	Adhesive deposits	Grain Boundaries
	Larger Rippling	Fine Rippling
	Fine Rippling	Burnishing
		Rotational Scratching
195°C 15 min	Adhesive deposits	Grain Boundaries
	Larger Rippling	Fine Rippling
	Fine Rippling	Burnishing

Table 3.13: Summary table categorising the types of wear observed on the UHMWPE plates with differing processing conditions.

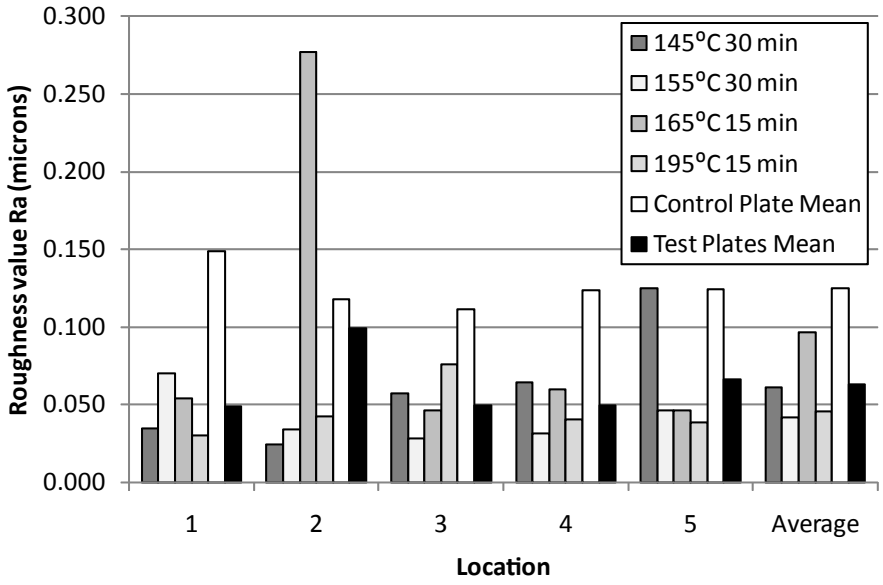

Figure 3.54: Mean surface roughness of the test plates in test 2. R_a readings were obtained using the Zygo at test conclusion of 3.0 MC.

difference between the 5 measured locations on the plates. The average R_a of the plates processed at 165°C was notably higher than the other three processing conditions, however as is clear from Figure 3.54, an abnormally high reading at location 2 has skewed the average. This high reading can be seen in Figures 3.55(g) and 3.55(h), and of additional interest in these figures is the conformation that the dark ripples occur on the most superior part of the surface. Single grain pullout on the 145°C plates can be seen in Figure 3.55(a), and what is thought to be multiple grain pullout can be seen in Figure 3.55(b). Unidirectional scratching on the 155°C plate can be seen in Figure 3.55(c). Raised grains and lower grain boundaries for the 155°C and 165°C plates can be seen in Figures 3.55(d) and 3.55(e) respectively. Figure 3.55(f) shows the topography of raised ripples on an otherwise burnished surface. Of special interest is the 'comet tail' material deposits that are not picked up by the optical analysis.

The surface roughness of the test pins was taken before the test start and at 0.5 MC then at the conclusion of the test at 3.0 MC. The surface roughness plot can be seen in figure 3.56. Here it can be seen that there are no differences between the pins used for plates of different processing conditions. There was also no significant difference between the R_a of the test pins with respect to the control pins.

Optical analysis of both sets of pins revealed no significant differences between the pins used for different processing conditions and the surface features observed were similar

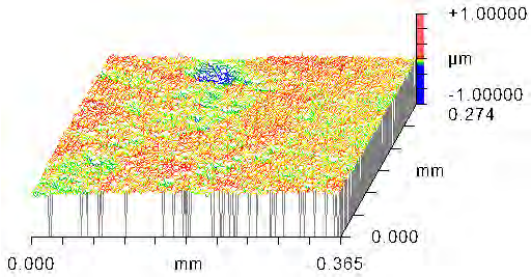

(a) Zygo scan of Plate D3 at location 1 after 3.0 MC (145) showing grain removed from surface. R_a=0.030μm.

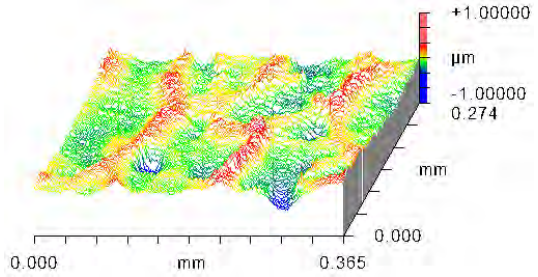

(b) Zygo scan of plate D3 at location 3 after 3.0 MC (145) showing large ridges (Grain boundaries). R_a=0.100μm.

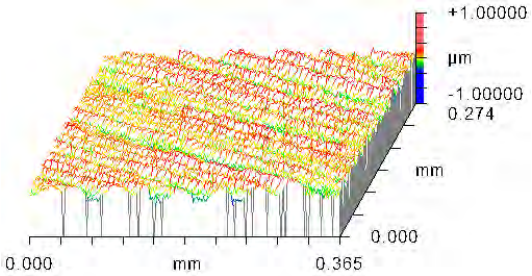

(c) Zygo scan of Plate D1 at location 1 after 3.0MC (155) showing uniform scratching of the surface. R_a=0.097μm.

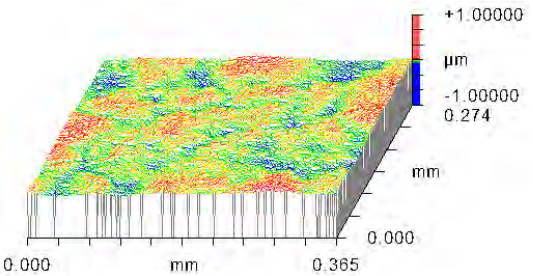

(d) Plate D2 at location 3 after 3.0 MC (155) showing raised grains and lower grain boundaries. R_a=0.022μm.

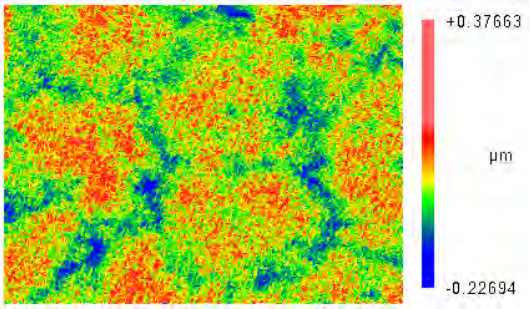

(e) Plate D5 at location 4 after 3.0 MC (165) showing larger raised grains. R_a=0.046μm.

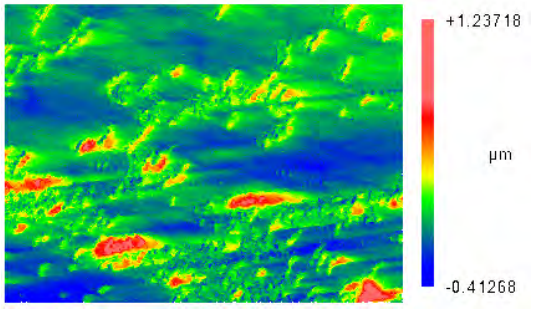

(f) Plate D7 at location 3 after 3.0 MC (195) showing raised ripples on burnished surface. R_a=0.112μm.

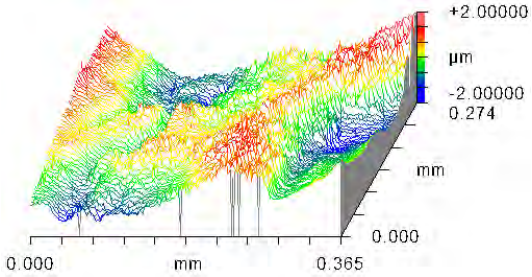

(g) Plate D6 at location 2 after 3.0 MC (195) showing ripples on raised areas. R_a=0.506μm.

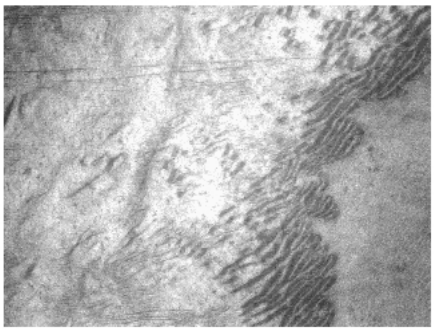

(h) Plate D7 at location 2 showing image of previous figure.

Figure 3.55: Zygo scans of various features on the UHMWPE plates with different processing conditions.

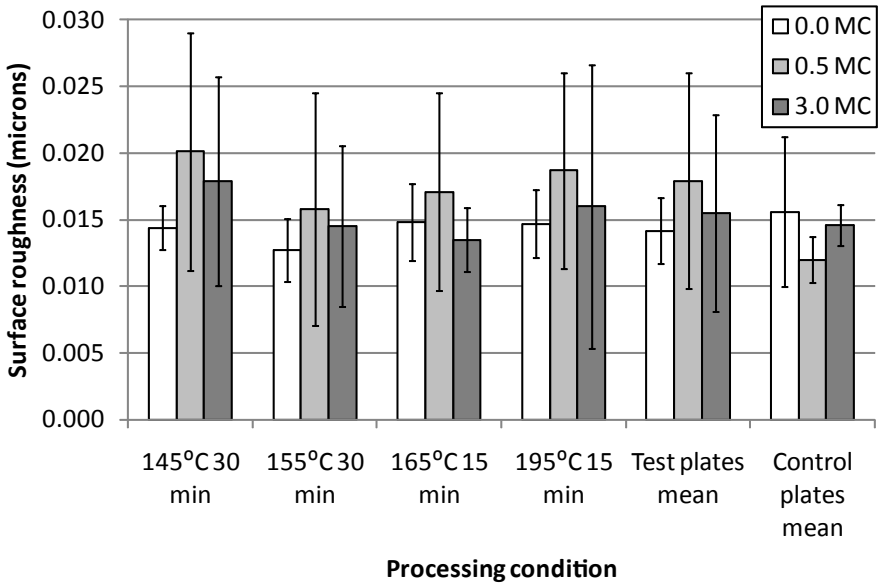

Figure 3.56: Surface roughness of the SS pins during test 2.

to those observed on the stainless pins used in the previous test with plates of differing molecular weight shown in Figure 3.31. No surface features were found to explain the higher mass loss of pins D1 and D7 indicated from Figure 3.42. Therefore it is assumed this mass loss was due to the contact between the pin and the pin holder.

3.4 Effect of rough counterface

During the lifetime of an implant, the polished counter-face of TKRs and THRs can become scratched due to third body wear. In this test the stainless steel pins were artificially scratched to see the effect on the wear of the UHMWPE plates.

3.4.1 Materials and methods

The 10 stainless steel pins used in the previous test 2 were artificially scratched using silicon carbide grinding paper with a grit value of P240. The contacting end of the pin was placed in contact with the grinding paper and rotated clockwise at 1Hz with 6N of axial loading to ensure contact. Each pin was rotated for 5 minutes and then rinsed with propan-2-ol. The contacting surface of each pin was analysed at 5 different points using a Zygo Newview 100 non-contacting surface profiler. The approximate position of the five points chosen is shown in Figure 3.3. A mean R_a of these 5 points was calculated and the 8 pins representing the smallest range of mean values were then chosen as the test pins and the remaining two

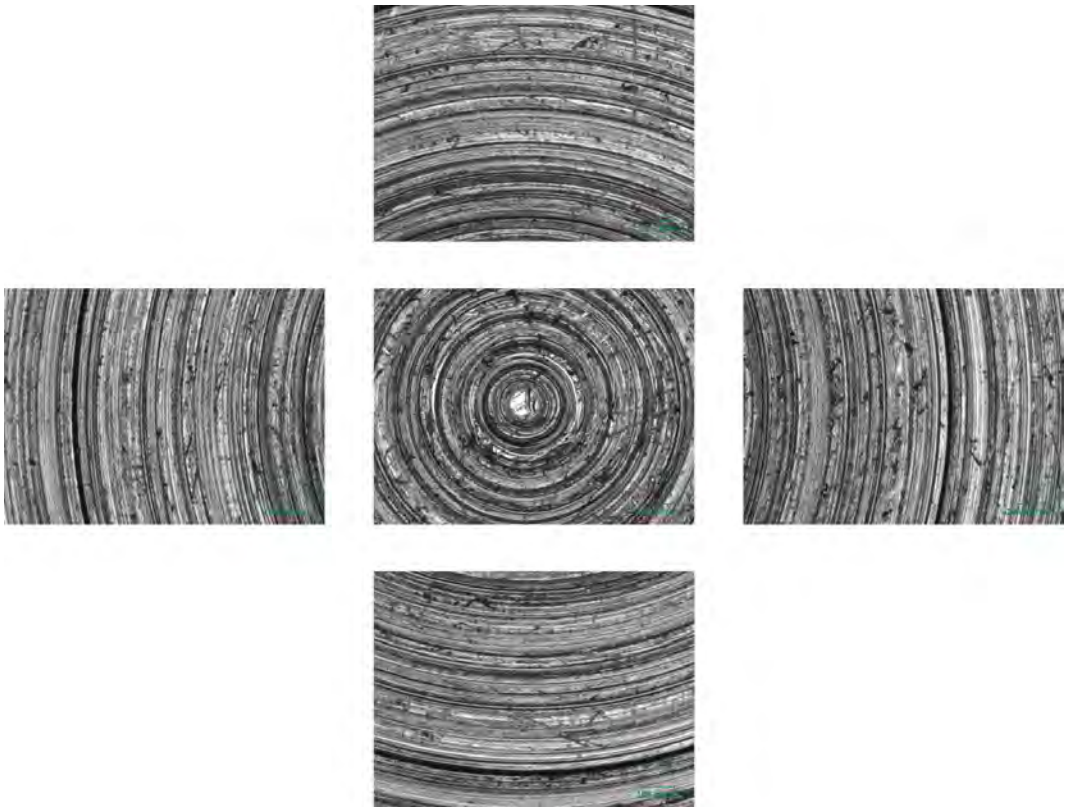

Figure 3.57: Optical micrographs of pin D5 after 0.5 MC.

were used as soak control samples. The mean R_a of the 8 test pins was 0.903μm, ranging between 1.001μm and 0.765μm. The circular scratches created on pin D5 using this method can be seen in figure 3.57 and in Figure 3.58. The test was run for approximately 2.0MC which equates to 82km total sliding distance.

The 8 test plates from the previous test 2 were also used so that a direct comparison of wear factors using smooth and rough counter-faces could be obtained. As the wear scar placement was unique to each station of each rig, the plates were located in the same rigs and stations as in the previous test.

Optical micrographs of the plates were taken at locations 1-15 on figure 3.4 both at pre test, then at 0.5 MC intervals thereafter until the conclusion of the test at 2.0 MC. Surface roughness measurements of the plates were taken pre test, then at 0.5 MC, 1.0 MC and finally at 2.0 MC upon conclusion of the test. Five R_a measurements in the wear track were obtained for each test sample the approximate location of these readings were locations 1-5 on figure 3.4.

As stated previously the surface roughness of the stainless steel pins was measured pre test. This was monitored throughout the test after 0.5, 1.0, and 2.0 MC.

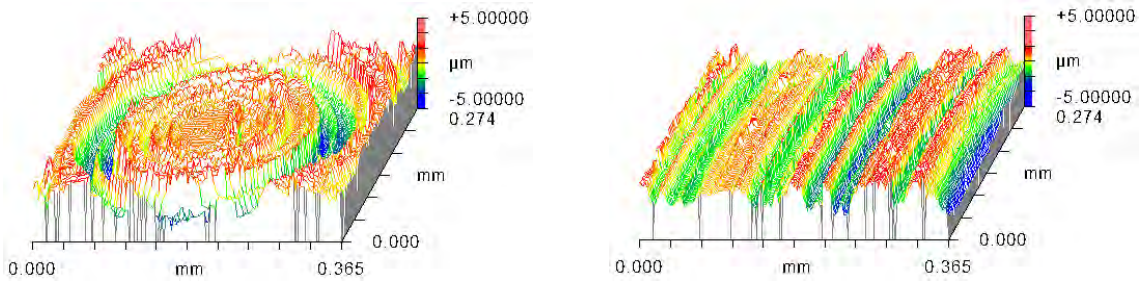

(a) Pin D5 at location 1 prior to testing.

(b) Pin D5 at location 2 prior to testing.

Figure 3.58: Zygo analysis of pin D5 prior to testing.

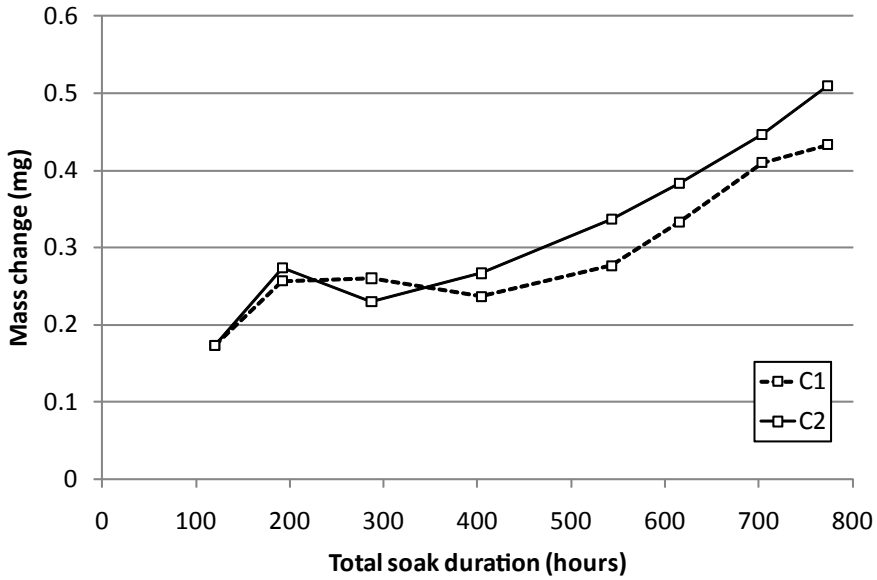

Figure 3.59: Mass change of the two control plates due to lubricant uptake.

3.4.2 Results

3.4.2.1 Fluid uptake

The fluid uptake of the two control plates can be seen in Figure 3.59. The fluid uptake rates for the two plates calculated using a linear least squares fit can be seen in Table 3.14.

Plate	Fluid uptake rate (mg/hour)	R^2
C1	0.00034	0.833
C2	0.00045	0.903

Table 3.14: Fluid uptake rates of the two control plates.

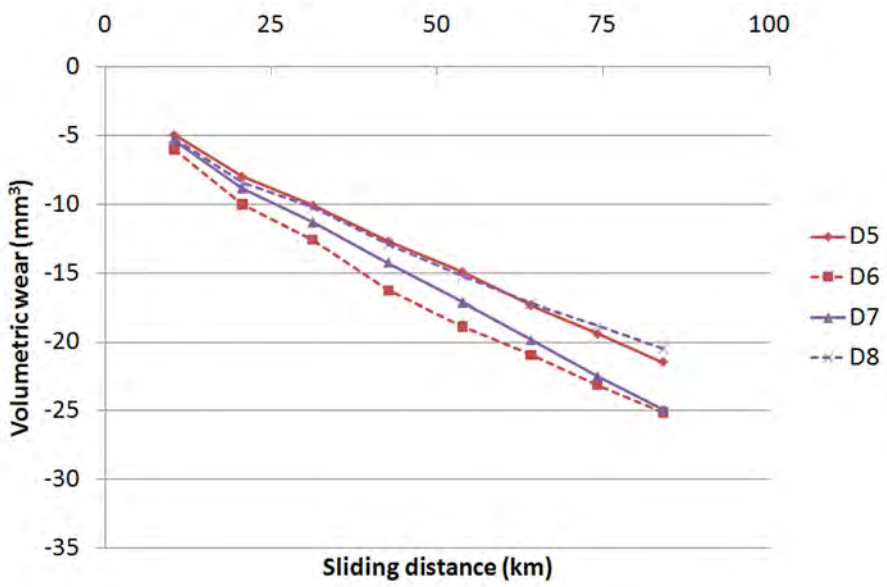

Figure 3.60: Test 1 Rig 2 Volumetric wear plot, D5 & D6 165°C 15min, D7 & D8 195°C 15min.

3.4.2.2 Wear

The individual wear plots for the four plates on rig 1 can be seen in figure 3.60. Due to the scratched pins, there are now larger variances between the individual plates of the same processing condition. The plates still seem to exhibit mainly a linear wear pattern, although plate D3 (145°C 30 Min) exhibited accelerated wear until approximately 20 km. Plates D2 (155°C 30 Min) and D4 (145°C 30 Min) also seemed to experience accelerated wear for the first 10km. The wear traces of the four plates on rig 2 can be seen in figure 3.61. Here the wear traces are again linear although there again seems to be accelerated wear for all samples until 20 km sliding distance. The combined data from both rigs can be seen in figure 3.62. Here it is clear that the average wear traces for the samples processed at 195°C, 165°C, and 155°C are indistinguishable and this is confirmed by the calculated wear factors shown in table 3.15. It is clear that the UHMWPE processed at 145°C was the worst performer. The magnitude of the standard deviation bars also show that there was much greater consistency between the pairs of plates processed at 195°C and 165°C than the two pairs processed at the lower temperatures. Comparing the mean wear factors from this test, shown in table 3.15, to the mean wear factors using polished pins, shown in table 3.11, it can be seen that there was a large increase in wear factors for the scratched pin samples. This is presented graphically in figure 3.64.

The wear factor of each plate can be seen in table 3.15 along with the mean wear factor

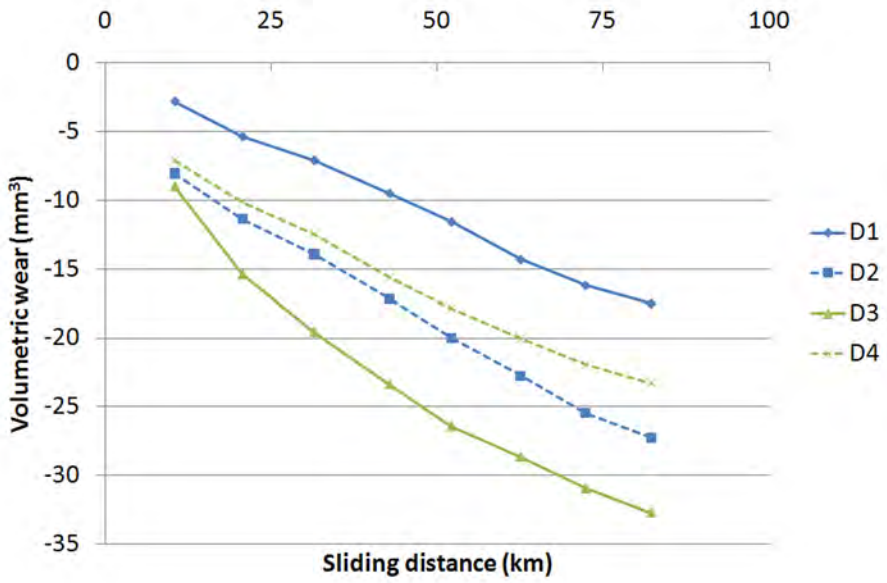

Figure 3.61: Test 1 Rig 2 Volumetric wear plot, D1 & D2 155°C 30min, D3 & D4 145°C 30min.

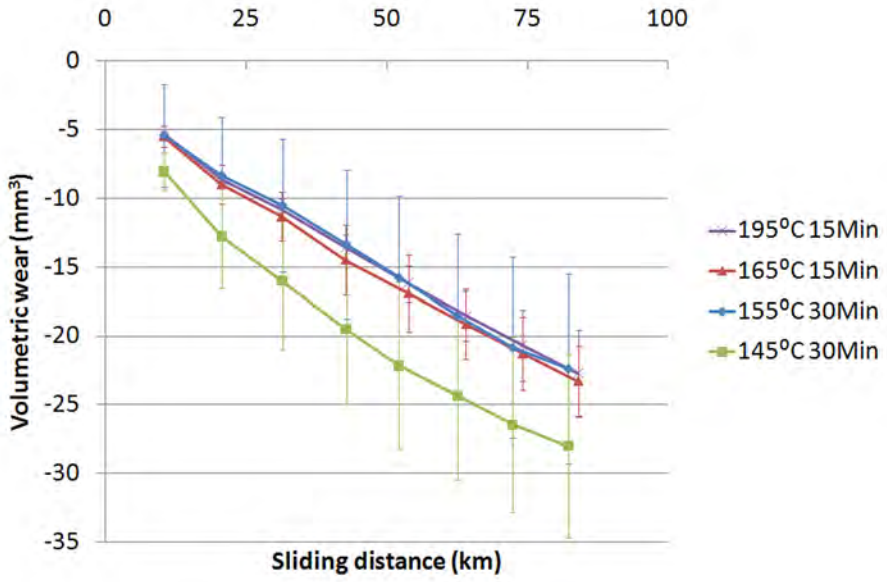

Figure 3.62: Average Volumetric wear plot ± 1SD of orthopaedic grade UHMWPE with scratched stainless steel pins.

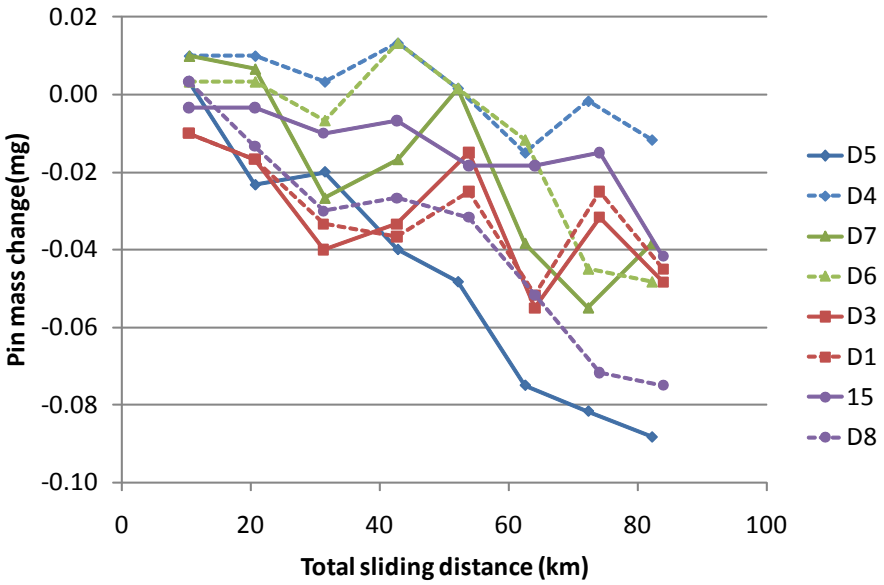

Figure 3.63: Mass change of the scratched pins.

for each condition. The trend is similar to that observed in the previous test with the plates processed with a max temperature of 145°C experiencing the greatest wear factor.

It can be seen that all conditions experienced a significant increase in wear factor due to the scratched counter face. The plates processed 145°C 30min had a wear factor 1.57 times that obtained for smooth counterface. 155°C 30min had an increase of 2.07 times, 165°C 15min increased 1.96 times, and 195°C 15min increased 2.22 times.

The difference in range between the min and max wear factors across different processing conditions the scratched pin test was 1.018 x10^{-6} $mm^3N^{-1}m^{-1}$ compared to 1.731 x10^{-6} $mm^3N^{-1}m^{-1}$ as observed in the previous smooth pin test.

3.4.2.3 Surface Analysis

The change in surface roughness (R_a) for the 8 tested plates over the course of the test can be seen in figure 3.65. It can be seen that for all processing conditions, the surface roughness increases from the initial value and remains higher at the end of the test. The mean R_a of the 8 plates upon conclusion of the previous test was 0.060±0.038μm. The previous test was conducted with smooth pins. After 0.5 MC, 1.0 MC and 2.0 MC the mean plate R_a had increased to 0.199±0.071μm, 0.151±0.081μm, and 0.163±0.077μm respectively. There were no significant differences between the processing conditions. However, the the surface roughness is location dependent. Figure 3.66 shows the mean surface roughness of the 8 plates at each location for each interval of recording. This again shows a large increase in

Proc. Cond.	Plate	Wear Factor	Test Mean
145°C 30min	D3	7.973	6.848±1.591
	D4	5.723	
155°C 30min	D1	5.242	6.014±1.091
	D2	6.786	
165°C 15min	D5	5.520	5.946±0.603
	D6	6.372	
195°C 15min	D7	6.543	5.830±1.009
	D8	5.117	

Table 3.15: Wear factors (x10^6 $mm^3N^{-1}m^{-1}$) of plates in scratched pin test.

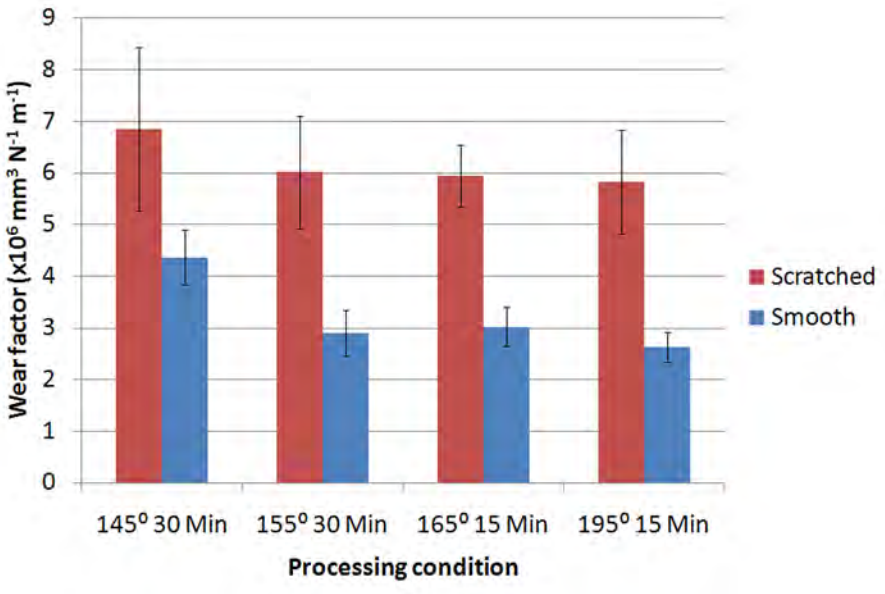

Figure 3.64: Comparison of plate wear factors for scratched and smooth stainless steel counter-face conditions. The smooth condition values are the mean of those shown in Figure 3.43 Error bars are ± 1 SD.

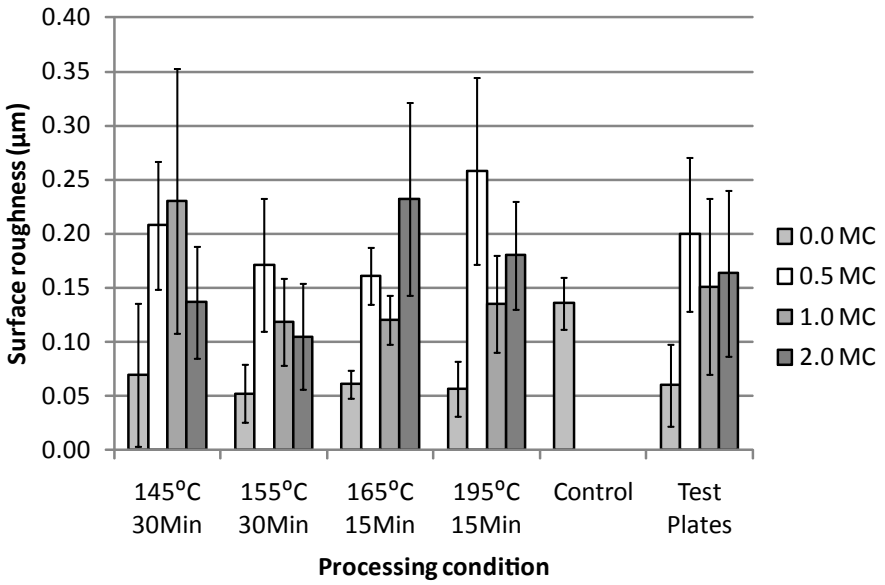

Figure 3.65: Change in surface roughness of the test plates during scratched pin wear test.

surface roughness from when smooth pins were used (0 MC). The values obtained at 0.5 MC were highest for all locations. There were minimal differences between 1.0 MC and 2.0 MC. Most interestingly is that for all intervals, the R_a at the extremities of the wear track (Locations 1 and 5) was observably lower than that at locations 2, 3, and 4. This could be because these locations are where there is lowest surface cross shear as the predominant motion would just be the rotation of the pin. At the locations in the centre of the wear track, there is rotation of the pin coupled with the reciprocation.

The surface roughness of the scratched pins throughout the course of the test can be seen in Figure 3.67. It was observed that there was no significant change in surface roughness to that which was recorded prior to the test start. The initial mean R_a of the 8 test pins was $0.878 \pm 0.176 \mu$m, and this remained at $0.851 \pm 0.224 \mu$m, $0.849 \pm 0.184 \mu$m, and $0.820 \pm 0.171 \mu$m, for 0.5MC 1.0MC, and 2.0 MC respectively.

Optical analysis of the plates revealed differences in appearance when compared to when they were scratched with smooth pins. In general, burnishing of the plates now no longer occurred. Images of the 145°C plate wear scar are shown in Figure 3.68. Zygo analysis showed that the ends of the wear track had a lower surface roughness, and this is corroborated by the images shown here. Figures 3.68(a) and 3.68(d) are located at the ends of the wear track and they have a smoother, more homogeneous appearance than Figures 3.68(b) and 3.68(c), that occur in the centre of the wear track. In these central images, larger ripples are visible and material pullout from the grain boundaries can be seen in Figure 3.68(c).

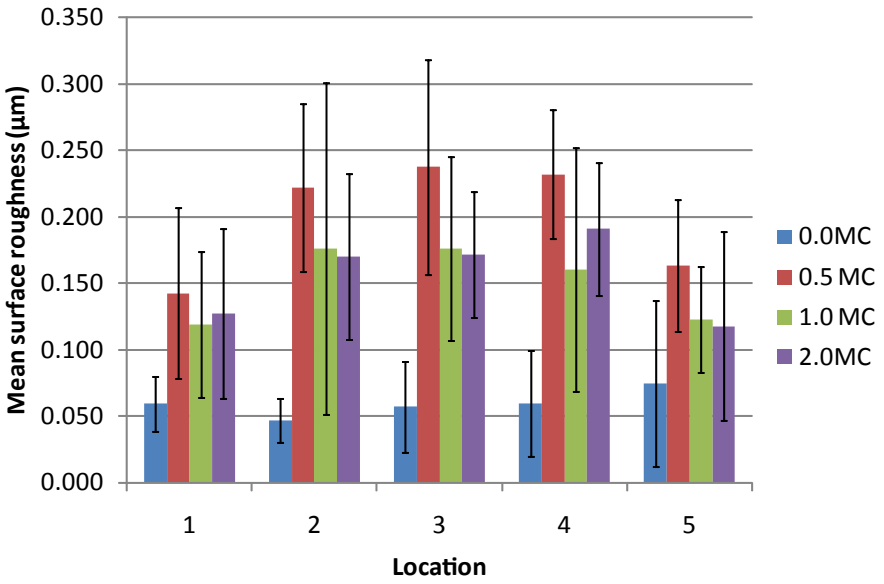

Figure 3.66: Mean surface roughness (R_a) $\pm$ 1 SD at each location on the UHMWPE plates worn with scratched pins at each interval of imaging.

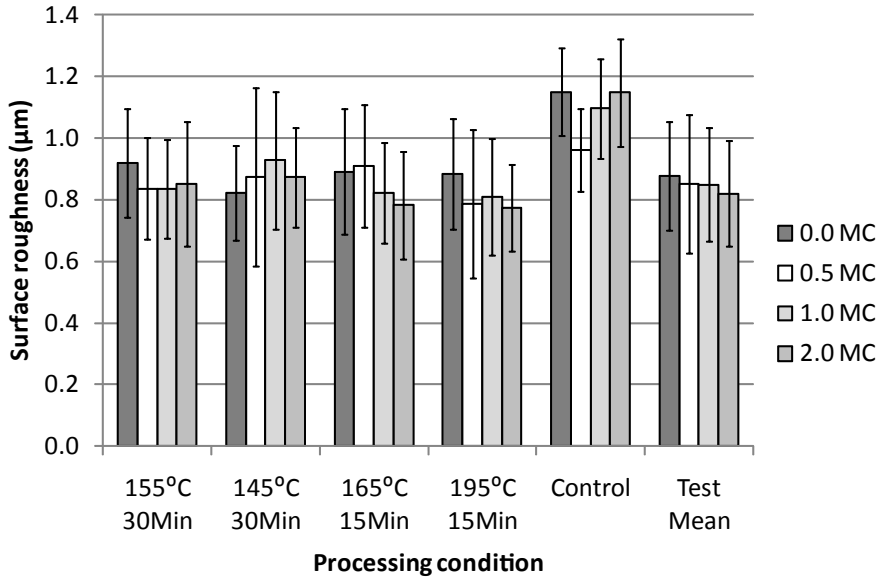

Figure 3.67: Change in surface roughness of the stainless steel pins throughout the course of the wear test.

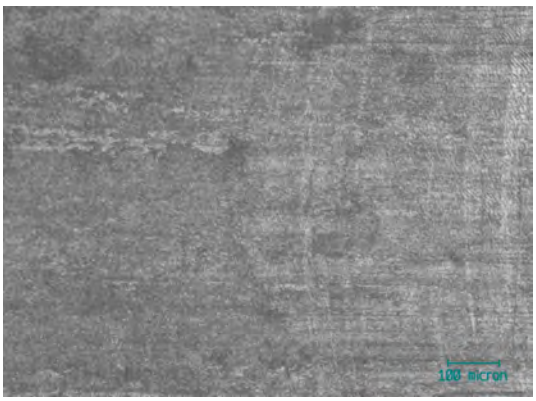

(a) Plate D3 at location 1 after 0.5 MC. Note the very fine ripples.

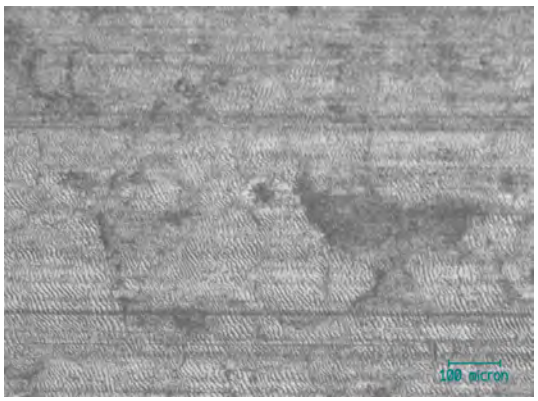

(b) Plate D3 at location 3 after 0.5 MC. Note the large ripples and the visible grain boundaries.

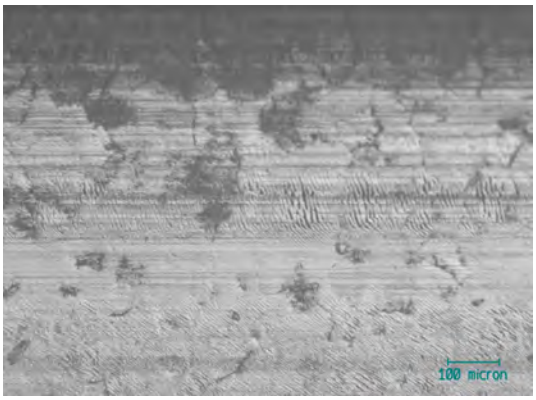

(c) Plate D4 at location 9 after 0.5 MC. Note the grain breakup at edge of wear track.

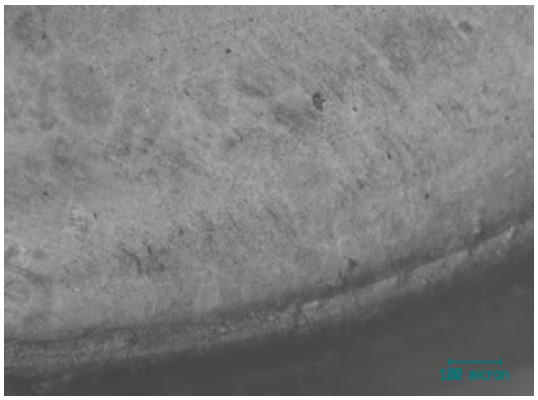

(d) Plate D4 at location 15 after 2.0 MC. Note the fine ripples and grains slightly visible.

Figure 3.68: Optical analysis of the wear track of plates processed at 145°C when worn with scratched pins.

Observations of the plates processed at 155°C are shown in Figure 3.69. Ripples were prevalent on these plates with the largest ripples occurring at the edge of the plate as seen in Figure 3.69(a). Finer ripples were observed centrally on the wear track as seen in Figure 3.69(b), and the finest ripples were observed in the centre of the wear track towards the ends such as location 5 shown in Figure 3.69(d). An additional observed feature was scratching at the edge of the wear track in the direction parallel to the plate translation as seen in Figure 3.69(c).

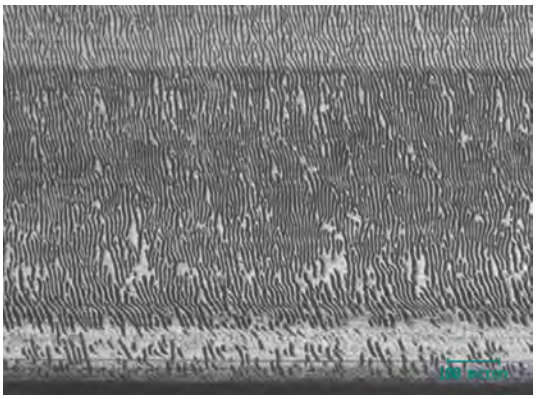

(a) Plate D1 at location 12 after 0.50 MC. Note the large dark ripples across the whole surface.

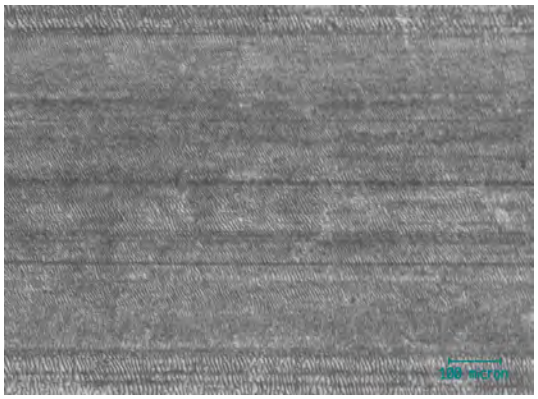

(b) Plate D1 at location 3 after 0.50 MC. Note the finer ripples at the centre of the wear track.

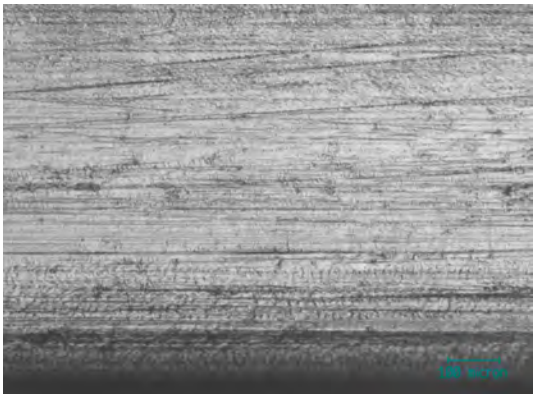

(c) Plate D2 at location 14 after 0.50 MC. Note the scratching in the translational direction at the wear track edge.

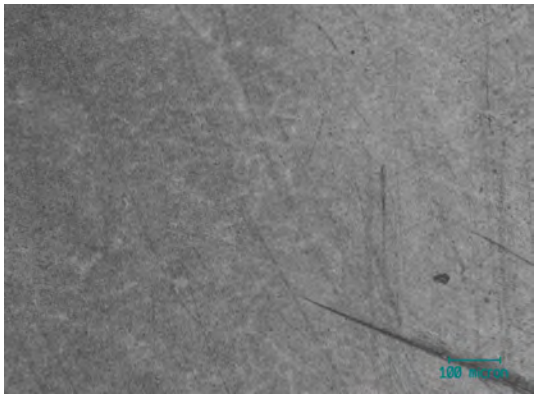

(d) Plate D2 at location 5 after 2.0MC. Note the very fine ripples giving a smoother appearance than the rest of the plate.

Figure 3.69: Optical analysis of the wear track of plates processed at 155°C when worn with scratched pins.

Optical analysis of the 165°C plate seen in Figure 3.70 revealed similar surface features to the 155°C plate shown previously. Dark ripples were observed at the wear track edge, seen in Figure 3.70(a), and these were at times worn away and replaced with translational scratching as seen in Figure 3.70(d). Finer ripples were observed in the centre of the wear track as seen in Figure 3.70(b), however larger ripples were not present when there was only

pin rotation and no translation as seen in Figure 3.70(c).

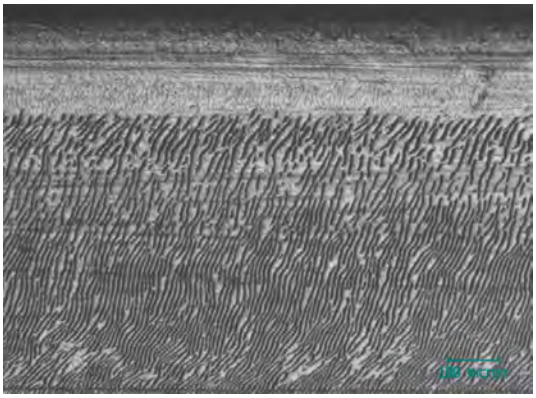

(a) Plate D5 at location 7 after 0.50 MC. Note the dark ripples at wear track edge.

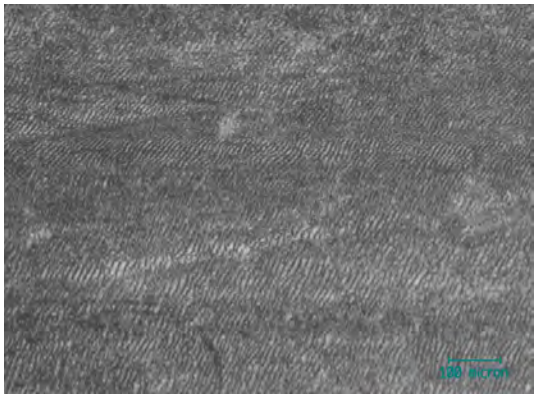

(b) Plate D6 at location 3 after 0.50 MC. Note the finer ripples at the centre of the wear track.

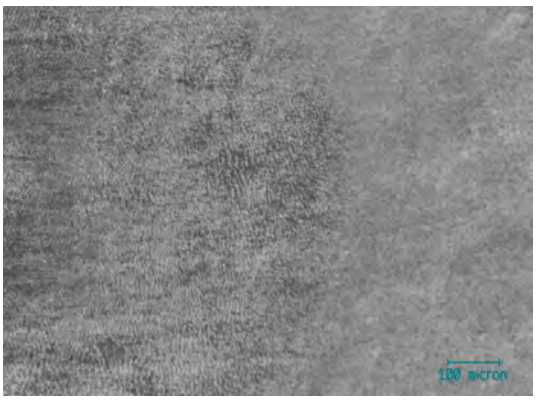

(c) Plate D5 at location 5 after 1.00 MC. Note that ripples stop where there would be no translation, only rotation.

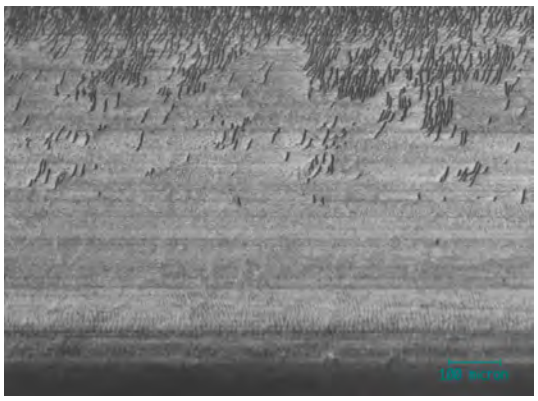

(d) Plate D5 at location 12 after 1.00 MC. Note the ripples being removed and replaced with translational scratches.

Figure 3.70: Optical analysis of the wear track of plates processed at 165°C when worn with scratched pins.

Surface analysis of the plate processed at 195°C revealed almost identical features to that of the plate processed at 165°C. However a few slight differences were observed and these are shown in Figure 3.71. A higher degree of burnishing was noted towards the wear track edge and the resistance to translational scratching appeared greater as illustrated in Figure 3.71(b). Also observed was a transitional area between this white burnished area and the dark finer ripples at the wear track ends as seen in Figure 3.71(a).

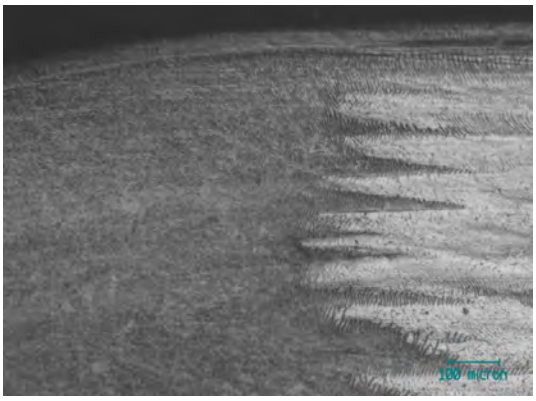

(a) Plate D5 at location 7 after 0.50 MC. Note the dark ripples at wear track edge.

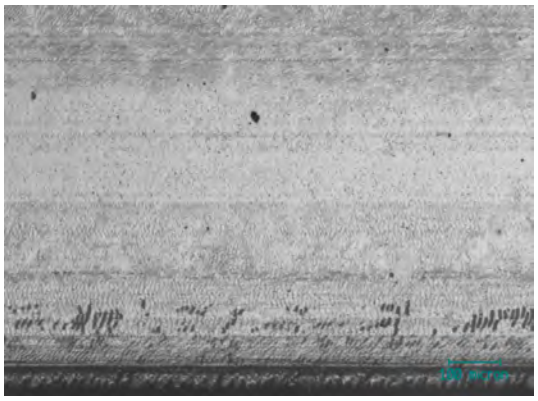

(b) Plate D8 at location 6 after 1.00 MC. Note a transitional are between very fine ripples and a white burnished like area.

Figure 3.71: Optical analysis of the wear track of plates processed at 195°C when worn with scratched pins.

3.5 Discussion

3.5.1 Lubricant Uptake

In the initial reproducibility test, the fluid uptake into the the UHMWPE control samples was monitored. It was observed that the samples soaked in lubricant at 37°C experienced a greater mass increase than those soaked at RT. A positive correlation was observed, although with a mean R^2 value of 0.533 the correlation can at best be described as weak. It should be noted that during the period of soaking, the ambient lab temperature RT was not explicitly controlled, therefore some environmental variation in temperature would be expected, therefore offering a possible explanation for the weak correlation. The increased fluid uptake of the samples soaked at 37°C could be attributed to two factors. Firstly the increased temperature could cause expansion of the polymer plates and consequently an increase in the free volume in the voids in the crystalline region. Creating a larger region in which the lubricant could ingress. Alternatively, or perhaps additionally, the increased temperature of the lubricant could reduce the viscosity and hence allow deeper ingress into the polyethylene plate. Increased lubricant uptake into UHMWPE at 37°C compared to RT has also been noted in a recent study on AMK tibial bearings (DePuy Orthopaedics Inc, Warsaw, IN) (Brandt et al., 2011) and a two-fold increase in fluid uptake into both irradiated and unirradiated UHMWPE discs when the soak temperature was 37°C compared to a soak temperature of 25°C (Blanchet et al., 2002). No hypothesis for this increased fluid absorption at increased soak temperature was given in either study.

The fluid uptake of the plates with varying molecular weights also revealed marked differences with the 5,000,000 g/mol and 9,000,000 g/mol control plates experiencing a greater mass increase due to immersion in fluid than the 600,000 g/mol control plate. Normalising this data with respect to the the 600,000 g/mol control plate indicated a linear increase in mass of the 5,000,000 g/mol and 9,000,000 g/mol plates. This links with density measurements which showed the 600,000 g/mol plate had a higher density of 0.950g/cm^3 compared to the 5,000,000 and 9,000,000 g/mol plates that had densities of 0.932 and 0.927 g/cm^3 respectively.

Analysis of the lubricant uptake in the test with plates of different processing conditions revealed indistinguishable fluid uptake trends between the two plates processed at 150°C and 175°C. However, density measurements also revealed a significant difference in density between the two plates with the plate processed at 150°C having a density of 0.947 g/cm^3 compared to the plate processed at 175°C which had a density of 0.930 g/cm^3, leading to a conclusion that it is the molecular weight of a polyethylene that is the biggest factor in determining its fluid uptake properties. The same two plates were also used in the scratched pin test, and again little difference in fluid uptake was found between them, confirming these initial observations.

Pin fluid uptake was monitored in the initial reproducibility test and was found to be negligible so was ignored for further tests. However, pin controls were still used to account for environmental changes when performing gravimetric analysis.

3.5.2 Reproducibility

The reproducibility test revealed differences in wear factors between supposedly identical materials and identical test conditions. The individual wear factors of the eight test plates ranged from 2.004 x10^{-6} mm^{3}N^{-1}m^{-1} to 2.999 x10^{-6} mm^{3}N^{-1}m^{-1}. This was an unexpectedly large range, the fact that this was UHMWPE manufactured by ram extrusion for industrial applications may be an explanation. For example, some plates may have come from the centre of the extruded rod, which commonly is less consolidated than the edges that would be in contact with the heating elements. Significant anisotropy in UHMWPE produced by ram extrusion has been noted previously (Kurtz et al., 2006). Inter-rig variability is another factor that cannot be ruled out. Slight differences in manufacture may contribute, and while every attempt was made to ensure reliable calibration, total confi-

dence can never be assumed. All test plates had an initial surface roughness with a mean value of 1.054μm consistent with the machining method used to create the plate geometry. In comparison the pin surface roughness was on average 0.021μm. As the harder material, this surface roughness was more important in influencing the wear factor than that of the softer UHMWPE material. By the end of the wear test a wear scar was clearly visible on all eight plates and had a burnished appearance with an absence of machining marks.

Comparison of the results with the literature is difficult due to the varying designs of simulator and methods used. For example in most tests reported at Durham 40N loads and 5mm diameter pins are used. This results in a contact stress of 2.04 MPa. At Leeds 3mm diameter pins are used with a loading of 80N. This results in a contact stress of 11.32 MPa. Higher contact stresses have been shown to give lower wear factors in a power law relationship, and variance of the loading at higher loads is less likely to cause big variances in the wear factor (Vassiliou and Unsworth, 2004). A notable difference in this set of pin on plate tests is that traditionally the pin is made from the softer material, whereas in the tests presented here the pin was made of the harder, metallic material, and the plate out of the polymer. However, as yet unpublished tests in the group revealed there was no significant difference between using a polished pin, or polished plate. The wear factor was purely dependent on the material combination. Additionally, in this thesis we are concerned with the wear of the UHMWPE surface. Using UHMWPE plates gave us a much larger wear scar area for analysis than if an UHMWPE pin was used.

3.5.3 Effect of Molecular Weight

The molecular weight of the polyethylene was found to affect the wear properties of the UHMWPE plates, with the greatest wear experienced by the plate with the lowest molecular weight of 600,000 g/mol. This was expected as it is known that a higher molecular weight. i.e. longer polymer chains, causes greater chain entanglement, which in turn improves the wear properties. However, it was found that the plate with the highest molecular weight of 9,000,000 g/mol, did not in fact have the best wear properties. In tests of acetabular cups with molecular weights ranging between 3 and 6 million g/mol little difference in wear rates was detected (McKellop et al., 1999). No literature could be found with published wear results for UHMWPE with a molecular weight greater than 6,000,000 g/mol. A potential reason being that this is the maximum molecular weight of the two most common resins

used in the orthopaedic market, GUR 1020 and GUR 1050. However, the results from this preliminary study indicate that by moving out of this range of molecular weights, there is a detrimental effect on the wear performance. Wear on the SS pins was found to be negligible.

The plates of different molecular weights exhibited visually different wear scars. Grain boundaries were visible on both the 5,000,000 and 9,000,000 g/mol plates, while none were found on the 600,000 g/mol plate. This is indicative of incomplete consolidation in the 5,000,000 and 9,000,000 g/mol plates. These visible grain boundaries have been termed 'Type 2 fusion defects' (Wu et al., 2002). Zygo scans revealed these grain boundaries were below the level of the visible grains. Rippling type features appeared to occur on the top of these grain surfaces and were orientated in a direction perpendicular to the translational motion, when sufficient wear had occurred to remove these rippling features, a burnished appearance was visible. These ripple features are thought to be caused by strain accumulation due to the repeated deformation of surface aspirates. and in tests on UHMWPE acetabular cups, the size of the ripples were determined by the roughness of the femoral head (Wang et al., 1995a). Plastic flow and deformation was observed on all plates, although most frequently on the 600,000 g/mol plate with large surface deformations detected using the Zygo interferometer. The lower degree of chain entanglement due to the lower molecular weight is thought to account for this increased plastic flow.

Surface roughness of the plate surfaces at the conclusion of the wear test was not able to differentiate between the three molecular weights, except for the central location (3) of the 600,000 g/mol plate, where the scan location fell on a large defect caused by plastic flow of the material. Other evidence of plastic flow was evident in raised particles of UHMWPE that appear to have adhered to the central wear track area. All other R_a values were lower than 0.5 μm, indicative of a generally burnished appearance, this value is approximately a 3-fold decrease on the initial surface roughness caused by the compression moulding process.

The pin surface roughness increased throughout the test. Evidence of pitting was found on the surface of the pins, possibly due to a combination of fatigue and corrosion. It is hypothesised that the material from these pits, then became trapped between the articulating surfaces, creating the circumferential scratching patterns seen on the optical micrographs. Thereby, causing an increase in the surface roughness.

3.5.4 The effect of processing conditions on the wear of UHMWPE plates

The dwell temperature during DCM of UHMWPE was found to affect the wear properties of the resultant plates. Of the four different processing conditions tested, the plates manufactured with a dwell temperature of 145°C and a dwell time of 30 minutes were found to have the highest wear factor of 4.362±0.535, and therefore, the poorest resistance to wear. Slight differences were observed in the wear resistance between the remaining three conditions, seen in Figure 3.43. In test 1 the 165°C 15 min plates had the second highest wear followed by the 195°C 15 min plates and finally the 155°C 30 min plates. However in the second test, the order in highest to least wear was 155°C 15 min, 165°C, and 195°C 15 min. This change of order was a possible indication of variability between the two rigs. The mean values of the two tests, seen in Figure 3.64, indicate that overall the plates processed at 195°C for 15 minutes had the lowest wear factor and hence the best wear performance. The plates processed at 155°C for 30 mins were the next best, followed by the plates processed at 165°C for 15 mins. This suggests that at similar temperatures, an increased dwell time also has an improving effect on elimination of type 2 fusion defects and hence a positive impact on the wear performance. It is accepted that the differences talked about here are small, but in biomedical applications, even seemingly small improvements in material design can potentially lead to large increases in implant survival.

This links well with observations made by Wu *et al* who found in tensile testing that specimens manufactured at 145°C had significantly lower elongation to break ratio than samples moulded at 155°C and above. This is the first study to examine the effect of molding temperature on the wear properties of DCM UHMWPE and as such it is impossible to compare the results with literature.

Evidence of the increased wear was clearly observed in the assessment of the articulating surfaces. Incomplete consolidation was visible in the plates manufactured at 145°C with type 2 fusion defects clearly visible and even material pull-out from the grain boundaries. Raised grain boundaries were also found, suggesting that complete grains had been pulled out from the surface. At the edge of the wear track, which is a particularly high shear environment, evidence of whole grain pull-out was seen. This rapid removal of material would account for the higher wear rates. Observations of the other processing conditions reveled better consolidated surfaces. Grain boundaries were visible, but no evidence of material removal from the grain boundaries was found, and the surfaces were worn in a far

more consistent way. Small ripples formed on the surface, and these were removed to leave a highly burnished finish. Some evidence of scratching was seen which is believed to be caused by 3rd body SS particles. Surface roughness measurements at the test conclusion showed high variability, but on average the roughness of the test plates was lower than that of the unworn controls.

3.5.5 The effect of a scratched counter-face

The circumferential scratching pattern achieved on the pin counterfaces was unique to this study, and was found to increase the wear factor of all the UHMWPE plates tested. The circumferential scratching pattern was chosen as it was believed a unidirectional scratching pattern on a rotating pin would be too severe. The mean R_a of the scratched pin surfaces was 0.903μm, compared to a mean R_a of 0.014 used in previous POP tests. This was a 64.5-fold increase in surface roughness. The wear factor increased approximately 100% for the plates manufactured at 155°C, 165°C, and 195°C and 50% for those manufactured at 145°C. Galvin *et al* also demonstrated increased wear factors of UHMWPE in POP tests when comparing scratched and smooth counter-faces. The increase in wear factor is due to an increase in abrasive wear, which is indicated by observations of the surface roughness. All test plates experienced an increase in surface roughness with the mean R_a of the four plates rising to 0.200 $\pm$ 0.071 μm from 0.060$\pm$0.038μm after just 0.5 MC. There was no difference in the surface roughness between processing conditions, but there was however a location dependance with the locations 1 and 5 having the lowest mean R_a and location 3 the highest. This is linked with the cross-shear on the plate. At the central location (3) this cross-shear is greatest as there is the combination of rotation and the peak velocity point of translation. At locations 1 and 5, the translational velocity is at a minimum. Observations using the optical microscope revealed a higher prevalence of translational scratches with all processing conditions, and there was clear evidence of grain pull-out in the centre of the wear track of samples manufactured at 145°C. A common feature amongst all plates is the absence of any adhesive deposits, both in the wear track centre or at the edges. Examples of rippling was common, with fine ripples mainly in the centre of the wear track, and larger ripples towards the edges. this difference in ripple size could be attributed to the fact that due to the rotation of the pin, the relative velocity between the two contacting surfaces is greatest at the edge of the wear track.

3.5.6 Summary

In summary, it has been demonstrated that the wear of DCM UHMWPE is dependent on the molecular weight of the original resin, and both the temperature and duration at which it was moulded. The surface roughness of the metal counter-face can also significantly affect the wear factor.

Chapter 4

Wear testing on the ProSim knee simulator

The ProSim Knee Simulator is a six station wear simulator designed to replicate the *in vivo* conditions of the knee joint, and can be seen in Figure 4.2. This enables TKRs to be placed in the simulator and their likely *in vivo* performance assessed. The simulator features four driven axes of motion, Flexion/Extension (FE), Axial Force (AF), Anterior/Posterior (AP) Displacement, and Tibial Rotation (TR). Abduction/Adduction (AA) is allowed and not constrained. The driven axes of motion and loading are shown in Figure 4.1. The simulator features two groups of three test stations. Group 1 is on the left when facing the PC and Group 2 is on the right. The individual stations are numbered left to right, from 0-2 on Group 1 and 3-5 on Group 2.

While standards do exist that list typical test conditions and processes for use in knee wear simulations BS ISO 14243, these are still general and not specific to a make or design of simulator. Therefore, significant time and effort was invested into translating the test standards for use in the Prosim knee wear simulator. This chapter discusses the calibration processes, fixation designs, test profiles, and experimental processes that were specifically developed for this simulator and the tested fixed bearing design Vanguard prostheses.

4.1 Calibration

The ProSim Knee Wear Simulator can be operated in a combination of displacement, force, or open loop control. Before each wear test was begun, careful calibration of the simulator

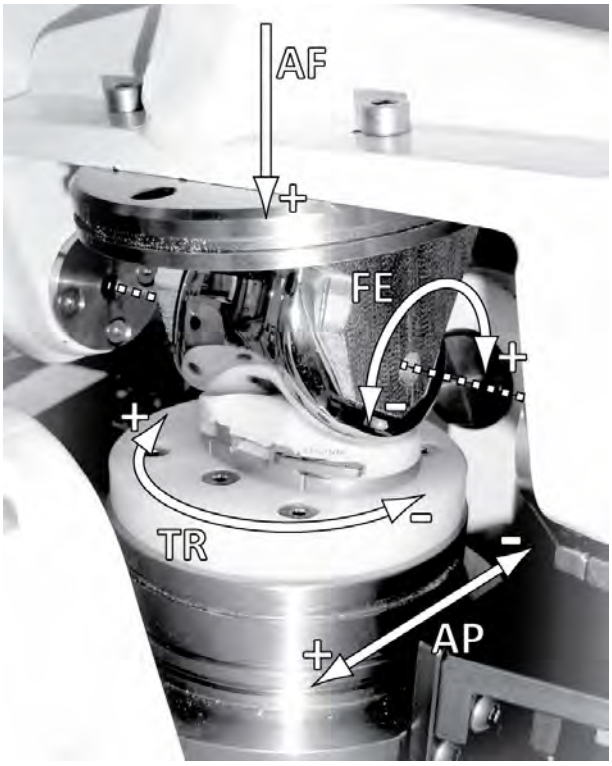

Figure 4.1: Driven axes of motion in the Prosim knee simulator articulating station. TKR is shown at approximately 35° of flexion.

Figure 4.2: The six station ProSim knee wear simulator.

stations was performed in order to ensure consistent results between stations.

4.1.1 Axial Force

Axial force is applied independently on each of the six stations by means of a pneumatic linear actuator. Each actuator is controlled by a computer controlled valve which can be run in either open-loop or force control. Feedback for the force control is provide by two load cells, one on station 1 and one on station 4. The supplied 'Kneesim' software was used to calibrate both the load cells and the individual pneumatic actuators. A detailed protocol was constructed in order to instruct users how to perform this calibration, this can be found in Appendix A.2.3.

4.1.2 Tibial Rotation

The internal/external rotation of the tibial component is achieved by the means of a linear pneumatic actuator connected to a rotary arm. It can be controlled in open-loop, displacement, or force control. Feedback for force control is again provided by load cells on stations 1 and 4, while feedback for displacement control is provided by an individual Linear Variable Differential Transformer (LVDT)s. A jig was constructed to enable calibration of each station at $\pm 5^\circ$, $\pm$-2.5°, 0° of tibial rotation. Again a detailed protocol was devised and this can be found in Appendix A.2.3. A home position alignment indicator was punched into each of the six tibial bearing cylinders to aid with future setup.

4.1.3 Anterior/Posterior

The displacement of the tibia components in the Anterior/Posterior direction is achieved through the use of six linear pneumatic actuators, each one directly attached to an AP translation sledge. The feedback for displacement control is provided by means of an LVDT positioned above the linear pneumatic actuator. Feedback for force control is by load cells on stations 1 and 4. Calibration of these LVDTs was conducted using a set of precision slip gauges. The gauges were placed between the anterior wall of the abduction/adduction cradle and the anterior edge of the AP translation sledge and the corresponding LVDT readout recorded. Twelve displacement ranging between 8.5mm and 30.0mm were obtained and the results used to calculate the displacement per ADC count. The home position of the AP translation sledge was set using a specially designed shaft and cup. The cup mounted

on the FE arm and located on the top of the shaft. The base of the shaft located in the AP translation sledge and due to the fixed FE axis this prevented movement of the sledge in the AP direction and hence the home(zero) position could be set in the software. This With the calibration shaft and cup inserted the home position of the FE arm could be set in the Medial/Lateral direction.

To enable quick calibration of the AP axis in the future, calibration rods were manufactured for each station that could be placed between the anterior edge of the AP translation sledge and the interior of the AA cradle. The larger end diameter was manufactured to calibrate the AP sledge to the zero home position, while the smaller end diameter was manufactured to calibrate the AP sledge to a home position 6mm to the anterior. This is to allow greater posterior displacements if required. The schematic for the six calibration rods can be seen in Appendix A.3.5.

4.1.4 Flexion/Extension

Flexion and extension of the femoral component is provided by two AC servomotors resulting in each group of 3 stations being capable of independent motion. Feedback to the servomotor is provided by two rotary encoders and optical switches are used to set the home position of the rotating shaft. These are fixed and cannot be adjusted. Adjustment of each individual FE cradle is possible through adjustment of the length of the linkage bar between each cradle and the rotating shaft. The home position of each FE cradle was set at 35°. This pre-set angle was incorporated into the design of the femoral mounts to ensure correct positioning.

4.2 Component Design

Mounts for the test components were designed and manufactured according to the British and International standard regarding wear testing of knee prostheses in a displacement controlled simulator (BS ISO 14243). The initial step was to define the FE axis of the Femoral component in accordance with the standard.

"...first considering the condyles of the femoral component in contact with an imaginary plane perpendicular to the tibial axis when the femoral component is at 30^0 and 60^0 of flexion, and then visualising four lines (contact normals) perpendicular to the imaginary plane running through the points where the two femoral condyles would contact the imaginary

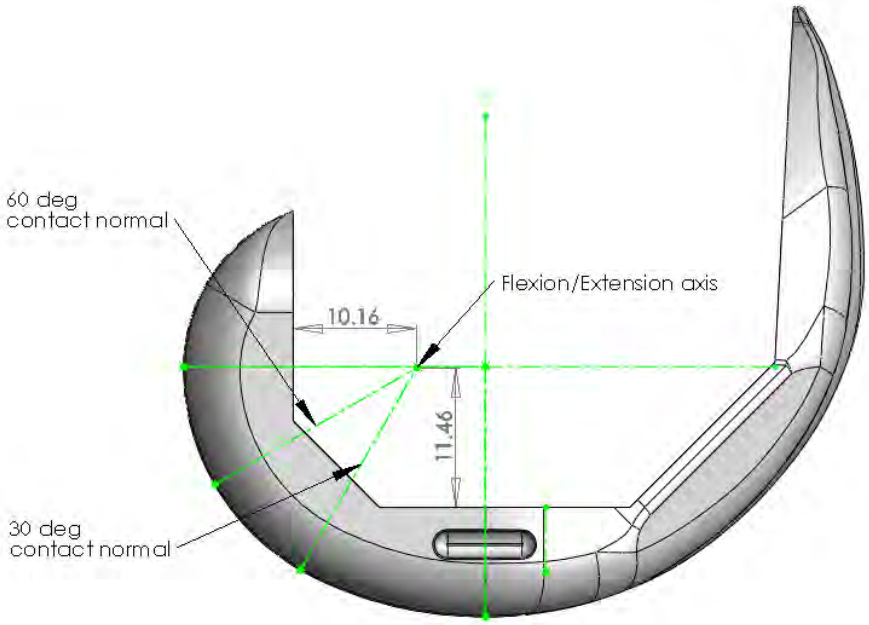

Figure 4.3: CAD model of Vanguard Femoral showing contact normals at 30° and 60° and FE axis. CAD model kindly provided by Biomet Ltd.

plane at each of these flexion angles. The flexion/extension axis is the line that would intersect all four contact normals."

This was achieved using Solidworks 2008 SP2.1 Computer Aided Design (CAD) package[1] and a electronic model of the femoral component supplied by Biomet. The four contact normals were connected using an intersecting line and this was defined as the FE axis as seen in Figure 4.3. This axis was then dimensioned from two reference surfaces as seen in Figure 4.3.

The standard also dictates that in order to obtain off centre loading, biased towards the medial condyle. The axial force axis is the...

"...line of action of the axial force taken to pass through a point on the tibial component of the knee joint prostheses which is offset by 0.07w ± 0.01w in the medial direction from the tibial axis, where w is the overall width of the tibial component..."

Again, using drawings supplied by Biomet the tibial component was found to have a width of 61.1mm resulting in a required medial offset of 4.28mm.

The final fixation mount design also included a 35° FE as this was the home position of the FE cradle. The femoral mounts were machined from Whale Brand Tufnol (Tufnol

[1] http://www.solidworks.com/

Composites Ltd., Birmingham, UK)[2] and the CoCrMo femoral components were affixed to the mounds using Dentine Cement (WHW Plastics, Hull, UK). The Tufnol mount was affixed to a stainless steel mounting plate by means of five stainless steel bolts and this was attached by 4 stainless steel bolts to the FE cradle.

The tibial mount was constructed from industrial grade UHMWPE. This was a 12mm thick disc that bolted to the stainless steel tibial plate by means of 4 stainless steel bolts. A section of the disc was removed to accommodate the stem of the tibial component. The tibial component was then cemented to the base using Dentine cement [3] (WHW Plastics, Hull, UK). The UHMWPE tibial insert was held in the tibial base by means of a titanium clip. This could be removed along with the UHMWPE tibial insert to allow for gravimetric analysis of the component.

4.3 Load Control Station Design

When testing the wear of arthroplasty components it is common to use one set of components as control samples that are just subjected to loads, but no motions. In many cases this means disabling the motions on one simulator station. In order to maximise the number of wear samples in this test, a novel load soak control station was designed with allowed all six stations to be used for wear samples.

The design specification required the control station to fully transmit the AF to the sample while restricting motion in the AP, FE, and TR axes. Two restricting rods were added either side of the component, so that FE, Tibial Rotation (TR), and AP displacement were restricted. Any movement on the FE axis was also restricted by the loaded contact between the flat surfaces of the Axial Force (AF) actuator and the AF spacer. A Computer Aided Design (CAD) schematic of the design can be seen in Figure 4.5. The control station was to be placed above one of the articulating stations directly below the linear pneumatic actuator providing the AF. The control sample was fully immersed in the test lubricant and was sealed inside a silicon gaiter identical to those used on the articulating stations. The load control station *in situ* can be see in Figure 4.6. For later tests in which two different types of component were tested concurrently in the same simulator, a second control station was built to enable a Load Soak Control (LSC) to be used for both types of component.

[2] http://www.tufnol.com/tufnol/default.asp?id=34
[3] http://www.whwplastics.com/ (Last accessed 18/11/2010)

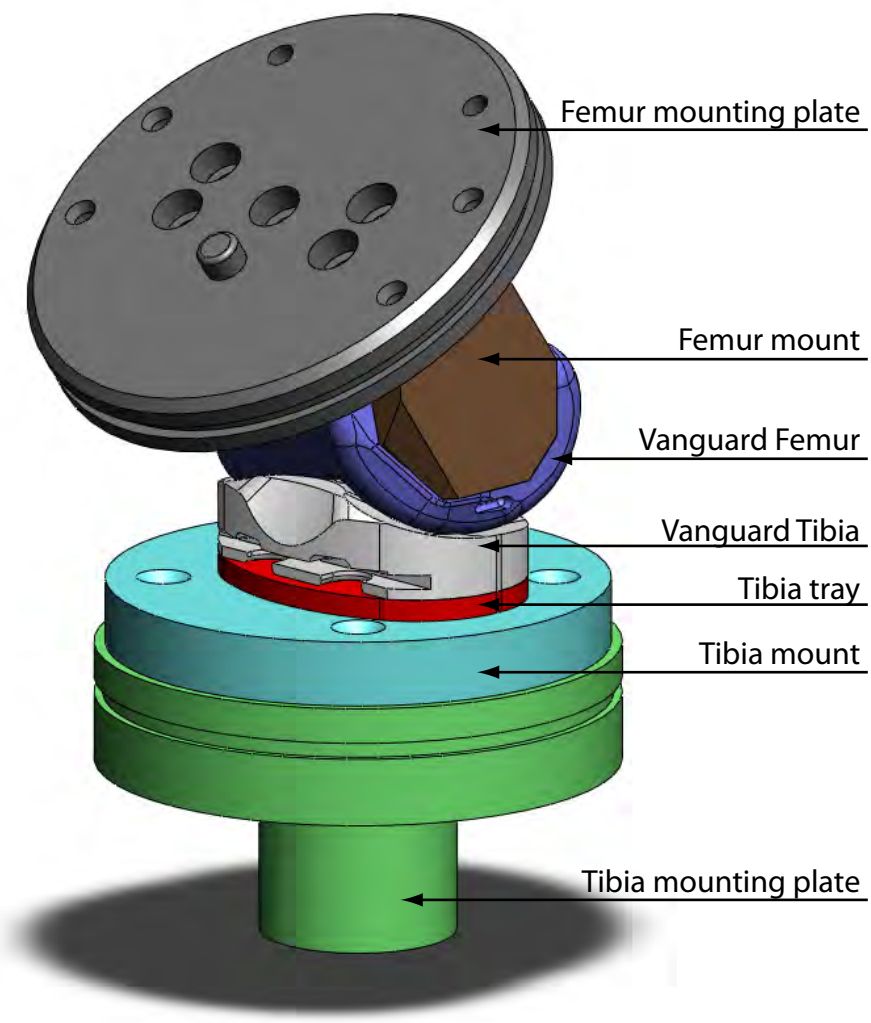

Figure 4.4: CAD schematic of station setup at home position.

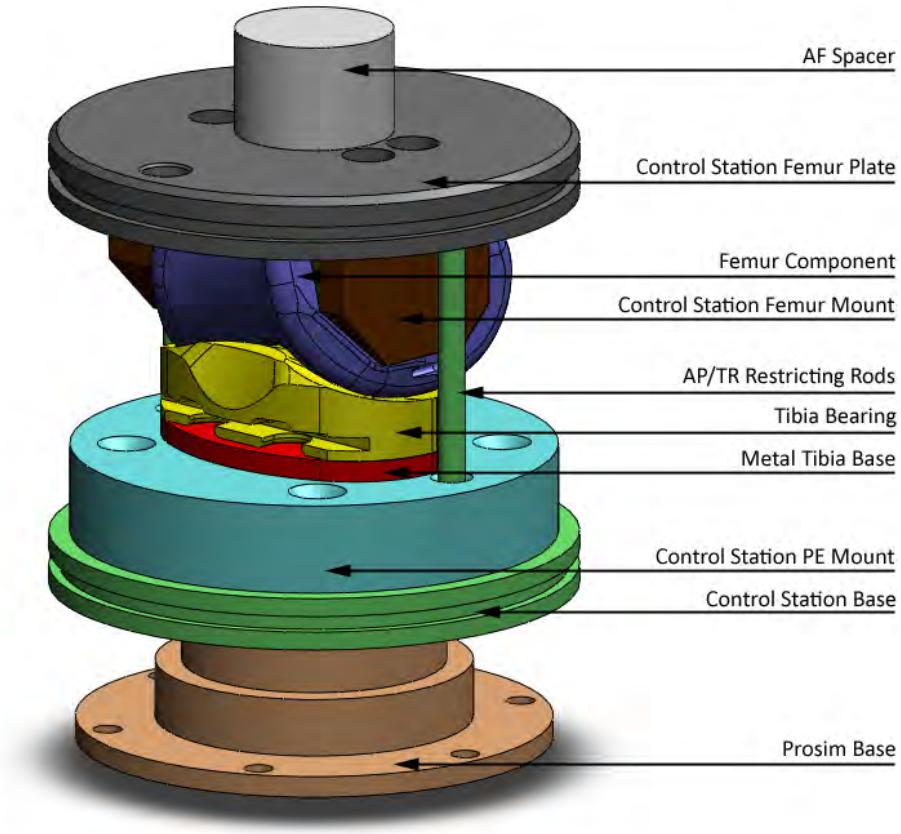

Figure 4.5: CAD schematic of the control station.

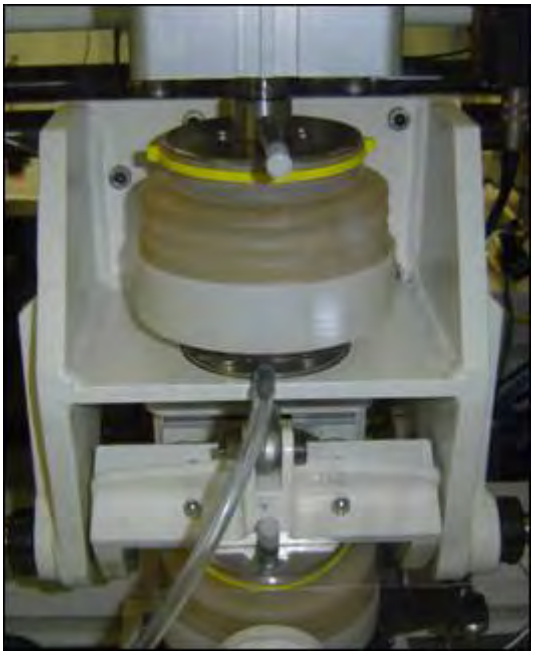

Figure 4.6: The load control station with gaiter *in situ*.

Full schematic drawings of the control station components can be found in Appendix A.3.3.

4.4 Simulator Setup

The Vanguard design Total Knee Replacement tested in this study consisted of three parts. A metal femoral component, a metal tibial component, and a Polyethylene tibial insert. From the outset of each test, each set of three components were kept tested together, i.e. it was always the same femoral component articulating against a given tibial bearing. The TKR sets were rotated around stations, in order to reduce any inter station variability. The specific intervals between rotations varied between tests, so specific details regarding this is presented in the relevant materials and methods sections.

A flexible silicon gaiter was placed over each TKR and secured onto the tibial stainless steel plate using a stainless steel cable tie. The gaiter was attached to the femoral plate using a plastic cable tie. This prevented any evaporation of the lubricant during the test. The gaiters were placed on the components while they were in a clean environment. The sealed unit was then transferred to the simulator in order to try to minimise the risk of any foreign bodies entering the test environment. The lubricant was administered to the components by means of a small plastic funnel.

Final alignment checks were conducted before commencement of the wear test. The tibial components were placed in the home position manually using the AP calibration rods and the TR home position indicator marks. The FE cradle holding the femoral component was placed at 35° to the horizontal. The Medial/Lateral (ML)clamping rings holding the FE cradle in place were then slackened off and tibial and femoral components allowed to come together and self centre. The ML clamping rings were then tightened. This was repeated for all six stations. In addition the periodic readings accessed through the kneesim software were checked to ensure that TR, AP displacements all confirmed that the stations were in the home position.

The lubricant used was New Born calf serum (Harlan UK) diluted with deionised water to a concentration of 25%. It was prepared in accordance with BS ISO 14243-3:2004. 0.2% 8g of sodium azide (NaN_3) was dissolved in the lubricant to prevent bacterial growth.

The Prosim simulator did not contain a facility to heat the lubricant to a desired level.

Therefore, any changes in the lubricant temperature were due to environmental conditions and frictional heating of the TKR components.

The wear tests were typically run at 0.5 million cycle intervals. Upon completion of an interval, the test components were removed from the simulator, whilst still sealed within the gaiter. The test lubricant was emptied from the gaiters and was retained and frozen for future analysis by the research group. The retaining clips were removed from the tibial mounts and the polyethylene inserts were carefully removed. Cleaning and gravimetric assessment details are outlined in the relevant materials and methods sections and were all conducted in accordance with the ISO standard (BS ISO 14243).

The gaiters and mounts were cleaned with water and neutracon solution and left to air dry ready for the commencement of the next test interval. The femoral components were carefully rinsed in a stream of water and left to air dry. If imaging of the surfaces was required, they were carefully cleaned with a lint free cloth and propan-2-ol.

The total test durations were different for all tests run, but were based on the findings of 111 patients, that on average, patients who have received a hip or knee replacement take approximately $0.9\text{x}10^6$ steps per year. However, within this average, it is possible to have patients taking up to $3.2\text{x}10^6$ steps per year (Schmalzried et al., 1998).

4.5 Test Profiles

Test profiles are input to the simulator in the form of tab-delimited data files. As previously stated it is possible to assign independent demand profiles of AP, AF, and TR for each individual station and independent demand profiles of FE for each group of 3 stations. Or conversely, it was possible to have a common profile operating across all six test stations. each individual station.

4.5.1 Demand profiles for wear testing

The profile for axial loading was taken from BS ISO 14243-3:2004 Implants for surgery - Wear of total knee joint prostheses. This data was presented as 100 data points so a simple linear interpolation was used to convert this to 128 data points as required by the Prosim knee simulator. Similarly, the FE profiles were also taken from the ISO and the same linear interpolation was used to convert the data to the required number of data points. Plots

of these two profiles can be seen in Figure 4.7. AP and TR displacements were based on those found in the natural knee (Lafortune et al., 1992). The profiles of tibial drawer and internal/external rotation were converted from a graphical figure to tabular values using Enguage Digitizer ver. 4.1.[4]. Plots of these demand profiles can be seen in Figure 4.8.

Lafortune profiles for AP and TR were selected as they contained higher kinematics than those defined in the ISO standard for displacement controlled simulators, and it was therefore felt that this would result in a test that was more relevant to the needs of a younger, more active patient. The higher kinematic profiles have been shown to significantly increase wear rates of UHMWPE tibial bearings (Barnett et al., 2001). FE data was identical for both the ISO and Lafortune profiles so no decision on which to use was needed. AF data was taken from the ISO standard as no force data was presented in Lafortune's work. A similar combination of profiles has been used previously, albeit with a different interpretation of the direction of AP displacement than used in this study (Barnett et al., 2001). The different interpretations arise because the amount of tibial drawer in the Lafortune study is measured from the vertical femoral axis, whereas in the Prosim knee simulator, the tibial drawer is measured from the FE axis of the femur These two reference locations on the femur are in different locations and therefore it may not be completely accurate to drive the simulator with the Lafortune profiles. However, presently there is little kinematic data available for the human knee joint, so there is little alternative. Other studies have reversed the AP direction as it was believed that this would result in a more anatomically relevant wear scar, however in this thesis, the AP direction was kept consistent with that defined by Lafortune. This mainly posterior translation of the tibia with respect to the femur is also consistent with the direction specified in the ISO standard BS ISO 14243.

4.5.2 Response profiles

The displacements and loads on each station were recorded once every 1000 cycles throughout all wear tests. So for a 5x10^6 cycle wear test this resulted in 5000 cycles being recorded for each of the five articulating stations. This data was output in a tab delimited format, with additional text strings detailing dates, times, and the cycle number for the particular profile. In order to be able to interpret the data using Matlab, the text strings were converted to tab delimited data using a conversion script. The response profiles of the Prosim

[4]http://digitizer.sourceforge.net

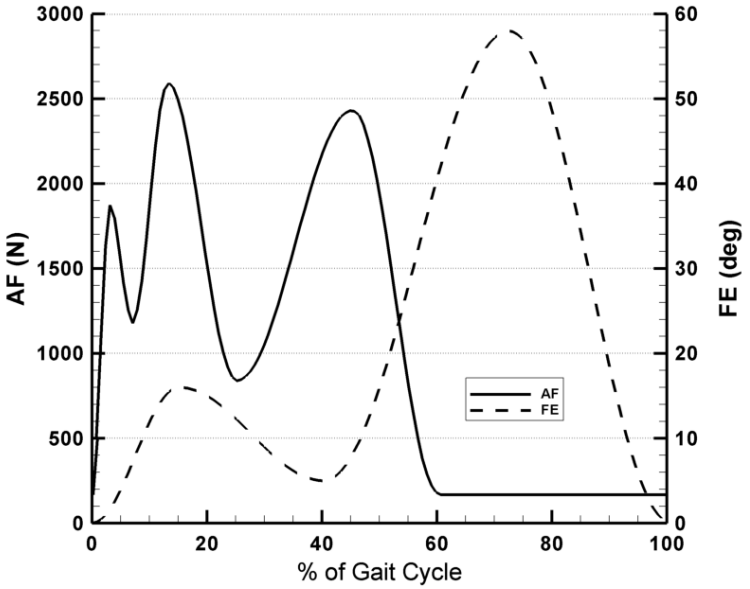

Figure 4.7: AF and FE demand profiles from ISO.

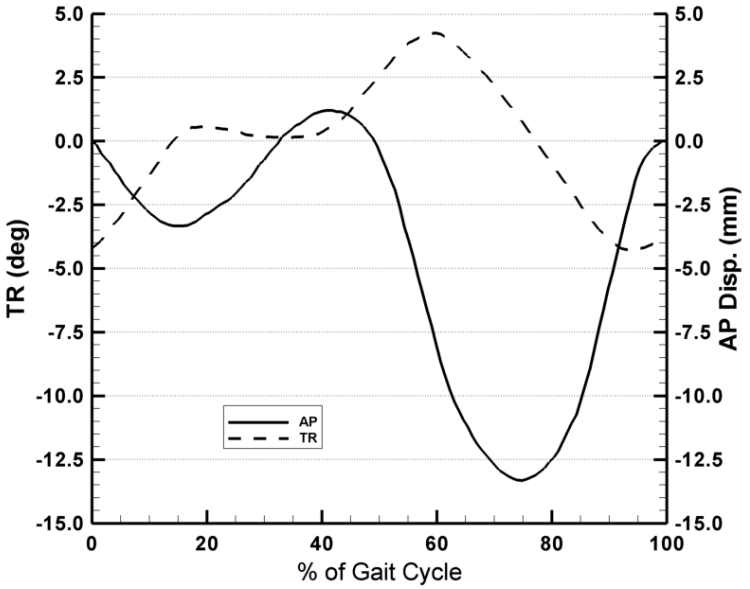

Figure 4.8: AP and TR profiles from Lafortune (Lafortune et al., 1992).

knee simulator are presented in the relevant results sections of each test.

Chapter 5

ArCom® non-crosslinked UHMWPE

Direct Compression Moulding has been proposed as a superior form of processing UHMWPE for use in TKR. The ArCom® process is a variation on this developed by Biomet (Warsaw, IN). The main aim in this chapter was to assess the potential *in vivo* performance of the ArCom® UHMWPE in a more active patient.

5.1 ArCom Wear Test

The six station Prosim knee simulator previously described in Chapter 4 was used to conduct a 5x10^6 cycle wear test to evaluate ArCom® UHMWPE wear properties in the Vanguard fixed bearing design. 5x10^6 cycles is considered to be approximately equivalent to 5 years of service *in vivo* (Schmalzried et al., 1998).

5.1.1 Materials and methods

The simulator was set up as described in Chapter 4. 5 stations were used and each station contained a Vanguard design TKR (Biomet UK Ltd.) with a cruciate retaining cobalt chrome (CoCr) as cast Femoral component articulating against an ArCom® UHMWPE tibial bearing. The ArCom® brand name denotes that the component is direct compression moulded in the presence of Argon. The bearing was held in a cobalt chrome molybdenum (CoCrMo) I-Beam one piece tibial tray using a sprung titanium clip. The components were mounted anatomically and were all left TKRs with a tibial bearing thickness of 10mm and

width of 63mm.

In order to take account of continuing lubricant uptake in to the UHMWPE, two control tibial components were used. One load soak control and one soak control. The load soak control was mounted in the novel load soak control station described in Section 4.3. The load soak control components were identical to those used in the five articulating test stations. The soak control tibia was mounted in the same one piece I-Beam tibial tray as the five test specimens. This was to ensure the surface area of UHMWPE exposed to the lubricant was consistent amongst all samples, as it has been noted in other studies that fluid sorption of UHMWPE is affected by both material type and surface area (Klapperich et al., 2000).

Prior to the wear test, the UHMWPE tibial inserts were soaked in a sealed container full of the test lubricant in order to try and minimise errors caused by fluid uptake of the lubricant. The tibial inserts were gravimetrically assessed at 5 day intervals in order to ascertain the mass gain. After weighing, they were immediately returned to soak. The 7 UHMWPE tibial bearings were left in soak until they exhibited a similar fluid uptake trend. This amounted to a total of 55 days in soak.

The wear test was run at 1Hz for a total of $5x10^6$ cycles, which is equivalent to approximately 5 years of service *in vivo*. At $2.5x10^5$ cycle intervals for the first $1.0x10^6$ cycles and then at $5.0x10^5$ cycle intervals thereafter, the UHMWPE inserts were removed from the simulator. They were cleaned as per the protocol in Appendix A.2.1.2 then gravimetrically assessed using a Mettler Toledo AX205 balance, which was accurate to 0.01mg. The tibia components were weighed in turn until three values were obtained for each component that were within a 0.1mg range in accordance with the ISO standard. The mean of these three values was then used as the mass of each tibia component. Volumetric wear of the UHMWPE was calculated using a density of $0.935g/cm^3$ which was obtained experimentally using a Mettler Toledo AX205 balance and accompanying density kit. At each $5.0x10^5$ cycle interval, the used lubricant was removed and retained for future analysis. It was replaced by fresh lubricant. To reduce the effect of inter-station variability, the TKRs were rotated around the stations at each $5.0x10^5$ cycle intervals. The locations of the individual components are shown in Table 5.1.

Assessment of the bearing surfaces was carried out using two methods. Firstly, an optical microscope fitted with a FireWire camera was used to observe the changes to the surface of the UHMWPE tibial components. Prior to testing and after $5.0x10^5$ cycles, this was

	0.0-0.5 MC		0.5-1.0 MC		1.0-1.5 MC		1.5-2.0 MC		2.0-2.5 MC	
	2.5-3.0 MC		3.0-3.5 MC		3.5-4.0 MC		4.0-4.5 MC		4.5-5.0 MC	
Station	Fem	Tib	Fem	Tib	Fem	Tib	Fem	Tib	Fem	Tib
0	5	5	2	2	6	1	3	7	4	6
1	4	6	5	5	2	2	6	1	3	7
2	3	7	4	6	5	5	2	2	6	1
3	6	1	3	7	4	6	5	5	2	2
4	2	2	6	1	3	7	4	6	5	5
5	NA	NA	NA	NA	NA	NA	NA	NA	NA	NA
LSC	7	4	7	4	7	4	7	4	7	4
SC	-	3	-	3	-	3	-	3	-	3

Table 5.1: Tibia(Tib) and Femoral(Fem) combinations and locations during 5.0x10^5 cycle wear test. Load soak control(LSC) and soak control(SC) are also shown for reference.

performed at random locations on the tibia component, with the majority of observations occurring in the apparent wear scar. From 2.5x10^6 cycles onwards, a custom built jig was used to enable the same location on the tibial bearing surface to be imaged at each removal from the simulator. Schematics can be found in Appendix A.3.5. Consequently, the variation in the bearing surface was catalogued between 2.5x10^6 and 5.0x10^6 cycles at 5.0x10^5 cycle intervals. The exact locations at which the optical micrographs were taken are shown in Figure 5.1. The apparent wear scars were also monitored, with the visibly worn area manually outlined and digitally photographed after both 2.5x10^6 and 3.0x10^6 cycles. Additionally, The area of each wear scar was then quantified using PixeLINK image processing software [1]. Additionally the backside of the tibias was also imaged as relative movement between the UHMWPE tibial insert and the fixed tibial base has been reported (Ash et al., 2003). The femoral components were imaged at random locations prior to testing and after 3.0 MC.

Secondly, a white light interferometer (Newview 100, Zygo, Middlefield, Connecticut, USA) was used to assess the changes in surface roughness at varying intervals during the test. For the tibia components, 5 readings at randomly selected locations were taken on both the medial and lateral articulating surfaces, giving a total of 10 readings per tibia. This

[1] http://www.pixelink.com/

was conducted prior to the test start (0 cycles) and after 0.25, 3.5, 4.0, 4.5 and 5.0 MC. 2 readings were taken on each articulating surface (total of 4 per tibia) after 0.5, 0.75, 1.0, 2.0, and 3.0 MC. For the femoral components, one randomly located reading per condyle (2 in total) was taken prior to the test start and then 5 readings per condyle (10 in total) were taken after 3.0, 4.0 and 5.0 MC. A cylinder of best fit was removed from the plot as to minimise the effect of the predetermined geometry of the femoral and tibial component on the R_a readings. Upon completion of the 5.0 MC wear test, the bearing surface of both the least worn (tibia 6), and the most worn (tibia 2) samples were analysed in detail using the Zygo white light interferometer. The 19 locations on tibia 2 (Figure 5.1(b)) and the 12 locations on tibia 6 (Figure 5.1(d)) were all imaged to enhance the optical micrographs collected after $5.0x10^6$ cycles with morphological data.

5.1.2 Results

The results from the initial soaking of components and the $5.0x10^6$ cycle wear test are shown in the following section. The results are discussed at the end of the chapter.

5.1.2.1 Fluid Uptake

Initial soaking of the 7 test components was performed to equalise the fluid content in the samples. The soaking was continued until all soak samples exhibited a similar mass change trend. This equated to 55 days in soak. The individual mass change for the plots can be seen in Figure 5.2. Tibias 1 and 2 both exhibited a different initial trend to the other 5 tibias. This was due to them being used in the initial setup of the simulator and for component design. Vaseline was used as a lubricant for these early setup tests and as a result a residue may have been left on the exterior surfaces. From 25 days of soaking onwards, tibias 1 and 2 exhibited a similar trend to the other 5 samples. It is thought that by this time all contaminants affecting the fluid uptake had been removed. The rates of fluid uptake for tibias 3 and 4 that later were used as the soak controls in the wear test can be found in Table 5.2.

5.1.2.2 Wear Data

Upon completion of $5x10^6$ cycles, the two soak control samples had both experienced a mass gain caused by lubricant uptake. Specifically, 3.41mg for the loaded soak control and

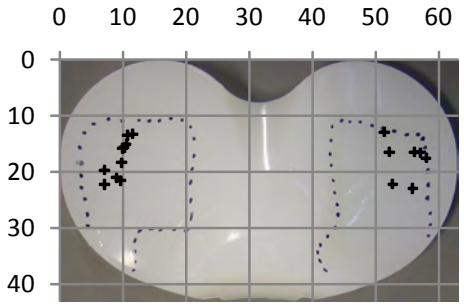

(a) Optical imaging locations on ArCom® tibia 1.

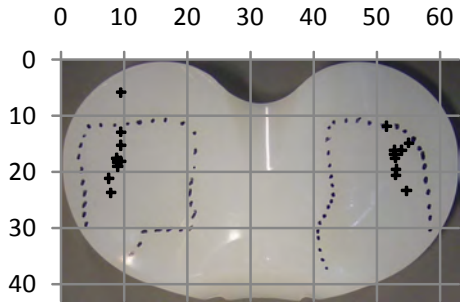

(b) Optical imaging locations on ArCom® tibia 2.

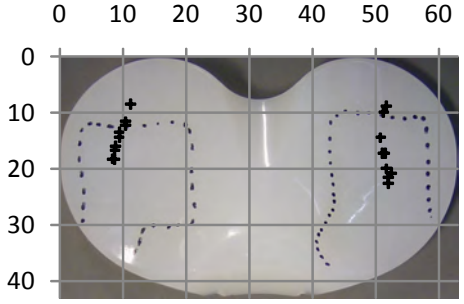

(c) Optical imaging locations on ArCom® tibia 5.

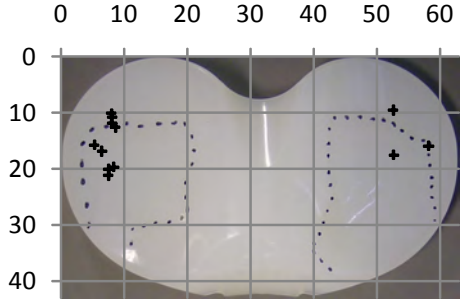

(d) Optical imaging locations on ArCom® tibia 6.

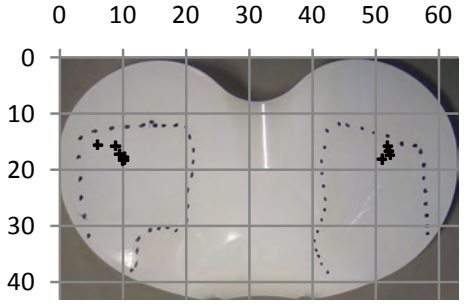

(e) Optical imaging locations on ArCom® tibia 7.

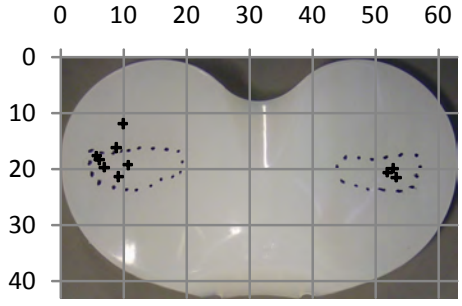

(f) Optical imaging locations on ArCom® tibia 4 (Load soak control).

Figure 5.1: Optical imaging locations on the ArCom® test tibia. Black crosses indicate exact locations imaged at 2.5x10^6 cycles then at every 5.0x10^5 cycle interval up to a total of 5.0x10^6 cycles. The dotted outlines are the visibly worn areas on each respective tibia after 3.0x10^6 cycles.

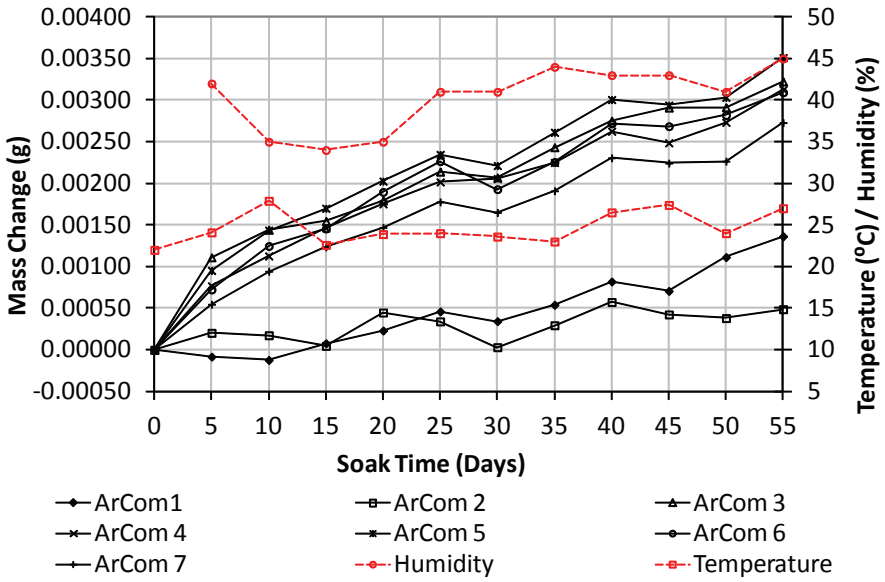

Figure 5.2: Fluid uptake of ArCom samples. Humidity and temperature at the time of gravimetric assessment are also shown.

1.38mg for the unloaded soak control. The absolute mass change of the two control tibias (3 and 4) both throughout the initial soak period and the wear test can be seen in Figure 5.4. During the initial soak the two soak controls remained tightly grouped in their fluid uptake trends. Upon the start of the wear test the two controls diverge, due to tibia 4 being loaded whereas tibia 3 is not. The relative difference between the two controls is shown in Figure 5.5. Here a clear linear relationship due to the loading of tibia 4 can be seen. The numerical values for all linear trend lines can be found in Table 5.2. The novel load soak control station performed as expected during the wear test with there being no visible motion between the femoral and tibial components. The mean volumetric wear rate (± one standard deviation) of the 5 articulating components, compensating for lubricant uptake of the load soak control was 6.46±1.80mm^3 per 1x10^6 cycles. The volumetric wear rate was calculated by combining the gravimetric measurements and a density value of 0.935 g/cm^3. The individual volumetric wear plots for the respective tibias can be seen in Figure 5.3. The 5 articulating tibias all experience a volume loss due to wear, however it is interesting to note that the wear of tibia 6 was approximately half that of the other 4 components despite rotating the TKRs around the 5 stations. Omitting tibia 6 from the mean volumetric wear calculation gives a value of 7.20±0.88mm^3 per 1x10^6 cycles.

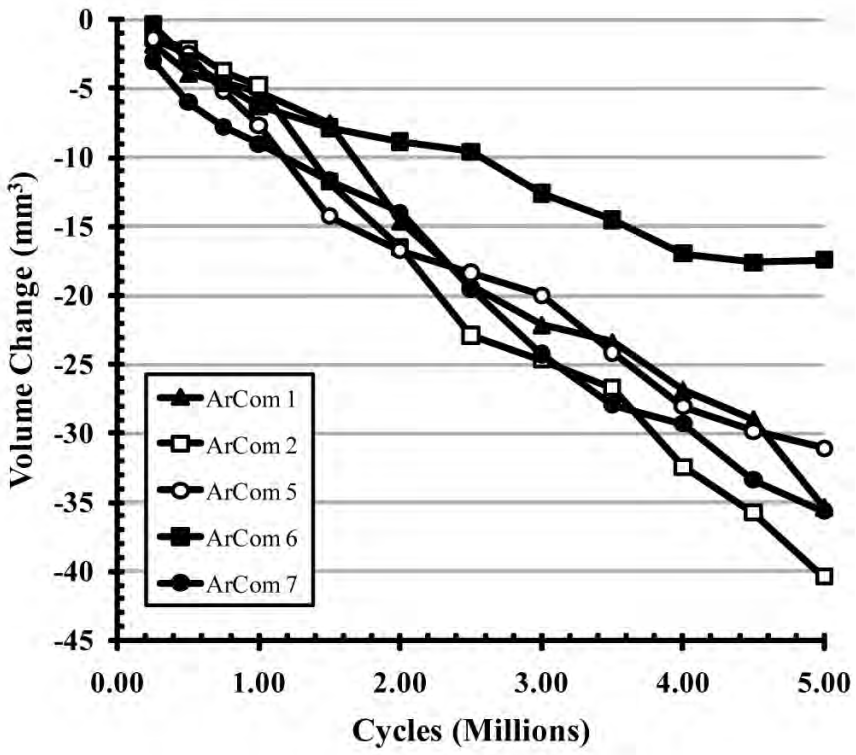

Figure 5.3: Volumetric wear plots of the five ArCom® tibias corrected with respect to the LSC.

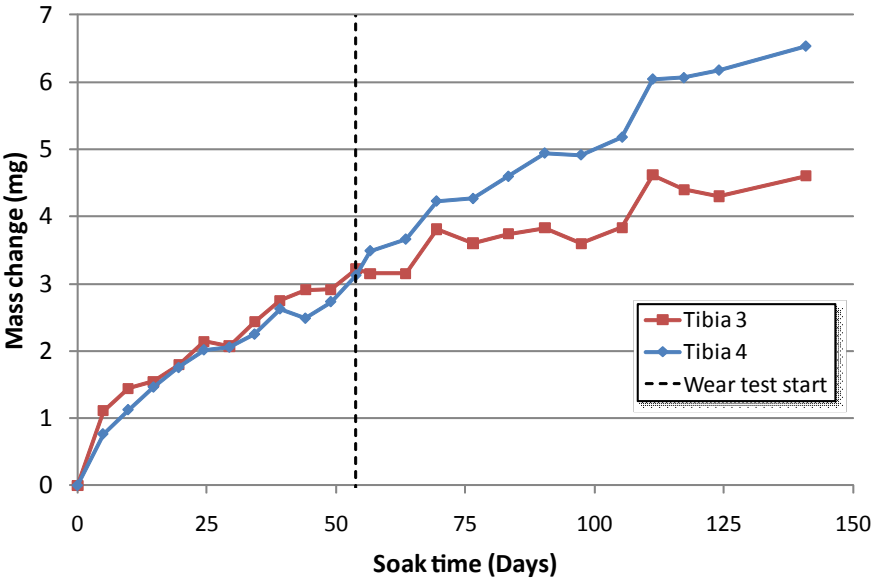

Figure 5.4: Absolute mass change of the two control tibias throughout both the initial soaking period and during wear test.

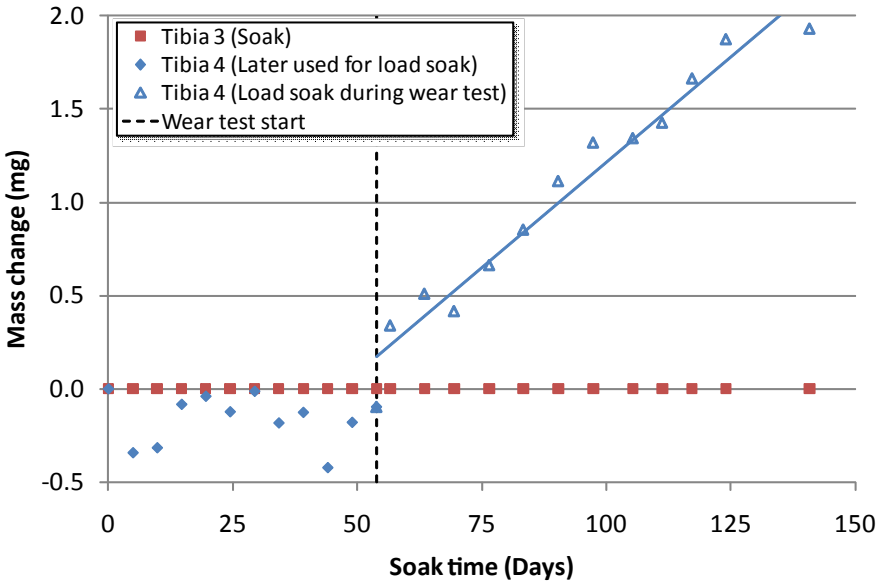

Figure 5.5: Relative mass change of the LSC (tibia 4) relative to the SC (tibia 3).

		3 (Soak)	4 (Load Soak)	4 relative to 3
Initial soak	mg/day	0.04224	0.04322	
	mg/hour	0.00176	0.00180	
	R^2	0.982	0.962	
Wear test	mg/day	0.01714	0.03834	0.02119
	mg/hour	0.00071	0.00160	0.00088
	R^2	0.792	0.962	0.966

Table 5.2: Fluid uptake rates for the ArCom® control tibias.

Station		0	1	2	3	4
AP Disp.	P	200	160	170	100	170
	I	1000	1000	1000	1000	1000
	D	100	100	100	100	100
TR Disp.	P	140	220	170	250	270
	I	500	500	500	500	500
	D	5	5	5	5	5

Table 5.3: PID Values for ArCom® wear testing.

Station	0	1	2	3	4
AP mm/ADC	0.0003711	0.0003287	0.0003512	0.0002646	0.0003462
AP Zero Disp. Offset	-5.46	-6.78	-5.12	-4.31	-7.92
TR °/ADC	0.0002201	0.0003505	0.0002978	0.0003661	0.0003432
TR Zero Disp. Offset	-0.7995924	0.9969632	0.8585027	0.1294384	0.4834549
AF Valve per N	0.055332	0.054887	0.055766	0.057188	0.056428
AF Valve Offset	0.226825	-2.542081	3.291981	0.041965	0.115496
AF Loadcell N/ADU	-	0.076295	-	-	0.078115
AF Loadcell Offset	-	-85.078627	-	-	-50.196001

Table 5.4: Calibration constants for ArCom® wear testing.

5.1.2.3 Simulator Setup and Response

The measured response profiles of the ProSim Knee Simulator are presented in this section. These were produced using logged data from the simulator and a Matlab script as described in Section 4.5.2. The Proportional-Integral-Differential (PID) values with which these plots were obtained are shown in Table 5.3 and the calibration constants are shown in Table 5.4. For all plots, the solid black line with circular markers represents the demand profile. The grey area represents the plotting of all the individually recorded profiles, therefore showing the full range of profiles. The dashed black lines are the mean response of each individual station. Finally, the thicker black line represents the mean response of all stations, in this case 5 of the possible 6 stations were used.

The FE demand and response of the simulator can be seen in Figure 5.6. The response profile followed the demand profile with high accuracy due to the fact it was motor controlled.

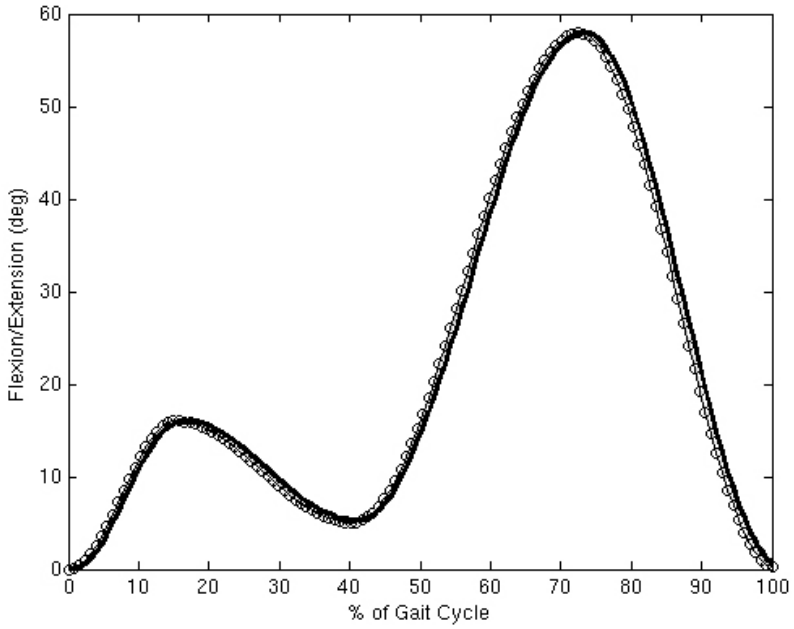

Figure 5.6: FE demand and response during ArCom® Wear test. Data was recorded 1 in every 1000 cycles. The circled black line indicates the demand profile. The grey area comprises of the individual plots of all recorded response profiles from all stations. The dashed black lines indicate the mean responses of each measured station. The heavy black line indicates the mean response of all recorded stations.

The AF response can be seen in Figure 5.7. The initial peak of 1.8kN was somewhat lost, however the two peak loads of 2.6kN and 2.5kN were achieved within tolerances. However, there was a time delay between the demand profile and achieved profile caused by the pneumatic lag of the loading cylinder. This was estimated to be 5% of one cycle or 0.05 seconds. There were no observed differences to the the two groups of stations recorded.

The tibial rotation response is shown in Figure 5.8. Here, the response profile mainly followed the demand profile with minimal high frequency oscillation. However, the mean peak-to-peak amplitude of all five stations was approximately 6.5° compared to the demand of 8.5°.

The AP displacement demand and response profile is shown in Figure 5.9. This profile proved to be the most difficult to achieve due to the fine levels of control required. A mean posterior displacement of 12mm in the swing phase was achieved compared to the demand of 13mm. However the 4mm posterior to anterior shift found in the stance phase was not obtained with any definition, a possible explanation being that the maximum force capable of being exerted by the AP pneumatic cylinder was not sufficient to act against the

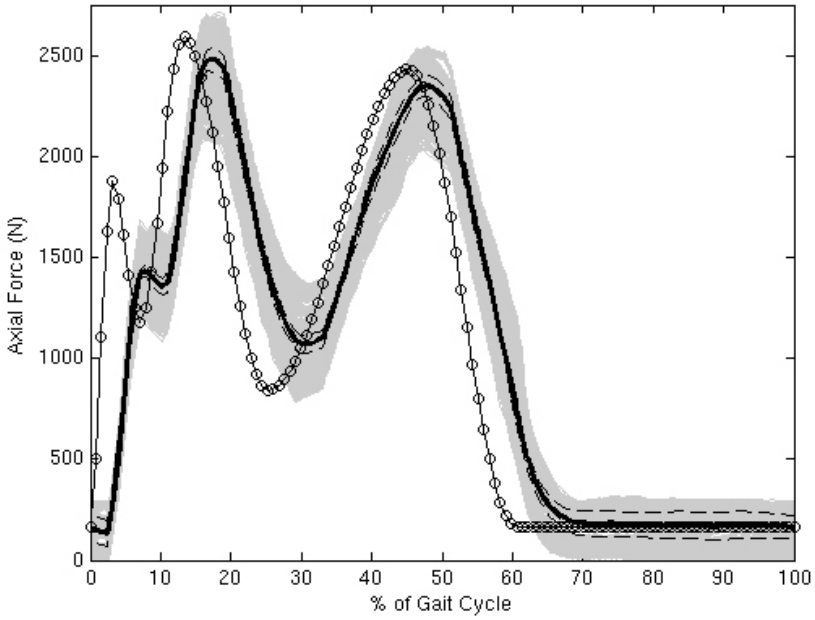

Figure 5.7: AF demand and response during ArCom 5x10^6 cycle wear test. Data was recorded 1 in every 1000 cycles. The circled black line indicates the demand profile. The grey area comprises of the individual plots of all recorded response profiles from all stations. The dashed black lines indicate the mean responses of each measured station. The heavy black line indicates the mean response of all recorded stations.

friction between the femoral and tibial components caused by the 2.6kN of AF. This was confirmed as a simulator limitation when additional tests with no axial loading obtained a good following of the demand profile in both the stance and swing phases as can be seen in Figure 5.10. Similar to what was observed with the AF response profile, there was a time delay between the demand and the AP response profile due to a pneumatic delay.

5.1.2.4 Surface Analysis

Both the Arcom tibias and the CoCrMo femurs were analysed using both the optical microscope and Zygo white light interferometer.

There was no observable change in the surface of the soak control tibia, indicating that the lubricant and cleaning process have no detrimental effects. Figure 5.11 shows zygo and optical micrographs of the soak control, both prior to the wear test starting and upon conclusion of the wear test. The average surface roughness of the soak component at the test start calculated from 10 points on the surface was 0.103±0.021μm, and on conclusion of the 5.0x10^6 cycle wear test it had remained at 0.083±0.019μm. The mean surface roughness

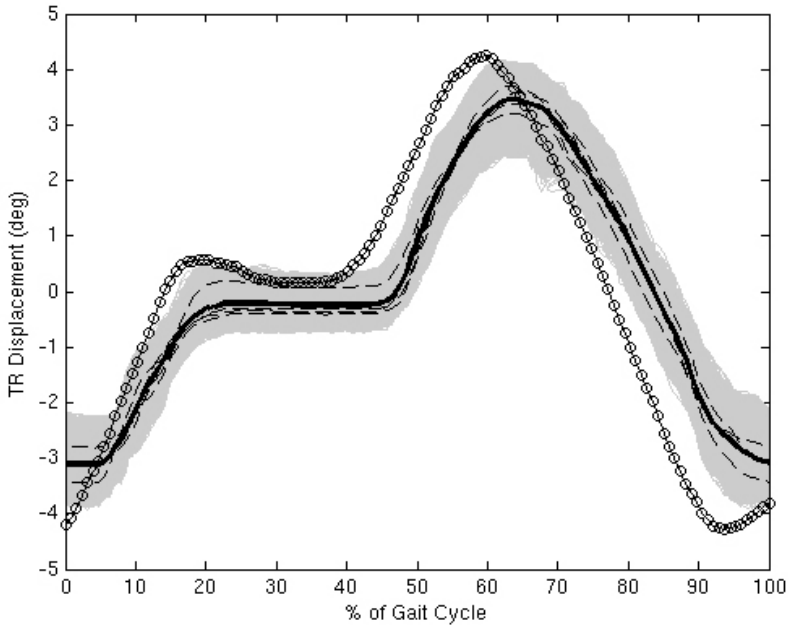

Figure 5.8: Tibial rotation demand and response during ArCom® wear test. Data was recorded 1 in every 1000 cycles. The circled black line indicates the demand profile. The grey area comprises of the individual plots of all recorded response profiles from all stations. The dashed black lines indicate the mean responses of each measured station. The heavy black line indicates the mean response of all recorded stations.

of all measured points throughout the whole wear test was 0.092±0.021μm. This can be seen graphically in Figure 5.14.

The load soak control also remained largely similar throughout the wear test. The initial surface roughness was 0.095±0.038μm, and at the conclusion of the test it was 0.091±0.061μm. The mean roughness for all points recorded during the whole test was 0.091±0.052μm. Analysis using the optical microscope revealed surface features, mainly around the edge of the contact between the tibia and femur. A selection of the these observations can be seen in Figure 5.12. Figure 5.12(b) shows splits in the surface, thought to be caused by the cyclical loading.

Analysis of the contact surface of the Load soak tibia (4) using the Zygo white light interferometer is shown in Figure 5.13. The area of tibia not in contact with the femur showed no change in surface features and remained similar to the surfaces of tibia 3 shown in Figure 5.11. However, observations around the boundary of the contact area (outlined in Figure 5.1(f)) showed some morphological damage that consisted of trenches running in both the ML and AP directions. It is thought that these trenches were caused by fatigue due

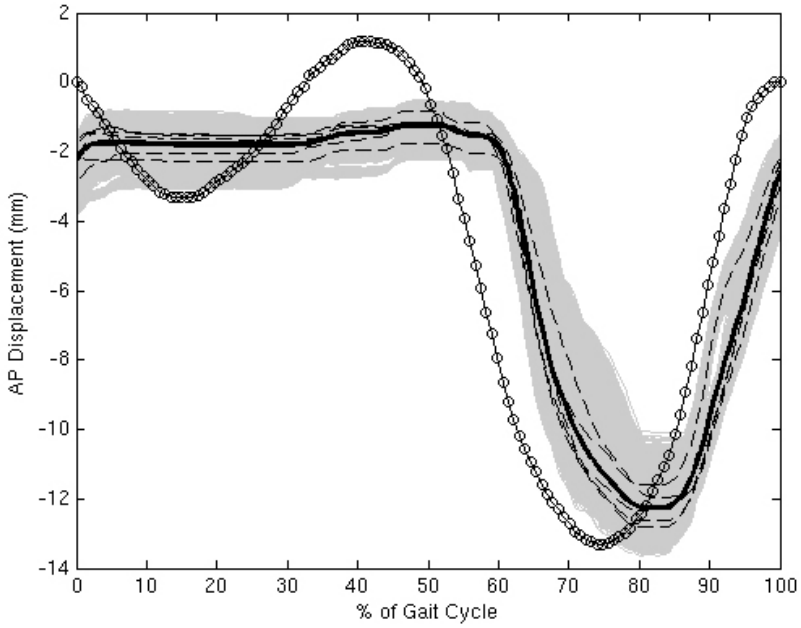

Figure 5.9: Anterior Posterior Demand and response during ArCom® wear test. Posterior displacement of the tibia component is defined as negative, and anterior displacement is defined as positive. Data was recorded 1 in every 1000 cycles. The circled black line indicates the demand profile. The grey area comprises of the individual plots of all recorded response profiles from all stations. The dashed black lines indicate the mean responses of each measured station. The heavy black line indicates the mean response of all recorded stations.

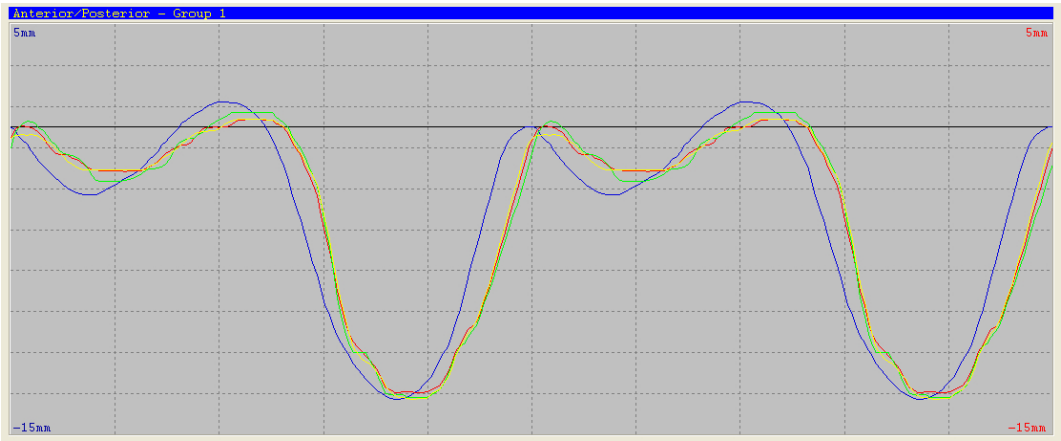

Figure 5.10: Screen capture from Kneesim software of displacement response of Group 1 stations when no AF is applied. Two complete cycles are shown. Blue line indicates demand, and the red, yellow, and green lines indicate the response.

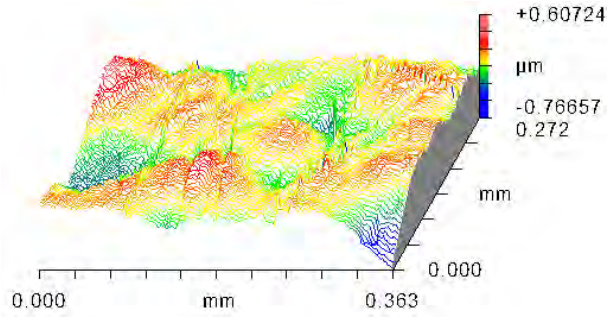

(a) ArCom® Load Soak Control (Tibia 3) prior to testing (R_a = 0.093 μm).

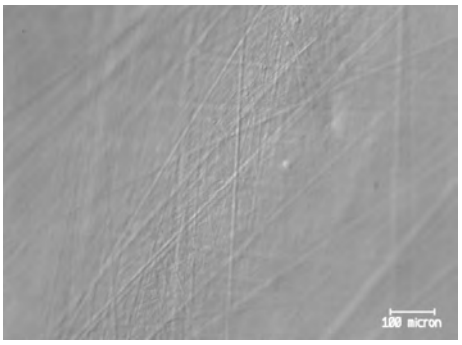

(b) Optical micrograph of soak control surface prior to testing.

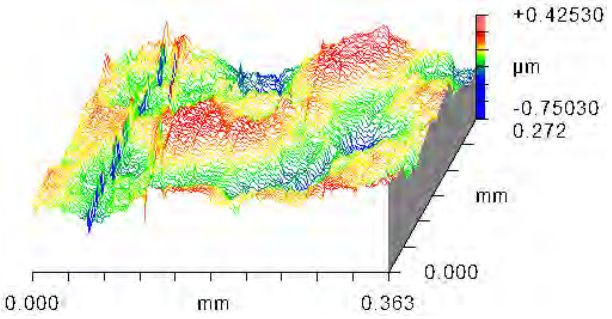

(c) ArCom ® Load Soak Control (Tibia 3) after 5MC (R_a = 0.090 μm).

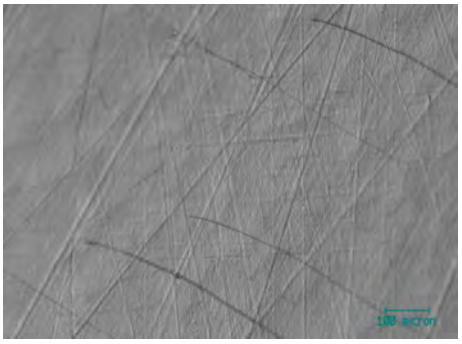

(d) Optical micrograph of soak control surface upon completion of the wear test.

Figure 5.11: Surface characterisation of Soak control (Tibia 3).

to the dynamic loading of the tibia. They are not thought to be due to scratching as they are generally short in length, and do not feature raised edges, which are typical for scratches. Figure 5.13(d) also showed some scratching in the AP direction which indicates that there may have been minor relative movement between the tibia and femur components.

The five test tibia components were also analysed. The mean combined R_a of all 5 test tibias compared to the two control tibias can be seen in Figure 5.14. It is clear that the mean R_a of the test tibias was greater than the two control samples throughout the whole test. No relationship between the test duration and surface roughness was seen. It should be noted that the mean R_a value for the articulating tibias at 0.00MC includes values for tibias 1 and 2 that were used to set up the Prosim knee simulator. If these are omitted, then the initial mean R_a of the remaining 3 articulating tibias is 0.074±0.020μm, which is similar to that of the two controls. Also of particular interest is the large standard deviations observed, an indication of the large variation in surface roughness between individual locations on the same plates. Analysis of the individual tibias is shown in Figure 5.15. Here the recorded surface roughness of the medial and lateral sides of the tibia are compared, as well as the

(a) Optical micrograph of tibia surface at the boundary of the contact patch after 0.5x10^6 cycles of loading.

(b) Optical micrograph of tibia surface at the boundary of the contact patch after 2.5x10^6 cycles of loading. Image was taken at coordinates 6.1x18.3 on Figure 5.1(f).

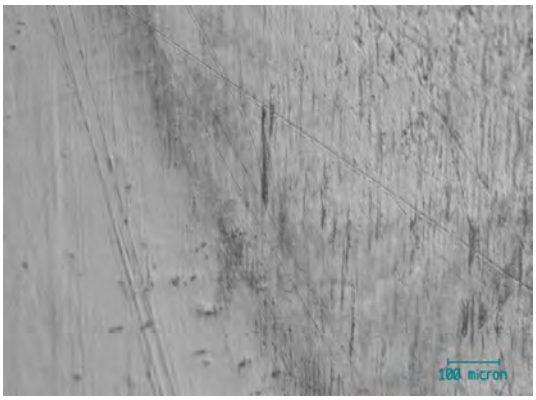

(c) Optical micrograph of tibia surface at the boundary of the contact patch after 3.5x10^6 cycles of loading. Image was taken at coordinates 6.1x18.3 on Figure 5.1(f).

(d) Optical micrograph of tibia surface at the boundary of the contact patch after 4.5x10^6 cycles of loading. Image was taken at coordinates 6.1x18.3 on Figure 5.1(f).

Figure 5.12: Surface characterisation of ArCom® Load soak control (Tibia 4).

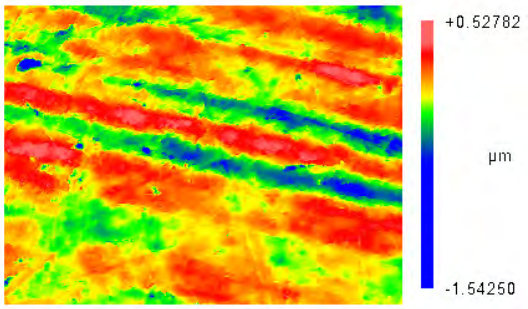

(a) Zygo scan of the lateral contact area of Tibia 4 after 0.5x10^6 cycles. Note the surface damage with trenches running in the approximate ML direction. The R_a of this surface is 0.147μm.

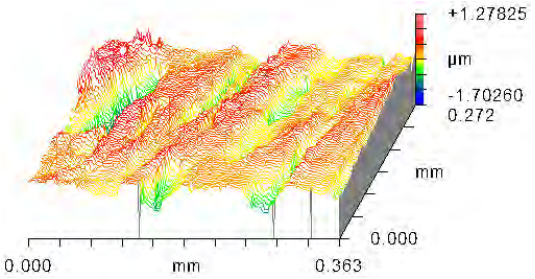

(b) Zygo scan of the lateral contact area of Tibia 4 after 3.0x10^6 cycles. Note the surface damage with trenches running in the AP direction. The R_a of the surface is 0.227μm.

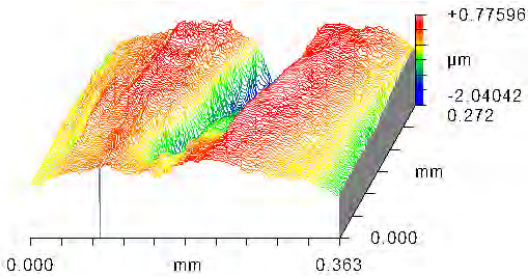

(c) Zygo scan of the lateral contact area of Tibia 4 after 3.5x10^6 cycles. Note the surface damage with one large trench running in the AP direction. The R_a of the surface is 0.351μm.

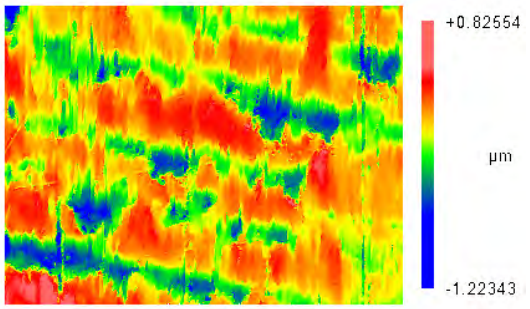

(d) Zygo scan of the lateral contact area of Tibia 4 after 4.0x10^6 cycles. Note the surface damage with trenches running in the ML direction and scratching in the AP direction. (R_a=0.178μm).

Figure 5.13: Surface characterisation of ArCom® Load soak control (Tibia 4) using Zygo white light interferometer.

average roughness of each individual tibia over the course of the wear test. It is clear from tibia 3 that without any contact, the surface roughness remains below 0.100μm. Addition of axial loading causes a slight increase in the variation of surface roughness, however the mean stays below 0.100μm as evidenced by tibia 4. All 5 articulating tibias saw an increase in surface roughness, and the standard deviation of all articulating tibias was high. There was no significant difference between the medial and lateral sides of the tibia.

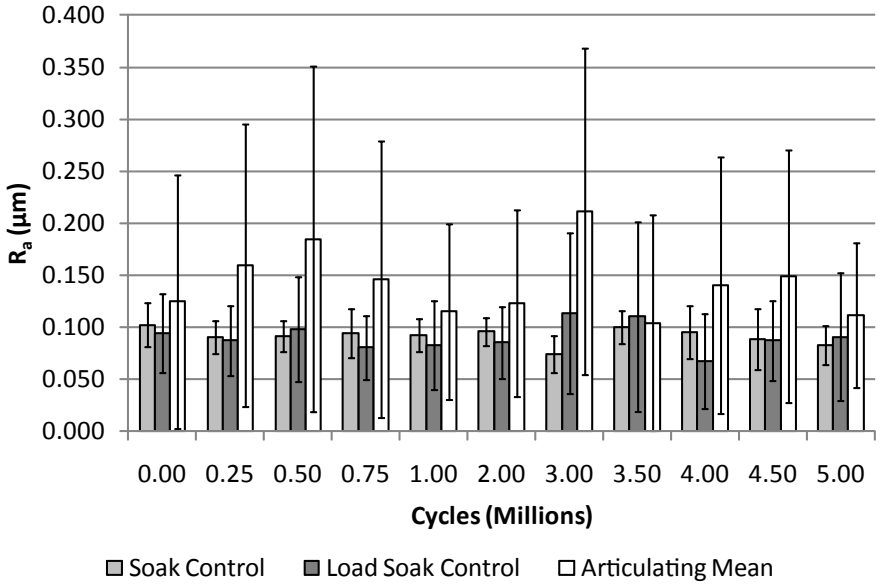

Figure 5.14: Mean R_a of the five articulating tibias compared to the two control tibias over the full course of the wear test. Mean values are shown ± 1SD.

Variation of the CoCrMo femur surface roughness is shown in Figure 5.16. Femur 7 was used to load the LSC tibia and as a result no motions were applied to it. As a result it showed very little change in surface roughness throughout the test. The articulating components showed greater variation, however the majority of the femur surfaces remained at a surface roughness value of 0.050μm or below, however the averages were upwardly skewed by readings being taken in the location of a scratch. This was especially the case for Femur 4, and to a lesser extent for Femur 5.

Optical observations of the femur component surfaces are shown in Figure 5.17. Prior to testing and the surfaces were homogeneous in appearance with carbides visible, protruding from the surface by 0.25μm as seen in Figures 5.18(a) and 5.17(a). While this image is not from the start of the test, it is of a non-contacting area of Femur 7, which was used with the LSC tibia. Damage to the articulating femurs occurred in the form of various size scratches running in the AP and FE direction. Shallow scratches with a depth of 0.05μm were seen

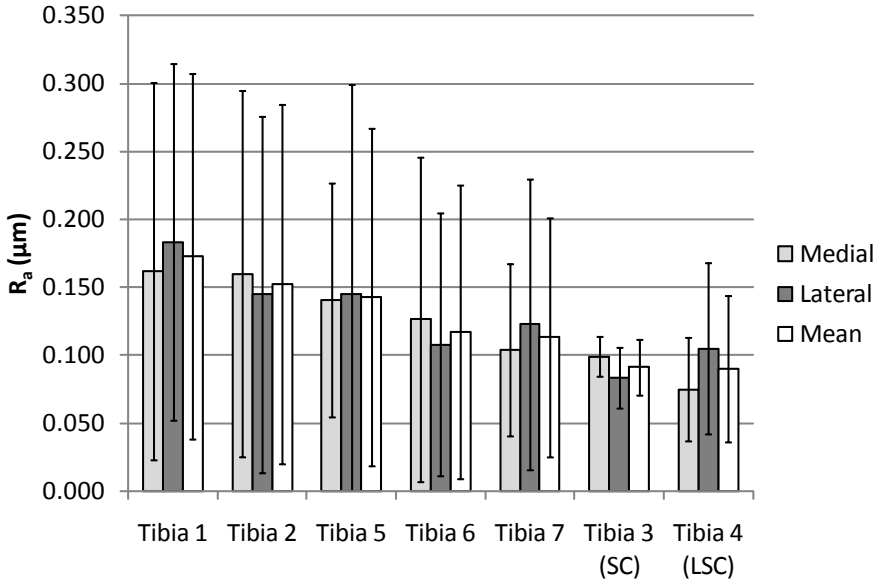

Figure 5.15: Comparison of the mean R_a for the medial and lateral sides of the tibia. Data shown is an average of all recorded points from 0.5MC to 5.0MC. Error bars are ± 1 SD.

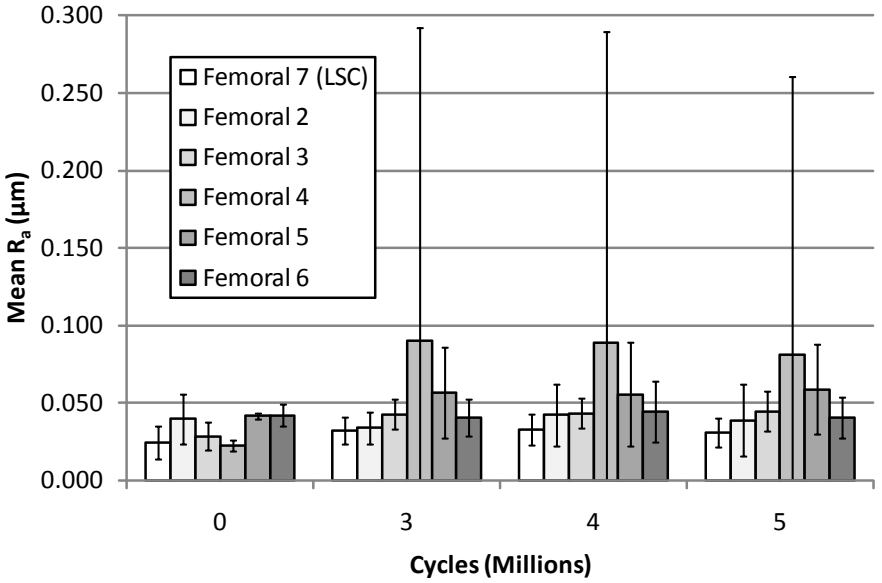

Figure 5.16: Variation in surface roughness of the 5 articulating femur components and the 1 load soak control. Mean values are shown ± 1 SD.

(a) Optical micrograph of Femur 7. This was contacting with the LSC and no surface damage is visible.

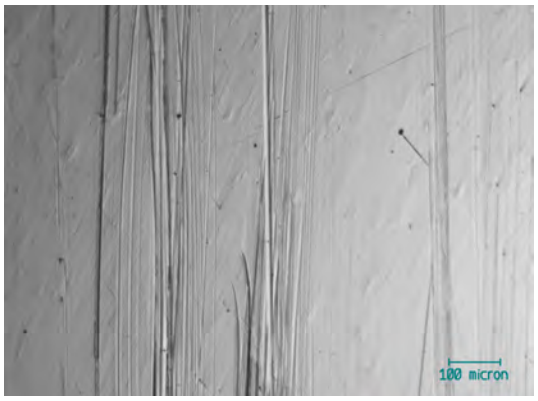

(b) Optical micrograph of Femur 2. Multiple fine scratches are visible running in the AP/FE direction.

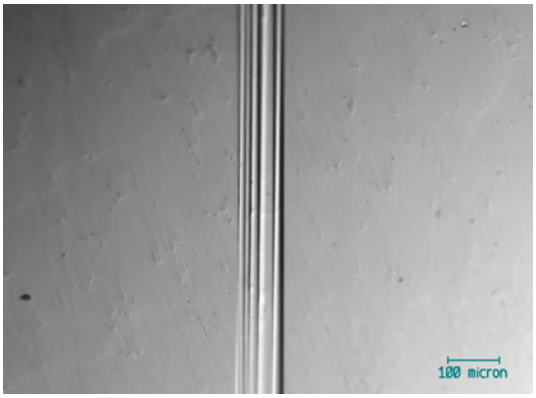

(c) Optical micrograph of Femur 4. Multiple medium size scratches are visible running in the AP/FE direction.

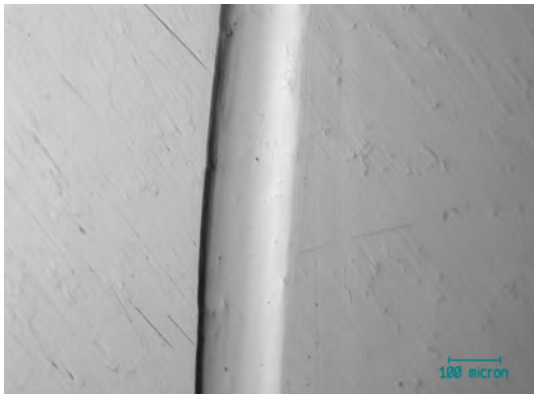

(d) Optical micrograph of Femur 4. A large scratch can be seen running in the AP/FE direction.

Figure 5.17: Optical micrographs the articular surface of the femoral components after 3.0 MC of testing.

in Figures 5.18(b) and 5.17(b). Deeper and wider scratches seen in Figures 5.18(c) and 5.17(c). Finally, small numbers of large scratches with a depth of 2.29μm were observed, such as that shown in Figures 5.18(d) and 5.17(d).

Observations on the backside of the tibia revealed that the machining marks were not evident in locations underneath the condyles as seen in Figure 5.19(a). In areas away from the loading they remained throughout the whole test duration as seen in Figure 5.19(b). at intermediate locations, evidence of both features could be seen, such as in Figure 5.19. This was similar for all five articulating tibias. The backside of the LSC is shown in Figure 5.19(d), where it can be seen that the effect is less pronounced.

Observations of the articulating tibia surfaces revealed several interesting features. Surface damage was categorised using seven descriptors of wear (Hood et al., 1983). These were; Surface deformation, pitting, embedded debris, scratching, burnishing, abrasion, and

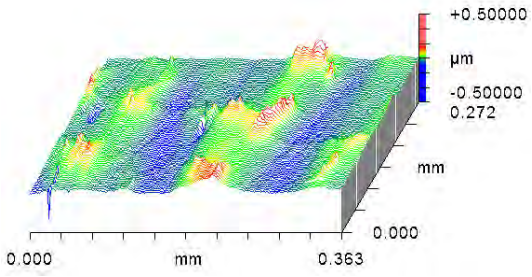

(a) Zygo scan of surface of Femur 7. Carbides can be seen protruding up to 0.25μm from the surface. R_a=0.030μm.

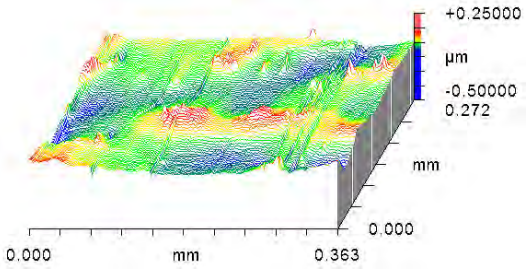

(b) Zygo scan of surface of Femur 2. Multiple fine scratches are visible running in the AP/FE direction. Scratch width is 5.7μm and scratch depth is 0.05μm. R_a=0.030μm.

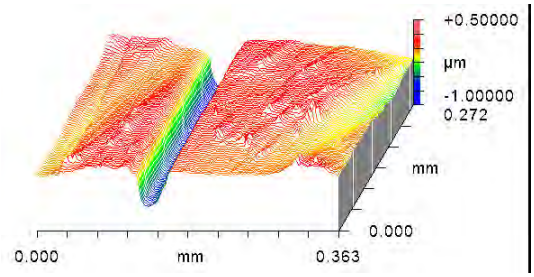

(c) Zygo scan of a medium scratch running in the AP/FE direction on Femur 5. Scratch width is 0.05mm and the scratch depth is 0.73μm. R_a=0.124μm.

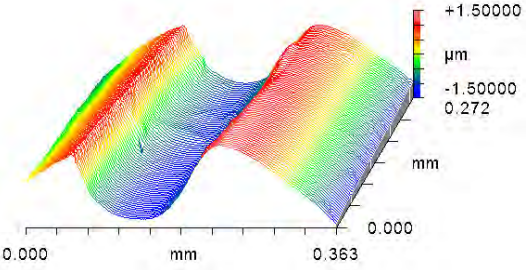

(d) Zygo scan of a large scratch running in the AP/FE direction on Femur 4. The scratch width is 0.16mm and the scratch depth is 2.29μm. R_a=0.665μm.

Figure 5.18: Zygo scans of the articular surface of the femoral components after 3.0 MC of testing.

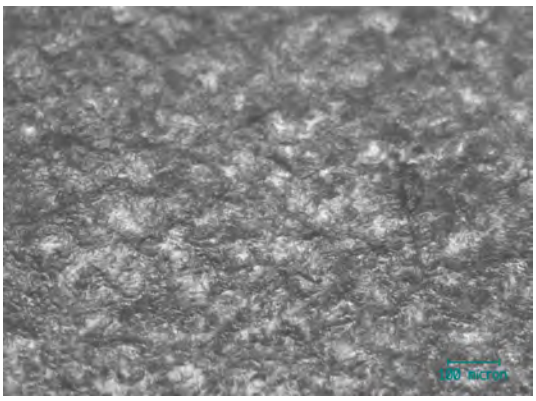

(a) No evidence of machining marks remain at location directly under condyle.

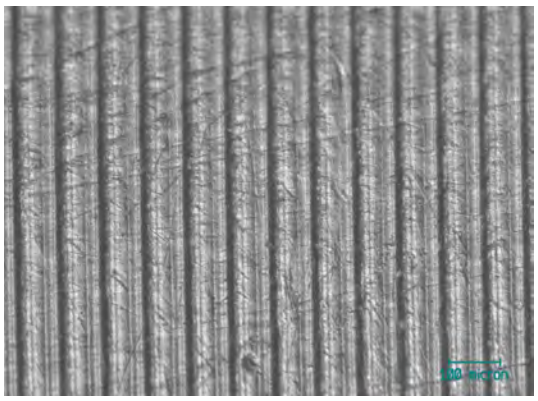

(b) Machining marks are still visible at location away from condyle.

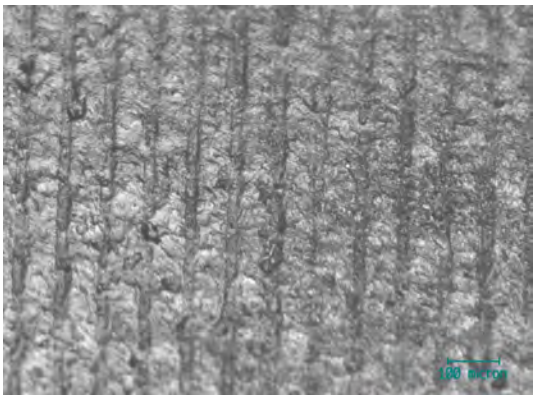

(c) Some machining marks remain at intermediate position.

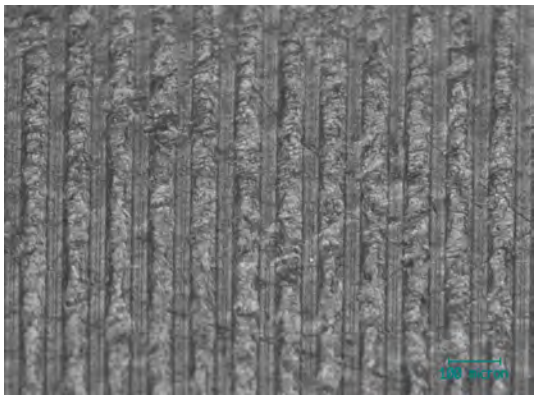

(d) The effect is less pronounced on the LSC (tibia 4).

Figure 5.19: Optical micrographs of the 'backside wear' observed on tibias 1 and 4 after $5.0 \text{x} 10^6$ cycles.

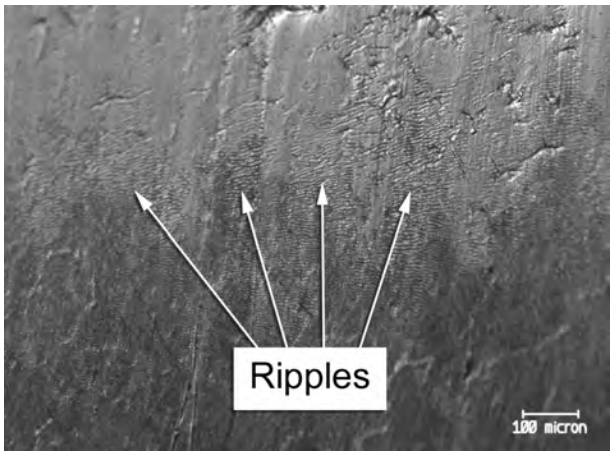

Figure 5.20: Ripples observed on ArCom® tibia 7 after 0.5x10^6 cycles.

delamination. however, additional 'rippling', 'adhesive', and 'finger' features were found that could not adequately be described by the Hood Scale descriptors.

Initial imaging of the unworn tibia components revealed that while much of the surface was uniform, there were small imperfections in the surface that may have been caused by either the direct compression moulding process, or the subsequent handling and packaging. After 0.5x10^6 cycles there was evidence of rippling on all 5 articulating tibial components, a typical example of which can be seen in Figure 5.20. All ripples wear orientated approximately perpendicular to the AP sliding direction. Scratching in the AP sliding direction was observed on all articulating tibias. Observations of the surface when the location was recorded revealed that the severity and type of surface damage was linked to the position of the tibia at which it occurred. With reference to the Hood descriptors, no evidence of abrasion, delamination, pitting, embedded cement, or deformation was observed on the UHMWPE components. The most common observed wear mechanisms were adhesion, scratching, burnishing, rippling, and 'finger like' protrusions. Figure 5.22 shows examples of these wear mechanisms and the locations at which they were found to occur with reference to the observed wear scar. Scratching was found mainly in the posterior areas of the wear track. Examples of rippling were found more centrally and often could be found in similar areas to examples of burnishing, adhesive wear, and the finger protrusions. Burnishing was found towards the anterior of the wear scars. The finger protrusions were highly location dependent and occurred in a region 15 - 20 mm from the posterior edge of the tibia, which corresponds to the outline created by the loading on the LSC seen in Figure 5.1(f).

Zygo scans of the six different types of wear mentioned are shown in Figure 5.21. It

can be seen from the R_a values that there was a large range between the burnishing, which was the smoothest wear type, and the raised protrusions, which had the highest values of surface roughness.

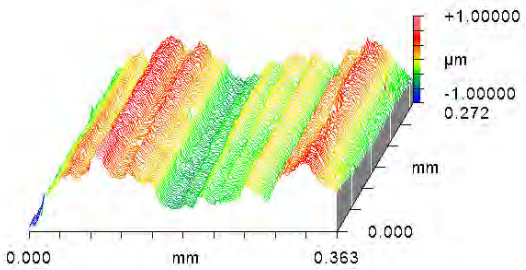

(a) Medial condyle of tibia 2 after 0.25 MC. Note the scratching in the AP/FE direction. R_a=0.256μm.

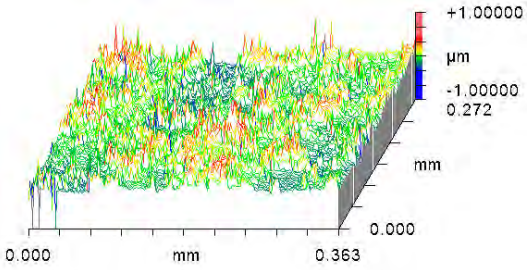

(b) Medial condyle of tibia 1 after 4.5 MC. Note the particles adhered to the surface. R_a=0.108μm.

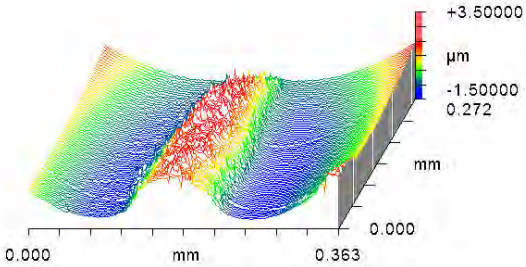

(c) Lateral condyle of tibia 5 after 3.5 MC. The protrusion width is 0.11mm and the height is 2.7μm. R_a=0.681μm.

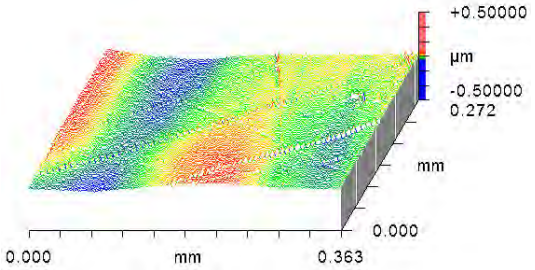

(d) Medial condyle of tibia 5 after 3.5 MC. Note the burnishing on the surface. R_a=0.020μm.

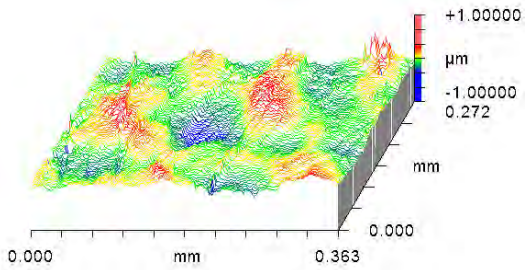

(e) Lateral condyle of tibia 3 after 3.5 MC. This tibia was not worn. R_a=0.096μm.

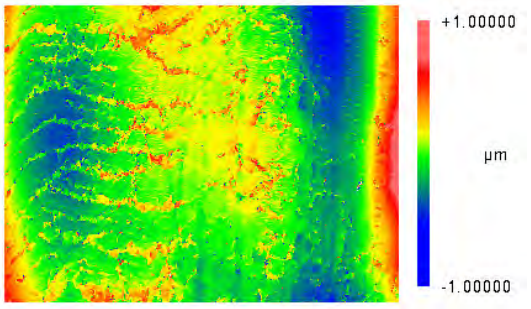

(f) Lateral condyle of tibia 2 after 3.0 MC. Note the rippling on the surface. R_a=0.179μm.

Figure 5.21: Zygo scans of the articulating surfaces of multiple ArCom® at various test durations.

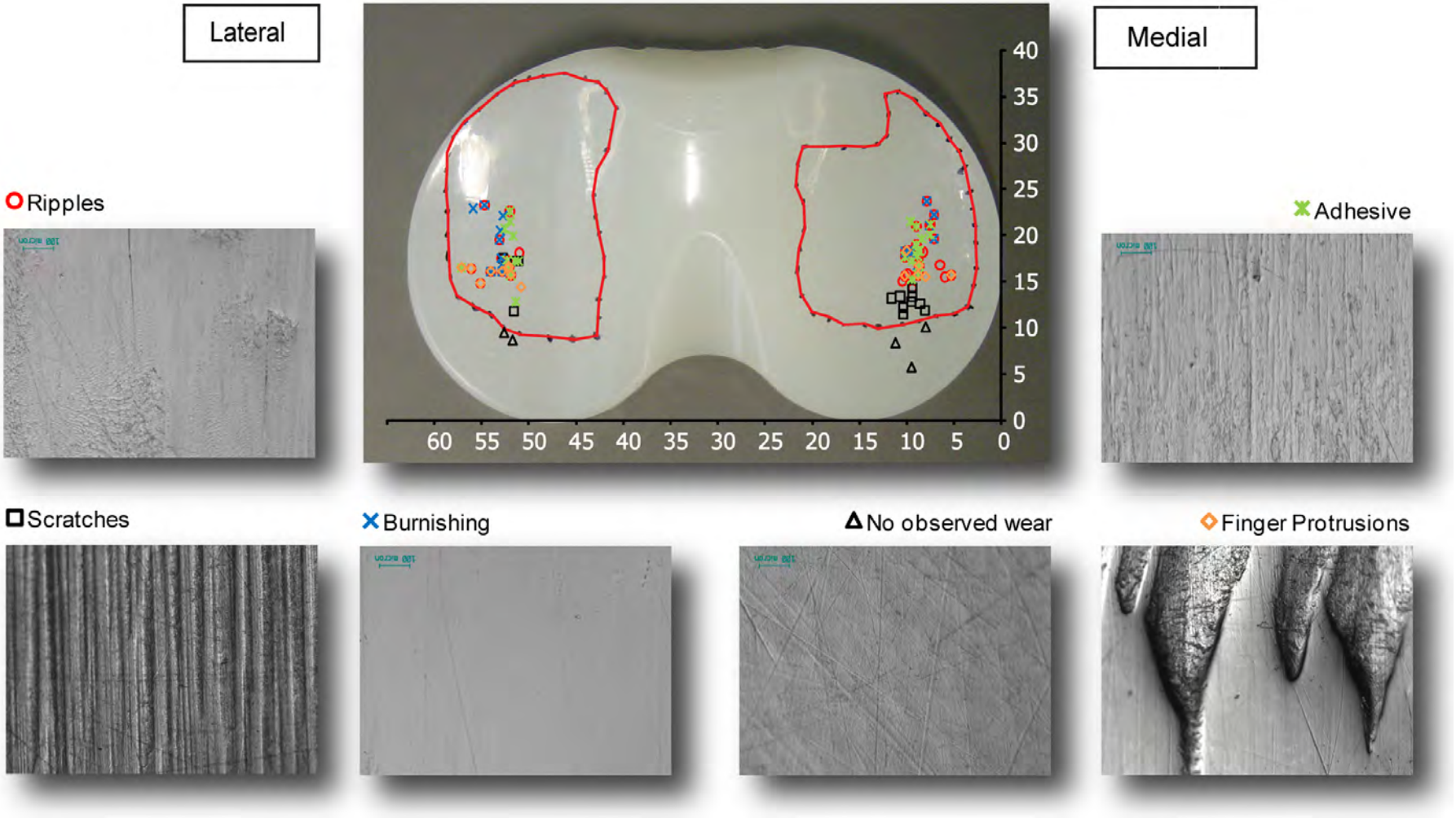

Figure 5.22: A typical wear scar on the ArCom® tibia with the locations of the different types of observed wear recorded. Data was compiled using observations from all 5 articulating tibias observed between 2.5x10^6 and 5.0x10^6 cycles.

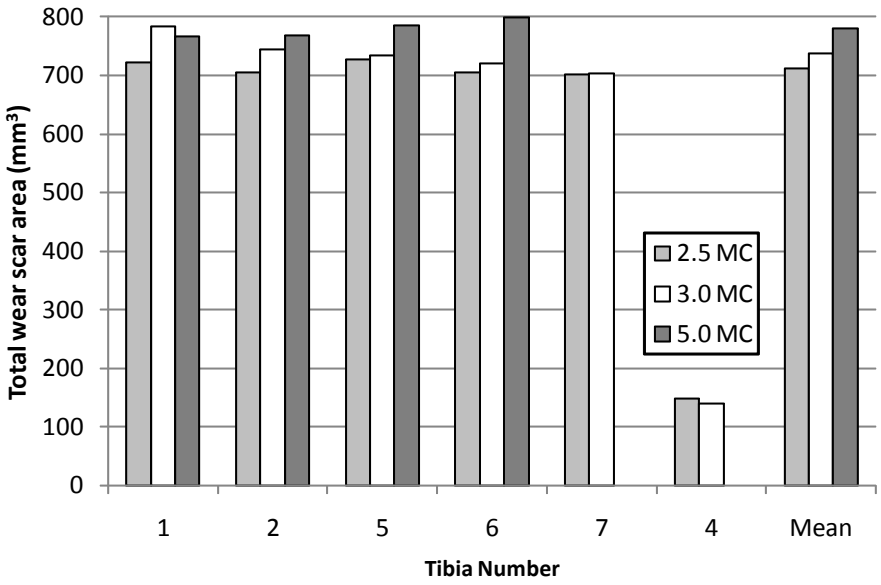

Figure 5.23: Total visible wear scar areas for the ArCom® test tibias. Note that tibia 4 was the load soak control and therefore no motions were applied to it. Both tibias 7 & 4 were used for other experiments at the conclusion of the wear test so were not available for wear scar area measurement.

5.1.2.5 Visible wear scars

The visible wear scar areas of all test tibias after 3.0×10^6 cycles can be seen in Figure 5.1. These visible wear scars are shown superimposed on one another in Figure 5.33, indicating that the visible wear scars were largely consistent between tibias. The visible wear scars were also outlined at 2.5×10^6 cycles, and additionally after 5.0×10^6 cycles for tibias 1, 2, 5, and 7. The total visible wear scar area for the five articulating tibias and the one LSC at each interval of imaging are shown in Figure 5.23. The total wear scar areas were consistent amongst test samples, with no significant increases or decreases during the test. The visible wear scar area on tibia 4 was significantly lower due to this being used as the LSC, therefore only AF and no motions were applied to this sample.

The mean ML distribution of the visible wear scar area for the test tibias is shown in Figure 5.24. For all tibias the visible wear scar area was greater on the lateral side of the tibia than on the medial. The mean distribution for all samples at all imaging periods was 53.2% on the lateral side and 46.8% on the medial side.

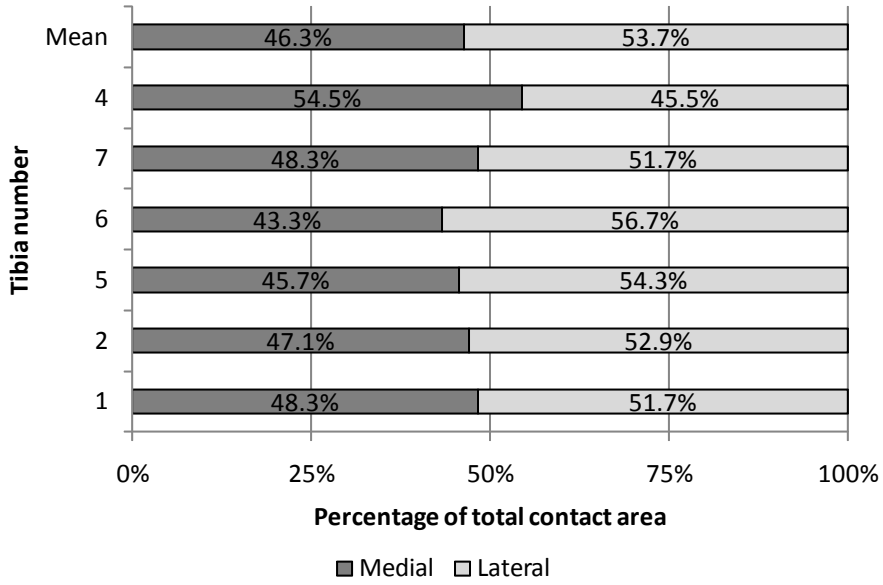

Figure 5.24: Mean ML distribution of visible wear scar area outlined at 2.5x10^6, 3.0x10^6, and 5.0x10^6 cycles.

5.2 Effect of Dynamic Axial Force on Lubricant Uptake

Results from the earlier wear test run for 5x10^6 revealed a difference in the rate of lubricant uptake between the soak and load soak control samples, as shown in Figures 5.4 and 5.5. In order to further investigate this result, a further two ArCom® tibias were immersed in lubricant, along with two tibias from the previous wear test. The aim of this experiment was to confirm the difference in fluid uptake between dynamically loaded and unloaded soak controls, and investigate if there are differences between previously worn, and unworn components.

5.2.1 Materials and methods

The regulators that supply air to the TR and AP cylinders on stations 0 and 1 were fully closed so that no movement of these cylinders was allowed. The AP calibration rods and wooden packing were also used to set and hold the AP sledges in the home position. The FE motors were disabled using the Kneesim simulator software. The AF profile used was the same as in the previous wear test and is displayed in Figure 4.7. The maximum applied load was 2.6kN. It was run in open loop control, in the same way as the previous 5x10^6 cycle wear test. A photograph of the test setup can be seen in Figure 5.25.

Two worn samples from the previous wear test were used, these were tibias 1 and 7.

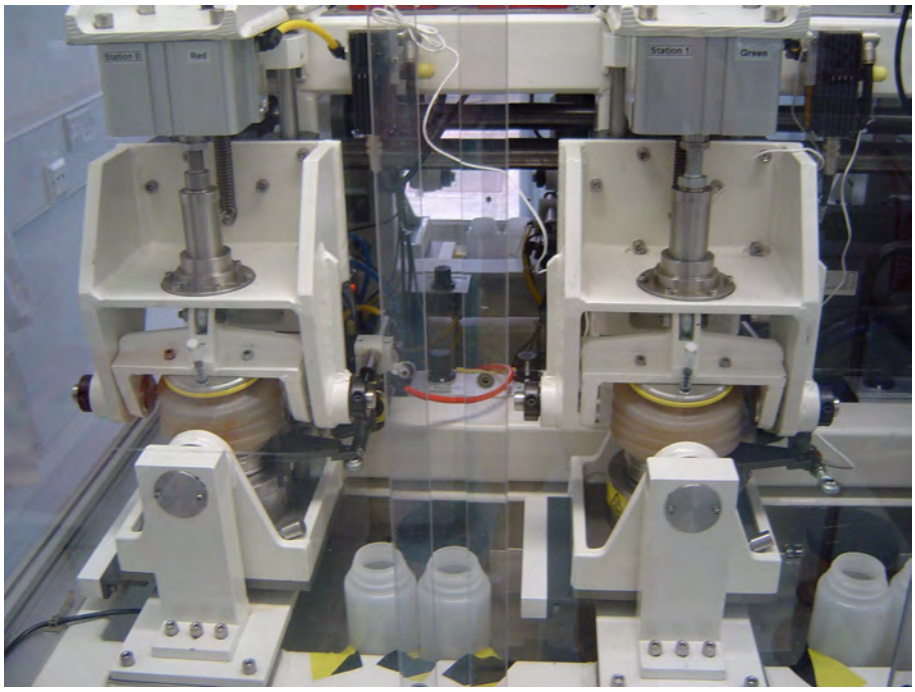

Figure 5.25: Stations 0 and 1 were used for the soak comparison test. FE, AP, and TR were restricted.

These two samples had undergone 55 days continuous soaking in lubricant and 5x10^6 cycles of wear testing. They were chosen as they had both experienced very similar mass change during the wear test and both had very similar fluid uptake trends. Two additional unworn tibias were also used and these were labeled tibias 8 and 9. During the test, one of the worn and one of the unworn tibias were placed in the test under dynamic load, and the remaining worn and unworn tibias were placed in the test lubricant under no load. The unloaded samples were soaked whilst fixed in their Co-Cr tibia trays as to ensure a consistent surface area exposed to the lubricant amongst all UHMWPE test samples.

Prior to testing, it was observed that there was minor discolouration of tibias 1 and 7 due to their previous immersion in the test lubricant. This can be seen in a photograph of the four samples shown in Figure 5.26.

The components were tested for a total duration of 2.5x10^6 cycles.

At approximately 5x10^5 cycle intervals the tibial components were removed from the simulator and cleaned according to the protocol in Appendix A.2.1.2. After cleaning, and gravimetric assessment, the components were returned to the simulator. Fresh test lubricant was poured into the test capsules and the test restarted.

Assessment of the bearing surface of the unworn load soak was performed after 1.0x10^6 cycles and 1.5x10^6 cycles in order to detect any changes in the surface due to the compres-

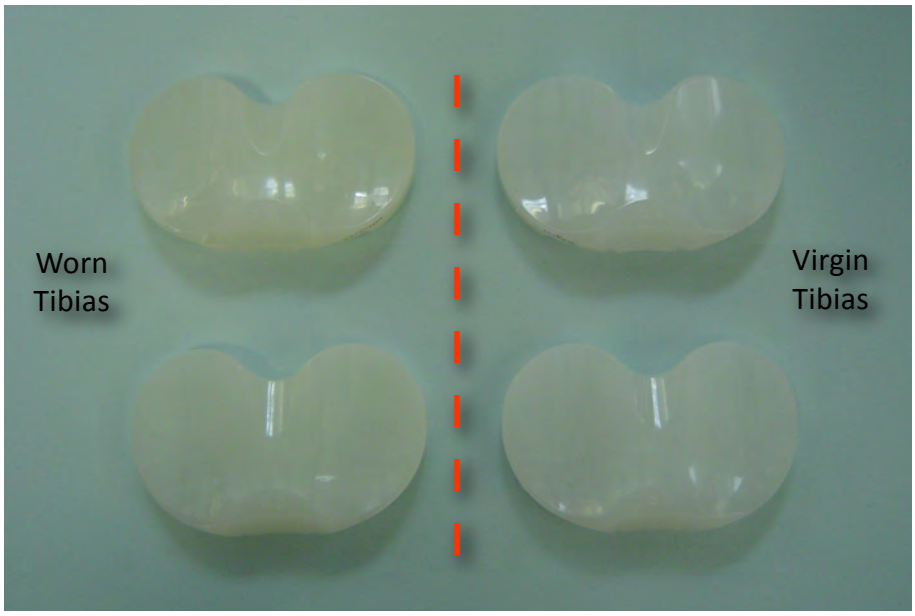

Figure 5.26: Photograph of the four tibia bearings used in the load soak test indicating the discolouration of the previously worn tibias (on left) compared to the virgin tibias (on right) caused by their previous immersion in the test lubricant for long periods of time.

sion.

5.2.2 Results

The absolute mass change of the four tibia samples during the soak test can be seen in Figure 5.27. All samples experienced a mass gain over the duration of the test, with a large initial increase over the first $5.0\text{x}10^5$ cycles. The absolute mass of all samples then fluctuates for the remainder of the test. In order to observe the difference between soaked and soaked under load samples the mass change of the worn and unworn load soak samples were calculated relative to their respective soak controls. This is shown in Figure 5.28, the test duration has also been converted from number of cycles to time in soak. The mean of both worn and unworn samples is also shown. applying a least squares linear regression to the mean value gives a mean mass increase of 0.00316mg/day, the R^2 value for the fit is 0.501, indicating a weak correlation in this case.

The contact area of loading was visible, much the same as it was on the LSC in the previous wear test, and was of the same dimensions as that shown in Figure 5.1(f). Analysis of the visible contact patch with the Zygo non-contacting interferometer revealed several changes in the morphology of the surfaces which would have otherwise been unnoticed if using just purely optical assessment. Damage was observed to the tibial bearing surface in

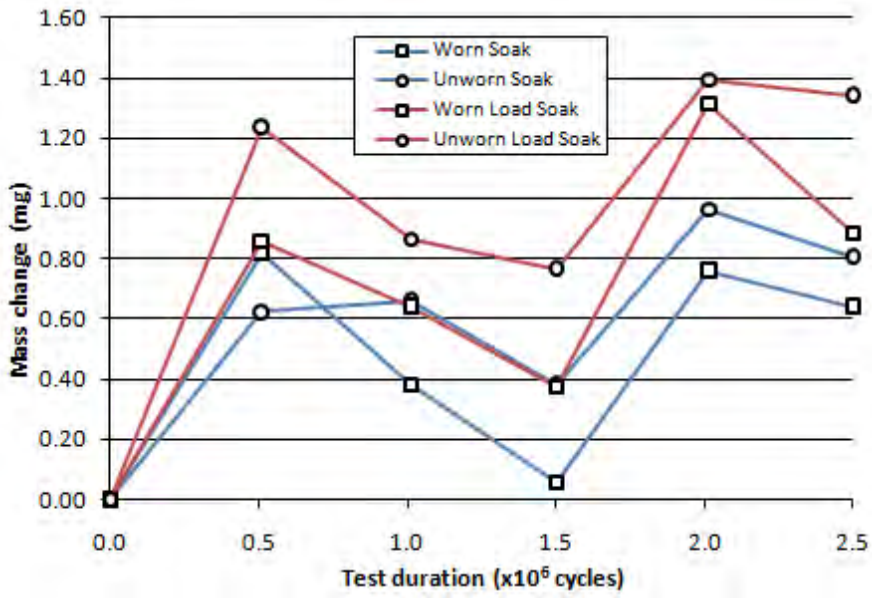

Figure 5.27: Absolute mass change of the four UHMWPE tibia samples during load soak test.

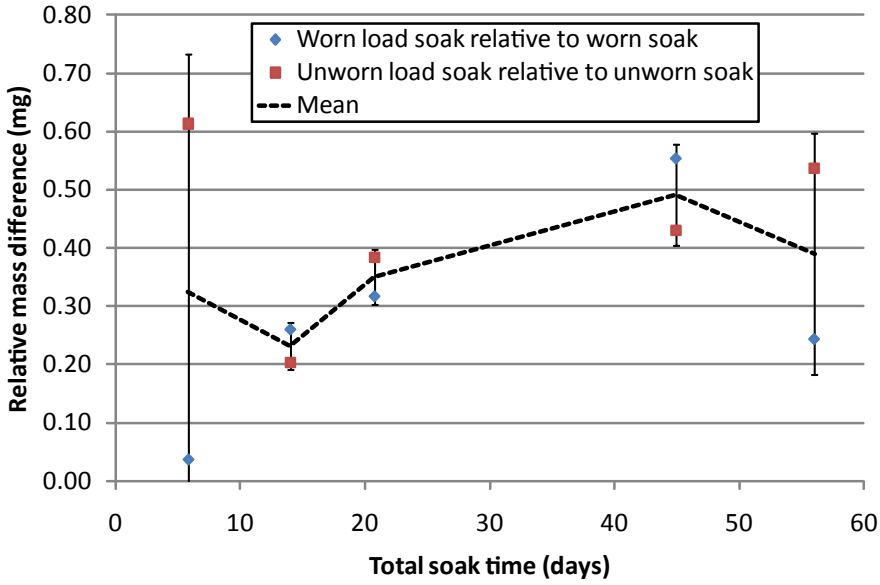

Figure 5.28: Relative mass change of the loaded unworn and worn samples relative to their respective soak samples.

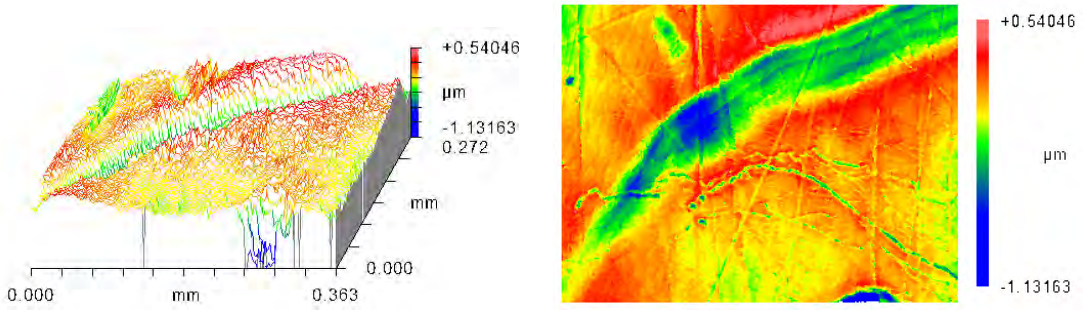

(a) 3D Plot of fissure. (b) 2D plot of fissure.

Figure 5.29: Zygo scans of fissure like feature observed on the lateral contact patch of the unworn load soak. Scans were taken after 1.0x10^6 cycles of dynamic loading.

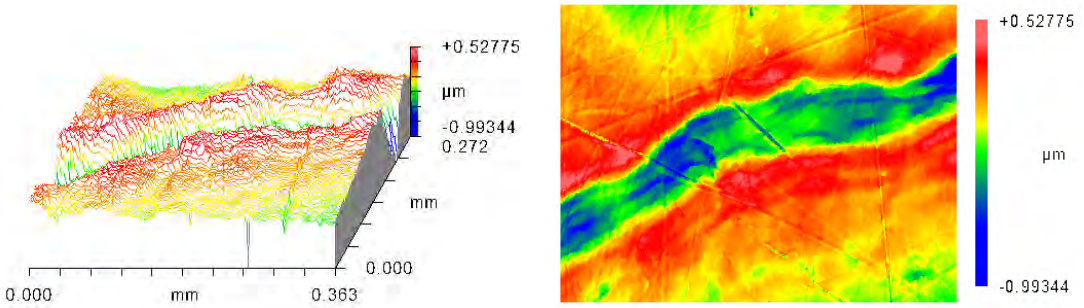

(a) 3D Plot of fissure. (b) 2D plot of fissure.

Figure 5.30: Continuation of the fissure like feature observed in Figure 5.29.

the form of fissures shown in Figure 5.29. It is hypothesised that this damage was caused by the cyclic loading and not by any motion due to the shape and orientation of the fissure. As seen in the wear test, scratches caused by motion are always predominantly in the AP direction, which in the specified figure would be top to bottom. Scratches are also often typified by a build up of material on the edges of the scratch, however in this case it is not seen. The fissure continued across the contact patch on the lateral side of the tibia and can be seen in Figure 5.30.

Also observed at another discrete point on the lateral contact patch were the distinctive saw-tooth fissures shown in Figure 5.31. The saw-tooth pattern was at 30° - 35° to the horizontal.

Imaging an area away from the contact patch, there was no evidence of surface damage caused by the dynamic loading. As evidenced by Figure 5.32.

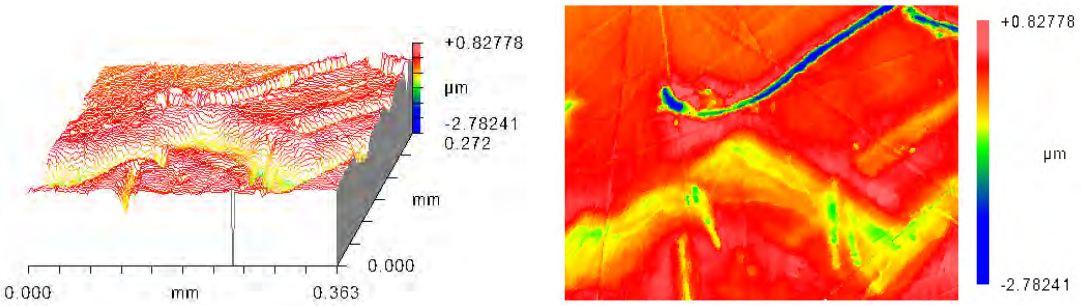

(a) 3D Plot of fissure. (b) 2D plot of fissure.

Figure 5.31: Zygo scan of more fissures on lateral condyle of tibia 9 at 1MC.

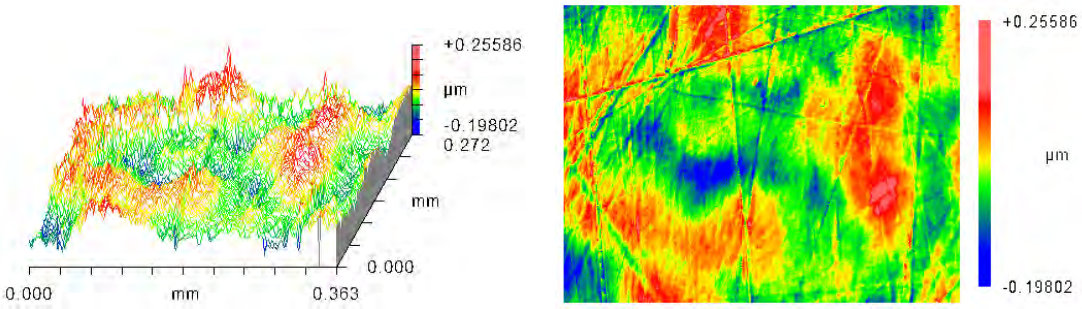

(a) 3D Plot of fissure. (b) 2D plot of fissure.

Figure 5.32: Zygo scan of the virgin tibia (9) after dynamic loading for 1.0×10^6 cycles. The point scanned is away from the visible contact area. No damage is visible on the surface.

5.3 Early detection of ripple formation

The optical imaging of the same points on the tibial surface in the 5 MC wear test produced very informative images on the types of wear, and the location at which it was occurring. However, the areas imaged were based on observed surface damage after 2.5 MC. In order to perform a more quantitative study, and examine the time it takes for this wear to occur, a more thorough investigation of the surface changes was conducted using a virgin UHMWPE tibia bearing. Increased amounts of images were taken as well as an increased frequency of image acquisition.

5.3.1 Materials and methods

The test was conducted using the same loading and displacement conditions as in the previous wear test, and was run for a total duration of $1.0\text{x}10^6$ cycles using a single virgin tibia. Optical imaging took place at every $0.1\text{x}10^6$ cycle interval. Gravimetric assessment was not performed as it was only the surface changes that were investigated. To enable a more rapid return to the simulator, the previous cleaning protocol was not used, a simple rinse with propan-2-ol proved adequate to remove the tibia of visible contaminants.

32 optical micrograph locations on the tibial component were selected prior to testing. The locations chosen were based on experience from the previous $5.0\text{x}10^6$ cycle wear test and on the physical limitations of the optical microscope, which could not produce images of sufficient contrast when it feature a large depth of field i.e areas with a large gradient. The 32 locations are illustrated in Figure 5.33. The specific locations were chosen to fall within, on the boundary, and out of the apparent wear area. The apparent wear scars for the five worn tibias from the previous wear test after $3.0\text{x}10^6$ cycles are also shown on the figure to illustrate this.

5.3.2 Results

The locations for the types of wear observed are shown in Figure 5.34. To produce this graphic, each one of the 352 individual optical micrographs was assessed and the most prevalent form of observed wear on each was recorded. Each type of wear was assigned a symbol and then these symbols plotted on the tibia at the location the image was taken. Some locations only contain one symbol which indicates that the same type of wear was

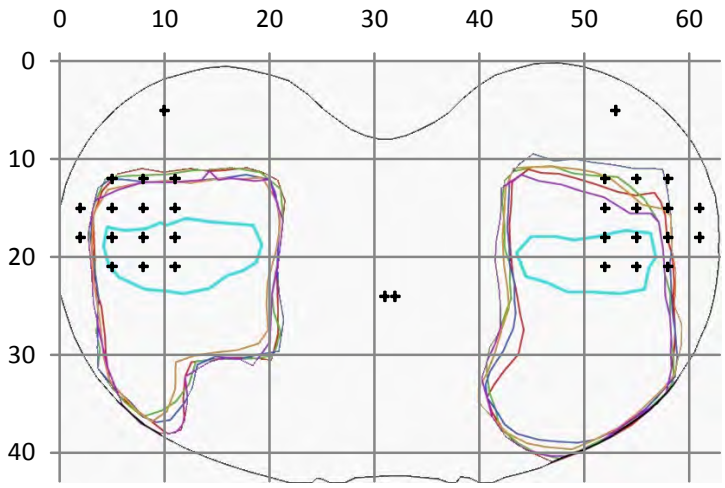

Figure 5.33: Optical micrograph locations indicated by black crosses on virgin tibia imaged at 1.0x10^5 cycle intervals for a total of 1.0x10^6 cycles. Locations were chosen based on physical limitations of the optical microscope (only shallow gradients could be imaged), and based on the observations of the apparent wear scars from the previous 5.0x10^6 cycle wear test. Wear scars shown are from the 5 test tibia analysed after 3.0x10^6 cycles. The light blue outline is the LSC.

observed at each observation interval. Some locations however, have up to four symbols. This indicates that each type of wear represented by the symbol was observed at least once during each observation interval.

All observations of no wear occurred at locations outside the apparent wear scar. There were more instances of no wear on the lateral side of the tibia than on the medial side, indicative of a wider, and therefore deeper wear scar on the medial side.

The raised protrusions were found in three locations which all fell within 18mm or 21mm from the posterior edge of the tibia. The protrusion observed at location X8 Y18 can be seen in Figure 5.36. Examples of the protrusions can be seen in all micrographs except those taken after 0.4x10^6 and 0.5x10^6 cycles. The remainder of the surface in the micrographs was burnished. It is also noted that these protrusions fall within the observable wear scar of the load soak control sample from the previous test, indicated by the light blue outline in figure 5.34.

Scratching was observed at several locations on both the medial and lateral sides. However, it was mainly found to occur towards the posterior of the observable wear scar. and it was common for the scratching to combine with burnishing, and adhesive features at the same location.

Rippling in the direction perpendicular to the AP motion was again observed at multiple

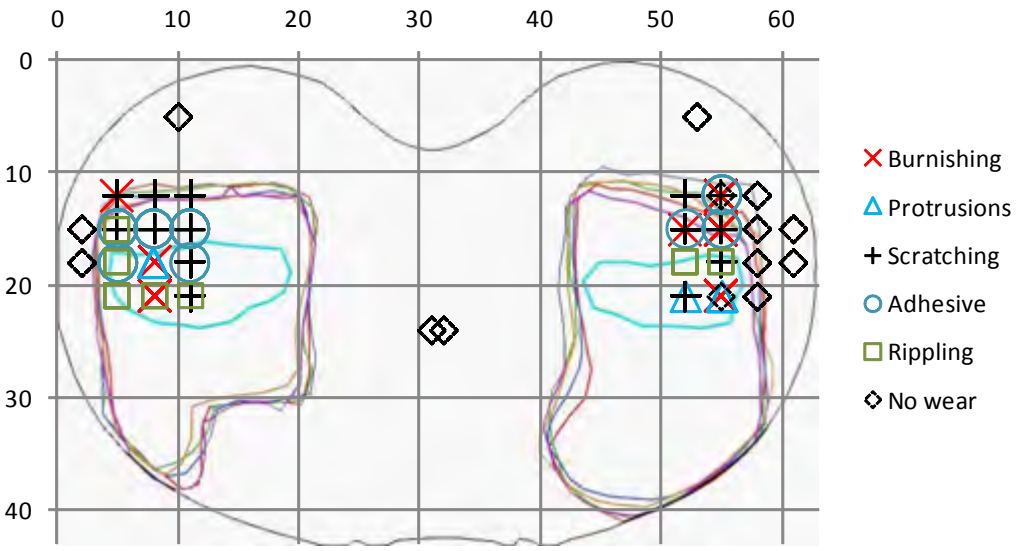

Figure 5.34: Locations of the different types of observed wear on the UHMWPE tibia tested for 1.0x10^6 cycles. The medial side of the tibia is the left side of the image.

locations indicated by the green squares in Figure 5.34. Rippling was more prevalent on the medial side of the tibia than on the lateral. The earliest indication of this was after just 0.1x10^6 cycles and it was observed at various points at each observation period. A clear example of rippling on the surface can be seen in Figure 5.35.

Burnishing was a common observation and this was characterised by an apparently smooth surface, an example of which can be seen in Figure 5.36(e). It regularly occurred at locations where scratching and adhesive wear were also observed.

Adhesive deposits were observed more commonly on the medial side than the lateral. On the lateral side it was observed at the more posterior locations, while on the medial side it fell more centrally in the recorded locations. No occurrences of adhesive wear were found at the most anterior location on both the lateral and medial side.

5.4 In-situ temperature measurement

Unlike some other knee wear simulators (Burgess et al., 1997), the Prosim knee simulator does not have the facility to heat the test lubricant. Therefore, it was unknown at what temperature the lubricant was during the previously run wear test. In order to assess the lubricant temperature and also the temperature of the articulating surfaces, k-type

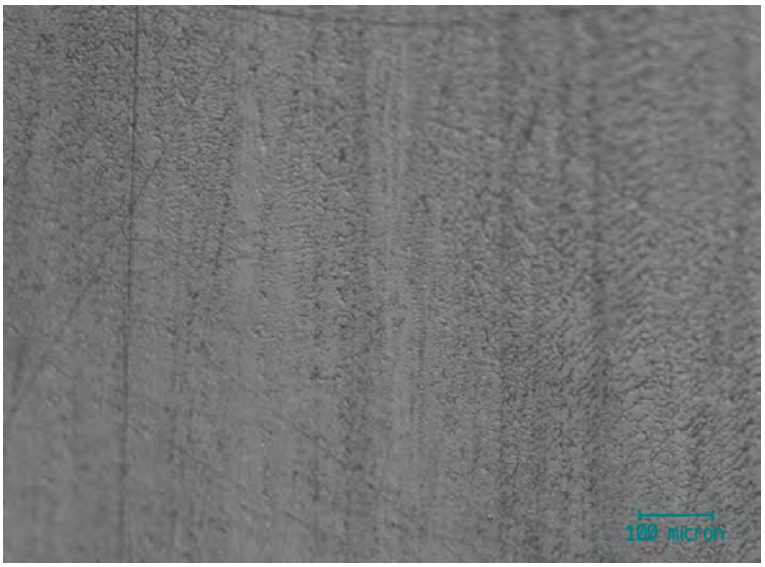

Figure 5.35: Clear example of rippling at location X5 Y21 at 0.1x10^6 cycles.

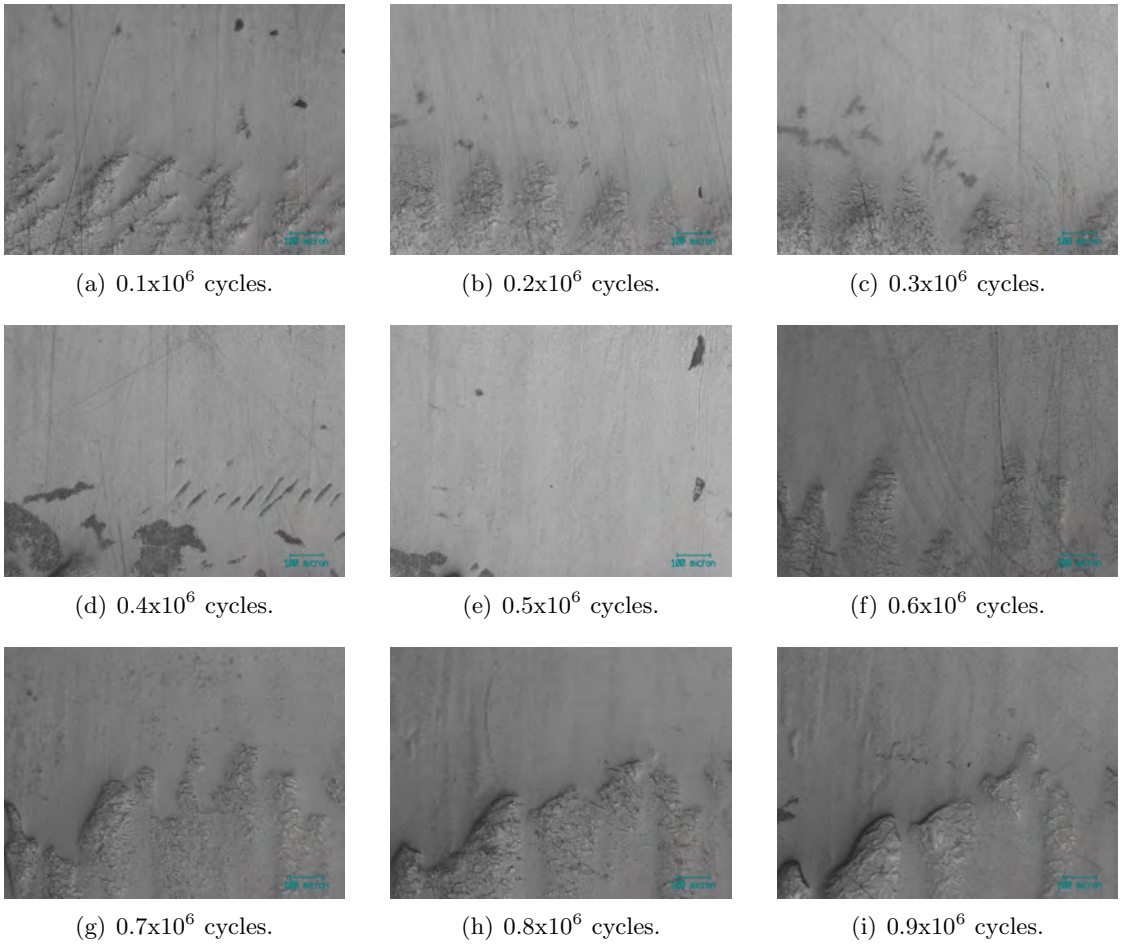

(a) 0.1x10^6 cycles. (b) 0.2x10^6 cycles. (c) 0.3x10^6 cycles.

(d) 0.4x10^6 cycles. (e) 0.5x10^6 cycles. (f) 0.6x10^6 cycles.

(g) 0.7x10^6 cycles. (h) 0.8x10^6 cycles. (i) 0.9x10^6 cycles.

Figure 5.36: Observations of surface features at 0.1x10^6 cycle intervals at location X8 Y18. 'Finger' like protrusions can be seen at all stages.

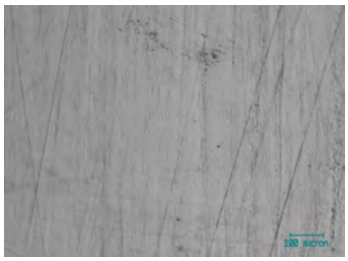

(a) 0.1x10^6 cycles.

(b) 0.2x10^6 cycles.

(c) 0.3x10^6 cycles.

(d) 0.4x10^6 cycles.

(e) 0.5x10^6 cycles.

(f) 0.6x10^6 cycles.

(g) 0.7x10^6 cycles.

(h) 0.8x10^6 cycles.

(i) 0.9x10^6 cycles.

Figure 5.37: Observations of surface features at 0.1x10^6 cycle intervals at location X5 Y15. Images show a combination of rippling, burnishing and scratching at the same location.

thermocouples were embedded at chosen locations in the TKR. Three locations in the UHMWPE tibial bearing, five locations on the CoCrMo femoral component and one in the lubricant were chosen.

5.4.1 Materials and methods

The locations of the thermocouples on the femoral component were chosen so that there was one thermocouple tip measuring the temperature in a non-contacting position, one on each condyle at the contact point at 0° of flexion, and finally one on each condyle at the contact point at 30° of flexion. These locations can be viewed in Figures 5.38(a) and Figure 5.38(c). Due to the hardness of the CoCrMo material, spark erosion was required to create the necessary cylindrical holes on the backside of the femoral component. The holes were eroded to a depth so that the tip of the thermocouple was 0.5mm below the articulating surface. Channels were created in the Tufnell femoral mount to allow the extraction of the thermocouple cables through the top of the stainless steel femoral mounting plate and can be seen in Figure 5.38(b). The thermocouple tips were held in place using Electrolube thermal bonding paste[2] which both secured the tips in place and provided a thermal conductivity of 1.1 W/m.K to minimise thermal transfer lag. The femoral component was then cemented to the mount with Dentine cement[3] as in previous tests. A view of the thermocouples in place before cementing can be seen in Figure 5.38(e).

Three thermocouples were placed 0.5mm below the surface of the UHMWPE bearing surface and held in place using the same Electrolube thermal bonding paste as in the femoral component. Channels were created in the PE mounting base and the tibial tray to allow extraction of the thermocouple cables, as seen in Figure 5.38(d) The tibial base was then cemented using Dentine cement as in previous tests. The tibial bearing before cementing can be seen in Figure 5.38(f). A fourth thermocouple protruded through the PE mount in order to monitor the lubricant temperature. One set of the Prosim SS mounting plates was also slightly modified to allow extraction of the cables without allowing any lubricant to escape. Detailed schematics of all modifications made to all components can be seen in Appendix A.3.2.

The test station was setup in the same manner as in the previous tests, and the 4.28mm

[2]http://www.electrolube.com/docs/thermalmain.asp?id=36 (Last accessed 18/11/2010)
[3]http://www.whwplastics.com/ (Last accessed 18/11/2010)

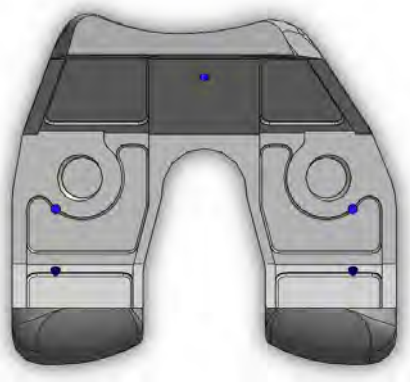

(a) Locations (in blue) of the five thermocouples place in the Vanguard femur component.

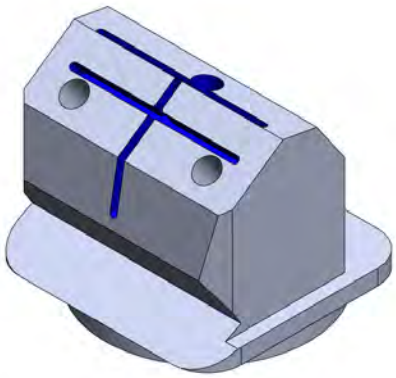

(b) Channels were created in the femur mount to facilitate thermocouple cabling.

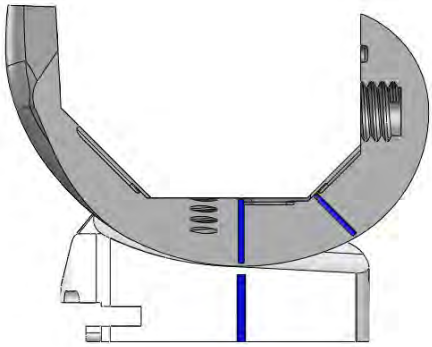

(c) Holes (blue) were created that allowed the thermocouple tip to be inserted 0.5mm below the contact surfaces.

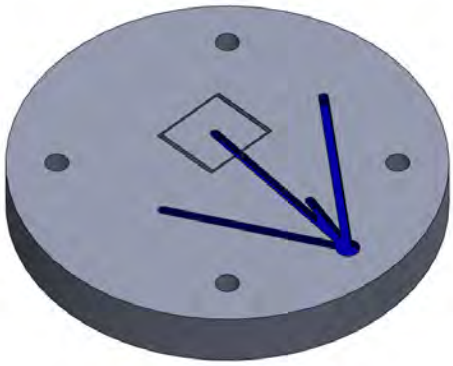

(d) Image showing underside of tibia mounting plate. Channels were created to route thermocouple cables out of the test cell.

(e) Photo of the five thermocouples in the test femur before cementing onto the mount.

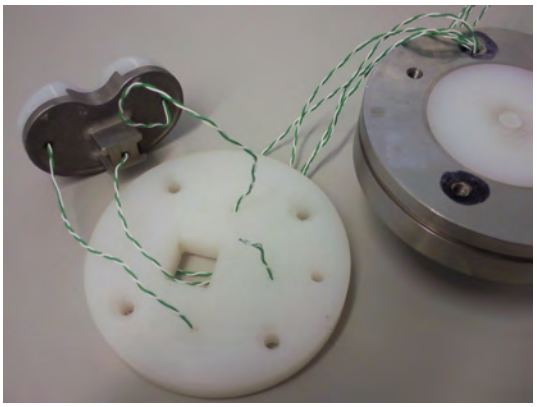

(f) Photo showing the three thermocouples in tibial component and one in lubricant before cementing onto the mount.

Figure 5.38: Images showing the location an fixation of thermocouples in one Vanguard design TKR.

offset of the TKR in the lateral direction was preserved. Care was taken to ensure that the thermocouple cables did not become entangled in the simulator mechanism. The thermocouple data was logged using a Pico TC-08 logger. This enabled 8 channels to be recorded. The ambient temperature was also recorded using the internal cold junction. Due to the length of the thermocouple cables, the data logger was placed inside the knee simulator safety cabinet. Data was recorded at 1Hz and the total test duration was 24 hours. Prior to commencement of the test the station was setup and the lubricant added, and then all components were left to equalise to RT. Once it was observed that all thermocouples had reached equilibrium, the data logger was activated, and the simulator motion was started. The profiles used were identical to those outlined in Figures 4.7 and 4.8.

5.4.2 Results

It was observed that during the initial period in which the test components and lubricant were left to equalise to RT the eight test thermocouples did not read the same equilibrium temperature. The average temperature of the 8 locations was 24.97 ± 0.16 °C, while the temperature of the cold junction at this point was 25.37°C. To account for these errors, when plotting the recorded temperatures, each thermocouple was assumed to be at the cold junction temperature at test start. All future recorded values were then adjusted to account for this assumption. The temperature plot of the whole test duration can be seen in Figure 5.39. The thermocouple embedded in the lateral side of the tibia failed after approximately 1.4 hours. The failure was attributed to relative movement between the UHMWPE tibia bearing and the CoCrMo tibial tray which sheared the thermocouple cable. The thermocouple measuring the non-contacting point on the center of the tibia bearing remained intact, possibly because the location was closer to the fixation points between the tibia tray and tibia bearing, therefore less relative movement between them would have occurred. All the temperature plots were quite tightly grouped, so to allow easier distinction between them, a magnified view of approximately the last 2 hours of data recording can be seen in Figure 5.40. All locations reached equilibrium temperature after approximately 9 hours (32400 sec). The greatest temperature increase was measured in the medial condyle at the location corresponding to 30° with a 6.75°C increase in temperature over the ambient condition. The location corresponding to 0° on the medial condyle experienced a 6.44°C rise. Both the locations on the lateral tibia experienced a similar rise in temperature of 6.14°C.

Location	Temperature (°C)
Fem Med 30	33.68
Fem Med 0	33.37
Fem Lat 30	33.08
Fem Lat 0	33.07
Lubricant	32.57
Fem Non Contact	32.54
Tib Non Contact	32.53
Ambient	26.93

Table 5.5: Absolute temperatures at different thermocouple locations at the conclusion of the test.

Both the non contacting positions experienced a rise in temperature of approximately 5.61°C and this was also the same as the lubricant temperature. The final recorded temperature of the Cold Junction was 26.93°C. Based on this value, the final recorded temperatures for the different locations in the TKR are shown in Table 5.5.

5.5 Discussion

Detailed response profiles from the ProSim knee wear simulator had not previously been seen in the literature. They are presented in this thesis to allow a more detailed comparison of the wear of the tibial components with other published studies. It is common for wear results to be published with just the idealised input profiles presented, however, it is clear from the results presented here that while on a well designed and calibrated simulator, the output profiles should largely match the inputs, there are variations that could possibly affect the wear results and contact areas and are therefore worth reporting. Overall following of the demand profile was good, with that obtained on the FE axis (Figure 5.6) the most accurate due to the electro-mechanical nature of the control.

The AF (Figure 5.7) was run in open loop control as this was found to give the smoothest response when compared to the alternative method of force control. Across the whole profile a time lag 0.05s or 5% was seen. This is attributed to the time constant of the pneumatic cylinder and control valve. The initial peak of 1900N was not obtained with a high degree of fidelity, due to the required speed of response, the demand load increases from 167N to

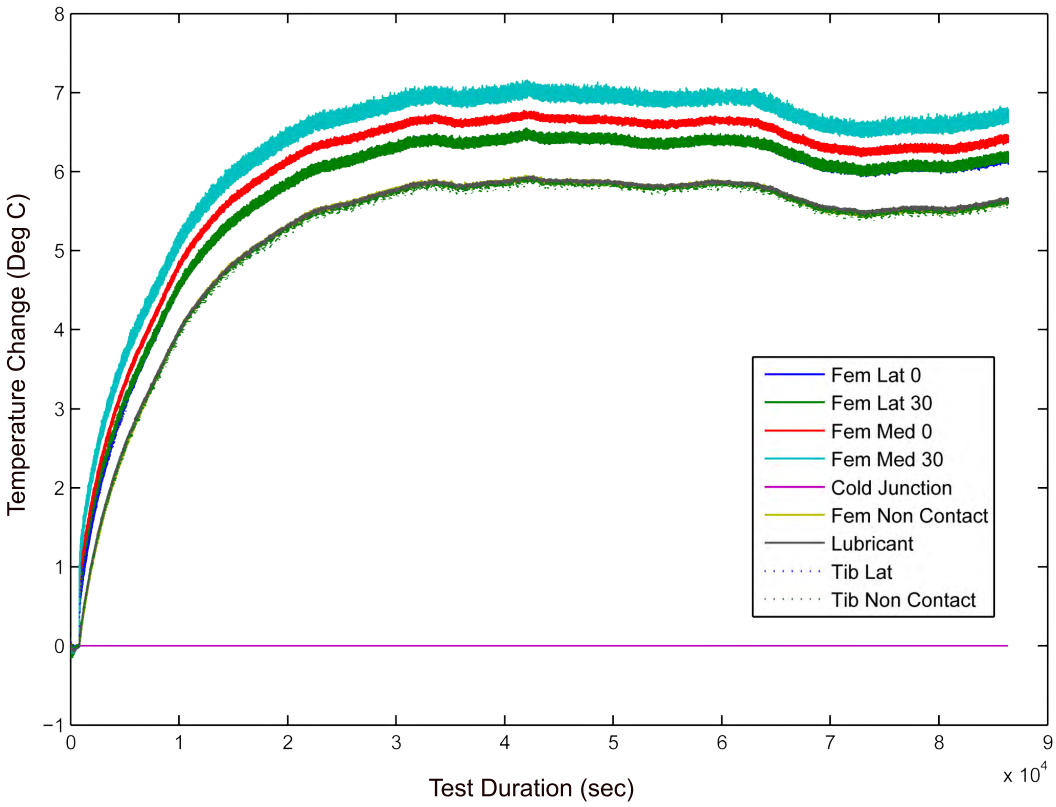

Figure 5.39: Recorded temperature traces for the eight K-type thermocouples embedded within the Vanguard TKR. All traces are plotted with respect to the ambient temperature (Cold Junction).

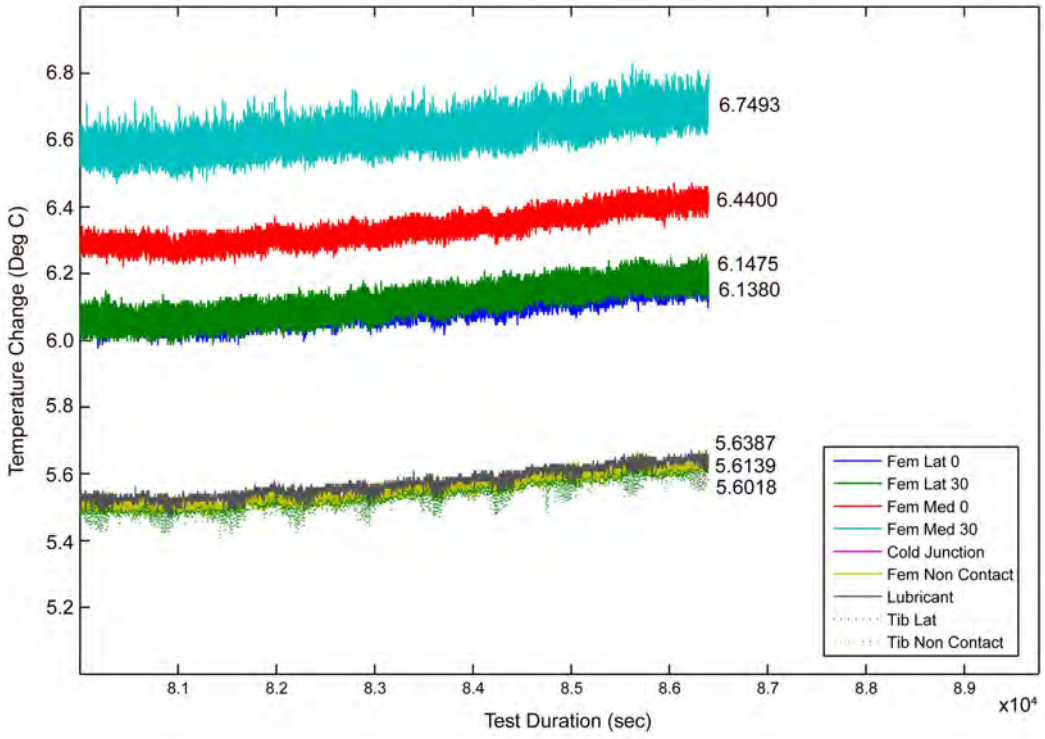

Figure 5.40: Magnified view of the final two hours of recording to allow clear distinction between the different traces. Final recorded temperatures (°C) are also shown.

1900N, this rate of increase was beyond the limitations of the Prosim simulator. The two peaks at approximately 15% and 45% of the gait cycle were achieved although in both cases the mean force applied was approximately 100N less than what was demanded. However, this was similar to, and in fact an improvement upon a previous output profile reported for the same kind of simulator (Barnett et al., 2002). The average response during the swing phase (60% to 100%) was identical to that of the demand, however the grey area during this time period indicates some degree of variation throughout the whole test duration. The tight grouping of the dashed black lines however, indicates that there was little variation between the mean response of the two recorded stations. This highlights one of the limitations of this plot in the fact it only records stations 1 and 4. On the other 3 stations used during this test, the AF was not recorded due to there not being load cells on that station. However, this is not thought to be detrimental to the test results as each cylinder was carefully calibrated prior to the test start using the protocols outlined, and any variation was not expected to be greater than that shown between the two recorded stations.

The two displacement controlled axis (TR and AP) were found to be far more difficult to control. The TR response shown in Figure 5.8 was found to largely follow that of the demand profile. For this axis all 5 stations were recorded. The grey area shows a maximum range of less than 2° between all stations for the whole duration of test. The mean responses of the individual stations, indicated by the dashed black lines show a tight grouping across all stations. The mean response of all stations combined compared to the demand response again shows a lag similar to that observed for the AF plot of around 0.05s or 5% of the gait cycle, again this is attributed to the time constants of the controller, control valve, and pneumatic actuator of the simulator. The minimum and maximum values of the demand profile were approximately -4.25° and +4.25° respectively. The recorded maximum and minimum values were less than these at +3.5° and -3° respectively. It was difficult to compare this to the responses obtained in other studies as the response profiles are not published alongside the results.

An acceptable response on the AP axis was the most difficult to obtain by a considerable margin. The response obtained is shown in Figure 5.9. The posterior then anterior shift demanded in the stance phase, between 0% and 50% of the gait cycle was not obtained. This was due to the 2.6kN axial force being applied at this time. This high force created a frictional force that was too great for the AP pneumatic cylinder to overcome. When the AF

was reduced to 167N from 50% of the gait cycle onwards, the AP response was improved and a posterior displacement of 12mm was achieved compared to the demand value of 13mm. A time lag that amounted to approximately 0.10s was also observed, again due to the time constant of the controller, control valve and pneumatic actuator. The influence of the AF on the AP response was confirmed by the trace shown in Figure 5.10. where no AF was applied to the tibia component and the response compared to the demand was far better.

All seven test UHMWPE tibia components were immersed in lubricant before the test commenced, until they all exhibited similar fluid uptake trends. This is a standard practice in the wear testing of porous components in order to equalise the fluid content and reduced to effect of fluid absorption on the wear results. In this study this amounted to 55 days soak in total. All components experienced a mass gain due to the immersion, as can be seen in Figure 5.2. All tibias bar 1 and 2 experienced highly similar fluid uptake trends. Tibias 1 and 2 were both used in the setup of the knee simulator, and to prevent excessive damage to the articulating surfaces, Vaseline was used as a temporary lubricant. It is believed that residue from this process remained on the exterior of the components and caused these two samples to have an initial fluid uptake rate that was lower than that experienced by the 5 tibias that went straight from the sterile packaging into the test lubricant. Once the two components had undergone several cleaning cycles, the barrier to normal fluid uptake was removed and after 30 days of soaking, they exhibited the same fluid uptake trend of the remaining 5 tibias. This trend was linear with an increase of 0.00178 mg/hour. The tibias were soaked at RT as it was assumed that this was the closest to the condition experienced in the Prosim knee simulator as the lubricant in the test cells was not heated (although later temperature monitoring in Section 5.4 using an instrumented TKR disproved that assumption).

During the wear testing of the five UHMWPE tibias, the fluid uptake of the two control tibias was monitored. Upon commencement of the wear test, one control sample was dynamically loaded in serum using the same load profile as the five articulating tibias loaded and the other just placed in serum at RT. Both control tibias continued to gain mass although the loaded sample (tibia 4) then experienced a greater mass increase than the soaked sample (tibia 3) this is illustrated in Figure 5.4. The rate of fluid uptake of the soak tibia reduced to 0.00071 mg/hour, a reduction of over 50% on the rate during the initial soak period. The dynamically loaded tibia however, continues at a rate of 0.00160 mg/hour, which

is comparable to the rate shown during the pre test soaking. A very interesting finding is the highly linear relationship between the mass increase of the loaded soak relative to the unloaded soak, which has not been explicitly presented in the literature to date. A later test in section 5.2 confirmed the increase in fluid uptake due to loading, but the linear trend was less clear, due to the shorter test time. It is hypothesised that the reduction in fluid uptake rate of the soak control tibia compared to the initial measured rates could be due to two factors. Firstly, during the wear test the soak controls were mounted inside the I-Beam tibial tray. The fit is tight, therefore the lower, non-articulating surface was not exposed to the lubricant as it was in the presoak, and as fluid uptake is proportional to surface area (Klapperich et al., 2000) this would have an effect. Secondly, it may indicate saturation of the voids within the sample. Although this is contrary to other observations that have shown that the total mass increase of UHMWPE tibia bearings due to fluid absorptions shows no difference between 48 and 92 days soak duration (Brandt et al., 2011). However, it should be noted that this test used Distilled Water (DW) as the soak media, and not diluted bovine serum as in this test. However, in a separate study of fluid absorption into UHMWPE acetabular cups, a biphasic curve was observed with 600% higher rate of fluid absorption noted in the first 30 days of soak than that observed between 30 and 400 days of soak (Clarke et al., 1985). Other ArCom samples have been shown to have a fluid uptake rate of 0.11 and 0.14 mg/day for 1900H and GUR1050 resins respectively when soaked in double distilled water (Tsukamoto et al., 2008). There is still a question of why the loaded soak control sample experiences a higher rate of fluid absorption than the unloaded sample. Fluid uptake experiments using diluted bovine serum and orthopaedic grade UHMWPE discs revealed a linear relationship between lubricant pressure and fluid uptake rates, the pressures tested were between 0 and 10 MPa (Blanchet et al., 2002). Now it is not suggested that the lubricant becomes pressurised in any way, rather that on loading the insert, the insert is compressed elastically and air is expelled from the voids in the polyethylene. On release of the load the insert recovers it original shape and draws the lubricant into the voids to replace the expelled air. In a similar way pressurising the lubricant creates a negative pressure in the voids within the insert. It is difficult to compare the fluid uptake rates with literature as they are highly dependent on a number of factors including temperature, pressure, UHMWPE type, sterilisation method, and surface area (Klapperich et al., 2000).

The volumetric wear rate of the 5 tested ArCom® joints was $6.46 \pm 1.80 mm^3$ per $1x10^6$

cycles. This was markedly lower than the PFC sigma (DePuy) joint that is currently the market leader (36%) in the UK for TKR procedures (NJR for England and Wales, 2010) which when tested in a similar simulator with comparable loads and displacements, exhibited a volumetric wear rate of 18.1 ± 3 mm^3/MC, approximately 3 times that of the ArCom joints in this test (Barnett et al., 2002). The components tested were size 3 with 10mm inserts, which corresponds to a ML width of the femur of 66mm, compared to the femurs in this test that had a ML dimension of 57.5mm. Although at present the influence of prosthesis size on wear rates is unknown, however an interesting question arises when testing TKRs of different sizes, in that usually a heavier patient would require a larger knee replacement. Hence, while the applied loads would be greater, the contact area would be greater also, and while the total volumetric wear may be larger, the total volumetric wear as a percentage of the total volume of the insert may not be that different. It should be noted though, that it is inherently difficult to compare results across research institutions due to the many variables that exist in simulator testing of joint replacement solutions. In the TKR field the main factors affecting simulated implant wear include: The geometry of the components; The material properties of the components; Kinematics and loads applied to the components; And the lubricants used. Standards have been developed in order to facilitate inter-laboratory comparisons, however, these are still very much used as a guide rather than a strict set of instructions. Additionally, due to the wide variety of gait, BMI, size, and activity of patients, different designs of TKR from different manufacturers may well be suited to different patients. It is hoped that future developments of computer wear simulations will allow matching of implants to individual patients.

Other tests of the ArCom® UHMWPE are difficult to find. The only test in literature is that by Tsukamoto *et al* which was conducted on posterior cruciate sacrificing TKRs, which exhibited a volumetric wear rates of 3.4 and 3.6 mm^3/MC for GUR1050 and 1900H UHMWPE resins respectively (Tsukamoto et al., 2008). The displacements and loads used were significantly smaller than those used in this study, however it does confirm the excellent wear properties afforded by the ArCom® UHMWPE. McEwen *et al* showed a slight increase in the PFC Sigma knee paired with GUR1020 inserts with a wear rate of 23±5.9 mm^3/MC and in the same study used a mildly cross-linked GUR1050 insert which exhibited a wear rate of 13±3.9 mm^3/MC using comparable conditions to this study (McEwen et al., 2005). This is approximately double that exhibited by the ArCom® tibia inserts in this

study. Wang *et al* tested Compression Moulded GUR 1020 inserts of the Triathlon CR design in a MTS simulator using a less severe ISO displacement profile and achieved a wear rate of 17.7±2.2 mm^3/MC (Wang et al., 2008). Finally Affatato *et al* tested a 913-MP design knee with GUR 1050 inserts in a Shore Western simulator using the ISO displacement profiles and achieved a wear rate of 22.6 mm^3/MC (Affatato et al., 2008). A summary of these results is listed in table 5.6 and more could be listed, however the conclusion would be the same. Being that the ArCom® variant of the DCM process produced tibia inserts with some of the lowest wear rates found in literature. No explanation can be offered for the lower wear of tibia 5 and all historical data regarding the manufacture of this component has been checked by the manufacturer[4].

Survivorship data for the PCR PFC Sigma (DePuy) indicates a 90% survival after 10 years (Schai et al., 1998), however wear related problems were evident in 8% of cases. It should be noted though that these components had been sterilised using gamma radiation in air, which leads to excessive oxidation and hence increased wear, compared to the newer method of gamma radiation in a vacuum (McEwen et al., 2005). It is therefore hypothesised that the clinical wear performance of the Vanguard CR TKR would be at least comparable, if not better than that of the PFC Sigma.

The thermocouple instrumented TKR revealed that even though there was no external heating of the test stations, there was still a temperature increase in the test cells due to frictional heating between the TKR components. It was observed that the temperature rose to approximately 6.5°C above the ambient lab temperature. In order to maintain the structure of the articulating surfaces the thermocouples were placed 0.5mm below the surface, therefore the temperatures measured would not be the surface temperatures. After normalising the data, it was found that the greatest temperature increase occurred on the medial condyle of the femur at 30° from the home position, with an increase 6.7°. With reference to the recorded response profiles, and assuming a flat plate contact, this point would be in contact when there is still approximately 2.0kN load, and maximum FE velocity. Additionally, the AF is applied more to the medial side than the lateral, thereby offering an explanation of why the temperature of the medial side was greater than on the lateral. The lubricant, and non-contacting positions on both the tibia and femur all experienced the lowest temperature increase of 5.6°C, indicating that the contact

[4]Personal communication with Biomet UK

areas that are generating the heat. The thermocouples on both the medial and lateral sides of the tibia failed early on in the test. These had to be routed through the I-Beam tibial tray into the UHMWPE bearing. It is hypothesised that there was enough relative movement between the two to cause the failure of the thermocouples. There is precious little data in the literature about experimental measurement of the heat generated at the bearing surfaces. Surface temperature increases of 12°C have been measured using a infra-red radiometric microscope when a UHMWPE ring was slid against smooth sapphire glass (Al_2O_3). Interestingly, lubricant temperature was also measured using a thermocouple and a linear relationship between lubricant and surface temperature was found, with a 6°C rise in lubricant temperature linked to a 11°C rise in surface contact temperature (Imado et al., 2004), thus linking well with the results found in our study. It only took 30mins for the lubricant temp to reach this value, rather than the 8 hours in our study, however, the volume of lubricant used was only 40cc compared to the 450ml (450cc) used in our test.

Observations of the backside of the tibia, which contacts the I-beam tibia tray revealed machining marks at the start of the test. These were gradually removed, although there were no scratches which suggests they were not removed by abrasion, rather by creep of the material due the high loads and motions applied on the articulating surface. This is corroborated by the finding that the greatest amount of machining marks removal on the backside occurred directly underneath the contact areas with the the two femoral condyles. The effect was greater on the articulating components, than on the load soak control, and was not observed at all on the soak control. It is hypothesised that the increase temperature in the articulating stations caused by frictional heating due to motion, would have allowed more flow of the material than in the LSC where there was no motions. This was confirmed in temperature measurement experiments conducted using the instrumented prosthesis, discussed earlier in this section.

Analysis of the wear scar areas revealed a larger (53.7%) wear scar on the lateral side of the tibia compared to the medial (46.3%). The design of the TKR was highly symmetrical, so this was somewhat unexpected, however in order to achieve the ML offset prescribed in the standard (BS ISO 14243) the tibia component had to be offset from the AF axis by 4.28mm in the lateral direction, however, this meant that it was also offset from the centre of TR by the same amount. This was unavoidable as the TR and AF axis are fixed in the simulator and cannot be adjusted. As a result of the offset from the TR centre of rotation,

a rotation of the tibia would then result in a larger displacement of the lateral side than the medial, therefore resulting in a larger wear scar area. Wear scar patterns were similar to those demonstrated in the literature (Schwenke et al., 2009).

Observations of the articulating surface of the tibia component revealed striking wear features and a location dependance for some. There is not a great deal of published data on surface observations as most seems to be concerned with the numerical wear data. However, with one of the main causes of joint failure being due to osteolyis caused by wear particles, analysis of the generation sites of these wear particles seems prudent. The wear of the modern DCM UHMWPE used in this study certainly seems less severe than that observed almost 3 decades ago (Hood et al., 1983). With wear modes such as embedded cement and delamination not observed. Five distinct modes of wear were observed, and attempts made to quantify the locations at which these occurred. Distinct protrusions were seen, and these are thought to have formed due to plastic flow of UHMWPE during the highly loaded stance phase. Adhesive wear was found mainly to occur to the anterior of the protrusions, suggesting that the material was transfered and adhered to the surface during the swing phase, in which the tibia moves posteriorly with respect to the femur. Scratching was mainly found towards the posterior of the wear scar area. Similar rippling features to those observed on UHMWPE acetabular cups (Wang et al., 1995b) were also found. Cyclic loading of the tibia inserts was found to cause fatigue cracks on the articular surface. femoral damage was found to occur in the form of scratches running in the AP and FE direction.

The surface roughness (R_a) was monitored using a Zygo non-contacting interferometer. The surface roughness of the articular components was found to be in-homogeneous, with some areas experiencing a smoothing effect and some become rougher. On average the articulating components were found to be rougher than they were at the commencement of the test. The surface roughness of the tibia components at the conclusion of the test ($0.122\pm0.069\mu$m) was higher than that observed on the UHMWPE plates with varying molecular weights used in the POP testing. These dropped from $0.139\pm0.037\mu$m, measured on the three control plates, to $0.050\pm0.047\mu$m, measured on the four test plates. This indicates differing trends, with the initial post processing surface condition of the tibial bearings being superior to that of the UHMWPE plates. A possible explanation for this improved surface finish is that although both the plates and tibial bearings were manufactured using the same DCM process, the tibial bearings were produced to orthopaedic device standards,

whereas the plates were produced for experimental purposes only. This is also reflected in the optical micrographs, with far less pitting observed on the tibial bearings when compared to the plates. At the conclusion of the respective wear tests The surface roughness of the tibial bearings had increased to 0.122±0.069μm, in contrast to the plates which had dropped to 0.050±0.047μm. This indicates that the relatively low loads and simple motions used in the POP simulators had a burnishing effect whereas the high loads and more complex motions found within the knee joint had a much more damaging effect on the UHMWPE surface.

5.5.1 Summary

In summary the ArCom® bearings were found to perform better than most comparable designs tested in the literature. This was true even under the high kinematic conditions that were using in this study. The importance of using a LSC was demonstrated due to increased fluid uptake over a non-loaded soak control. Analysis of the wear particle generation sites revealed five distinct types of surface feature and the location dependance of these. Examples of surface rippling were found after just 0.1 MC. The friction between the articulating components raised the test cell temperature to approximately 6°C above RT and it is hypothesised that the surface temperature could be greater still.

Study	PE Type	Aged	Design	Simulator	Profile	Lubricant	Duration	Wear Rate
This study	ArCom UHMWPE	No	Vanguard CR	Prosim (Pneumatic)	ISO AF, FE - Lafortune AP, TR	25% BS	5.0 MC	6.46 ± 1.80 mm^3/MC
Barnett et al. (2002)	GV UHMWPE GUR1020	No	PFC Sigma (Size 3)	Prosim (Pneumatic)	ISO AF, FE - Lafortune AP, TR	25% BS	2.0 MC	18.1 ± 3 mm^3/MC
Tsukamoto et al. (2008)	ArCom GUR1050	No	Vanguard PCR sacrificing	Shore Western	Stance Phase only. Max AF 2kN, Max FE 20°, TR ±5°, AP 6mm	50% BS	2.5 MC	3.4 mm^3/MC
Tsukamoto et al. (2008)	ArCom 1900H	No	Vanguard PCR sacrificing	Shore Western	Stance Phase only. Max AF 2kN, Max FE 20°, TR ±5°, AP 6mm	50% BS	2.5 MC	3.6 mm^3/MC
McEwen et al. (2005)	GUR1020 Gamma Air	Shelf 29-33 months	PFC	Prosim (Pneumatic)	ISO AF, FE - Lafortune AP, TR	25% BS	3.0 MC	41±14 mm^3/MC
McEwen et al. (2005)	GUR1020 GVF	No	PFC Sigma	Prosim (Pneumatic)	ISO AF, FE - Lafortune AP, TR	25% BS	5.0 MC	23±5.9 mm^3/MC
McEwen et al. (2005)	GUR1050 Marathon GP (Mildly XL)	No	PFC Sigma	Prosim (Pneumatic)	ISO AF, FE - Lafortune AP, TR	25% BS	5.0 MC	13±3.9 mm^3/MC
Wang et al. (2008)	Com. Mould. GUR 1020	No	Triathlon CR	MTS	ISO Disp.	50% BS	5.0MC	17.7±2.2mm^3/MC
Affatato et al. (2008)	GUR 1050	No	913-MP	Shore Western	ISO Disp.	25% BS	2.0 MC	22.6 mm^3/MC

Table 5.6: Comparison of ArCom wear rates with other non-crosslinked UHMWPE in literature

Chapter 6

Vitamin E infused highly cross-linked UHMWPE

The addition of Vitamin E (α-Tocopherol) to XL UHMWPE has been shown in the literature to reduce post-irradiation oxidation without the need for re-melting of the UHMWPE samples. Thereby, retaining a high degree of cross-linking combined with good fatigue resistance. However, questions remain about the general suitability of using highly XL UHMWPE in TKRs due to higher contact stresses involved compared to THRs. In this chapter, Vitamin E infused, highly cross-linked UHMWPE (termed E1^{TM}) tibia bearings have been tested in multiple ways in order to assess their suitability for use in TKR.

6.1 E1^{TM} Wear Test

In order to assess the possible *in vivo* wear characteristics of the E1^{TM} material, a wear test was conducted using similar conditions to that of the ArCom® components to allow for a direct comparison. The test was run for a total of 9x10^6 cycles. This was 4x10^6 cycles longer than run in the previous ArCom® wear test, with the rationale that the fatigue resistance of the E1^{TM} tibias is of particular interest, and this would more likely be highlighted with a longer test duration.

The demand profiles for the simulator were modified slightly from the form used for the previous ArCom® test, as there were delays in the output profile when compared to the demand profile. To counteract this the AF profile was phase shifted by 5% in the

leading direction. The AP displacement demand profile was also modified in a similar way with a phase shift of 10% in the leading direction. The maximum AP displacement in the anterior direction was also limited to 11mm, in an attempt to limit the oscillation at the limit of posterior movement experienced in the previous test. Some small adjustments in the PID settings of the simulator were also conducted and these are listed in Table 6.2. The calibration constants used during the simulation can also be seen in Table 6.3. The response of each test station was logged once in every 1000 cycles and processed as described in Section 4.5.2.

6.1.1 Materials and methods

Eight complete Vanguard design TKRs (Biomet, UK) were used in the wear test and these had identical geometry as the ArCom® Vanguard components used in the previous test. The design of the fixation mounts for both the tibia tray and femoral component was therefore identical to those previously used. The schematics for these components can be found in Appendix A.3.1. The tibia bearings were manufactured from ArCom® bar-stock, which in turn was manufactured from GUR1050 UHMWPE resin using a hot-isostatic compression moulding process. The bar-stock is machined into smaller specimens and irradiated with 10 Mrad (100kGy) which caused cross-links to form between the polymer chains. Vitamin E was infused into the cross-linked material, then the components were machined into the final geometry, cleaned, packaged, and gamma sterilised. All processes were conducted at a temperature lower than the melting temperature in order to preserve the mechanical properties of the cross-linked UHMWPE.

The TKR sets were rotated around the six test stations at 1MC intervals in order to minimise the influence of inter station variability. The station locations of each femoral and tibia component during the wear test is shown in table 6.1.

Extensive optical analysis was conducted on the articulating surfaces of the E1™ tibia samples. 15 locations were selected on each condyle with the majority of these selected so that they fall within or on the edge of the wear scar. The tibia inserts were imaged on removal from the sterile packaging then at 0.5 MC intervals up until 5.5 MC then again at 8.0 MC. The backside of each tibia was also imaged in six locations at each observation interval.

	0-1 MC 6-7 MC		1-2 MC 7-8 MC		2-3 MC 8-9 MC		3-4 MC		4-5 MC		5-6 MC	
Station	Fem	Tib	Fem	Tib	Fem	Tib	Fem	Tib	Fem	Tib	Fem	Tib
0	A2	1	A7	6	A6	5	A5	4	A4	3	A3	2
1	A3	2	A2	1	A7	6	A6	5	A5	4	A4	3
2	A4	3	A3	2	A2	1	A7	6	A6	5	A5	4
3	A5	4	A4	3	A3	2	A2	1	A7	6	A6	5
4	A6	5	A5	4	A4	3	A3	2	A2	1	A7	6
5	A7	6	A6	5	A5	4	A4	3	A3	2	A2	1
LSC	A1	7	A1	7	A1	7	A1	7	A1	7	A1	7
SC	-	8	-	8	-	8	-	8	-	8	-	8

Table 6.1: Tibia (Tib) and Femoral (Fem) station locations during 9.0 MC wear test.

6.1.1.1 Simulator Setup

The simulator was setup in accordance with the procedures outlined in chapter 4. However for this test some minor changes were made to the test procedure. In order to minimise any medial/lateral alignment errors between the femoral and tibial components, both the tibial and femoral and components were set in their home position and the medial lateral clamping rings were slackened off. The tibial and femoral components were then brought together and the femoral component was allowed to self align in the medial lateral direction. Once the components were aligned, the medial/lateral clamping rings were tightened. Slight adjustments were also made to the gains in the PID controller in an attempt to improve the following of the demand profile.

6.1.2 Results

The results from the wear test conducted on the E1^{TM} tibial bearings are presented in this section. The fluid uptake of the tibia components is shown, followed by the volumetric wear of the tibial components during the 9 MC wear test. Optical and topographical data is also presented of both the tibial or femoral components. Finally, the results of the increased loading test are also shown.

Station		0	1	2	3	4	5
AP Disp. Gain	P	200	200	350	150	350	300
	I	4000	4000	4000	1500	3500	500
	D	375	375	350	50	375	15
TR Disp. Gain	P	150	200	150	200	300	75
	I	2000	1500	1500	1500	1500	1000
	D	50	50	50	50	50	25
AP Disp. Average	P	6	6	6	6	6	6
	I	1	1	1	1	1	1
	D	2	2	2	2	2	2
TR Disp. Average	P	1	1	1	1	1	1
	I	1	1	1	1	1	1
	D	1	1	1	1	1	1

Table 6.2: Simulator PID controller settings for E1^{TM} wear testing.

Station	0	1	2	3	4	5
AP mm/ADC	0.0003711	0.0003287	0.0003512	0.0002646	0.0003462	0.0002495
AP Zero Disp. Offset	-4.58	-6.71	-3.20	-4.44	-7.83	-5.05
TR °/ADC	0.000298	0.000359	0.000297	0.000373	0.000355	0.000163
TR Zero Disp. Offset	-0.44	-0.94	-0.79	0.037	0.068	0.60
AF Valve per N	0.055332	0.054887	0.055766	0.057188	0.056428	0.057174
AF Valve Offset	0.226825	-2.542081	3.291981	0.041965	0.115496	-0.562775
AF Loadcell N/ADU	-	0.076295	-	-	0.078115	
AF Loadcell Offset	-	-85.078627	-	-	-50.196001	

Table 6.3: Simulator calibration constants for E1^{TM} wear testing.

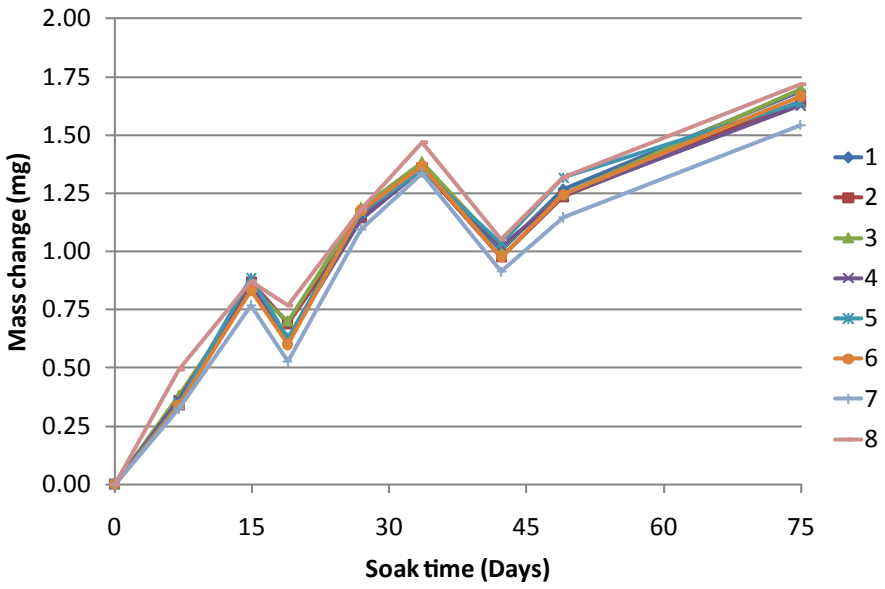

Figure 6.1: Fluid uptake of the eight E1^{TM} tibias (prior to wear testing).

Tibia	1	2	3	4	5	6	7	8
mg/day	0.017	0.016	0.017	0.016	0.017	0.017	0.016	0.016
RSQ	0.771	0.744	0.765	0.759	0.757	0.742	0.708	0.768

Table 6.4: Mass increase rates (linear) of E1^{TM} tibias prior to wear testing.

6.1.2.1 Lubricant Uptake

Prior to testing the eight E1^{TM} test components were soaked in lubricant for a total of 75 days. The tibias were gravimetrically assessed at approximately 7 day intervals. All eight tibias experienced a similar mass increase as can be seen in Figure 6.1.

6.1.2.2 Gravimetric Results

The wear test was run for a total of 9x10^6 cycles with gravimetric analysis occurring at 5x10^5 cycle intervals. Volumetric wear rates were calculated using a density value obtained using the Mettler Toledo AX205 balance with accompanying density kit. Two cores were taken from tibia 8 (soak control tibia) after it had been in soak for 8x10^6 cycles, this equated to approximately 219 days in soak. The density of each core was measured seven times and a mean value taken. This was 0.914 g/cm^3. The volumetric wear plots of the six test samples and the mean are shown in Figure 6.2. The volumetric wear rates are shown in Table 6.5. The mean wear rate was 0.853 mm^3 per 1x10^6 cycles.

The mass change of the two control samples can be seen in Figure 6.3. Upon commence-

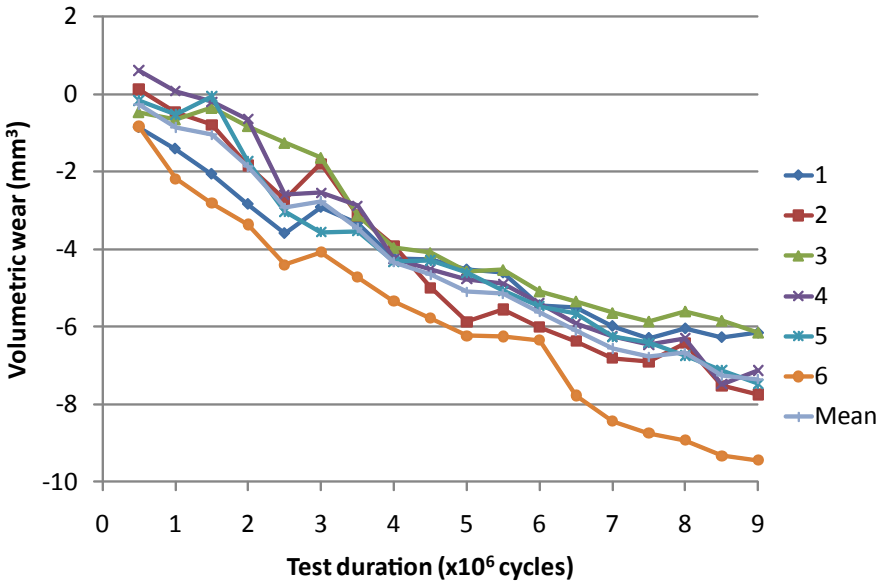

Figure 6.2: Volumetric wear plots of individual E1^{TM} tibia bearings during 9.0 MC wear test

Tibia	1	2	3	4	5	6	Mean
Vol. Wear (mm^3 per MC)	0.628	0.944	0.774	0.948	0.861	0.961	0.853
RSQ	0.943	0.944	0.926	0.951	0.949	0.977	0.970

Table 6.5: Volumetric wear rates of E1^{TM} tibia samples.

ment of the wear test at approximately 75 days the two soak samples take two distinct paths. Prior to commencement of the wear test both the samples increased in mass at a rate of 0.016mg/day however, during the wear test, the fluid uptake rate of the soak control (tibia 8) dropped to 0.008 mg/day while the fluid uptake of the load soak control (tibia 7) increased to 0.024 mg/day.

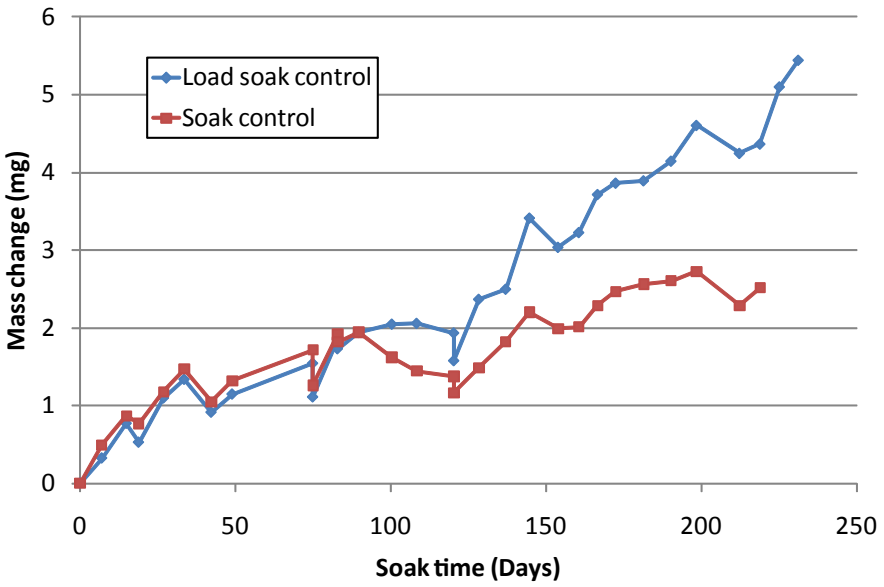

Figure 6.3: Mass change of the two E1^{TM} control tibias.

Observing the relative difference between the two control tibias by normalising the data to the soak control gives the plot shown in Figure 6.4.

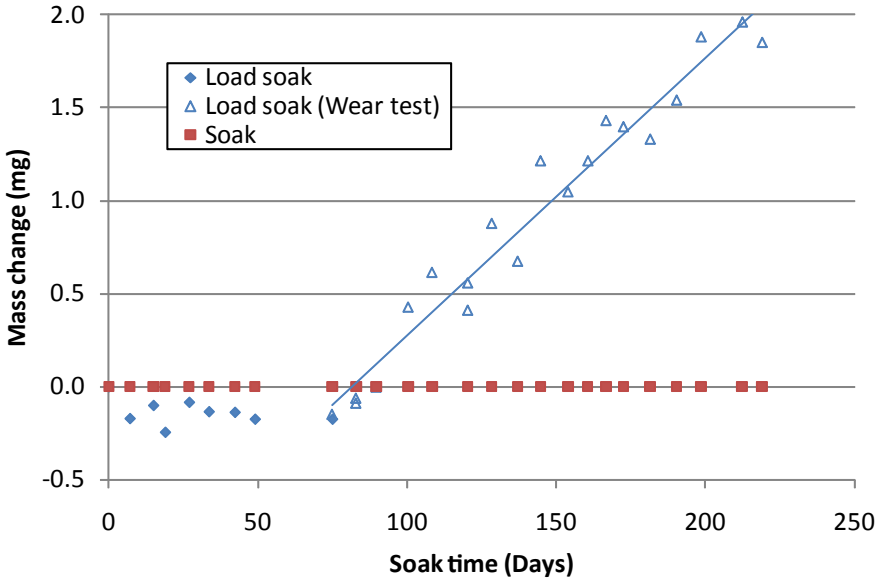

Figure 6.4: Relative mass change of the load soak compared to the soak control over the course of pre-soak and wear test.

Applying a least squares fit to the difference in mass increase between the load soak and soak control during the wear test gave a figure of 0.015 mg/day.

6.1.2.3 Apparent wear scars

The wear scars on the six wear tested tibias and the one LSC after 2.5x10^6 cycles of testing are shown in Figure 6.5.

6.1.2.4 Surface Analysis

The mean surface roughness if the worn areas for each of the E1^{TM} test tibias is shown in Figure 6.9. Readings were taken at 28 locations on each tibia, chosen to fall within, on the boundary of, and outside the predicted wear scar area. The locations were symmetrical for the medial and lateral sides of the tibia. Prior to testing the machined finish of the eight E1^{TM} tibia components had a mean surface roughness of 1.776$\pm$0.044μm. The small standard deviation indicating that the manufacturing methods culminated in comparative surface finishes for all components. An example of the typical surface finish is shown in Figure 6.12.

After 2.5x10^6 cycles of testing, a significant reduction in surface roughness was observed for the 6 E1^{TM} tibias that had undergone wear testing. For the purposes of the mean surface roughness, only locations that fell within the wear scar area were used for the calculation, this resulted in 2 locations on the medial side, and 8 locations on the lateral side of the tibia being omitted from the calculation at both 2.5x10^6 and 8.0x10^6 cycles. After 2.5x10^6 cycles the mean surface roughness of the 6 wear tested tibias was 0.162$\pm$0.058μm, and after 8.0x10^6 cycles this reduced even further to 0.080$\pm$0.013μm. It was also observed that some areas on the extremities of the wear scar that were previously unworn after 2.5x10^6 cycles, had a detectable drop in surface roughness after 8.0x10^6 cycles, indicating a larger wear scar area, due to penetration of the femoral component into the tibia. There was no detectable difference between the medial and lateral sides of the tibia. The mean surface roughness of LSC tibia 7 remained consistently high throughout the test with mean values of 1.748$\pm$0.204μm, 1.864$\pm$0.455μm, and 1.806$\pm$0.393μm after 0.0, 2.5, and 8.0 x10^6 cycles respectively.

A clear demonstration in the removal of the machining marks can be seen in Figure 6.10. This set of scans shows the same location on tibia 3 and the burnishing action that reduces

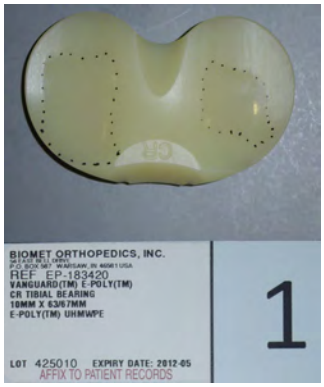

(a) Wear scar on E1^{TM} tibia 1 after 2.5x10^{6} cycles of testing.

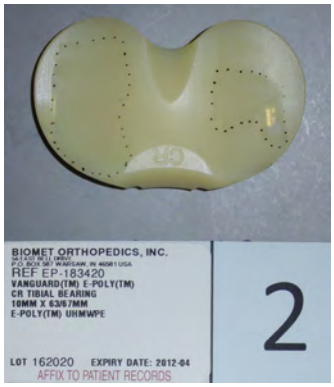

(b) Wear scar on E1^{TM} tibia 2 after 2.5x10^{6} cycles of testing.

(c) Wear scar on E1^{TM} tibia 3 after 2.5x10^{6} cycles of testing.

(d) Wear scar on E1^{TM} tibia 4 after 2.5x10^{6} cycles of testing.

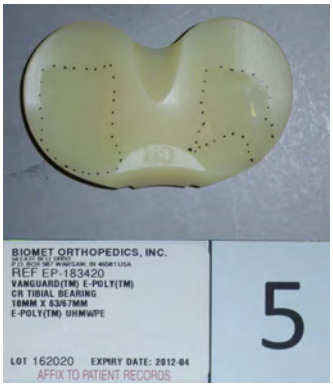

(e) Wear scar on E1^{TM} tibia 5 after 2.5x10^{6} cycles of testing.

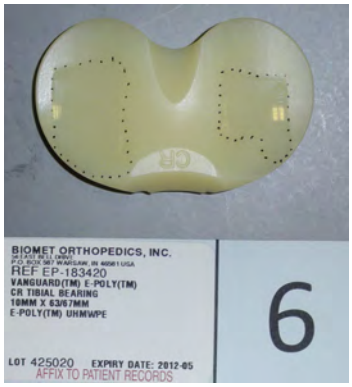

(f) Wear scar on E1^{TM} tibia 6 after 2.5x10^{6} cycles of testing.

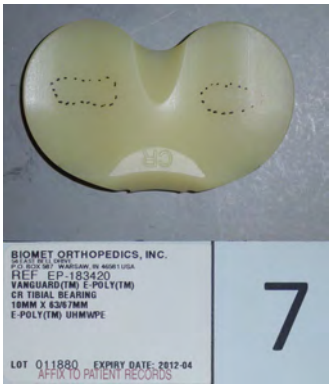

(g) Wear scar on E1^{TM} tibia 7 (LSC) after 2.5x10^{6} cycles of testing.

Figure 6.5: Observed wear scars on the articulating surfaces of the E1^{TM} tibia after 2.5x10^{6} cycles of wear testing. Areas have been assessed with the naked eye and the observed area marked using a non permanent marker pen.

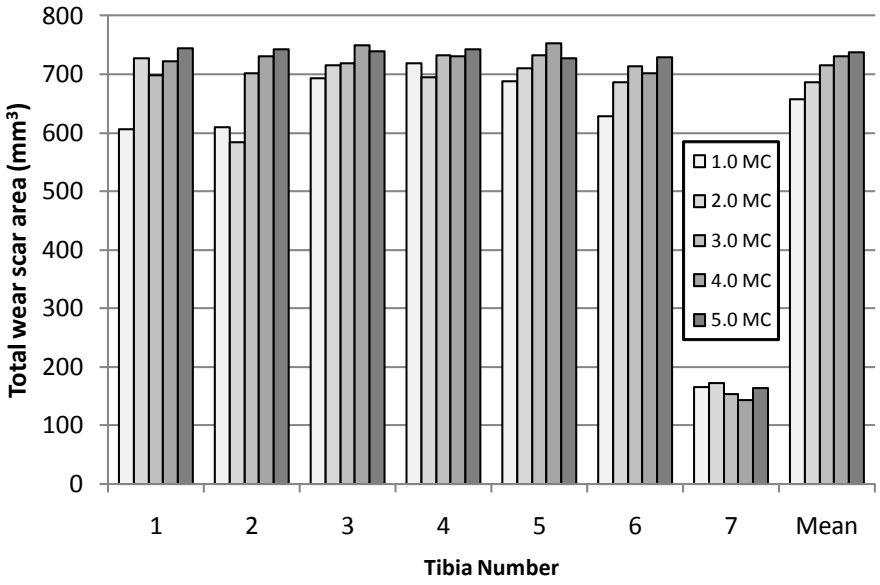

Figure 6.6: Total apparent wear scar areas for the E1^{TM} test tibias.

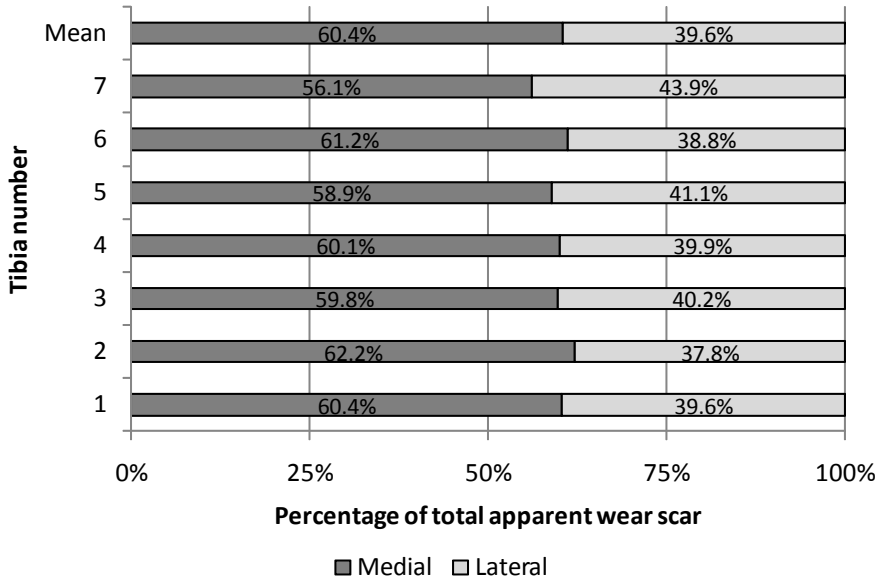

Figure 6.7: Proportion of the apparent wear scar area on the medial and lateral condyles.

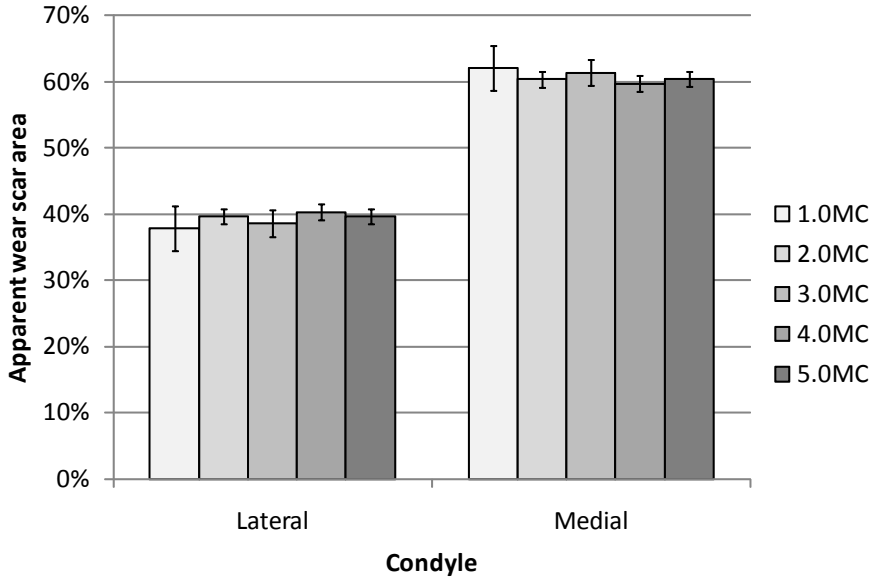

Figure 6.8: Proportion of apparent wear scar area on each tibia condyle at increasing test durations.

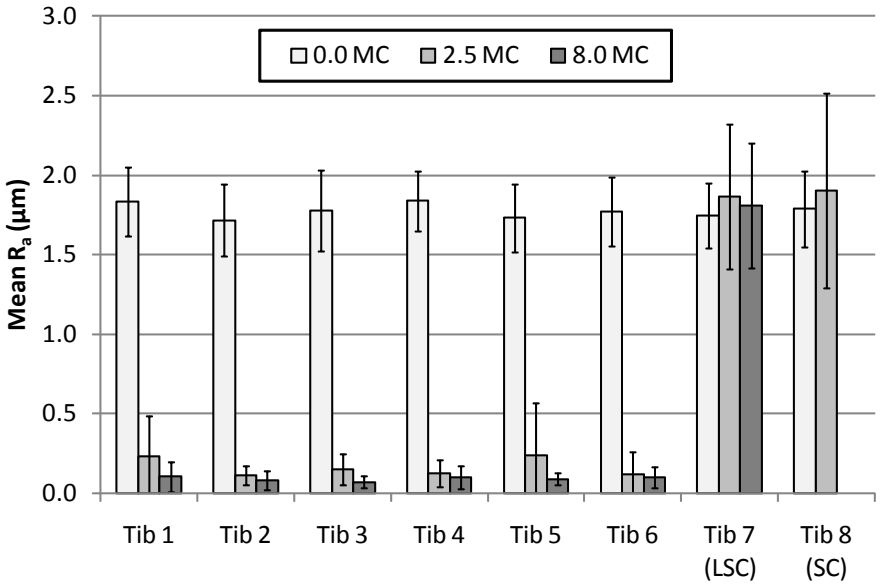

Figure 6.9: Plot showing the mean $R_a \pm 1$SD of the worn area of each of the E1^{TM} tibias prior to testing, and at 2.5MC and 8.0MC durations. The soak control (tibia 8) was required for other testing so was unavailable for measurement at 8.0MC.

the surface roughness of the surface from 1.624μm prior to testing, to 0.071μm after 8.0 MC of testing.

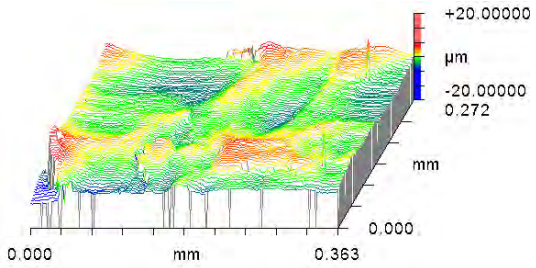

(a) Surface prior to testing at 0.0 MC. R_a=1.624μm.

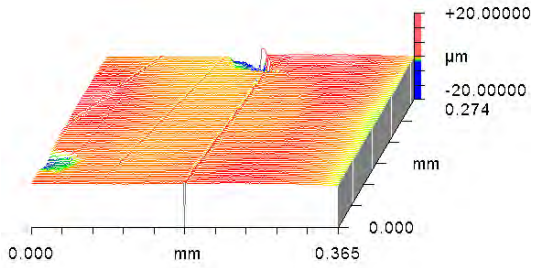

(b) Surface after 2.5 MC of testing. R_a=0.277μm.

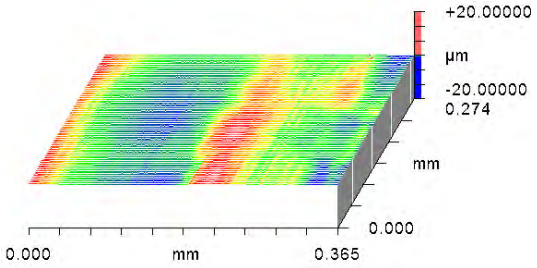

(c) Surface after 8.0 MC of testing. R_a=0.071μm.

Figure 6.10: Zygo scans demonstrating the smoothing effect of machine mark removal on E1^{TM} Tibia 3 at location X55 Y15 at various stages throughout the test. Note that the z-axis has been set to $\pm$20μm for all images.

Zygo scans of additional types of observed wear are shown in Figure 6.11. Here an example of the rippling and scratching type features observed on the surface of the E1^{TM} are shown.

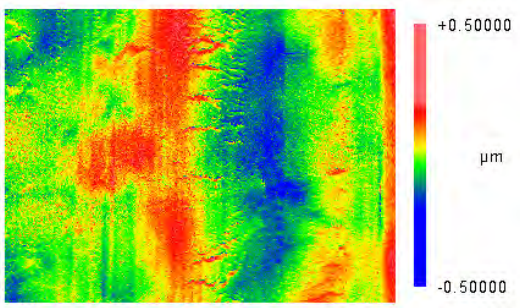

(a) Zygo scan showing evidence of rippling features at location X5 Y21. R_a=0.068μm.

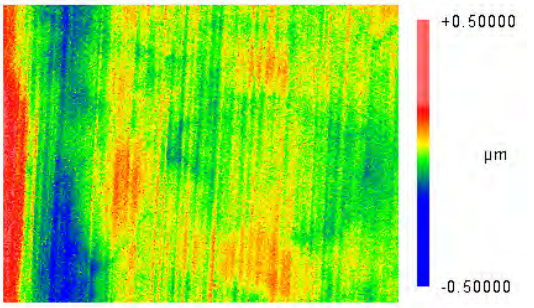

(b) Zygo scan showing evidence of fine scratching in the AP direction at location X52 Y21. R_a=0.045μm.

Figure 6.11: Zygo scans demonstrating the smoothing effect of machine mark removal on E1^{TM} Tibia 3 at different locations after 8.0 MC of wear.

Surface analysis using the optical microscope upon removal of the E1^{TM} tibias from

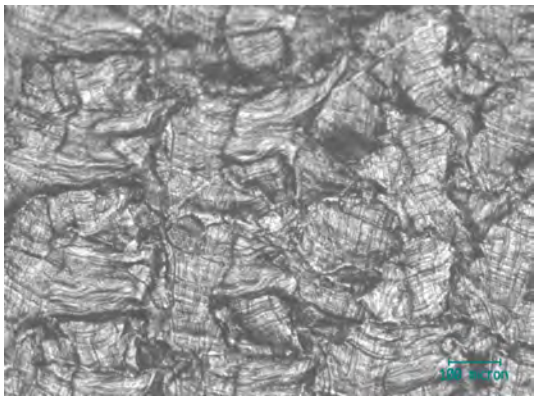

Figure 6.12: Optical micrograph of E1^{TM} tibia 2 at location X55 Y15 on removal from packaging. Machining marks can clearly be seen.

their packaging showed distinct tessellation like features caused by machining post infusion. All eight tibias were highly similar so only on example is shown in Figure 6.12. Outside of the wear track, there was no observable change in the appearance of the E1^{TM} surface. At locations on the edge of the wear scar area here initially was no change in the surface appearance, but as the central area of the wear area became more worn, the edges started to show partial wear as seen in the sequence of images in Figure 6.13. It can be seen that by 5.0 MC most evidence of the machining marks had been removed. Observations towards the centre of the wear scar area revealed that the machining marks were removed after just 0.5MC cycles as can be seen in Figure 6.14. In general, the E1^{TM} tibias had a highly homogeneous appearance when compared to the previously tested ArCom® tibia bearings. The most commonly observed wear mechanisms were scratching and burnishing. Rippling was also observed, although this was limited to the central areas of the medial wear scar, mainly in the area defined by X 5-8 and Y 15-18. Only 6 occurrences of rippling were observed on the lateral side of the tibia compared to 23 on the medial side. Typical examples of the observed rippling can be seen in Figure 6.15. Burnishing was commonly seen on all areas of the wear scar area and often featured fine scratches running in the AP direction. Examples of the burnishing type wear can be seen in Figure 6.16. Scratching was also prevalent across the whole of the wear scar area at all time points, as shown in Figure 6.17. Examination of the underside of the E1^{TM} revealed the removal of machining marks in areas underneath the contact points. At areas away from the contact the machining marks remained as can be seen in Figure 6.18.

The location of each optical micrograph was also recorded. An assessment was made of the predominant type of wear on each image, and these results are plotted in Figure 6.19.

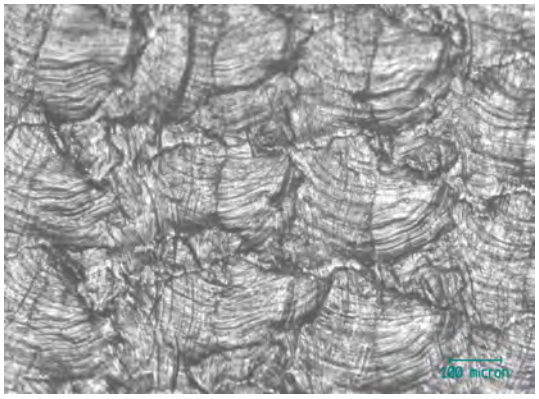

(a) Optical micrograph at removal from packaging.

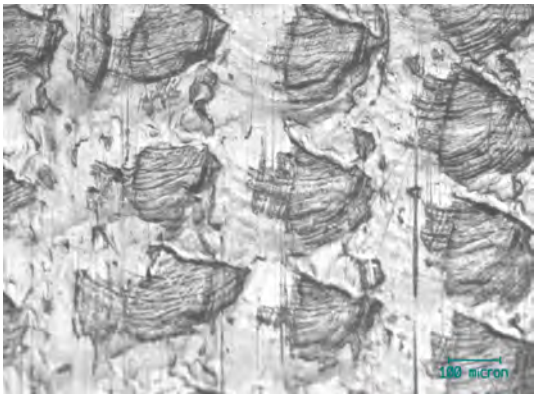

(b) Optical micrograph after 0.5 MC of wear testing.

(c) Optical micrograph after 2.5 MC of wear testing.

(d) Optical micrograph after 5.0 MC of wear testing.

Figure 6.13: Concurrent optical micrographs of E1^{TM} tibia 3 at location X55 Y15 showing various stages of wear.

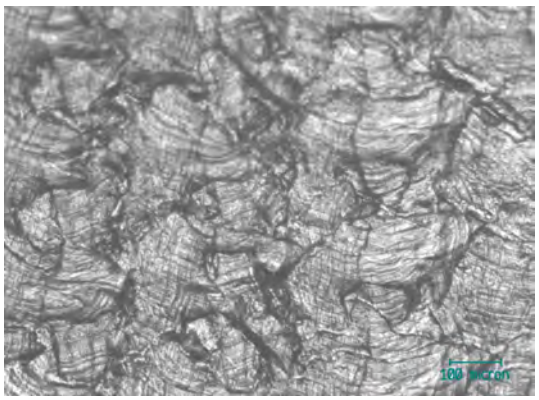

(a) Optical micrograph at removal from packaging.

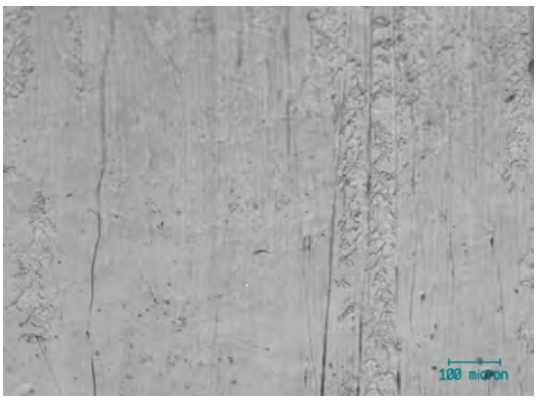

(b) Optical micrograph after 0.5 MC of wear testing.

Figure 6.14: Concurrent optical micrographs of E1^{TM} tibia 5 at location X58 Y18 showing removal of all machining marks after just 0.5 MC.

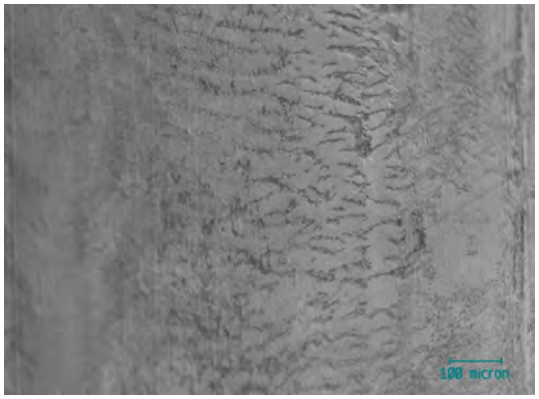

(a) Optical micrograph of tibia 5 at location X5 Y18 after 1.0 MC.

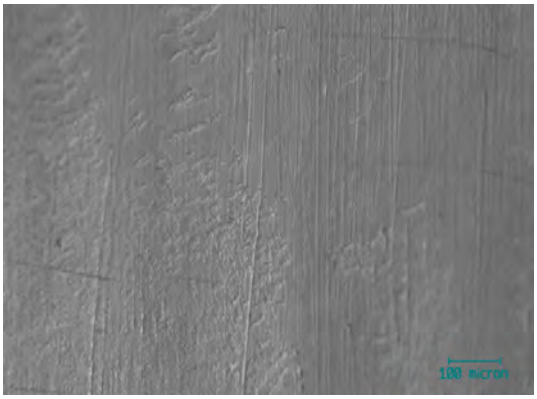

(b) Optical micrograph of tibia 1 at location X11 Y18 after 0.5 MC.

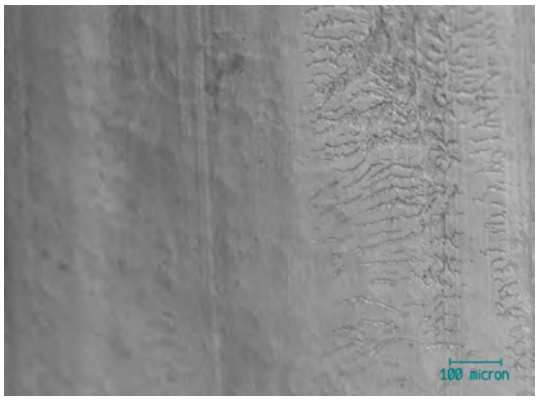

(c) Optical micrograph of tibia 2 at location X5 Y18 after 3.5 MC.

(d) Optical micrograph of tibia 6 at location X5 Y18 after 2.5 MC.

Figure 6.15: Optical micrographs showing examples of rippling type wear on E1^{TM} tibia bearings.

(a) Optical micrograph of tibia 6 at location X8 Y12 after 5.5 MC.

(b) Optical micrograph of tibia 5 at location X8 Y21 after 5.0 MC.

(c) Optical micrograph of tibia 4 at location X55 Y18 after 5.0 MC.

(d) Optical micrograph of tibia 3 at location X8 Y18 after 3.0 MC.

Figure 6.16: Optical micrographs showing examples of burnishing type wear on E1^{TM} tibia bearings.

(a) Optical micrograph of tibia 1 at location X52 Y18 after 4.5 MC.

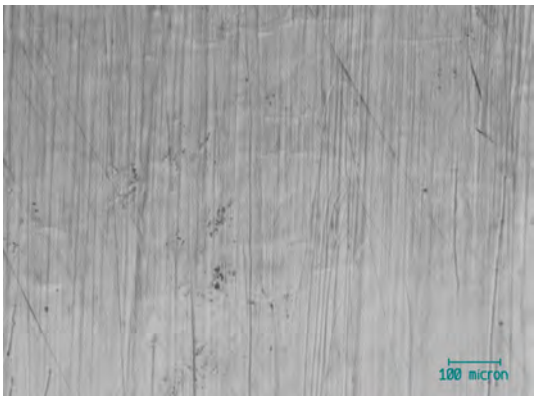

(b) Optical micrograph of tibia 2 at location X8 Y12 after 3.0 MC.

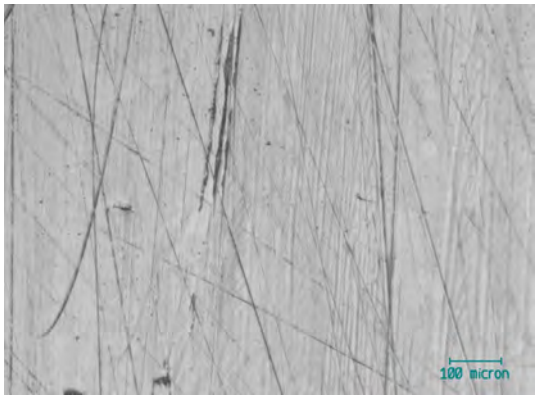

(c) Optical micrograph of tibia 3 at location X8 Y12 after 4.0 MC.

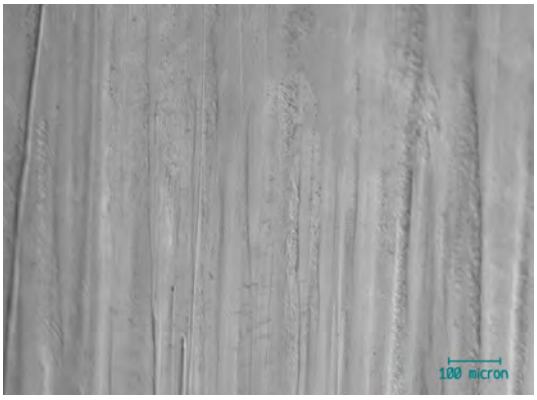

(d) Optical micrograph of tibia 4 at location X52 Y15 after 1.5 MC.

Figure 6.17: Optical micrographs showing examples of scratching type wear on E1^{TM} tibia bearings.

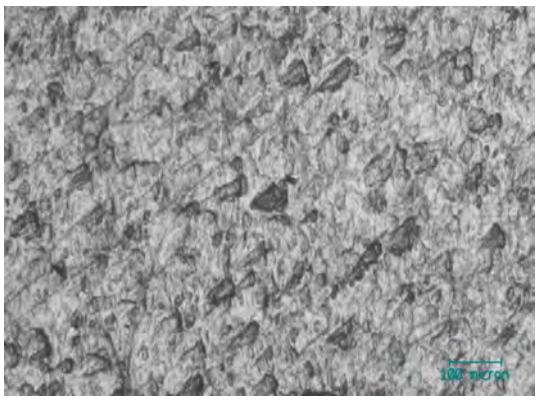

(a) Optical micrograph of the backside of tibia 1 underneath the contact point after 2.5 MC.

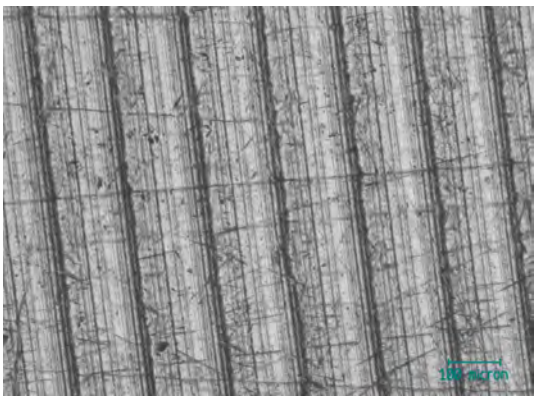

(b) Optical micrograph of the backside of tibia 1 away from the contact point after 2.5 MC.

Figure 6.18: Optical micrographs showing example of backside wear on E1^{TM} tibia bearings.

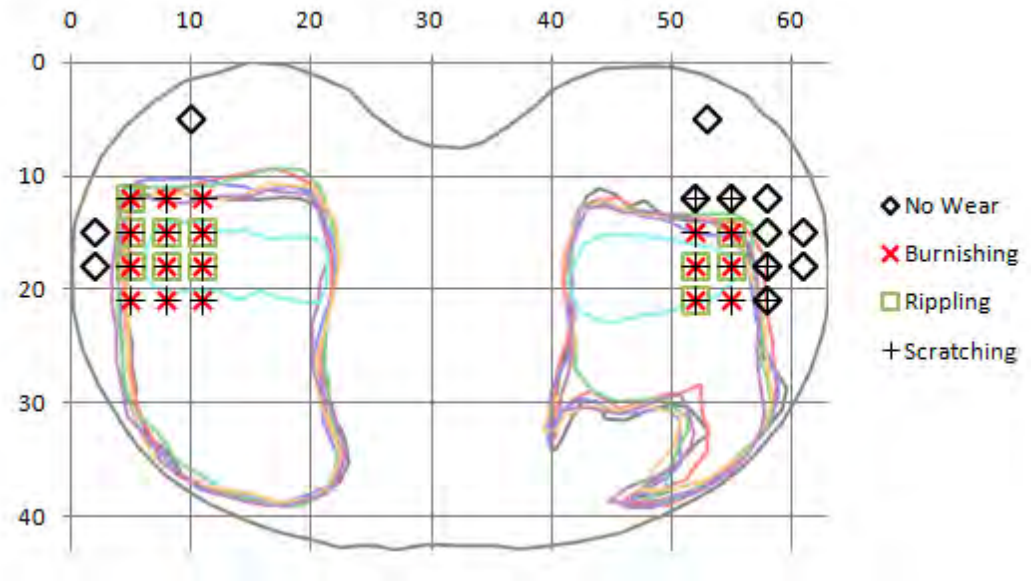

Figure 6.19: Illustration showing the types of wear at different locations on the E1^{TM} tibias. Wear scars shown are from the six articulating and one LSC tibia after 5.0 MC. The lateral side of the tibia is the right of the image and the medial side is the left of the image.

The correlation between observed wear on the optical microscope and that of the naked eye was good, except from two locations on the lateral side of the tibia, where scratching was observed on the optical micrographs, but none was seen using the naked eye.

6.1.2.5 Simulator Response

The measured response profiles of the ProSim Knee Simulator are shown in this section. For all plots, the solid black line with circular markers represents the demand profile. The grey area represents the plotting of all the individual recorded profiles showing the full range of profiles. The dashed black lines are the mean response of each of the individual stations. Finally, the thick black line represents the mean response of all stations.

The Flexion/Extension response of the two groups of stations throughout the 9MC is shown in figure 6.20. Similar to the previous ArCom® test conducted, there was no discernible difference between the demand and the recorded profile. This clearly shows the benefits of using servo motors for displacement control.

The Axial Force response of the simulator, recorded using load cells on stations 1 and 4, is shown in figure 6.21. It should be noted that in this figure a leading phase shift of 5% (0.05 seconds) has been applied to the AF demand profile to compensate for simulator lag.

The Axial Force response plotted against the ideal demand profile can be seen in Figure

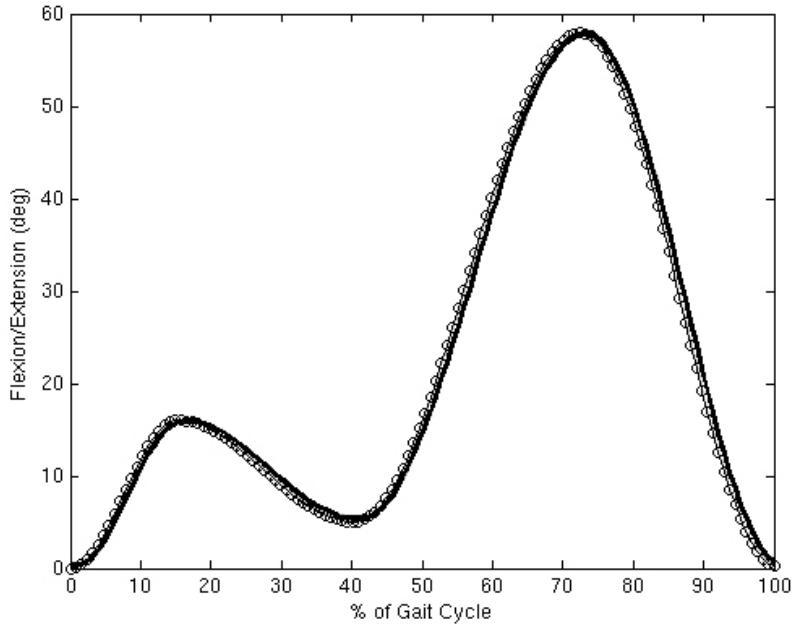

Figure 6.20: Flexion/Extension demand and response during E1^{TM} wear test.

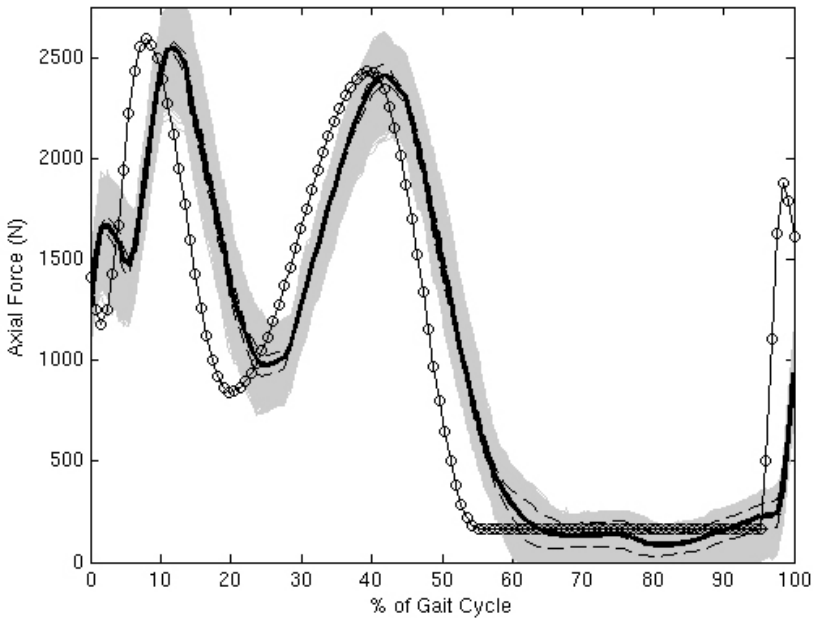

Figure 6.21: Axial Force demand (leading 5%) and response during E1^{TM} wear test.

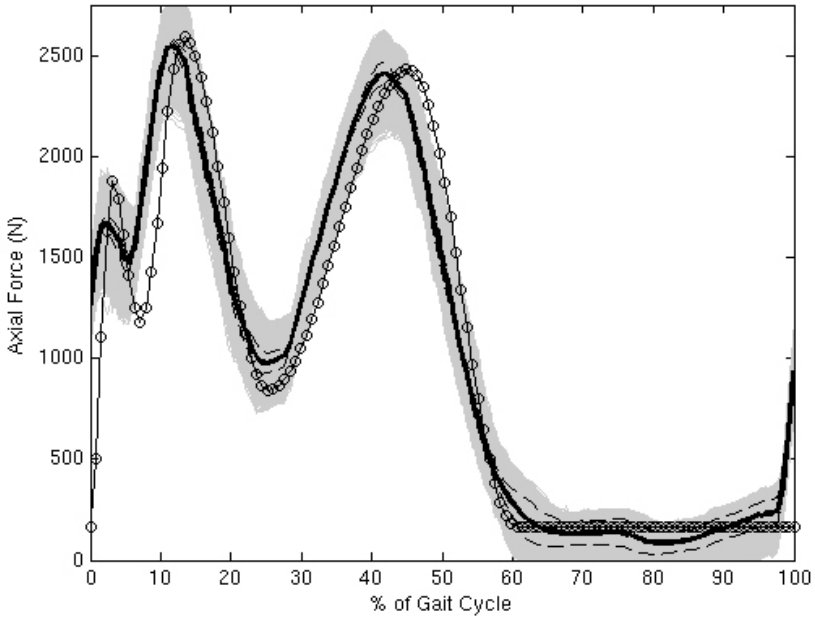

Figure 6.22: Axial Force demand and response during E1^{TM} wear test.

6.22. Here it can be seen that the manual modification of the demand profile has resulted in a response that is closer to that of the ideal demand. The only significant variation of the mean response from the demand was in the first 10% of the gait cycle, where the initial peak of 1900N and drop off to 1200N was not obtained with any fidelity. However, the peak loads at approximately 13% and 45% of the gait cycle were obtained. The period of static loading during the swing phase was obtained, although there were measurable differences between the two stations measured.

The Tibial Rotation response of the six stations can be seen in figure 6.23. The mean response of all stations followed closely that of the demand. However, the maximum values obtained were $\pm 3.5^{\circ}$ compared to the demand of $\pm 4.2^{\circ}$.

The Anterior/Posterior displacement response is shown in figure 6.24. This demand profile featured a 10% leading phase shift to account for simulator lag and also an 11mm posterior cutoff in an attempt to prevent oscillation at the limit of posterior displacement

The response of the simulator compared to the desired demand profile is shown in figure 6.25. It can be seen that the general profile has been achieved. However, there are some areas in which all the detail has not been realised. In the stance phase of the cycle, between 0 and 50% the -3.5mm & +1.0mm peaks were not achieved. The mean traces for each station show measured movement in each, but only with maximum magnitude of

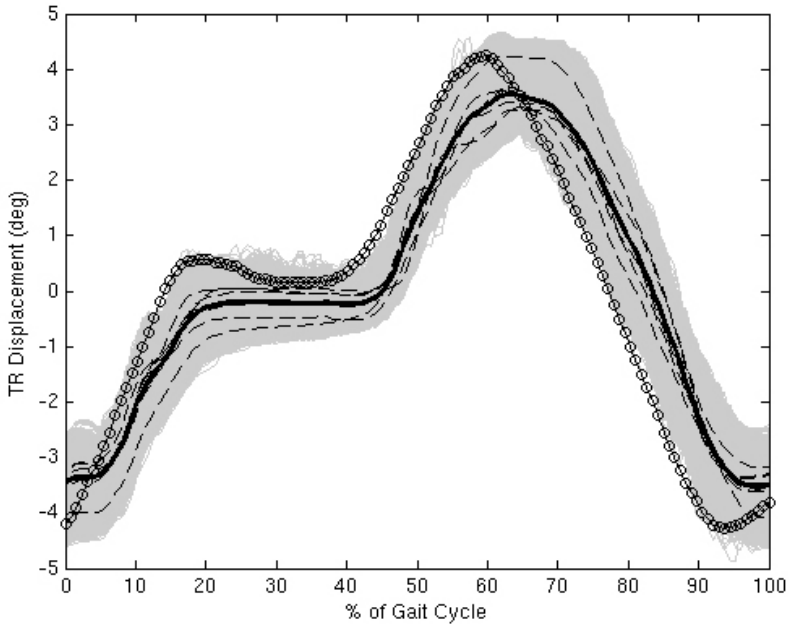

Figure 6.23: Tibial Rotation demand and response during E1^{TM} wear test.

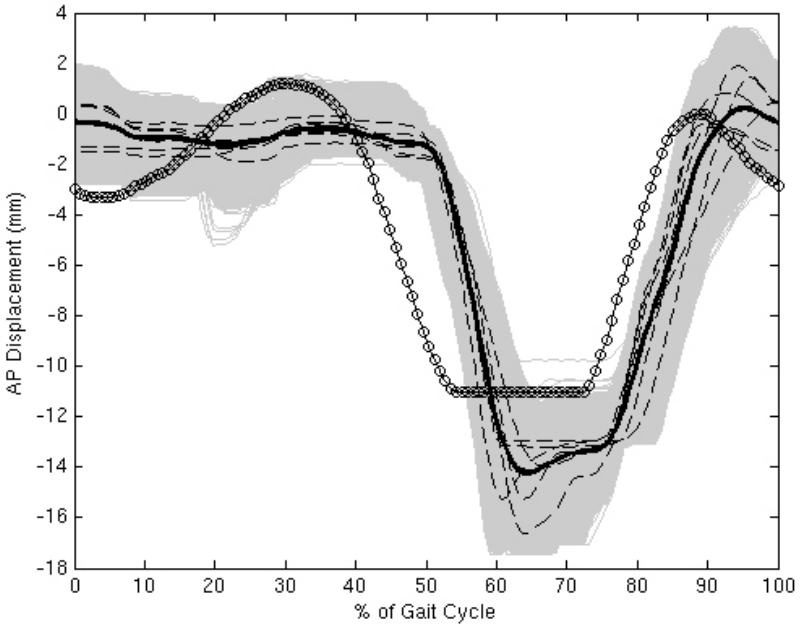

Figure 6.24: Anterior/Posterior demand (leading 10%) and response during E1^{TM} wear test.

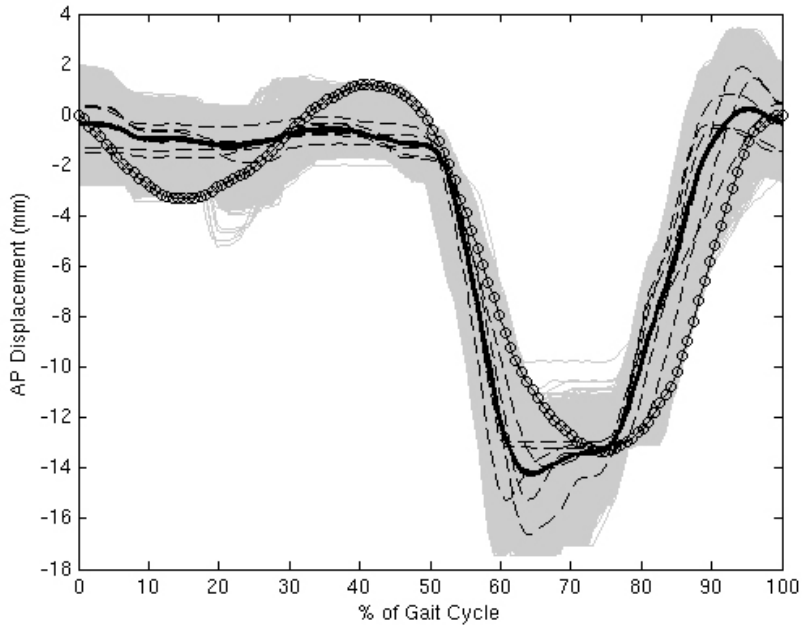

Figure 6.25: Anterior/Posterior demand and response during E1^{TM} wear test.

approximately 1mm. The swing phase was achieved with more success. The mean trace of all stations shows a posterior displacement of approximately 14.1mm compared to the demand of 13.5mm. However, looking at the mean traces for each individual station, there was significant deviation at the limit of posterior movement. The presence of two flat traces at the limit of movement also indicates that the limit of the LVDT had been reached.

6.2 E1^{TM} High Load Testing

Upon completion of the wear test described in section 6.1 the components were subjected to a further test of approximately 2 million cycles, in which three articulating components and the load soak control were placed under a maximum dynamic load of 4kN. The remaining three articulating components had a peak load of 2.6kN as normal.

6.2.1 Materials and Methods

The standard load profile taken from the British and International standard BS ISO 14243 was scaled linearly so that the peak load was 4.0kN instead of 2.6kN. FE displacement was taken from the same standard while AP and TR displacements were based on observations of the human knee (Lafortune et al., 1992). This magnified load was only applied to the TKRs in the three stations in Group 1. The three stations in Group 2 were unmodified

Test interval	Station	Peak load	Tibia	Femoral
0 - 0.5MC 1.0 - 1.5MC	0	4.0kN	2	A3
	1		3	A4
	2		5	A6
	3	2.6kN	1	A2
	4		4	A5
	5		6	A7
0.5 - 1.0MC 1.5 - 2.2MC	0	4.0kN	1	A2
	1		4	A5
	2		6	A7
	3	2.6kN	2	A3
	4		3	A4
	5		5	A6

Table 6.6: Tibia and femoral combinations and station locations during high load test.

so that the peak load was 2.6kN as used in all previous tests. This was to allow a direct comparison between the loading regimes, independent of any environmental conditions. The lubricant used was 25% bovine serum solution and was renewed every 5x10^5 cycles. A load soak control was used to account for fluid uptake of the the tibial components. The load soak control was placed inside the novel load soak control station and placed above station 0 (4.0 kN) for the full duration of the test. The mass change of the tibia bearings was assessed gravimetrically us ing the cleaning protocol listed in appendix A.2.1.3. The articulating surface of each tibia bearing was also assessed at each removal from the simulator using an optical microscope. Eight images, four on each condyle, were taken at predetermined locations on each tibia bearing. Upon completion of gravimetric and surface assessment, the TKRs were returned to the simulator. The three TKRs that had previously been under 4.0kN (Group 1) were now placed in the stations with a 2.6kN (Group 2) and vice versa. This process was continued until test completion at 2.0x10^6 cycles. The tibia and femoral combinations along with station locations can be seen in Table 6.6.

Additionally, for a period of approximately 2.0x10^5 cycles, thermocouples were used to monitor the lubricant temperature in both the high load and normal load stations.

6.2.2 Results

The load soak control was subjected to a 4.0kN peak load throughout this wear test, in contrast to a peak load of 2.6kN in previous tests. The absolute mass increase of the load soak control tibia can be seen in Figure 6.26. Calculating a least squares fit of these points, omitting the zero value gave a mass increase of 0.034 mg/day.

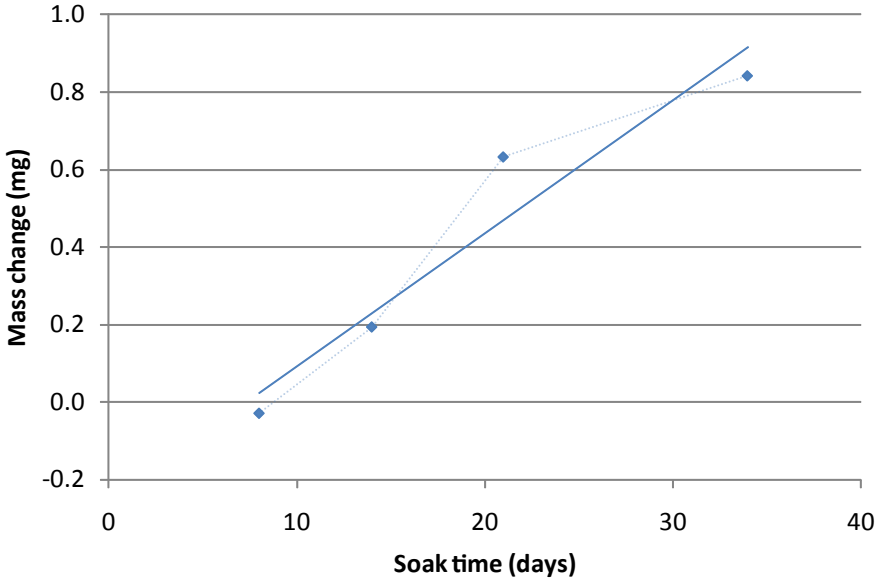

Figure 6.26: Absolute mass increase of load soak control tibia (7) during 4.0kN test.

This compares to an absolute value of 0.024 mg/day when under a dynamic peak loading of 2.6kN, and a value of 0.008 mg/day when under no load. Plotting this gives a linear relationship between peak dynamic load and fluid uptake rate, with each 1 kN extra loading resulting in an extra 0.0065 mg/day lubricant uptake.

Due to this differing fluid uptake between different peak loading conditions, the LSC data obtained in this test for the 4.0kN samples could not be used for the 3 articulating samples with a peak load of just 2.6kN. Therefore, an estimation of the fluid uptake of a sample under peak loading of 2.6kN was made. It had previously been observed in the 9 MC wear test, the 2.0 MC ageing test, and the 3.0 MC scratched femoral test, that the mean fluid uptake rate of an E1^{TM} tibia under the normal loading profile was 0.022±0.002 mg per day. From this value it was therefor assumed that the fluid uptake experienced by the three samples loaded at 2.6kN was 0.012mg/day less than that measured using the load soak control loaded at 4.0kN. The mean volumetric wear of the two loading conditions can be seen in Figure 6.28. Using a least squares linear regression the mean volumetric wear

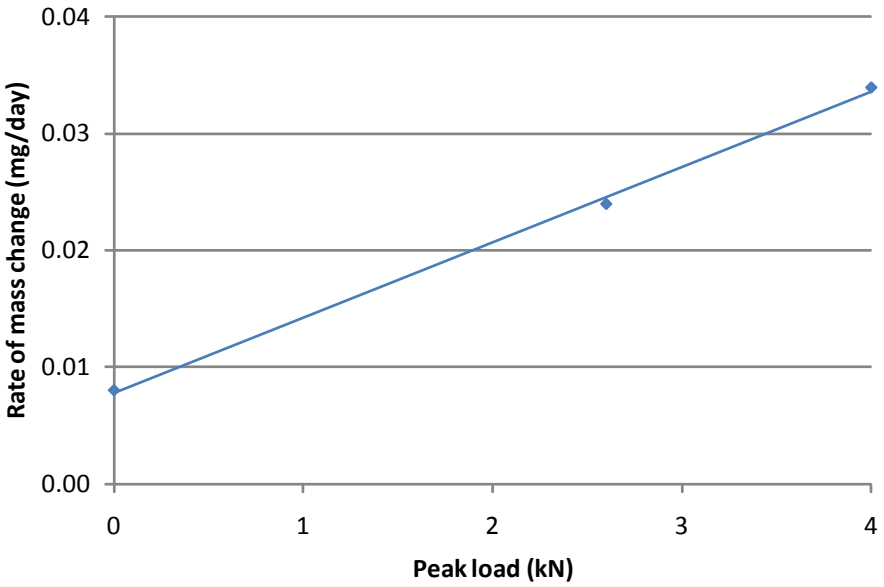

Figure 6.27: Rate of mass change vs load for E1^{TM} soak controls.

rates for the 4.0kN and 2.6kN samples was 0.001±0.150 and 0.318±0.231 mm^3 per 1x10^6 cycles respectively.

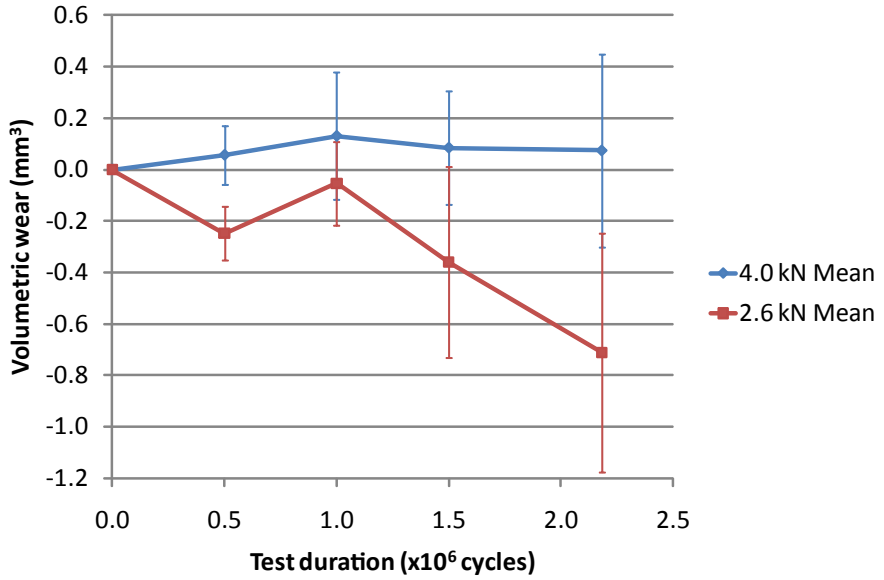

Figure 6.28: Mean volumetric wear plots for stations loaded at 4.0kN and 2.6 kN.

The recorded temperature profiles were normalised to the cold junction temperature as in the previous temperature tests conducted in Section 5.4. This was to enable comparisons between the two loading conditions, that were recorded at different times.

Surface analysis of the E1^{TM} tibias revealed no differences in surface conditions between the highly loaded and normally loaded tibias.

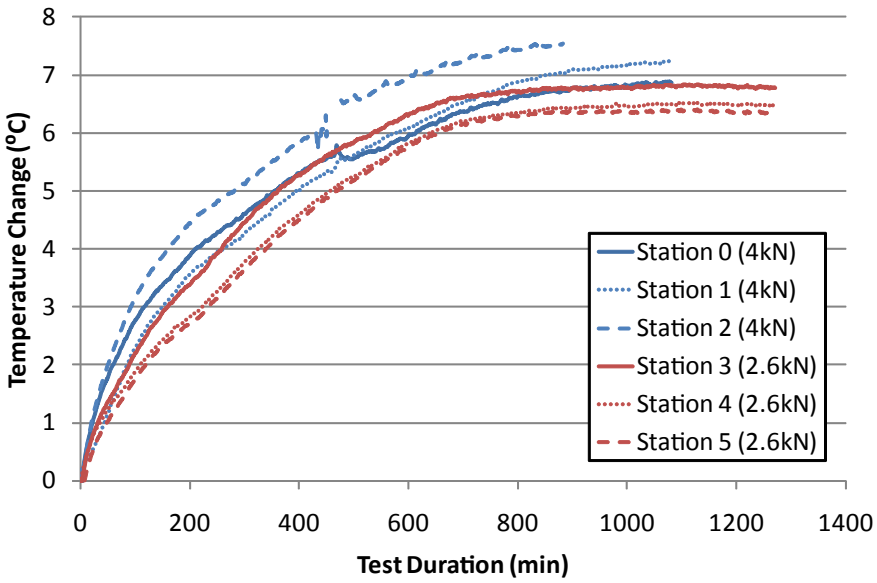

Figure 6.29: Recorded temperature profiles of lubricant temperature under different loading conditions.

6.3 Accelerated ageing of Vitamin E infused UHMWPE

The diffusion of Vitamin E within the cross-linked UHMWPE is to prevent oxidative ageing of the components. Several different ageing processes have been mentioned in the literature, however one of the most common, and also the one with defined standards attached is the process of ageing components at 70°C at 5 bar in the presence of oxygen for a 14 day duration. As noted in the standard, this process was originally designed to simulate the shelf ageing of components when packaged in air, however it has been used extensively in the literature to test a components resistance to oxidation in general.

6.3.1 Materials & Methods

Due to a limited number of components, only three tibia bearings were available to be aged. These three components had previously undergone 10.0×10^6 cycles of wear testing with a peak load of 2.6kN, 1.0×10^6 cycles of wear testing with a peak load of 4.0kN. Femoral and tibial pairings were kept consistent with previous tests. The locations of the pairs of specimens can be seen in figure 6.7.

The three tibia bearings were aged in accordance to the ASTM standard. This involved keeping the components at a temperature of 70°C and a pressure of 5 bar (73 psi). The environment was defined to be 99% oxygen and the ageing duration was 14 days.

	0.0 - 0.5 MC		0.5 - 1.0 MC		1.0 - 1.5 MC		1.5 - 2.0 MC	
Station	Fem	Tib	Fem	Tib	Fem	Tib	Fem	Tib
0	-	-	A4	E3	-	-	A6	E5
1	A4	E3	-	-	A6	E5	-	-
2	A6	E5	-	-	A7	E6	-	-
3	-	-	A6	E5	-	-	A7	E6
4	A7	E6	-	-	-	-	A4	E3
5	-	-	A7	E6	A4	E3	-	-
LSC	A1	E7	A1	E7	A1	E7	A1	E7

Table 6.7: Location of femoral and aged tibias during 2.0x10^6 cycle wear test

A specialised rig was designed an constructed in order to age the components. Great care was taken during the design and component selection process due to the volatility of pure oxygen. An exploded diagram of the final design can be seen in Figure 6.30 and after construction can be seen in Figure 6.31. The pressure vessel base and top were manufactured from 10mm thick 316 Stainless Steel (TW Steam, Durham, UK) and sealing between the base and top was achieved through the use of a Klingersil gasket which is resistant to oxidative degeneration and creep, which was compressed between the top and base using eight stainless steel nuts and washers. 4 threaded holes were machined into the pressure vessel top to allow for oxygen entry and exit and monitoring of the test conditions. The pressure was monitored using a pressure gauge (Swagelok) with a range of 0-100 psi. The internals of the gauge were cleaned by the manufacturer prior to assembly to ensure compatibility with the oxygen rich environment. The internal temperature of the vessel was monitored using a Resistance Temperature Detection (RTD) probe. This was inserted into a SS thermowell which was permanently sealed to the pressure vessel top. The RTD probe was held inside the thermowell by means of a locking nut. The RTD probe was attached to a HH505 Digital Thermometer (Omega, Manchester, England) and the min, max and average temperatures recorded during the ageing process. The oxygen cylinder was attached by means of a hose to the female quick connect, and this in turn connected to the male quick connect. This allowed easy removal of the oxygen supply if required. Oxygen flow into the vessel was controlled using the inlet needle valve, which was supplied with a polytetrauoroethylene (PTFE) seal that would not react with the oxygen. A pressure relief valve was also incorporated into

the design. It was set to release the pressure if it rose to above 100 psi, therefore reducing the risk of any failure of the pressure vessel in the unlikely event of an increase in pressure. A bleed valve was also used to allow the pressure to be released with the oxygen cylinder attached.

Polyethylene samples were placed inside the vessel on a specially made rack which featured perforated platforms. This allowed the underside of the samples to be exposed. The samples were placed so that the main articulating surface was fully exposed to the oxidising environment. 3 E1^{TM} tibias were chosen for oxidation, addition pin-on-plate specimens were also aged for other tests within the research group.

In order to achieve a oxygen atmosphere with the oxygen bomb, the vessel was pressure purged with oxygen a total of five times, (the ASTM standard suggests a minimum of 3). In each cycle of purging, the vessel was filled with oxygen up to a pressure of 73 psi, then vented to atmospheric pressure. This ensured a concentration of oxygen within the vessel of close to 100%. The final pressurisation was performed up to 62.5 psi.

Heating of the pressure vessel to 70°C was conducted a heated water bath (Fisher Scientific UK Ltd., Loughborough, UK). two rails were placed over the water bath and the flanges of the vessel base rested on these. Therefore the base of the vessel was wholly surrounded by water. Due to heat losses the water was heated to 75°C. A piece of polystyrene sheeting with a circular cutout was placed over the pressure vessel and this prevented evaporation of the heated water. It was held to the top of the water bath using tape. Expanded polystyrene pieces were placed around the top of the pressure vessel to insulate against heat loss. The temperature, pressure, water level was checked at approximately 12 hour intervals throughout the whole duration of the test. The samples were aged for a total of 14 days in accordance with the standard.

Upon removal of the aged components from the oxidation chamber, the components were cleaned and weighed as per stated protocols and then a wear test was conducted for a total of 2.0x10^6 cycles using the protocols and methods outlined in Chapter 4. Optical microscopy was conducted upon removal from the ageing chamber and after 0.5, 1.5 and 2.0x10^6 cycles. 14 locations on each condyle of the tibias were imaged giving a total of 28 images per tibia. Image locations were as in Figure 5.33, minus the four locations furthest from the wear scars.

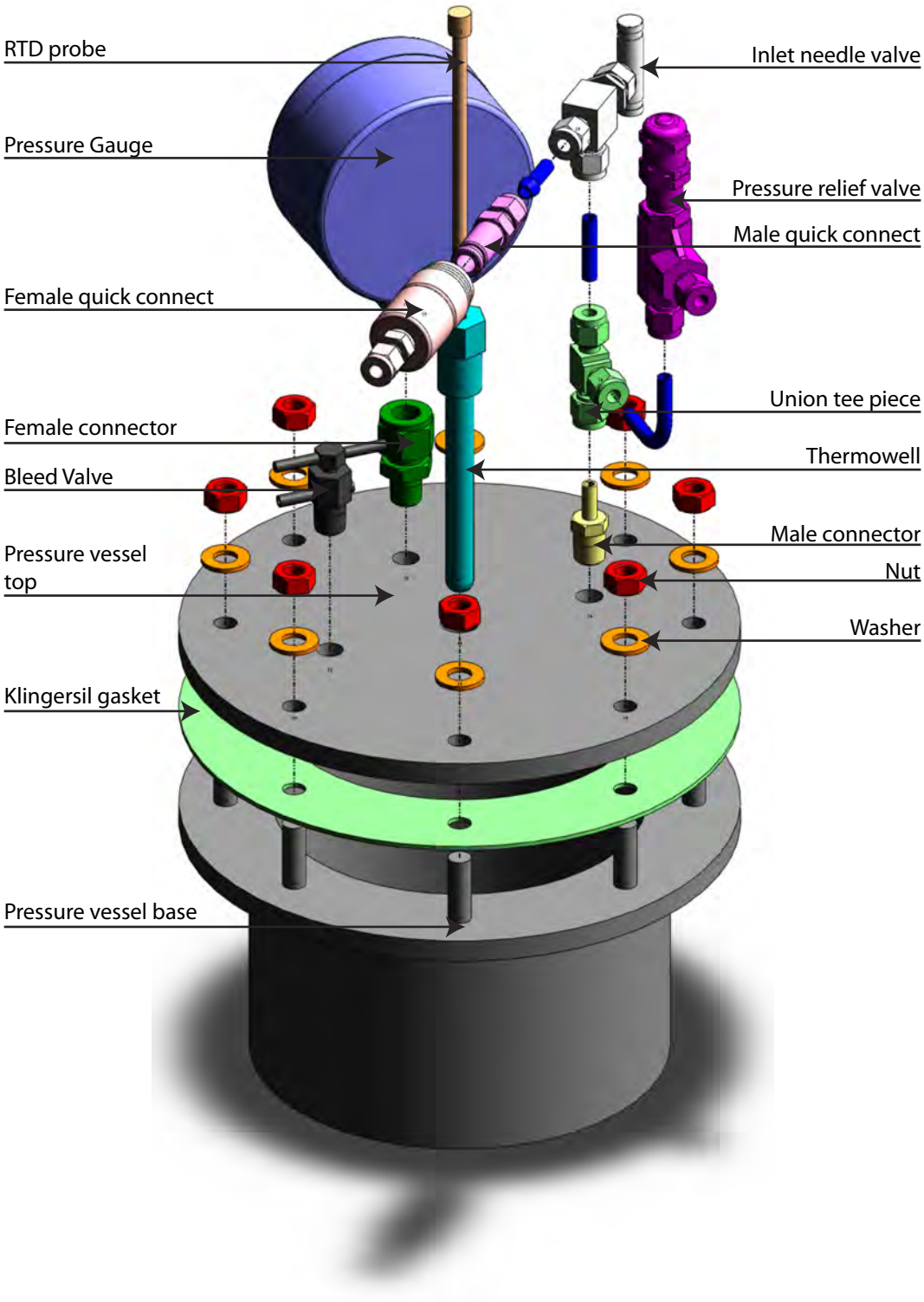

Figure 6.30: Exploded and labeled view of accelerated ageing rig.

Figure 6.31: Ageing rig.

Figure 6.32: Setup of the base of the pressure vessel immersed in water bath.

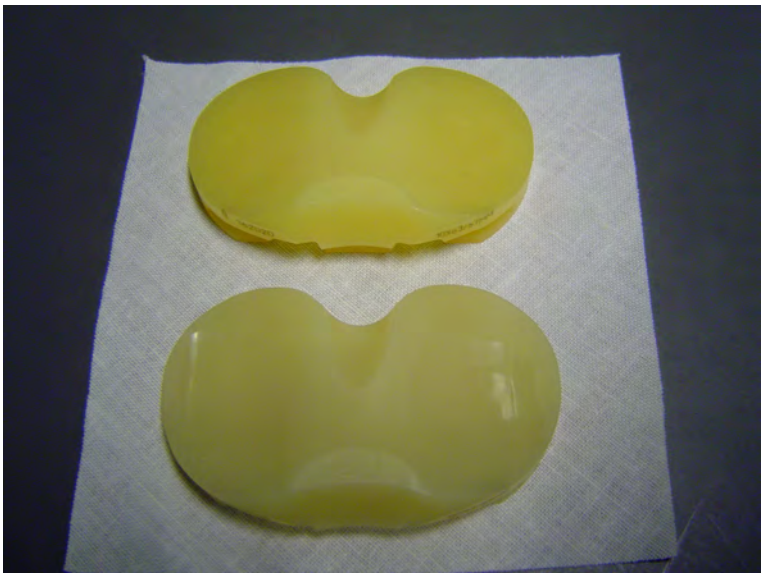

Figure 6.33: Appearance of a E1^{TM} tibia after undergoing ageing (top) compared to an unaged tibia (bottom). Note the brighter yellow appearance.

Tibia	E3	E5	E6	Mean
Mass increase (mg)	5.21	5.51	5.79	5.50

Table 6.8: Mass change of aged tibias due to the accelerated ageing process.

6.3.2 Results

Upon removal form the oxidation chamber at the conclusion of ageing, the E1^{TM} tibia samples had experienced a colour change from a dull to vibrant yellow, as seen in Figure 6.33.

All three aged tibias experienced an increase in mass due to the ageing process. The mean mass increase was 5.50±0.29 mg. The individual mass changes of the three tibias can be seen in Table 6.8.

The individual volumetric wear plots of the three Vitamin E infused UHMWPE tibias after accelerated ageing can be seen in Figure 6.34. The average volumetric wear rate of the three individual aged E1^{TM} tibias was 0.767±0.329 mm^3 per 1x10^6 cycles, and the individual volumetric wear rates are summarised in Table 6.9.

Tibia	E3	E5	E6	Mean
Vol. wear (mm^3 per MC)	1.013	0.392	0.894	0.767
RSQ	0.981	0.173	0.684	0.798

Table 6.9: Individual volumetric wear rates of the three aged tibias.

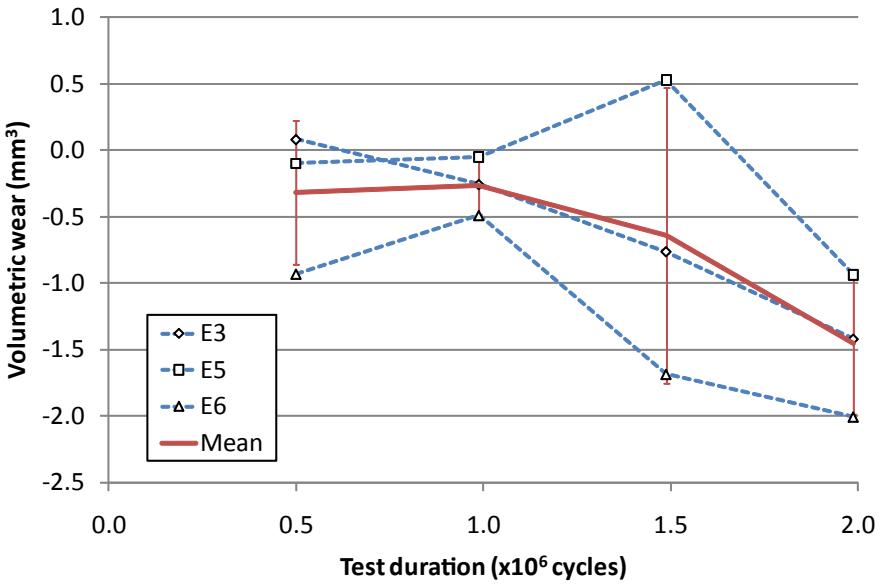

Figure 6.34: Volumetric wear of the three Vitamin E infused UHMWPE tibias during the 2.0 MC wear test conducted after accelerated ageing.

Fluid uptake of the LSC tibia, E7, is shown in Figure 6.35. A linear trend was observed and using a least squares linear regression fit, a fluid uptake rate of 0.023 mg/day was calculated (R^2=0.867).

Observations using the optical microscope revealed no change in the wear mechanisms post ageing.

6.4 Discussion

The use of highly crosslinked UHMWPE in TKR is an exciting new area which researchers are currently exploring in order to increase the product life of implanted prostheses. The aim of this chapter was to assess the new E1^{TM} UHMWPE in *in vitro* testing and therefore assess its potential performance *in vivo*. A standard wear test was conducted, with the exception of the AP and TR profiles which were based on observations of the natural knee (Lafortune et al., 1992). These were more aggressive profiles than were stated in the ISO standard. It is believed that the increasing incidence of operations on younger patients, and the inevitable increases in activity thereafter will be more accurately simulated using these profiles.

Slight changes to the PID controller and profiles were made prior to the test start. This was in order to achieve a better following of the demand profile to that which had been

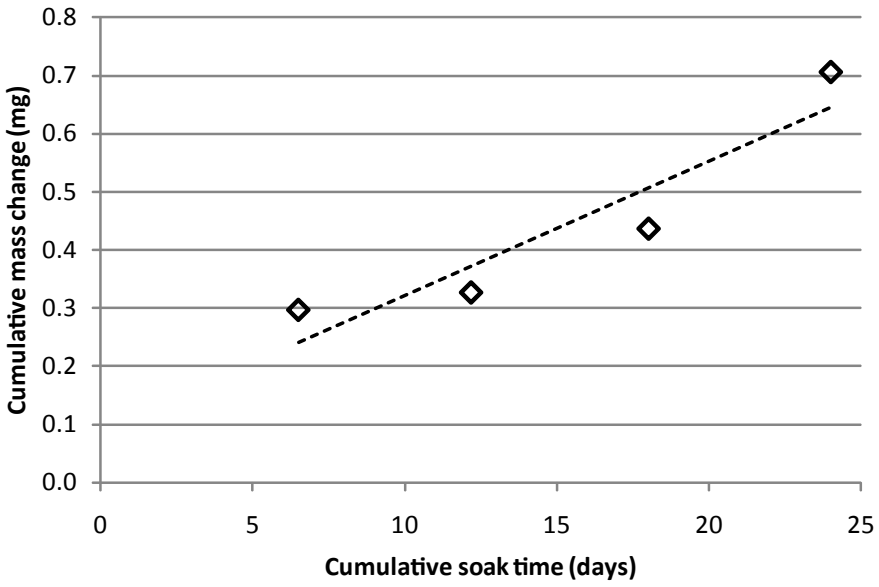

Figure 6.35: Mass change of the E1^{TM} LSC control sample due to lubricant uptake throughout the 2.0x10^6 cycle wear test.

achieved in the previous chapter in which ArCom® tibial components had been tested. Care was taken though in order to ensure that the two profiles still allowed a comparison of the respective wear rates. The simulator response of the FE axis was effectively the same as the demand due to being driven using an electric motor. The AF demand was shifted by 5% to account for lag in the control system and actuators. This adjustment worked well and there was little difference between the demand profile and recorded response. The AP demand was adjusted by 10%, again to account for lag in the controllers and actuators. Again this change ensured a more accurate following of the demand profile. The mean values of AP displacement in the stance phase indicated little movement, however observing the range of values indicated by the shaded grey area in the response plots, it is clear that some displacement, equal to the ranges of motion required was obtained. This indicates that there was some degree of oscillation, possibly due to the increased P values used in the PID controller for this test. The mean traces during the swing phase indicated that there was some overshoot of the stations in the large posterior displacement region (-ve values), again this is thought to be due to the larger P values used in the PID controller. Two stations exhibited a flat trace at the limit of posterior displacement, indicating that the limit of the LVDT had been reached. It is thought that the profile of these two stations would have followed the same pattern of the other four, with a small overshoot. It was felt that the general following of the AP demand was good, although the increased proportional

gain values had introduced some undesirable overshoots and oscillations. The TR had no lag adjustment, although examining the response trace suggest that it may have benefitted from a 5% leading shift, which could possibly be implemented in later tests on the simulator. The mean magnitudes were approximately 1° lower than that of the demand. Steps were taken to rectify this using the control system, however it was found that increases in the gains caused undesirable oscillations. The demands and PID control values remained the same for all further testing on the E1^{TM} components.

The wear test was continued past the standard 5.0x10^6 duration on to a total of 9.0x10^6 cycles. This was in order to assess the fatigue resistance properties, as highly irradiated ($\geq$100 kGy), and therefore, highly cross-linked UHMWPE has a lower fatigue propagation resistance than unirradiated controls, which is in turn attributed to a reduction in plastic deformation ahead of the crack tip (Baker et al., 2003). However, in the present study, no change of the wear rate was observed throughout the test duration, indicating that fatigue was not currently an issue. All six E1^{TM} experienced linear wear rates throughout the full 9.0 MC duration of testing, with a mean wear rate of 0.85$\pm$0.13 mm^3/MC. There were several challenges during the experiment, the main one being the sensitivity of the gravimetric readings to the mass change of the LSC. The absolute mean value of mass change, not compensating for fluid uptake, of the six articulating tibias was -2.38mg after 9.0MC. The absolute mass change of the LSC was +4.34mg after 9.0MC. Therefore, it is clear that errors in the measurement of lubricant uptake could have a large influence on the calculated wear rate. Improvements to the cleaning protocol was made after 2.0MC in order to ensure less variation between the six samples. No difference was noted in the grouping of the volumetric wear plots, however, the number of weighing repetitions required before 3 were within acceptable limits was reduced.

Comparing the volumetric wear rate achieved by the E1^{TM} tibias to that achieved by the ArCom® an 87% reduction in wear was seen. This was achieved using identical test conditions. The achieved volumetric wear rate is incredibly low and if this wear rate was achieved throughout the life of the implant, then there would be no question of failure of the implant due to polyethylene wear. McEwen *et al* have also demonstrated the effectiveness of cross-linking on the wear properties in the knee with a 43% reduction in wear when using a moderately cross linked UHMWPE compared to standard UHMWPE of the same geometric design (McEwen et al., 2005). Muratoglu *et al* demonstrated similar levels of

wear (0.7mm^3/MC) of aged highly cross-linked inserts in a knee simulator test with similar displacements, although the peak load was approximately half that used in this study (Muratoglu et al., 2004a). However, it should be stated that the inserts used in Muratoglu's study had been completely re-melted after irradiation so questions remain about their fatigue resistance. Wang *et al* tested highly cross-linked GUR1020 inserts using the less severe ISO displacement profile and achieved a higher wear rate of 5.7±1.5mm^3/MC (Wang et al., 2008), although these components were just annealed post irradiation so may be susceptible to oxidation post implantation. Similarly irradiated (100 kGy), KOM knee tibias with blended Vitamin E have a wear rate of 0.66mm^3/MC (Akagi et al., 2006), slightly lower than measured in this study. However, the simulator profile used was just that of the stance phase similar to that used in other studies (Tsukamoto et al., 2008). The rationale behind this was that wear only occurs in the highly loaded stance phase, although no evidence was given to corroborate these claims and in this authors opinion this is highly questionable.

Fluid uptake of the control specimens followed the same trend seen in the previous test with ArCom® tibias. In the initial pre-soak period all eight E1™ tibias experienced very similar fluid uptake rates with a mean rate of 0.016 mg/day, this was less than the 0.042 mg/day experienced by the ArCom® tibias, a similar finding to Blanchet *et al* (Blanchet et al., 2002). Upon commencement of the wear test, the Soak Control (SC) fluid uptake rate dropped by 50% a clear consequence of insertion in the metal tibia tray and a similar finding to that of the ArCom® SC. A linear relationship was found to the relative difference between the lubricant uptake of the SC and LSC much like that of the earlier test, although this difference was 0.015 mg/day compared to 0.021 mg/day seen with the ArCom® , indicative perhaps of the higher elastic modulus of crosslinked UHMWPE under compression (Pruitt, 2005).

Monitoring of the visible wear scar areas revealed a greater proportion of the visible wear was on the medial side (60.4%) of the tibia compared to the lateral side (39.6%). This is opposite to the observations on ArCom® tibias in the previous chapter and is illustrated in Figures 6.36 and 6.37. This difference can be attributed to the increased hardness of the E1™ UHMWPE, coupled with the presence of machining marks on the surface. The higher loads on the medial side due to the ML offset are adequate to remove all the machining marks, however on the lateral side where the applied load is lower, some machining marks still remain. Similar observations have been found in highly crosslinked acetabular cups, on

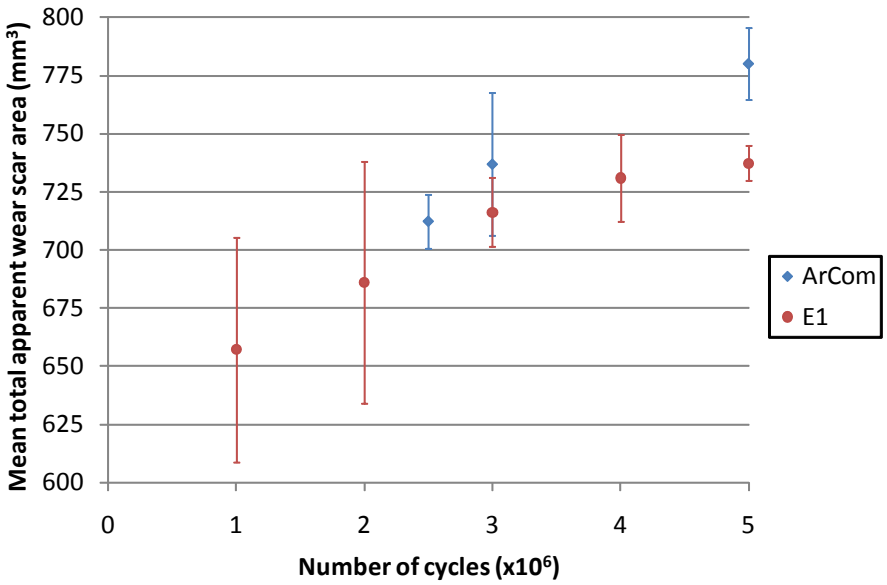

Figure 6.36: Comparison of the mean apparent wear scar areas for both the ArCom® and E1™ components at increasing test durations. Plot shows mean of E1™ tibias (n=6) ± 1SD and mean of ArCom® tibias (n=5) except at 5x10^6 cycles (n=4) ± 1SD.

which the machining marks remain after several million cycles of wear testing (Muratoglu et al., 2004c). In terms of total wear scar area, there was little difference between the six test tibias. There was a general rising trend from 1.0 to 5.0 MC indicative of continued femoral penetration into the tibia surface. The total wear scar area after 5.0 MC was less approximately 50mm^2 less than that of the ArCom® tibias at the same test duration. The lack of machining mark removal on the lateral side is thought to account for this discrepancy.

Observation of the wear surfaces revealed predominant wear modes of scratching and burnishing with rippling features observed in areas around the 'home' position contact points, on the flatter areas of the tibia. This would suggest that these rippling type features are a result of combined FE and high AF. It was also interesting that a greater incidence of rippling was found on the medial side of the tibia, indicating it may well be dependent on the size of axial loading as the medial side experienced greater loading due to the ML offset that was intentionally introduced in the simulator setup. In comparison with the ArCom® no evidence of adhesive wear or protrusions caused by cold flow of the UHMWPE were found. In general the E1™ tibias had a far more homogeneous appearance. Analysis of the tibia surface roughness revealed an initial R_a 1.776±0.044μm, caused by machining marks on the surface. After 2.5 MC this had reduced to 0.162±0.058μm, and after 8.0 MC reduced further to 0.080±0.013μm. This was lower than that of the ArCom® tibias, and therefore

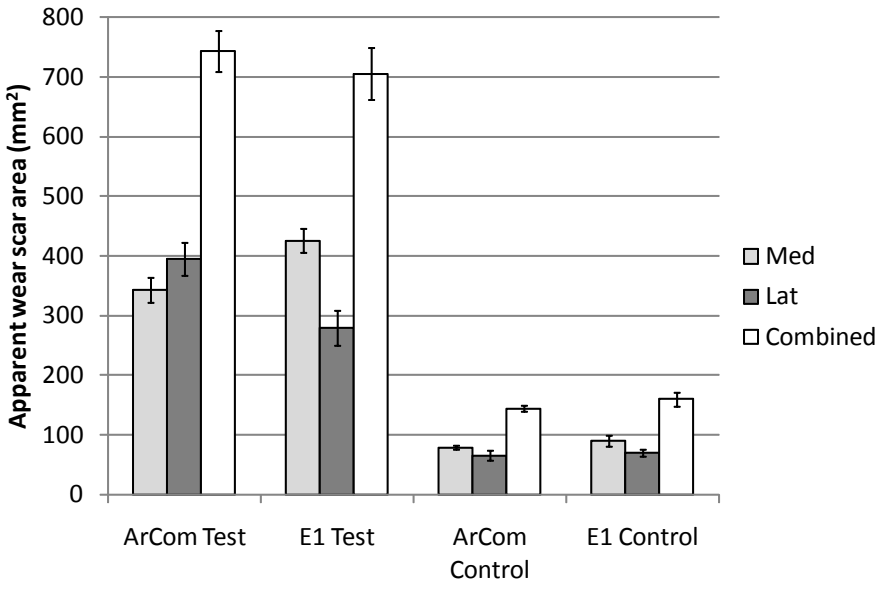

Figure 6.37: Comparison of apparent wear scar areas for ArCom® and E1™ tibias during wear tests. Values shown are the mean ± 1SD. For ArCom® tibias, apparent wear scars were measured after 2.5x10^6, 3.0x10^6, and 5.0x10^6 cycles. For E1™ tibias apparent wear scars were measured after 1.0x10^6, 2.0x10^6, 3.0x10^6, 4.0x10^6, and 5.0x10^6 cycles.

links well with the observed burnished areas.

On application of higher axial loads, the volumetric wear of the E1™ appeared to decrease. However, further experimentation needs to be conducted before this can be substantiated. With the wear rates being very low, further investigation into fluid uptake under varying loading conditions should be conducted, and separate load soak control specimens should be used. Furthermore, due to simulator limitations, the test specimens could not be fully rotated around the six stations, as they were during previous tests. Therefore, it is currently only prudent to say that increasing the AF caused no detectable increase in wear. This is similar to findings in THR simulator tests where high stress conditions caused by near impingement do not cause increases of wear for highly cross-linked UHMWPE acetabular cups when compared to standard test conditions (Kelly et al., 2010). Lubricant uptake into the LSC tibia was found to increase with increasing load, and a linear relationship, albeit with just three data points, was found. Observation of the tibia bearing surface revealed no differences in wear types between the two loading conditions. The lubricant temperature was found to increase by approximately 0.5° with the increase in loading. The temperatures generated, approximately 7° above RT were comparable to those observed in the test with ArCom® tibia bearings.

The E1^{TM} tibia components feature infused α-tocopherol in order to increase the oxidative stability once implanted in the body. In order to assess the effectiveness of this solution E1^{TM} tibias were aged according to the recommendations outlined in ASTM F2003 standard, which was developed from research by Sanford *et al* (Sanford et al., 1997). The oxygen bomb was designed in-house and operated largely as expected. However, there were a small number of variations from the standard that it is only prudent to mention. Firstly, the standard suggested a rate of temperature increase of 1.0±0.1°C/min. However, due to the use of a water bath, rather than a heater element, a heating rate of approximately 0.15°C was achieved. However, taking into account the 14 day duration of the test, the samples were held at 70°C only 1.1% less than the total time specified in the standard. However, it has been observed that an increased heating rate can lead to a reduction in density of the aged components (Lu et al., 2002) albeit only in small amounts with an increase from 0.1 to 0.2°C giving a 0.002 g/cm^3 drop in density. Other, issues that presented themselves during ageing included slight loss of oxygen pressure due to small leaks in the chamber. To counteract this, the pressure was monitored twice daily and addition oxygen added if required. No pressures outside the 72±1 psi specified in the standard were recorded.

The 3 aged components experienced a mass gain of 5.50mg over the course of the 14 days of ageing. This is similar to another study in which a mean mass rise 4.9mg was observed in the same ageing period (Vaidya et al., 2011). However, in the test performed by Vaidya *et al* the tibia component's mass was allowed to 'stabilise', a process that took a total of 13 days. It is not clear from the text what is meant by the word 'stabilise', possibly a reduction in weight to that of before the ageing process. No rationale was given for this choice in experimental method. In this study the wear test was commenced immediately after removing the components from the oxygen bomb. In the ageing test, an assumption was made that the lubricant uptake of an unaged E1 tibia is the same as an aged one, as due to a limited number of test components, a LSC specimen could not be aged. Therefore the LSC specimen used during wear testing of the aged components was unaged.

The wear performance of the three aged tibias was unaffected by the ageing process, with a volumetric wear rate of 0.767±0.330 mm^3/MC post ageing compared to a volumetric wear rate of 0.85±0.13 mm^3/MC prior to ageing. Optical assessment of the tibia surface revealed no abnormal wear features when compared to those seen prior to ageing. This builds upon findings by Wannomae *et al* where both the post ageing oxidation and subsequent

wear performance of GUR1050 infused with α-tocopherol was found to be unaffected in simple unidirectional motion wear tests (Wannomae et al., 2010). In contrast the wear performance and oxidation levels exhibited by conventional GUR1050 UHMWPE after ageing was severely affected, with delamination of the UHMWPE observed.

6.4.1 Summary

In summary, Vitamin E infused, highly cross linked UHMWPE tibia inserts have been assessed in physiologically relevant wear simulations. In a test simulating the high activity of a younger patient, the volumetric wear rate was found to be 87% less than that of a conventional DCM UHMWPE tibia insert tested under the same conditions. Concerns in the literature regarding the long term suitability of Cross-linked UHMWPE in the knee joint due to lower fatigue resistance were not upheld, with no evidence of fatigue damage found. Tests simulating a patient with increased BMI were found to have no negative effect on the wear of the implant. Finally, the oxidation resistance of the inserts were assessed using an accelerated ageing technique, and the wear performance of the Vitamin E infused inserts was found to be unaffected.

Study	PE Type	Aged	Design	Simulator	Profile	Lubricant	Duration	Wear Rate
This study	E1 UHMWPE	No	Vanguard CR	Prosim (Pneumatic)	ISO AF, FE - Lafortune AP, TR	25% Bovine Serum	9.0 MC	0.85 ± 0.13 mm^3/MC
This study	E1 UHMWPE	No	Vanguard CR	Prosim (Pneumatic)	ISO AF (4kN max load), FE - Lafortune AP, TR	25% Bovine Serum	2.2 MC	0.001±0.150 mm^3/MC
This study	E1 UHMWPE	No	Vanguard CR	Prosim (Pneumatic)	ISO AF, FE - Lafortune AP, TR	25% Bovine Serum	2.0 MC	0.318±0.231 mm^3/MC
This study	E1 UHMWPE	Yes (ASTM F2003)	Vanguard CR	Prosim (Pneumatic)	ISO AF, FE - Lafortune AP, TR	25% Bovine Serum	2.2 MC	0.767 ± 0.330 mm^3/MC
Vaidya et al. (2011)	HXL VitE Blended UHMWPE	Yes (ASTM F2003)	3D Knee (DJO Surgical) (Size 6)	Stanmore KC	ISO Force Control	25% BS	5.0 MC	1.9±1.9 mg/MC
Akagi et al. (2006)	GUR1050 (100kGy) annealed at 110°	No	KOM Knee	Shore Western	Stance Phase 0-20$^{/circ}$ FE, 4mm AP, ±5° TR, AF (Paul)	50% BS	4.0 MC	0.6 mg/MC (0.66 mm^3/MC)
Wang et al. (2008)	Com. Mould. GUR 1020 XL(90kGy) + Annealed	No	Triathlon CR	MTS	ISO Disp.	50% BS	5.0MC	5.7±1.5mm^3/MC
Muratoglu et al. (2004a)	GUR1050 (95kGy) remelted	80°C Air 35 days	Natural Knee 2 (Zimmer)	AMTI	Modified ISO Disp	100% BS	5.0 MC	0.7 ± 0.1 mm^3/MC

Table 6.10: Comparison of E1^{TM} UHMWPE wear rates with other Vitamin E infused and/or highly XL UHMWPE in literature. Where gravimetric values have been converted to volumetric a density of 0.914g/cm^3.

Chapter 7

The Influence of Counterface Surface Roughness on UHMWPE wear

THERE EXISTS IN LITERATURE several studies on the effects of scratches on the metal femoral components on the wear of polyethylene tibia components. However, to the author's knowledge, no data exists for highly cross-linked UHMWPE infused with vitamin E. This chapter describes a wear test conducted in the same manner as in the previous two chapters, with the difference being artificially scratched femoral components were used in order to increase the severity of the test conditions. The rationale for this is that the wear observed on explanted TKRs is often more severe than is achieved through *in vitro* simulator testing. The CoCr femoral component is often damaged which results in an increase in surface roughness of the component. The severity of the scratching was greater than any that had previously been observed in literature.

7.1 Materials and methods

A total of six stations were used, three stations contained tibias manufactured from E1^{TM} highly cross-linked UHMWPE and the remaining three stations contained tibias manufactured from non-cross-linked ArCom® UHMWPE. All six of the tibia samples had previously been used in a wear test. The three ArCom® tibias had undergone 5x10^6 cycles and the three E1^{TM} tibias had undergone a total of 10x10^6 cycles wear testing with a peak load of 2.6kN

and an additional 1x10^6 cycles of wear testing with a peak load of 4.0kN. Two load soak control stations were used, one for each type of UHMWPE. The ArCom® LSC used in previous tests was not available so a fresh scrap tibia, labeled A14 was used. The pairing of femoral and tibial components from the previous wear tests was continued. Testing was performed in accordance with the procedures previously outlined in Chapter 4. The tibial and femoral pairs and station locations throughout the test can be seen in Tables 7.1 and 7.2. Wear was measured using the gravimetric method as before, and measurements were taken every 0.5x10^6 cycles. The densities for the two types of polyethylene obtained in previous chapters were used again for volumetric calculations. Fluid uptake into the tibias was also compensated for using the LSCs.

Zygo analysis was performed on the femoral components prior to scratching, post scratching, then at 1.0x10^6 cycle intervals throughout the test until the test conclusion at 3.0x10^6 cycles. Ten Zygo scans were taken for each femoral component, five on the medial condyle and five on the lateral condyle. These were taken at predetermined locations and the same locations were imaged at each interval. Optical analysis of the femoral components was carried out both pre and post scratching, and again after 2.0x10^6 cycles.

The tibial components were also analysed using both the Zygo and optical microscope. eight locations on each tibia were chosen and these were imaged both prior to testing and at 1.0x10^6 cycle intervals thereafter until the conclusion of the test at 3.0x10^6 cycles. Optical analysis was performed prior to testing, then at 0.5x10^6 cycle intervals until a total of 2.0x10^6 cycles, then additionally at 3.0x10^6 cycles. The same 32 locations as indicated on Figure 5.33 were imaged.

Multiple scratching methods had previously been mentioned in the literature. The method chosen in this study consisted of scratching thee surface of the femoral using P240 grade emery paper. Scratching was performed by hand in the approximate directions 0°/180°, 45°/225°, 90°/270°, 135°/315°. Surface roughness measurements were taken using the Zygo non-contacting profilometer. This was conducted both prior and post scratching and at various intervals throughout the testing.

	0-0.5MC		0.5-1.0MC		1.0-1.5MC		1.5-2.0MC		2.0-2.5MC		2.5-3.0MC	
Station	Fem	Tib	Fem	Tib	Fem	Tib	Fem	Tib	Fem	Tib	Fem	Tib
0	2	A2	-	-	-	-	4	A6	5	A5	-	-
1	4	A6	-	-	2	A2	-	-	-	-	5	A5
2	5	A5	-	-	4	A6	-	-	-	-	2	A2
3	-	-	2	A2	5	A5	-	-	4	A6	-	-
4	-	-	4	A6	-	-	5	A5	2	A2	-	-
5	-	-	5	A5	-	-	2	A2	-	-	4	A6
LSC 0	7	A14	-	-	7	A14	-	-	7	A14	-	-
LSC 3	-	-	7	A14	-	-	7	A14	-	-	7	A14

Table 7.1: ArCom® Tibia (Tib) and Femoral (Fem) locations during 3x10^6 cycle wear test using scratched femoral components.

	0-0.5MC		0.5-1.0MC		1.0-1.5MC		1.5-2.0MC		2.0-2.5MC		2.5-3.0MC	
Station	Fem	Tib	Fem	Tib	Fem	Tib	Fem	Tib	Fem	Tib	Fem	Tib
0	-	-	A2	E1	A5	E4	-	-	-	-	A3	E2
1	-	-	A3	E2	-	-	A5	E4	A2	E1	-	-
2	-	-	A5	E4	-	-	A2	E1	A3	E2	-	-
3	A2	E1	-	-	-	-	A3	E2	-	-	A5	E4
4	A3	E2	-	-	A2	E1	-	-	A5	E4	-	-
5	A5	E4	-	-	A3	E2	-	-	-	-	A1	E7
LSC 0	-	-	A1	E7	-	-	A1	E7	-	-	A1	E7
LSC 3	A1	E7	-	-	A1	E7	-	-	A1	E7	-	-

Table 7.2: E1™ Tibia (Tib) and Femoral (Fem) locations during 3x10^6 cycle wear test using scratched femoral components.

Figure 7.1: Photo showing artificially created scratches on femoral components (top) compared to femoral components after 11x10^6 cycles of wear testing (bottom).

7.2 Results

7.2.1 Wear Data

The volumetric wear plots for the six tibias tested can be seen in Figure 7.2. It can be seen that all six tibias exhibited a linear volumetric wear rate. The mean wear rates of the two types of tibia can be seen in Figure 7.3. The mean volumetric wear of the three E1™ tibias was lower than that of the 3 ArCom® tibias. Additionally the absolute variation in wear rate between the three E1™ tibias was far lower than that of the three ArCom® tibias, indicated by the size of the standard deviation error bars. The mean volumetric wear rates for the E1™ and ArCom® tibias were 50.7±17.3 and 100±38.5 mm^3 per 1x10^6 cycles respectively. Observing the results from the ArCom® tibias, tibia 6 was again the least wearing, as it was in the test with smooth counter-faces.

The individual wear rates of the six tested tibia are summarised in Table 7.3.

7.2.2 Surface Analysis

The effect of scratching the femoral surfaces can be seen in Figure 7.4. Here the pre and post scratching images can be seen.

The surface roughness of the femoral components can be seen in Figure 7.5. The mean surface roughness of the six tibias prior to scratching was 0.067±0.065μm, however omitting femur A2 from the mean calculation, as the scan location fell on deep scratches not typical of the rest of the surface, gives a value of 0.041±0.012μm. Note the large reduction in standard

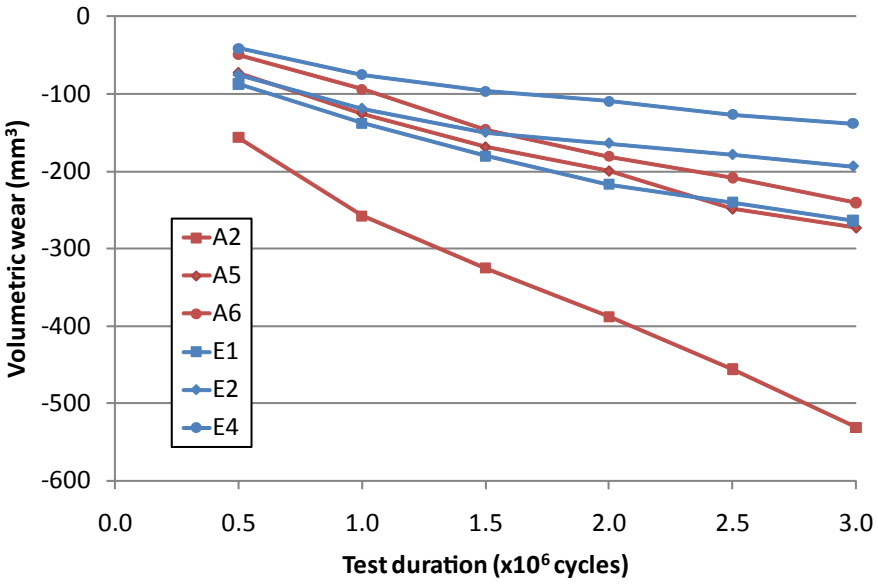

Figure 7.2: Volumetric wear plots of the six individual tibia components articulating against artificially scratched femoral components. Tibias A2, A5, and A6 were manufactured from ArCom® UHMWPE and tibias E1, E2, and E4 were manufactured from Vitamin E infused UHMWPE.

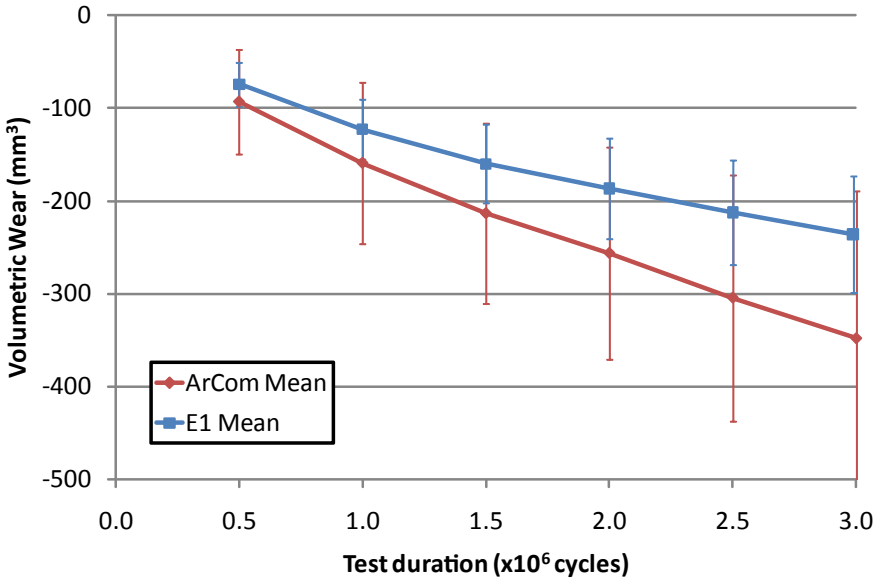

Figure 7.3: Mean volumetric wear plots of the 3 ArCom® tibias and 3 E1™ tibias, with LSC compensation. Error bars shown are ± 1 SD.

	Tibia	Volumetric Wear	Mean	R^2
ArCom	A2	145	100 ± 38.5	0.994
	A5	80.0		0.990
	A6	76.1		0.986
$E1^{TM}$	E1	70.4	50.7 ± 17.3	0.976
	E2	45.0		0.938
	E4	37.4		0.964

Table 7.3: Table showing individual and mean wear rates (mm^3/MC) of the six tibias worn with scratched femoral components.

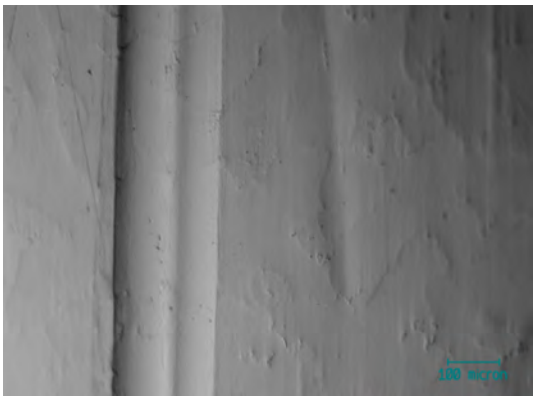

(a) Optical micrograph of the lateral condyle of femoral A5 at approximately 35° of flexion prior to scratching. It should be noted that this femoral component had previously been used for testing, hence the scratches running in the AP/FE direction.

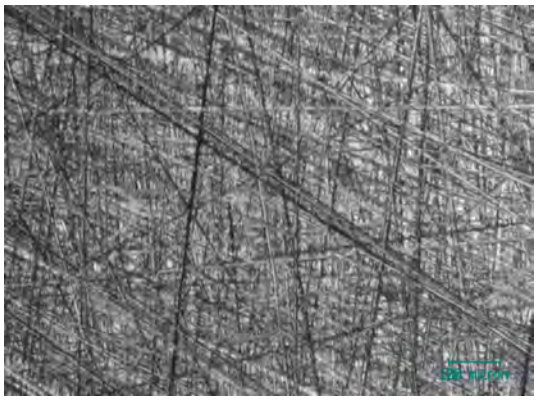

(b) Optical micrograph of the medial condyle of femoral A3 at approximately 35° of flexion post scratching.

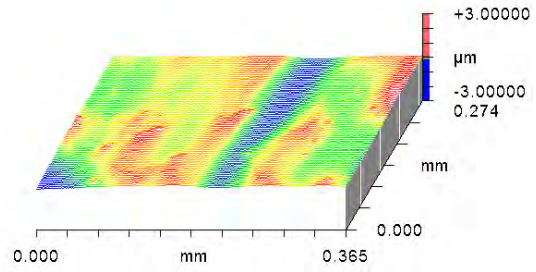

(c) 3D Zygo scan of the lateral condyle of femoral 5 prior to scratching. R_a=0.040μm.

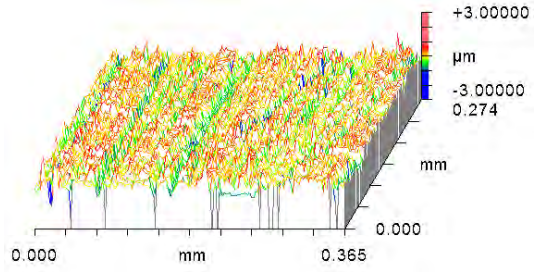

(d) 3D Zygo scan of the lateral condyle of femoral 5 showing the scratching pattern created. R_a=0.304μm.

Figure 7.4: Zygo scans and optical micrographs indicating both the pre and post scratching conditions of the CoCr femoral components. Z axis scale on the Zygo images is identical, to allow for direct comparison.

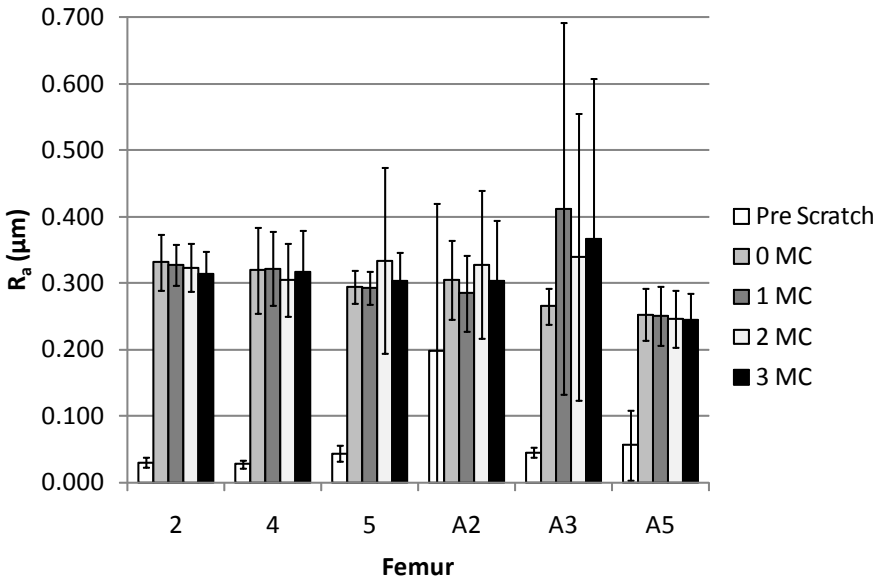

Figure 7.5: Plot showing the change in the R_a of the test femurs. Values shown are the mean of 10 points ± 1 SD. Femurs 2, 4, and 5, articulated with ArCom® tibias. Femurs A2, A3, and A5, articulated with E1™ tibias.

deviation. The scratching process using emery paper increased the surface roughness of all 6 tibias significantly to a mean value of 0.295±0.031μm. Approximately a 700% increase on the previous typical value. After 1x10^6 cycles of wear the mean surface roughness increased slightly to 0.315±0.055μm. Looking individually at the different femoral components it can be seen that femur A3 experiences a large increase in surface roughness from 0.265±0.028μm to 0.412±0.280μm. This was due to two image areas having abnormally high surface roughness' of close to 1μm. These two areas are shown in Figure 7.6 and it is clear that the high reading was caused by a large scratch running in the AP direction. The locations shown are locations 1 and 4 which are in line with other in the ML axis, therefore it is highly likely that this is the same scratch. This is confirmed when looking at the scratch dimensions. It was approximately 4μm deep and 0.1mm wide. Also visible in Figures 7.6(c) and 7.6(d) is the roughened surface on the main articulating surface. These scratches remained for the duration of the test, hence the mean roughness of Femur A3 remained higher than that of the other 5 femurs. Looking at the remaining 5 femurs, there was no significant change in the mean roughness throughout the test duration. The mean roughness of all 6 femurs at the conclusion of the test after 3x10^6 cycles was 0.308±0.039μm.

Analysis of the articulating surfaces of the six tibia components revealed that both types of tibias experienced an increase in surface roughness from the initial pre test value, this is

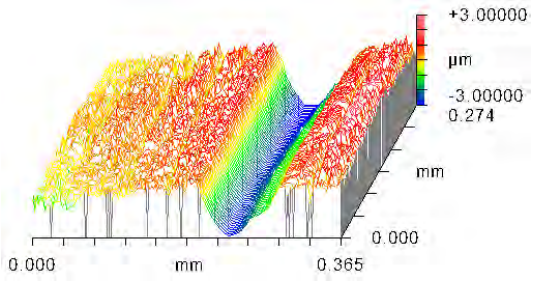

(a) 3D Zygo scan of Femoral A3 at location 1 after 1.0x10^6 cycles showing the large scratch running in the AP direction (R_a=0.857μm).

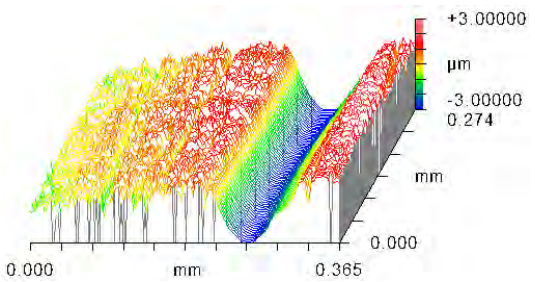

(b) 3D Zygo scan of Femoral A3 at location 4 after 1.0x10^6 cycles showing the large scratch running in the AP direction (R_a=0.983μm).

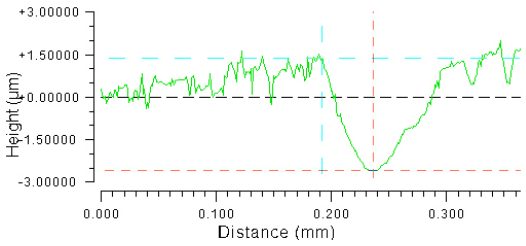

(c) 2D Zygo plot showing profile of the scratch observed on Femoral A3 at location 1 after 1.0x10^6 cycles. The depth of the scratch is 3.99μm and the width is 0.105mm.

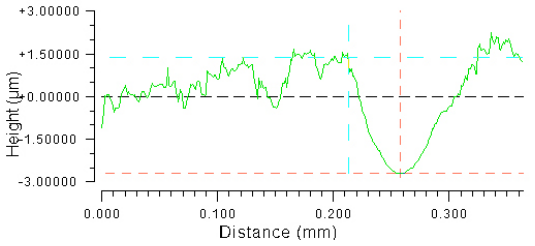

(d) 2D Zygo plot showing profile of the scratch observed on Femoral A3 at location 4 after 1.0x10^6 cycles. The depth of the scratch is 4.05μm and the width is 0.108mm.

Figure 7.6: Zygo scans of the above average readings of surface roughness on Femoral component A3 after 1x10^6 cycles of testing.

shown in Table 7.4. It should be noted that all components had been used in previous wear testing.

The surface roughness of the six individual tibia components is shown in Figure 7.7. Tibia A14 was used as the LSC and is included for comparison purposes. It can be seen that while a increase in surface roughness was seen for all tibias, the three ArCom® tibias demonstrated more consistent readings. There were high standard deviations for the E1™ tibias at most measurement intervals, indicating a large range of R_a values. Examples of the spread in R_a values can be seen in Figure 7.8.

Duration	ArCom®	E1™
0.0 MC	0.146±0.028μm	0.138±0.038μm
1.0 MC	0.210±0.011μm	0.291±0.059μm
2.0 MC	0.213±0.031μm	0.437±0.327μm
3.0 MC	0.180±0.056μm	0.346±0.108μm

Table 7.4: Table showing the change in mean surface roughness (±1SD) of the three ArCom and three E1 tibias articulated against scratched femoral components

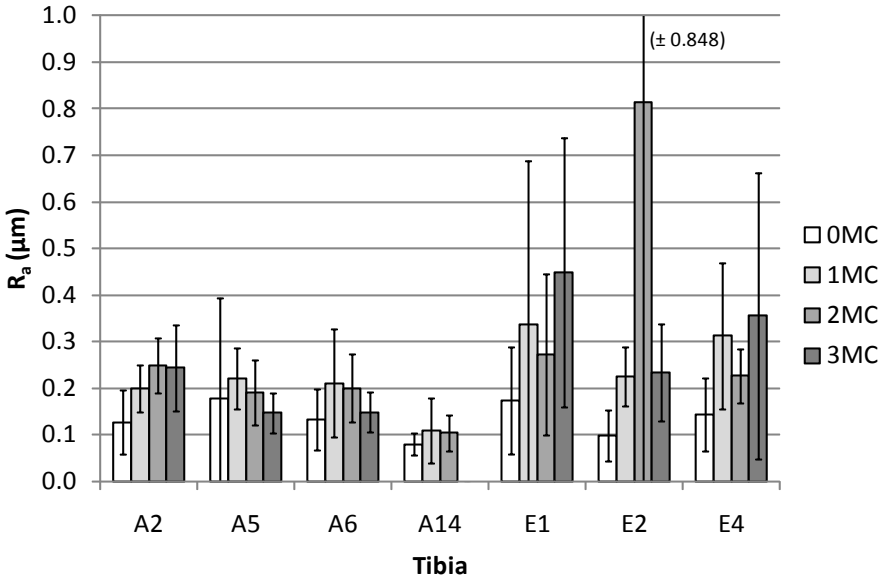

Figure 7.7: Plot showing the change in R_a of the test tibias. Values shown are the mean of 8 points, except for some isolated cases where the reading fell outside the wear track. Tibias prefixed with A are ArCom® , tibias prefixed with E are E1™. Tibia A14 was used as a LSC.

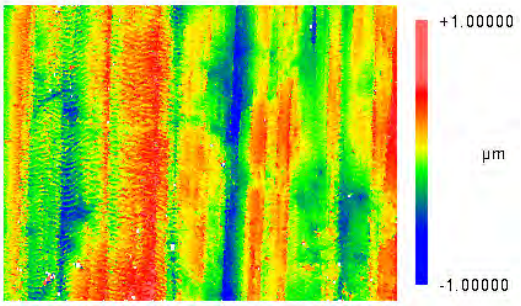

(a) ArCom tibia 2 at location X5 Y15 after 2.0 MC. R_a=0.174μm. Note the AP scratching and ripples perpendicular to AP motion.

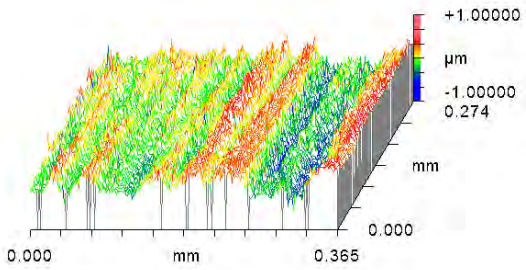

(b) ArCom tibia 5 at location X5 Y15 after 3.0 MC. R_a=0.166μm. Note the clearly defined scratching in the AP direction.

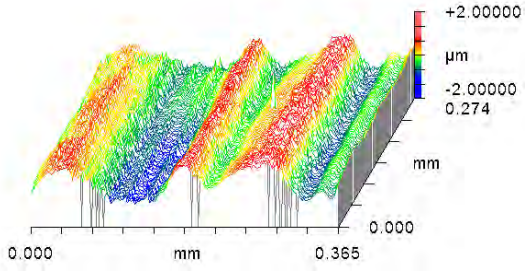

(c) E1™ tibia 2 at location X5 Y18 after 2.0 MC. R_a=0.407μm. Note the deep AP scratching.

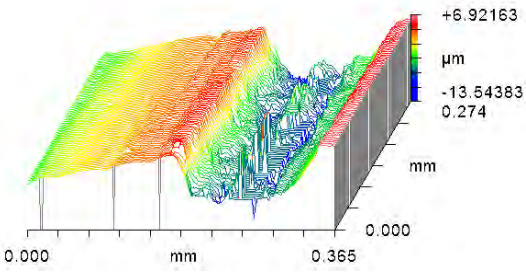

(d) E1™ tibia 2 at location X55 Y15 after 2.0 MC. R_a=2.739μm. Note the deep gouge running in the AP direction. It was this scan that caused the high average and SD on Figure 7.7.

Figure 7.8: Zygo scans of the tibia surfaces of both the E1™ and ArCom® tibias articulating against scratched femoral components.

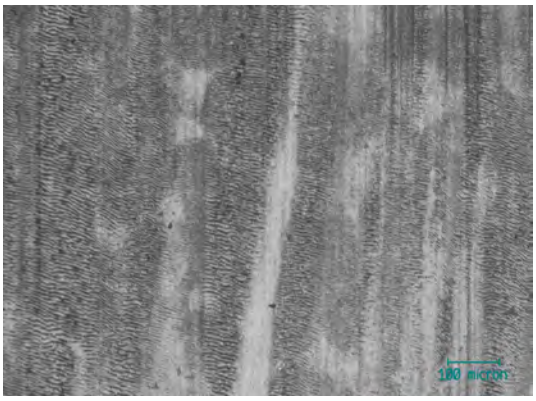

(a) ArCom® tibia 2 at location X55 Y15. Note the increased number of ripples combined with scratching in the AP direction.

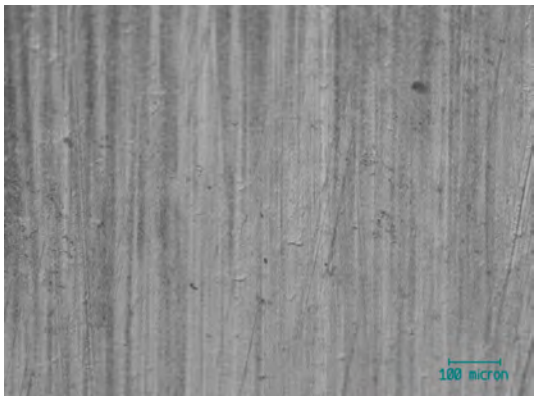

(b) ArCom® tibia 5 at location X8 Y18. Note the increased scratching in the AP direction.

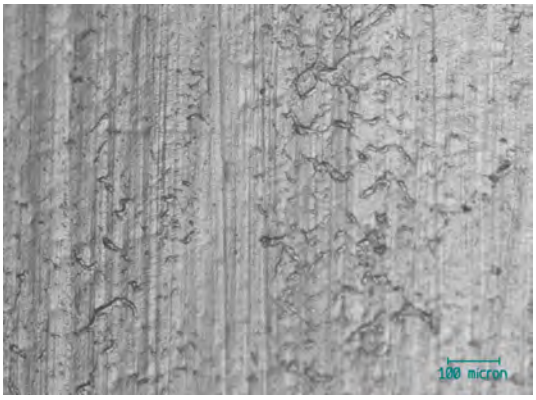

(c) E1™ tibia 2 at location X8 Y15. Note the cracking perpendicular to the AP direction and scratching parallel to the AP direction.

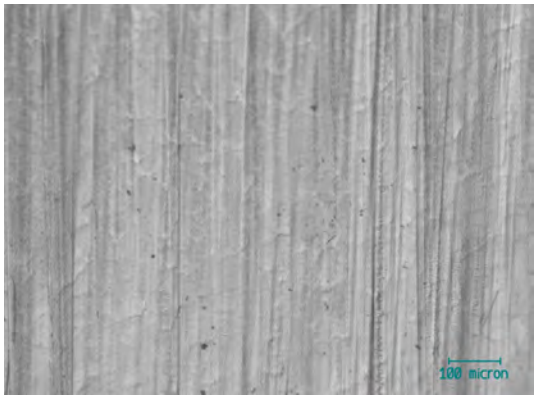

(d) E1™ tibia 4 at location X8 Y15. Note the increased scratching parallel to the AP sliding direction.

Figure 7.9: Optical micrographs of both the ArCom® and E1™ tibias after 2.0 MC of testing with the scratched femoral components.

Analysis using the optical microscope revealed a change in the wear mechanisms from the observations made in previous tests with smooth femoral components. Scratching in the AP direction and rippling perpendicular to the AP direction were much more prevalent for both the E1™ and ArCom® tibias. This change was observed after just 0.5 MC and continued through to the conclusion of the test at 3.0MC. Examples of this increased scratching and rippling can be seen in Figure 7.9.

7.3 Discussion

Damage to the femoral component and it's effect on wear is a concern in TKR. Some studies regarding THR have revealed that in some cases of roughened femoral heads, wear of the acetabular cups was found to be greater when using mildly cross-linked UHMWPE than in

conventional UHMWPE (Jedenmalm et al., 2009).

In this chapter, the primary aim was to assess the performance of both the ArCom® and E1 components using severely damaged femoral components, the likes of which had not previously been seen in the literature. Damage was imparted to the surface of the femoral components using Emery paper, and was such that it was a general roughening effect and no preference to scratch orientation was used.

The wear of both the E1™ and ArCom® tibia bearings was found to increase substantially when articulated with an artificially scratched femoral component. The wear rates from this test and that of the smooth femoral component conditions are summarised in Figure 7.10. A 16 fold increase for the ArCom® bearings and a 74-fold increase for the E1™ bearings was observed. Observing the volumetric wear plots seen in Figure 7.2, it is clear that excluding tibia A2 the wear performance of the remaining two ArCom® bearings was very similar to that of the three E1™ bearings. Investigations into the test history between the three ArCom® tibias reveal that bearing A2 was used for the initial setup procedures of the Prosim simulator. While no differences were seen in testing with smooth counter-faces, it is possible that damage to the micro-structure of tibia A2 was caused during the setup procedures, and this has only become apparent with the roughened counter-face. Closer analysis of the volumetric wear rates however, reveals similar ranges volumetric wear for the two tibia types. With the highest wearing E1™ tibia (E1 - 70.4 mm^3/MC) having twice the wear rate of the lowest wearing (E4 - 37.4 mm^3/MC). With the ArCom® tibias the relationship was similar with the highest wearing (A2 - 145 mm^3/MC) having approximately double the wear rate of the lowest wearing (A6 - 76.1 mm^3/MC). What is clear though is that with a counter-face with higher surface roughness, the performance difference between the two material types becomes less, as evidence by the wear rates of tibias E1 and A6, that were almost identical.

However, the absolute mean volumetric wear of the E1™ tibias remained remained 49% lower than that of the ArCom® tibias. This indicates that in both smooth and scratched counterface conditions, the highly cross-linked E1™ tibias had lower wear rates. What is apparent however is that under these extreme conditions, the performance benefit of the E1™ highly cross-linked tibias was not as pronounced as in the smooth femoral conditions with 49% and 87% reductions in wear over the ArCom® tibias for each condition respectively.

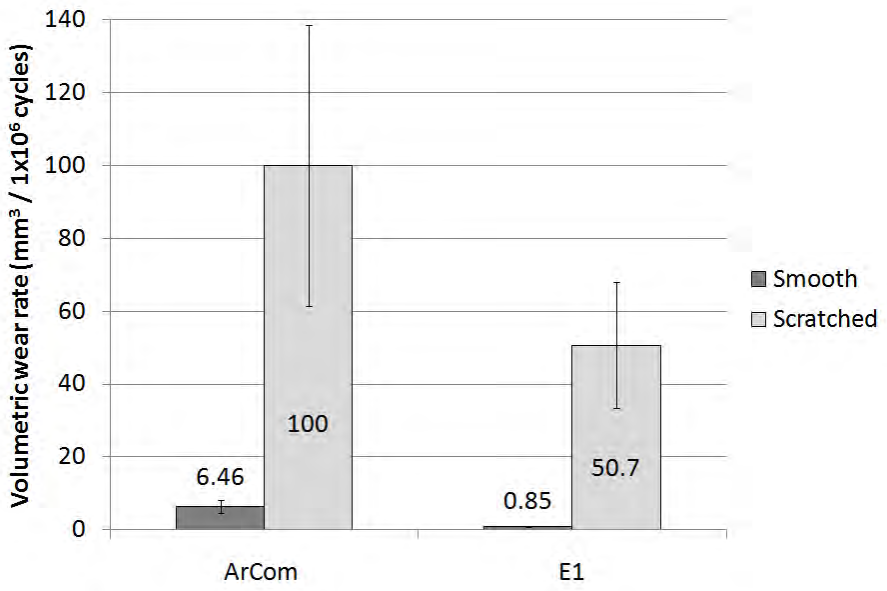

Figure 7.10: Comparison of volumetric wear rates of the ArCom® and E1™ tibias for both the smooth and scratched femoral tests. Mean values are shown ±1SD.

Optical and Zygo analysis of the femoral heads prior to testing revealed a 7-fold increase in surface roughness of the CoCr components with a rise from 0.041±0.012μm to 0.295±0.031μm. The R_a of the femoral components did not change throughout the wear test and remained consistently around 0.300μm. There was some variation of Femoral component A3 although this was due to the measured surface location being of a large scratch running in the AP direction.

Surface roughness of the six tibia components was found to increase, with a greater increase observed for the E1™ tibia components. This increase in surface roughness was reflected in optical observations which showed AP scratching and rippling as the predominant wear types. Evidence of burnishing was not found on any regions of the surface.

Existing studies had previously examined the effect of using explanted, rough femoral components articulating against both conventional and highly cross-linked UHMWPE in a knee simulator study. The explanted femoral components produced a wear rate approximately 5 times higher on the conventional inserts (32.9 mg/MC) than on the highly-crosslinked inserts (6.35 mg/MC) (Muratoglu et al., 2004b). Conventional GUR1050 UHMWPE articulating against artificially scratched femoral components (R_a=0.172μm) of the Genesis 2 design have a wear rate of 92.0±24.4mm^3/MC (DesJardins et al., 2008). This is similar to that observed in this study although the R_a in this study was over 50% higher.

With regards to clinical relevance, it is accepted that the surface roughness values used in

this test are significantly higher than any that would commonly found *in vivo* (Lakdawala et al., 2005; Que et al., 2000). However, this test was designed to assess the limits of performance of the chosen materials. It was found that under these extreme conditions, highly-crosslinked UHMWPE could perform as well as, in a wear perspective, conventional UHMWPE using non-damaged femoral components (McEwen et al., 2005).

7.3.1 Summary

In summary the wear of the E1™ and ArCom® tibia components was assessed using artificially roughened femoral components. The degree of roughening was more severe than any reported in the current literature. Wear rates of both the E1™ and ArCom® tibias increased dramatically, however the highly cross-linked E1™ tibias had approximately half the wear of the conventional ArCom® tibias, even under these extreme surface conditions. Spread of the wear rates for each condition was much greater however, with the least wearing ArCom® tibia wearing by approximately the same amount as the highest wearing E1™ tibia. ArCom® tibia 6 was again the least wearing of the three ArCom® tibias, as it was in the smooth counter-face wear test.

Study	PE Type	Design	Simulator	Profile	Lubricant	Duration	Wear Rate	Counterface Ra
This study	E1 UHMWPE	Vanguard CR	Prosim (Pneumatic)	ISO AF, FE - Lafortune AP, TR	25% Bovine Serum	3.0 MC	50.7 ± 17.3 mm^3/MC	0.295±0.031μm
This study	ArCom UHMWPE	Vanguard CR	Prosim (Pneumatic)	ISO AF, FE - Lafortune AP, TR	25% Bovine Serum	3.0MC	100 ± 38.5 mm^3/MC	0.295±0.031μm
DesJardins et al. (2008)	GUR1050 UHMWPE	Genesis 2 (CR) CoCr	Instron/Stanmore	ISO Force	50% BS	5.0MC	92.0±24.4mg/MC	0.172±0.029μm
DesJardins et al. (2008)	GUR1050 UHMWPE	Genesis 2 (CR) OxZr	Instron/Stanmore	ISO Force	50% BS	5.0MC	16.6±7.6mg/MC	0.058±0.016μm
Muratoglu et al. (2004b)	Con. UHMWPE	-	-	-	100-50% BS	2.0 MC	32.9 mg/MC	Explant
Muratoglu et al. (2004b)	Highly XL UHMWPE	-	-	-	100-50% BS	2.0 MC	6.35 mg/MC	Explant

Table 7.5: Comparison wear rates of UHMWPE tibia components articulating against damaged femoral components.

Chapter 8

Clinical Relevance, Conclusions, and Future Work

The challenge of any clinical research is to directly relate the outcomes of the research to improvements for patients and health professionals. In this section the outcomes of the current study and their relevance in the wider clinical community will be discussed. Additionally recommendations for further research are made in order to enhance and increase the impact of the work outlined in this thesis.

8.1 Clinical Relevance

Current TKR designs that are implanted into patients have an excellent survivorship rate and most can last for 10 years and beyond. The most common materials currently used in TKRs are a metal femoral component articulating on a UHMWPE bearing surface that is mounted into a metal tibial tray. Whereas in THR there are several hard-on-hard bearings available. The increased forces and contact stress in the knee joint, as well as less favourable lubrication regimes have encouraged development of the metal on UHMWPE rather than straying too far into other material combinations. Alternative methods of UHMWPE component fabrication have been developed, one example being the DCM process. This has been shown, in this study to produce components that perform exceptionally well in knee simulator wear testing. Investigations into the processing methods used has shown the importance of correct moulding temperatures on the consolidation and subsequent wear performance of DCM UHMWPE.

Cross-linking of UHMWPE has been used successfully in THR and it has been touted as the next advance on longer lasting TKRs due to its improved wear resistance. Concerns were raised about first generation cross-linked UHMWPE as the cross-linking process increased its tendency towards oxidative degeneration and subsequent early failure. Thermal treatments were developed to combat this, but these had the negative side effect of reducing the fatigue resistance of the UHMWPE and therefore reducing its suitability for long term implant survival. Third generation Vitamin E infused, highly cross-linked UHMWPE aims to solve this problem by significantly reducing oxidative degeneration, whilst eliminating the need for thermal treatments higher than the melt temperature of UHMWPE. This maintains the fatigue resistance of the component whilst also retaining the excellent wear properties. This study, went someway onto validating all these claims with excellent wear properties, no measurable oxidative degeneration, and no evidence of fatigue.

Future directions in TKR may take researchers down roads already travelled by those researching hard-on-hard bearings for THR. There are currently clinical trials ongoing for ceramic-on-UHMWPE bearings as ceramic femoral components have been shown to be more scratch resistant than their CoCr counterparts (DesJardins et al., 2008). A successful hard-on-hard TKR is a very challenging prospect, as shock absorbency is another key feature of the natural knee. The elastic and plastic properties of UHMWPE create shock absorbency to some extent, but where this would come from in a hard-on-hard material pairing is difficult to see.

8.2 Conclusions

8.2.1 Influence of molecular weight and processing conditions

The effect of molecular weight and different conditions during the DCM process were examined using pin-on-plate simulators. Additional tests were also conducted using a scratched counterface. The results showed:

- UHMWPE Plates moulded at 145°C exhibited visible fusion defects in the subsurface of the material, whereas plates moulded at 155°C, 165°C, and 195°C showed improved resin consolidation.
- UHMWPE plates moulded at 145°C had a higher wear factor of 4.362±0.535 com-

pared to the plates moulded at 155°C, 165°C, and 195°C which had wear factors of 2.903±0.443, 3.026±0.379, and 2.631±0.295 respectively (all values x10^6 $mm^3N^{-1}m^{-1}$).

- Circumferential scratching of the metal pin counter-face was found to increase the wear factor for all four processing conditions.
- Out of three different molecular weights tested, the optimum molecular weight was found to be 5,000,000 g/mol which exhibited a lower wear factor than 9,000,000 g/mol and 600,000 g/mol plates.

8.2.2 ArCom® non-crosslinked UHMWPE

- The mean volumetric wear rate of the ArCom® DCM UHMWPE tibias using a standard load and aggressive displacement profile was 6.46±1.80mm^3 per 1x10^6 cycles. This compares favourably to other PCR designs on the market today.
- Even though the test cells were not externally heated, frictional heating between the components was found to increase the test cell temperature to approximately 33°C, or approximately 6.5°C above ambient temperature.
- Dynamic loading of the control tibia increased the rate of lubricant uptake by 0.021mg/day over the unloaded soak sample.

8.2.3 Vitamin E infused, highly crosslinked UHMWPE

Six vitamin E infused, highly crosslinked UHMWPE tibias were wear tested in near identical conditions to the ArCom® UHMWPE components for a total of 9.0 MC. A comparison of wear rates was made when the peak loading was scaled to 4.0kN. Three E1™ tibias were aged and the wear performance assessed.

- Dynamic loading of the control tibia was found to increase the rate of lubricant uptake by 0.015mg/day over the unloaded soak sample. The importance of a load soak control tibia was demonstrated. This is especially important in samples that feature very low wear rates.
- The volumetric wear rate of the 6 Vitamin E infused UHMWPE tibia bearings was 0.853±0.131 mm^3/MC. This was an 87% reduction in volumetric wear compared to the geometrically identical ArCom® tibias tested previously.

- The wear rate remained constant for the whole 9.0 MC test duration, therefore presenting no evidence of fatigue.
- Increased loading on the E1^{TM} tibias during the wear test was not found to adversely affect wear. Contrarily, it was found to reduce the wear rate, although the test duration was short and further study should take place to confirm this.
- Accelerated ageing of the E1^{TM} tibias did not affect their wear performance indicating excellent resistance to oxidation, and hence less risk of oxidative degeneration once implanted.

8.2.4 The influence of a roughened counter-face

Three ArCom® and three E1^{TM} tibias were tested under the same standard conditions as the previous wear test with the exception that the femoral component had been artificially scratched.

- An increase in femoral surface roughness from 0.041±0.012μm to 0.295±0.031μm resulted in an increase in wear rate of the ArCom® tibias from 6.46±1.80 mm^3/MC to 100±38.5 mm^3/MC, and of the E1^{TM} tibias from 0.853±0.131 mm^3/MC to 50.7±17.3 mm^3/MC.
- Increasing the roughness of the femoral component was found to also increase the roughness of the resultant tibia surface for both the E1^{TM} and ArCom® tibia bearings. Surface analysis revealed no burnishing which previously was the surface feature with the lowest R_a.

8.3 Future work

The work within this thesis has substantially increased the knowledge of the performance of UHMWPE as a bearing material in TKRs. Particularly with regards to: the processing factors influencing the performance of DCM components; techniques to categorise the performance of knee wear simulators; the influence of lubricant uptake on gravimetric wear results; the performance of DCM components in TKR; the performance of highly cross-linked UHMWPE components in TKR; the influence of Vitamin E on UHMWPE wear; the

influence of a scratched counterface on UHMWPE wear. There are several future directions in which work from this thesis could be continued. These include:

- There is evidence that oxidation of UHMWPE occurs mostly at 1mm below the surface. It is unlikely that the E1™ tibias would have worn to this depth in the current 2.0 MC study. Therefore, continued wear testing of the oxygen aged E1™ tibias would show whether they are resistant to this subsurface oxidation. Fourier Transform Infra-Red (FTIR) spectroscopy would also be useful in determining the degree of oxidation caused by the accelerated ageing process.

- Particle analysis of the serum collected during wear testing would reveal whether the particles generated by both the ArCom® and E1™ UHMWPE tibias under smooth and scratched counterface conditions are within the size range that triggers osteolysis.

- Accelerated ageing and subsequent wear testing of the ArCom® manufactured would quantify the resistance of DCM components to oxidation.

- A comparison of the lubricant uptake rate for aged and un-aged E1™ specimens would inform the assumption made during the wear testing of the aged E1™ tibia components.

- Scratched counterface tests were conducted with highly scratched femoral components that led to very large increases in wear of the UHMWPE tibia components. Intermediate tests could be conducted in order to assess whether there is a threshold in counterface roughness, over which wear significantly increases.

- In order to accurately report simulator response behaviour, a form of reporting protocol could be investigated and introduced. This would allow better comparison of wear results across different research centres.

- Improvements could be made to the accelerated ageing rig, namely the addition of an oven rather than a water bath to provide the heating. This would allow a more rapid rise in temperature as prescribed in the ASTM standard, rather than the five hours it took using the water bath.

- A repeat experiment of the thermocouple instrumented TKR could be carried out to confirm higher temperatures on the medial side of the tibia.

Bibliography

S. Affatato, W. Leardini, M. Rocchi, A. Toni, and M. Viceconti. Investigation on wear of knee prostheses under fixed kinematic conditions. *Artificial Organs*, 32(1):13–18, JAN 2008. ISSN 0160-564X. 170, 174

M. Akagi, T. Asano, I.C. Clarke, N. Niiyama, M. Kyomoto, T. Nakamura, and C. Hamanishi. Wear and toughness of crosslinked polyethylene for total knee replacements: A study using a simulator and small-punch testing. *Journal Of Orthopaedic Research*, 24(10):2021–2027, OCT 2006. ISSN 0736-0266. 23, 209, 214

H.C. Amstutz, P. Campbell, N. Kossovsky, and I.C. Clarke. Mechanism and clinical-significance of wear debris-induced osteolysis. *Clinical Orthopaedics And Related Research*, 276:7–18, MAR 1992. ISSN 0009-921X. 14

T. P. Andriacchi, T. S. Stanwyck, and J. O. Galante. Knee biomechanics and total knee replacement. *J Arthroplasty*, 1(3):211–9, 1986. 7, 8

T.P. Andriacchi, J.O. Galante, and R.W. Fermier. The influence of total knee-replacement design on walking and stair-climbing. *Journal Of Bone And Joint Surgery-american Volume*, 64(9):1328–1335, 1982. ISSN 0021-9355. 13

H.E. Ash, S.C. Scholes, R. Parkin, and A. Unsworth. Relative movements between kinemax plus tibial inserts and the tibial base-plates. *Proceedings Of The Institution Of Mechanical Engineers Part H-Journal Of Engineering In Medicine*, 217(H2):99–104, 2003. ISSN 0954-4119. 126

ASTM F2003 - 02. Accelerated aging of ultra-high molecular weight polyethylene after gamma irradiation in air. 3

G.A. Ateshian, W.M. Lai, W.B. Zhu, and V.C. Mow. An asymptotic solution for the contact

of 2 biphasic cartilage layers. *Journal Of Biomechanics*, 27(11):1347–1360, NOV 1994. ISSN 0021-9290. 5

D.A. Baker, A. Bellare, and L. Pruitt. The effects of degree of crosslinking on the fatigue crack initiation and propagation resistance of orthopedic-grade polyethylene. *Journal Of Biomedical Materials Research Part A*, 66A(1):146–154, JUL 1 2003. ISSN 0021-9304. 22, 208

P. I. Barnett, J. Fisher, D. D. Auger, M. H. Stone, and E. Ingham. Comparison of wear in a total knee replacement under different kinematic conditions. *Journal of Materials Science: Materials in Medicine*, 12:1039–1042, 2001. 121

P. I. Barnett, H. M. J. McEwen, D. D. Auger, M. H. Stone, E. Ingham, and J. Fisher. Investigation of wear of knee prostheses in a new displacment/force-controlled simulator. *Proc Instn Mech Engrs Part H: J Engineering in Medicine*, 216:51–61, 2002. 27, 166, 169, 174

D.L. Bartel, V.L. Bicknell, and T.M. Wright. The effect of conformity, thickness, and material on stresses in ultra-high molecular weight components for total joint replacement. *J Bone Joint Surg Am*, 68(7):1041–51, September 1986. 12

C.J. Bell, P.S. Walker, M.R. Abeysundera, J.M. H. Simmons, P.M. King, and G.W. Blunn. Effect of oxidation on delamination of ultrahigh-molecular-weight polyethylene tibial components. *The Journal of Arthroplasty*, 13(3):280–290, April 1998. ISSN 0883-5403. 30

A. Bellare and R. E. Cohen. Morphology of rod stock and compression moulded sheets of ultra-high molecular-weight polyethylene used in orthopaedic implants. *Biomaterials*, 17 (24):2325–2333, December 1996. 2

A. Bellare, H. Schnablegger, and R. E. Cohen. A small-angle x-ray-scattering study of high-density polyethylene and ultrahigh molecular-weight polyethylene. *Macromolecules*, 28(23):7585–7588, November 1995. 15

A.A. Besong, J.L. Hailey, E. Ingham, M. Stone, B.M. Wroblewski, and J. Fisher. A study of the combined effects of shelf ageing following irradiation in air and counterface roughness on the wear of UHMWPE. *Bio-medical Materials And Engineering*, 7(1):59–65, 1997. ISSN 0959-2989. 16, 29

T.A. Blanchet, S.L. Peterson, and K.D. Rosenberg. Serum lubricant absorption by UHMWPE orthopaedic bearing implants. *Journal Of Tribology-transactions Of The Asme*, 124(1):1–4, JAN 2002. ISSN 0742-4787. Stle/asme Tribology Conference, San Francisco, California, Oct 21-24, 2001. 104, 168, 209

J.G. Bowsher and J.C. Shelton. Hip simulator study of the influence of patient activity level on the wear of crosslinked polyethylene under smooth and roughened femoral conditions. *Wear*, 250(Part 1):167–179, OCT 2001. ISSN 0043-1648. 13th International Conference On Wear Of Materials, Vancouver, Canada, Apr 22-26, 2001. 28

J.M. Brandt, K.D.J. Charron, S.J. MacDonald, and J.B. Medley. Mass gain behaviour of tibial polyethylene inserts during soak testing. *Proceedings Of The Institution Of Mechanical Engineers Part H-journal Of Engineering In Medicine*, 225(H3):324–331, 2011. ISSN 0954-4119. 104, 168

BS ISO 14243. Implants for surgery - wear of total knee joint prostheses. 111, 114, 120, 121, 171, 196

I.C. Burgess, M. Kolar, J.L. Cunningham, and A. Unsworth. Development of a six station knee wear simulator and preliminary wear results. *Proc Instn Mech Engrs Part H*, 211: 37–47, 1997. 27, 158

J. Charnley. The lubrication of animal joints in relation to surgical reconstruction by arthroplasty. *Annals Of The Rheumatic Diseases*, 19(1):10–19, 1960. ISSN 0003-4967. 10

J. Charnley. Arthroplasty of hip - a new operation. *Lancet*, 1(718):1129–&, 1961. ISSN 0140-6736. 1

J. Charnley. *Low friction arthroplasty of the hip: theory and practice.* Berlin: Springer-Verlag., 1979. 12

I.C Clarke, W. Starkebaum, A. Hosseinian, P. Mcguire, R. Okuda, R. Salovey, and R. Young. Fluid-sorption phenomena in sterilized polyethylene acetabular prostheses. *Biomaterials*, 6(3):184–188, 1985. ISSN 0142-9612. 168

M. T. Clarke, P. T. H. Lee, A. Arora, and R. N. Villar. Levels of metal ions after small- and large-diameter metal-on-metal hip arthroplasty. *Journal of Bone and Joint Surgery-british Volume*, 85B(6):913–917, August 2003. 26

A.F. Cooke, D. Dowson, and V. Wright. The rheology of synovial fluid and some potential synthetic lubricants for degenerate synovial joints. *Engineering in Medicine*, 7(2):66–72, 1978. vi, 9, 10

A. Deburge. Guepar Hinge Prosthesis Complications And Results With 2 Years Follow-up. *Clinical Orthopaedics And Related Research*, 120:47–53, 1976. ISSN 0009-921X. 12

J.D. DesJardins, B. Burnikel, and M. LaBerge. UHMWPE wear against roughened oxidized zirconium and CoCr femoral knee components during force-controlled simulation. *Wear*, 264(3-4):245–256, FEB 4 2008. ISSN 0043-1648. 29, 226, 228, 230

D. DOWSON, A. UNSWORTH, and V. WRIGHT. Analysis of boosted-lubrication in human joints. *Journal of Mechanical Engineering Science*, 12(5):364–&, 1970. 10

D. Dowson, S. Taheri, and N.C. Wallbridge. The role of counterface imperfections in the wear of polyethylene. *Wear*, 119(3):277–293, OCT 15 1987. ISSN 0043-1648. 28

A.P.D. Elfick, S.L. Smith, S.M. Green, and A. Unsworth. The quantitative assessment of UHMWPE wear debris produced in hip simulator testing: the influence of head material and roughness, motion and loading. *Wear*, 249(5-6):517–527, JUN 2001. ISSN 0043-1648. 28

E.L. Feng, S.D. Stulberg, and R.L. Wixson. Progressive subluxation and polyethylene wear in total knee replacements with flat articular surfaces. *Clinical Orthopaedics And Related Research*, 299:60–71, FEB 1994. ISSN 0009-921X. 14

J. Fisher, P. Firkins, E. A. Reeves, J. L. Hailey, and G. H. Isaac. The influence of scratches to metallic counterfaces on the wear of ultra-high molecular weight polyethylene. *Proc Inst Mech Eng H*, 209(4):263–4, 1995. 28

T. Fukubayashi, P. A. Torzilli, M. F. Sherman, and R. F. Warren. An invitro biomechanical evaluation of anterior-posterior motion of the knee - tibial displacement, rotation, and torque. *Journal Of Bone And Joint Surgery-American Volume*, 64(2):258–264, 1982. 9

J. Furmanski, M. Anderson, S. Bal, A. S. Greenwald, D. Halley, B. Penenberg, M. Ries, and L. Pruitt. Clinical fracture of cross-linked UHMWPE acetabular liners. *Biomaterials*, 30 (29):5572–5582, OCT 2009. ISSN 0142-9612. 22

A. Galvin, L. Kang, J. Tipper, M. Stone, E. Ingham, Z.M. Jin, and J. Fisher. Wear of crosslinked polyethylene under different tribological conditions. *Journal Of Materials Science-materials In Medicine*, 17(3):235–243, MAR 2006. ISSN 0957-4530. doi: 1. 23, 28

A. Gomoll, T. Wanich, and A. Bellare. J-integral fracture toughness and tearing modulus measurement of radiation cross-linked UHMWPE. *Journal Of Orthopaedic Research*, 20 (6):1152–1156, NOV 2002. ISSN 0736-0266. 22

H. Gray. *Anatomy of the human body*. Philadelphia: Lea and Febiger, 1918. vi, 6

T.R. Green, J. Fisher, M. Stone, B.M. Wroblewski, and E. Ingham. Polyethylene particles of a 'critical size' are necessary for the induction of cytokines by macrophages in vitro. *Biomaterials*, 19(24):2297–2302, DEC 1998. ISSN 0142-9612. 15

C.J. Grobbelaar, T.A. Duplessis, and F. Marais. Radiation improvement of polyethylene prostheses - preliminary-study. *Journal Of Bone And Joint Surgery-british Volume*, 60 (3):370–374, 1978. ISSN 0301-620X. 2, 21

W.H. Harris and O.K. Muratoglu. A review of current cross-linked polyethylenes used in total joint arthroplasty. *Clinical Orthopaedics And Related Research*, 430:46–52, JAN 2005. ISSN 0009-921X. 21

W.H. Harris and C.B. Sledge. Total hip and total knee replacement .2. *New England Journal Of Medicine*, 323(12):801–807, SEP 20 1990. ISSN 0028-4793. 12

D.A. Heck, C.A. Melfi, L.A. Mamlin, B.P. Katz, D.S. Arthur, R.S. Dittus, and D.A. Freund. Revision rates after knee replacement in the United States. *Medical Care*, 36(5):661–669, MAY 1998. ISSN 0025-7079. 14

B. Heinlein, F. Graichen, A. Bender, A. Rohlmann, and G. Bergmann. Design, calibration and pre-clinical testing of an instrumented tibial tray. *Journal Of Biomechanics*, 40: S4–S10, 2007. 7

R.W. Hood, T.M. Wright, and A.H. Burstein. Retrieval Analysis Of Total Knee Prostheses - A Method And Its Application To 48 Total Condylar Prostheses. *Journal Of Biomedical Materials Research*, 17(5):829–842, 1983. ISSN 0021-9304. 142, 172

K Imado, A Miura, M Nagatoshi, Y Kido, H Miyagawa, and H Higaki. A study of contact temperature due to frictional heating of UHMWPE. *Tribology Letters*, 16(4):265–273, MAY 2004. ISSN 1023-8883. Austrib 2002 Meeting, Perth, Australia, 2002. 171

J.H. Ingram, M. Stone, J. Fisher, and E. Ingham. The influence of molecular weight, crosslinking and counterface roughness on TNF-alpha production by macrophages in response to ultra high molecular weight polyethylene particles. *Biomaterials*, 25(17):3511–3522, AUG 2004. ISSN 0142-9612. 15

S.P. James, K.R. Lee, G.P. Beauregard, E.D. Rentfrow, and J.R. McLaughlin. Clinical wear of 63 ultrahigh molecular weight polyethylene acetabular components: Effect of starling resin and forming method. *Journal Of Biomedical Materials Research*, 48(3):374–384, JUN 5 1999. ISSN 0021-9304. 17, 18

M. Jasty, H. E. Rubash, and O. Muratoglu. Highly cross-linked polyethylene - The debate is over - In the affirmative. *Journal of Arthroplasty*, 20(4):55–58, June 2005. 20

A.. Jedenmalm, S. Affatato, P. Taddei, W. Leardini, U. W. Gedde, C. Fagnano, and M. Viceconti. Effect of head surface roughness and sterilization on wear of UHMWPE acetabular cups. *Journal Of Biomedical Materials Research Part A*, 90A(4):1032–1042, SEP 15 2009. ISSN 1549-3296. 28, 225

E.S. Jones. Joint lubrication. *The Lancet*, 227(5879):1043–1045, May 1936. ISSN 0140-6736. 9

L.C. Jones and D.S. Hungerford. Cement disease. *Clinical Orthopaedics And Related Research*, 225:192–206, DEC 1987. ISSN 0009-921X. 14

T. J. Joyce and A. Unsworth. A comparison of the wear of cross-linked polyethylene against itself with the wear of ultra-high molecular weight polyethylene against itself. *Proc Inst Mech Eng H*, 210(4):297–300, 1996. 24

T. J. Joyce, D. Monk, S. C. Scholes, and A. Unsworth. A multi-directional wear screening device and preliminary results of UHMWPE articulating against stainless steel. *Bio-Medical Materials And Engineering*, 10(3-4):241–249, 2000. 27, 32

N.H. Kelly, A.D. Rajadhyaksha, T.M. Wright, S.A. Maher, and G.H. Westrich. High Stress Conditions Do Not Increase Wear of Thin Highly Crosslinked UHMWPE. *Clinical Or-*

thopaedics And Related Research, 468(2):418–423, FEB 2010. ISSN 0009-921X. Annual Symposium of the Hip-Society, Las Vegas, NV, FEB 28, 2009. 211

H. Kim, R.R. Pelker, D.H. Gibson, J.F. Irving, and J.K. Lynch. Rollback in posterior cruciate ligament-retaining total knee arthroplasty - A radiographic analysis. *Journal Of Arthroplasty*, 12(5):553–561, AUG 1997. ISSN 0883-5403. 61st Annual Meeting of the American-Academy-of-Orthopaedic-Surgeons, NEW ORLEANS, LA, FEB 24-28, 1994. 13

C. Klapperich, S. Niedzwiecki, M. Ries, and L. Pruitt. Fluid sorption of orthopedic grade ultrahigh molecular weight polyethylene in a serum environment is affected by the surface area and sterilization method. *J Biomed Mater Res (Appl Biomater)*, 53:73–75, 2000. 125, 168

S.M. Kurtz. *The UHMWPE Handbook: Ultra-High Molecular weight Polyethylene in Total Joint Replacement*. Elsevier Academic Press, 2004. 17

S.M. Kurtz, O.K. Muratoglu, M. Evans, and A.A. Edidin. Advances in the processing, sterilization, and crosslinking of ultra-high molecular weight polyethylene for total joint arthroplasty. *Biomaterials*, 20(18):1659–1688, SEP 1999. ISSN 0142-9612. 16, 17

S.M. Kurtz, D. Mazzucco, C.M. Rimnac, and D. Schroeder. Anisotropy and oxidative resistance of highly crosslinked UHMWPE after deformation processing by solid-state ram extrusion. *Biomaterials*, 27(1):24–34, JAN 2006. ISSN 0142-9612. 105

M.A. Lafortune, P.R. Cavanagh, H.J. Sommer III, and A. Kalenak. Three-dimensional kinematics of the human knee during walking. *J. Biomechanics*, 25(4):347–357, 1992. vi, xi, 6, 8, 121, 122, 196, 206

A. Lakdawala, S. Todo, and G. Scott. The significance of surface changes on retrieved femoral components after total knee replacement. *Journal of Bone and Joint Surgery-british Volume*, 87B(6):796–799, June 2005. 28, 227

G. Lewis. Properties of crosslinked ultra-high-molecular-weight polyethylene. *Biomaterials*, 22(4):371–401, FEB 2001. ISSN 0142-9612. vi, 21, 23

P. Lewis, C.H. Rorabeck, R.B. Bourne, and P. Devane. Posteromedial tibial polyethylene

failure in total knee replacements. *Clinical Orthopaedics And Related Research*, 299:11–17, FEB 1994. ISSN 0009-921X. 14

S. Li and A.H. Burstein. Ultra-high-molecular-weight Polyethylene - The Material And Its Use In Total Joint Implants. *Journal Of Bone And Joint Surgery-american Volume*, 76A (7):1080–1090, JUL 1994. ISSN 0021-9355. 16

S. Lu, F.J. Buchanan, and J.F. Orr. Analysis of variables influencing the accelerated ageing behaviour of ultra-high molecular weight polyethylene (UHMWPE). *Polymer Testing*, 21 (6):623–631, SEP 2002. ISSN 0142-9418. 212

M.A. Macconaill. The Function of Intra-Articular Fibrocartilages, with Special Reference to the Knee and Inferior Radio-Ulnar Joints. *J Anat*, 66(Pt 2):210–27, January 1932. 9

A. Maroudas. Hyaluronic acid films. *ARCHIVE: Proceedings of the Institution of Mechanical Engineers, Conference Proceedings 1964-1970 (vols 178-184), Various titles labelled Volumes A to S*, 181(310):122–124, June 1967. 10

C.W. McCutchen. The frictional properties of animal joints. *Wear*, 5(1):1 – 17, 1962. ISSN 0043-1648. 10

H.M.J. McEwen, J. Fisher, A.A.J. Goldsmith, D.D. Auger, C. Hardaker, and M.H. Stone. Wear of fixed bearing and rotating platform mobile bearing knees subjected to high levels of internal and external tibial rotation. *Journal Of Materials Science-Materials In Medicine*, 12(10-12):1049–1052, 2001. ISSN 0957-4530. 16th Conference of the European-Society-for-Biomaterials, LONDON, ENGLAND, SEP 12-14, 2001. 27

H.M.J. McEwen, P.I. Barnett, C.J. Bell, R. Farrar, D.D. Auger, M.H. Stone, and J. Fisher. The influence of design, materials and kinematics on the in vitro wear of total knee replacements. *Journal Of Biomechanics*, 38(2):357–365, FEB 2005. ISSN 0021-9290. 29, 169, 170, 174, 208, 227

H.A. McKellop, F.W. Shen, P. Campbell, and T. Ota. Effect of molecular weight, calcium stearate, and sterilization methods on the wear of ultra high molecular weight polyethylene acetabular cups in a hip joint simulator. *Journal of Orthopaedic Research*, 17(3):329–339, May 1999. 106

D. McMinn, R. Treacy, K. Lin, and P. Pynsent. Metal on metal surface replacement of the hip - Experience of the McMinn prosthesis. *Clinical Orthopaedics and Related Research*, 329:S89–S98, August 1996. 26

J.B. Morrison. Mechanics of knee joint in relation to normal walking. *Journal Of Biomechanics*, 3(1):51, 1970. ISSN 0021-9290. 9

O.K. Muratoglu, C.R. Bragdon, D.O. O'Connor, M.Jasty, and W.H. Harris. A novel method of cross-linking ultra-high-molecular-weight polyethylene to improve wear, reduce oxidation, and retain mechanical properties: Recipient of the 1999 HAP Paul Award. *The Journal of Arthroplasty*, 16(2):149 – 160, 2001. ISSN 0883-5403. xviii, 15, 21, 24

O.K. Muratoglu, C.R. Bragdon, M. Jasty, D.O. O'Connor, R.S. Von Knoch, and W.H. Harris. Knee-simulator testing of conventional and cross-linked polyethylene tibial inserts. *Journal Of Arthroplasty*, 19(7):887–897, OCT 2004a. ISSN 0883-5403. 29, 209, 214

O.K. Muratoglu, B.R. Burroughs, C.R. Bragdon, S. Christensen, A. Lozynsky, and W.H. Harris. Knee simulator wear of polyethylene tibias articulating against explanted rough femoral components. *Clinical Orthopaedics and Related Research*, (428):108–113, November 2004b. 226, 228

O.K. Muratoglu, E.S. Greenbaum, C.R. Bragdon, M. Jasty, A.A. Freiberg, and W.H. Harris. Surface analysis of early retrieved acetabular polyethylene liners - A comparison of conventional and highly crosslinked polyethylenes. *Journal Of Arthroplasty*, 19(1):68–77, JAN 2004c. ISSN 0883-5403. 210

NJR for England and Wales. 7th annual report, 2010. URL www.njrcentre.org.uk. 1, 12, 169

P.C. Noble, M.A. Conditt, K.F. Cook, and K.B. Mathis. The John Insall Award - Patient expectations affect satisfaction with total knee arthroplasty. *Clinical Orthopaedics And Related Research*, 452:35–43, NOV 2006. ISSN 0009-921X. Annual Meeting of the Knee-Society, San Diego, CA, 2006. 1, 14

E. Oral, K.K. Wannomae, N. Hawkins, W.H. Harris, and O.K. Muratoglu. alpha-tocopherol-doped irradiated UHMWPE for high fatigue resistance and low wear. *Biomaterials*, 25 (24):5515–5522, NOV 2004. ISSN 0142-9612. vi, 2, 24, 25

E. Oral, E.S. Greenbaum, A.S. Malhi, W.H. Harris, and O.K. Muratoglu. Characterization of irradiated blends of alpha-tocopherol and UHMWPE. *Biomaterials*, 26(33):6657–6663, NOV 2005. ISSN 0142-9612. 25

E. Oral, S.D. Christensen, A.S. Malhi, K.K. Wannomae, and O.K. Muratoglu. Wear resistance and mechanical properties of highly cross-linked, ultrahigh-molecular weight polyethylene doped with vitamin E. *Journal Of Arthroplasty*, 21(4):580–591, JUN 2006a. ISSN 0883-5403. 23, 26

E Oral, A.S. Malhi, and O.K. Muratoglu. Mechanisms of decrease in fatigue crack propagation resistance in irradiated and melted UHMWPE. *Biomaterials*, 27(6):917–925, FEB 2006b. ISSN 0142-9612. 24

E. Oral, A.S. Malhi, K.K. Wannomae, and O.K. Muratoglu. Highly cross-linked ultrahigh molecular weight polyethylene with improved fatigue resistance for total joint arthroplasty - Recipient of the 2006 Hap Paul Award. *Journal Of Arthroplasty*, 23(7):1037–1044, OCT 2008. ISSN 0883-5403. 26

H. Pandit, S. Glyn-Jones, P. McLardy-Smith, R. Gundle, D. Whitwell, C.L.M. Gibbons, S. Ostlere, N. Athanasou, H S. Gill, and D W. Murray. Pseudotumours associated with metal-on-metal hip resurfacings. *Journal of Bone and Joint Surgery-british Volume*, 90B (7):847–851, July 2008. 26

L.A. Pruitt. Deformation, yielding, fracture and fatigue behavior of conventional and highly cross-linked ultra high molecular weight polyethylene. *Biomaterials*, 26(8):905–915, MAR 2005. ISSN 0142-9612. 209

L. Que, L.D.T. Topoleski, and N.L. Parks. Surface roughness of retrieved CoCrMo alloy femoral components from PCA artificial total knee joints. *Journal of Biomedical Materials Research*, 53(1):111–118, February 2000. 28, 227

MD Ries. Highly cross-linked polyethylene - The debate is over - In opposition. *Journal Of Arthroplasty*, 20(4, Suppl. 2):59–62, JUN 2005. ISSN 0883-5403. 4th Annual Spring Meeting on Current Concept in Joint Replacement, Las Vegas, NV, 2004. 20

V Saikko. A multidirectional motion pin-on-disk wear test method for prosthetic joint

materials. *Journal Of Biomedical Materials Research*, 41(1):58–64, JUL 1998. ISSN 0021-9304. 32

W.M. Sanford, W..C Moore, D McNulty, C Frisinger, and T.P. Schmalzried. Hip simulator study of the e!ect of sterilization and oxidation on UHMWPE wear. In *Trans 43rd Orthop Res Soc*, number 22, page 95, 1997. 212

P.A. Schai, T.S. Thornhill, and R.D. Scott. Total knee arthroplasty with the PFC system - Results at a minimum of ten years and survivorship analysis. *Journal Of Bone And Joint Surgery-british Volume*, 80B(5):850–858, SEP 1998. ISSN 0301-620X. 11, 170

T.P. Schmalzried, E.S. Szuszczewicz, M.R. Northfield, K.H. Akizuki, R.E. Frankel, G Belcher, and H.C. Amstutz. Quantitative assessment of walking activity after total hip or knee replacement. *Journal Of Bone And Joint Surgery-american Volume*, 80A(1): 54–59, JAN 1998. ISSN 0021-9355. 120, 124

S.C. Scholes. *The tribology of hard bearing surfaces for use in hip prostheses.* PhD thesis, University of Durham, 1999. 39

S.C. Scholes and A. Unsworth. Pin-on-plate studies on the effect of rotation on the wear of metal-on-metal samples. *Journal Of Materials Science-Materials In Medicine*, 12(4): 299–303, 2001. 32

S.C. Scholes and A. Unsworth. The wear properties of CFR-PEEK-OPTIMA articulating against ceramic assessed on a multidirectional pin-on-plate machine. *Proceedings Of The Institution Of Mechanical Engineers Part H-Journal Of Engineering In Medicine*, 221 (H3):281–289, 2007. vi, 32, 34

T. Schwenke, D. Orozco, E. Schneider, and M.A. Wimmer. Differences in wear between load and displacement control tested total knee replacements. *Wear*, 267(5-8):757 – 762, 2009. ISSN 0043-1648. 17th International Conference on Wear of Materials. 27, 172

P.F. Sharkey, W.J. Hozack, R.H. Rothman, S. Shastri, and S.M. Jacoby. Why are total knee arthroplasties failing today? *Clinical Orthopaedics and Related Research*, 404:7–13, NOV 2002. ISSN 0009-921X. Annual Meeting Of The Knee-Society/Association Of-hip-and-knee-surgeons, Dallas, Texas, 2002. 2, 14

T.F. Sibly and A. Unsworth. Wear of cross-linked polyethylene against itself - a material suitable for surface replacement of the finger joint. *Journal Of Biomedical Engineering*, 13(3):217–220, 1991. 24, 26

T. Siebel, S. Maubach, and M.M. Morlock. Lessons learned from early clinical experience and results of 300 ASR (R) hip resurfacing implantations. *Proceedings of the Institution of Mechanical Engineers Part H-Journal of Engineering In Medicine*, 220(H2):345–353, February 2006. 26

K.S. Simis, A. Bistolfi, A. Bellare, and L.A. Pruitt. The combined effects of crosslinking and high crystallinity on the microstructural and mechanical properties of ultra high molecular weight polyethylene. *Biomaterials*, 27(9):1688–1694, MAR 2006. ISSN 0142-9612. 22

T.W. Stapleton, J. Ingram, J. Katta, R. Knight, S. Korossis, J. Fisher, and E. Ingham. Development and characterization of an acellular porcine medial meniscus for use in tissue engineering. *Tissue Engineering Part A*, 14(4):505–518, APR 2008. ISSN 1937-3341. 11

J.B. Stiehl, R.D. Komistek, D.A. Dennis, R.D. Paxson, and W.A. Hoff. Fluoroscopic analysis of kinematics after posterior-cruciate-retaining knee arthroplasty. *Journal Of Bone And Joint Surgery-British Volume*, 77B(6):884–889, NOV 1995. ISSN 0301-620X. 7, 13

J.L. Tipper, P.J. Firkins, E. Ingham, J. Fisher, M.H. Stone, and R. Farrar. Quantitative analysis of the wear and wear debris from low and high carbon content cobalt chrome alloys used in metal on metal total hip replacements. *Journal Of Materials Science-materials In Medicine*, 10(6):353–362, JUN 1999. ISSN 0957-4530. 32

R.B.C. Treacy, C.W. McBryde, and P.B. Pynsent. Birmingham hip resurfacing arthroplasty - a minimum follow-up of five years. *Journal of Bone and Joint Surgery-british Volume*, 87B(2):167–170, February 2005. 26

R. Tsukamoto, P.A. Williams, H. Shoji, K. Hirakawa, K. Yamamoto, M. Tsukamoto, and I.C. Clarke. Wear in Molded Tibial Inserts: Knee Simulator Study of H1900 and GUR1050 Polyethylenes. *Journal of Biomedical Materials Research Part B: Applied Biomaterials*, 85B:314–319, 2008. 17, 19, 168, 169, 174, 209

M. B. Turell and A. Bellare. A study of the nanostructure and tensile properties of ultra-high molecular weight polyethylene. *Biomaterials*, 25(17):3389–3398, August 2004. 15

A. Unsworth. Tribology of human and artificial joints. *Proc Inst Mech Eng H*, 205(3): 163–72, 1991. 10, 11

C. Vaidya, E. Alvarez, J. Vinciguerra, D.A. Bruce, and J.D. DesJardins. Reduction of total knee replacement wear with vitamin E blended highly cross-linked ultra-high molecular weight polyethylene. *Proceedings Of The Institution Of Mechanical Engineers Part H-journal Of Engineering In Medicine*, 225(H1):1–7, 2011. ISSN 0954-4119. 25, 212, 214

K. Vassiliou and A. Unsworth. Is the wear factor in total joint replacements dependent on the nominal contact stress in ultra-bigh molecular weight polyethylene contacts? *Proceedings Of The Institution Of Mechanical Engineers Part H-Journal Of Engineering In Medicine*, 218(H2):101–107, 2004. 106

P.S. Walker, C. Ranawat, and J. Insall. Fixation of tibial components of condylar replacement knee prostheses. *Journal Of Biomechanics*, 9(4):269, 1976. ISSN 0021-9290. 12

P.S. Walker, D. Greene, D. Reilly, J. Thatcher, M. Bendov, and F.C. Ewald. Fixation of tibial components of knee prostheses. *Journal Of Bone And Joint Surgery-American Volume*, 63(2):258–267, 1981. ISSN 0021-9355. 12

A. Wang, C. Stark, and J. H. Dumbleton. Role of cyclic plastic deformation in the wear of UHMWPE acetabular cups. *J. Biomed. Mater. Res.*, 29(5):619–626, 1995a. ISSN 1097-4636. 107

A. Wang, D.C. Sun, C. Stark, and J.H. Dumbleton. Wear mechanisms of UHMWPE in total joint replacements. *Wear*, 181-183(Part 1):241–249, February 1995b. ISSN 0043-1648. 172

A. Wang, C. Stark, and J.H. Dumbleton. Mechanistic and morphological origins of ultra-high molecular weight polyethylene wear debris in total joint replacement prostheses. *Proc Inst Mech Eng H*, 210(3):141–55, 1996. 32

A. Wang, S.S. Yau, A. Essner, L. Herrera, M. Manley, and J. Dumbleton. A highly crosslinked UHMWPE for CR and PS total knee arthroplasties. *Journal Of Arthroplasty*, 23(4):559–566, JUN 2008. ISSN 0883-5403. 170, 174, 209, 214

S. Wang and S. Ge. The mechanical property and tribological behavior of UHMWPE: Effect of molding pressure. *Wear*, 263(Part 2 Sp. Iss. SI):949–956, SEP 10 2007. ISSN 0043-1648. 19

K.K. Wannomae, S.D. Christensen, B.R. Micheli, S.L. Rowell, D.W. Schroeder, and O.K. Muratoglu. Delamination and adhesive wear behavior of alpha-tocopherol-stabilized irradiated ultrahigh-molecular-weight polyethylene. *J Arthroplasty*, 25(4):635–43, June 2010. 213

C. Wolf, C. Macho, and K. Lederer. Accelerated ageing experiments with crosslinked and conventional ultra-high molecular weight polyethylene (UHMW-PE) stabilised with alpha-tocopherol for total joint arthroplasty. *Journal Of Materials Science-materials In Medicine*, 17(12):1333–1340, DEC 2006. ISSN 0957-4530. 10th International Conference on Polymers in Medicine and Surgery (PIMS2004), Cambridge, ENGLAND, SEP 06-08, 2004. 29

J.J. Wu, C.P. Buckley, and J.J. O'Connor. Mechanical integrity of compression-moulded ultra-high molecular weight polyethylene: effects of varying process conditions. *Biomaterials*, 23(17):3773–3783, SEP 2002. ISSN 0142-9612. 2, 18, 107

Appendix A

Appendix

A.1 Theory and coding

A.1.1 R^2 Calculation

The R^2 value for all linear fits was calculated using the Pearson product moment correlation coefficient r, which is:

$$r = \frac{\sum_{i=1}^{n}(x_i - barx)(y_i - \bar{y})}{\sqrt{\sum_{i=1}^{n}(x_i - \bar{x})^2 \sum_{i=1}^{n}(y_i - \bar{y})^2}} \tag{A.1}$$

The r^2 value gives an indication of the linearity of the data and ranges between 0 (no linearity) and 1 (complete linearity).

A.1.2 Matlab scripts

Below are two Matlab scripts that were used to extract the profile data from the Prosim logs and subsequently plot the data. Appreciation is extended to Dr. Andrew Gallant for his assistance with the coding.

converter.m

```
[filename,pathname] = uigetfile('*.txt','Select the log file to
convert');
f_load = fopen(fullfile(pathname, filename),'r');

[filename, pathname] = uiputfile('*.txt', 'Save converted file as',
'default.txt');
f_save = fopen(fullfile(pathname, filename),'w');
```

```
disp('Running');
d_1 = ' ';
d_2 = ' ';
s = 0;
flag = 0;
while (s~= -1)
    s = fgetl(f_load);
    if (s~= -1)
        if s(1)=='2'
             [d_1, d_2] = strtok(s(29:42));
             [d_2] = strtok(d_2);

        elseif (s(7)=='I' && flag == 0)
             fprintf(f_save,'No1\tNo2\t%s\r\n', s);
             flag = 1;
        elseif s(7)~='I'
             fprintf(f_save, '%s\t%s\t%s\r\n', d_1, d_2, s);
        end
    end
end

fclose(f_load);
fclose(f_save);
```

data-importer.m

```
clear

\newpage

[filename,pathname] = uigetfile('*.txt','Select the converted log
file');
f_load = fopen(fullfile(pathname, filename),'r');

headerline = fgetl(f_load);
headerlinemod = strrep(headerline, ' ', '_');
data = textscan(f_load,'','Delimiter','\t','MultipleDelimsAsOne',1);
```

```
fclose(f_load);
headers = textscan(headerlinemod,'%s','Delimiter','\t',
'MultipleDelimsAsOne',1);

[m,n] = size(data{1,1});

p = m/128;
q = 128;
r = repmat(q,1,p);

for k = 1:length(headers{:})
    data{1,k} = mat2cell(data{1,k}, r, 1);
    eval([headers{1}{k} '= data{k};']);
end
```

A.2 Protocols

A.2.1 Cleaning Protocols

A.2.1.1 Pin-on-plate samples

- Rinse under a stream of distilled water to remove bulk contaminants.
- Degas a bath of 1% solution of Neutracon and distilled water for 5 minutes.
- Sonicate pins and plates in 1% solution of Neutracon and distilled water for 7.5 minutes.
- Turn plates over and sonicate for a further 7.5 minutes.
- Remove components from bath and rinse under a stream of distilled water.
- Degas a bath of distilled water for 5 minutes.
- Soncate pins and plates for 2.5 minutes.
- Turn plates over and sonicate for a further 2.5 minutes.
- Immerse pins and plates in Propan-2-ol for 3 minutes.

- Air dry components for a total of 30 minutes.

A.2.1.2 ArCom UHMWPE tibial bearings

- ArCom tibial components carefully removed from titanium CoCrMo bases.
- Rinse under a stream of distilled water to remove bulk contaminants.
- Degas a bath of 1% solution of neutracon and distilled water for 5 minutes.
- Sonicate ArCom components in 1% solution of neutracon and distilled water for 10 minutes.
- Turn components over and sonicate for a further 10 minutes.
- Rinse under a stream of distilled water to remove any contaminants.
- Degas a bath of distilled water for 5 minutes.
- Sonicate ArCom components in a bath of distilled water for 2.5 minutes.
- Turn components over and sonicate for a further 2.5 minutes.
- Place components in propan-2-ol for 3 minutes.
- Air dry components for a total of 30 minutes, turning after 15.

A.2.1.3 EPoly tibial bearings

From 2×10^6 cycles the EPoly components were no longer cleaned using the same protocol as the ArCom samples, but with the following protocol.

- EPoly tibial components carefully removed from titanium CoCrMo bases.
- Rinse under a stream of distilled water to remove bulk contaminants.
- Degas a bath of 1% solution of neutracon and distilled water for 5 minutes.
- Sonicate Epoly in components in 1% solution of neutracon and distilled water for 20 minutes.
- Turn components over and sonicate for a further 20 minutes.
- Remove components and use air duster to remove any contaminants.

- Rinse under a stream of distilled water to remove any contaminants.
- Degas a bath of distilled water for 5 minutes.
- Sonicate EPoly components in a bath of distilled water for 5 minutes.
- Turn components over and sonicate for a further 5 minutes.
- Remove components and use an air duster to remove any contaminants.
- Place components in propan-2-ol for 3 minutes.
- Air dry components for a total of 30 minutes, turning after 15.

A.2.2 Gravimetric Assessment Protocol

The following protocol was used for gravimetric assessment of all test samples. It was performed using the Mettler Toledo AX205 balance.

- Take cleaned components and place on lint free tissue next to balance.
- Turn on balance an use the 'Internally adjust' function to zero the balance.
- Record the time, date, temperature, and humidity.
- Take the first sample and place on the balance. Wait for the reading to stabilise and record the value.
- Remove the sample and replace with the second sample.
- Continue this process until three readings have been obtained for each sample with a maximum range of 0.01mg.
- The mean of these three values is the value that will be used for mass and volumetric change calculations.

A.2.3 ProSim Calibration

A.2.3.1 Axial Force

Axial force on the Prosim knee simulator can be controlled by two methods, open loop control and force control. In order to allow an accurate following of the demand profile, two

load cells, six pneumatic linear actuators, and six control valves must be calibrated. Stations 1 and 4 both contain a load cell, which in both force control and open loop control is used to provide a real-time visual readout of the applied load. Also, in force control, the load cell is used as feedback for the PID controller. All six stations contain individual pneumatic linear actuators and a control valve. While all actuators are of the same model, there may be small manufacturing differences between them which makes calibration necessary.

Equipment Required: RDP E275 Digital indicator
Load Cell
Short Loading Bolt

1. Ensure all guards are fully closed and that the air supply is on on and the compressor is activated.

2. Log on to the controller PC and double click the 'Kneesim' icon on the desktop. This will open the knee simulator program and the machine will automatically initialise.

3. If the simulator does not initialise, then either the guards are open or the air supply is turned off. Remedy the situation and then press the green button in the keyboard well to initialise the simulator.

4. Navigate to 'Machine Properties and deselect the 'Enable motor drives when running' option. This ensures the FE cradle does not inadvertently move during calibration, which may cause damage to both the calibrating load cell or the simulator itself.

5. Attach the digital indicator to the RDP load cell. Plug it into the mains and switch it on. Allow the load cell to stand for 20 minutes under no load.

6. Open the safety guards. The simulator will automatically discharge any pressure in the system for safety. Place the externally calibrated load cell into the first simulator station, ensuring that both the top and bottom surfaces are sitting flush. Some manual movement of the FE cradle will be required.

7. Screw the shorter loading bolt into the pneumatic linear actuator.

8. Zero the external load cell, now add the spacing cylinder and cap. This ensures that the loading on the external load cell is identical to that of the internal load cell.

9. Close the safety guards and press the green button to initialise the simulator.

10. Navigate to 'Machine' then 'Auto Load Calibrate' this will bring up the calibration option menu. Select the station and the axis, in this case AF, and input a comment to identify the calibration. at least your name and the date of calibration are recommended. Click 'OK' and the test screen will appear. Click 'Go' to commence the calibration.

11. During the calibration the control valve is opened to five evenly spaced intervals between 0 (fully closed) and 255 (fully open) at each stage the load measured on the external load cell is entered manually, then the next load is applied. Enter all five load values then click 'Finish ' to produce a calibration test report. This can be saved as a tab delimited text file.

12. Determine whether the values obtained are sensible and that the derivations from the actual recorded values are within tolerances. If they are not then you may want to run the test again.

13. Repeat the previous 7 steps for all six stations and record the calibration constants.

14. To input the calibration constants navigate to 'Machine' then 'Set Calibration Constants'.

15. This will open the 'Machine Calibration dialog box. Click the 'AF Axis' tab at the top then enter the calibration constants for one station. Click 'OK' to save the values, then repeat for all stations. Remember to enter zeros for the load-cell constants in stations 0,2,3,5 as there is no load cell.

16. To check the variances of loading between stations, move the small internal load-cell to Station 0 and run a test cycle. Use the 'History Viewer' to export tabular values of the applied load. Repeat this for all stations and plot the profiles.

17. If all the profiles are within accepted tolerances of each other then save the test to keep these updated constants.

A.2.3.2 Tibial Rotation

Tibial rotation on the Prosim knee simulator is obtained through the use of a pneumatic linear actuator and monitored by a LVDT. Each of the six stations has its own actuator and LVDT. In order to obtain an accurate experimental implementation of the demand profile, the LVDT must be calibrated.

Equipment Required: ±2.5° TR calibration block
±5.0° TR calibration block

1. Ensure all guards are fully closed and that the air supply is on and the compressor is activated.
2. Log on to the controller PC and double click the 'Kneesim' icon on the desktop. This will open the knee simulator program and the machine will automatically initialise.
3. If the machine does not initialise, then either the guards are open or the air supply is turned off. Remedy the situation and then press the green button in the keyboard well to initialise the machine.
4. In the menu bar, click 'Machine' then select 'Periodic readings'. This will open a new window that contains real-time readouts from all the sensors on the machine. There is a drop down box in which you can select the station number, and tabs for all the axis of load/displacement. (Axial Force, Tibial Rotation, Anterior/Posterior, and Flexion/Extension)
5. Open one of the machine guards and discharge the pressure from the system.
6. Take the ±2.5° TR calibration block and place the 90° edges flush against the most anterior wall of the Abduction/Adduction cradle and the flat edge of the tibial bearing mount.
7. Ensure that both edges are conforming then record the ADC value listed in the real time display.
8. Repeat using the 2.5° to get ADC values for ±2.5° and the 5.0° to get ADC values for ±5.0°

9. Repeat for all 6 stations

10. For each individual station, plot ADC values on the x axis versus degree of displacement on the y axis. Insert a trend line, and obtain an expression in the form y=mx+c for this line. m= displacement per ADC count and c = zero displacement offset. If you are happy with the trend line in relation to the data points record the m and c values for each station.

11. In the machine software, navigate to 'Machine' then 'Set Calibration Constants'. Click on the TR tab and input the constants for station 0. Click 'OK' then repeat for the rest of the stations. Remember to navigate to 'Test' then 'Save' in order to keep these updated constants.

12. The TR Displacement should now be calibrated. To check the accuracy of the calibration repeat steps 6-9 but, instead of recording ADC values, make a note of the value in the 'Disp' box.

A.2.3.3 Anterior/Posterior Displacement

Anterior and posterior displacement on the Prosim knee simulator is obtained through the use of a pneumatic linear actuator and monitored by a LVDT. Each of the six stations has its own actuator and LVDT. In order to obtain an accurate experimental implementation of the demand profile. The LVDT must be calibrated.

Equipment Required: Metric Slip Gauges
Calibration Shaft & Cup

1. Ensure all guards are fully closed and that the air supply is on and the compressor is activated.

2. Log onto the controller PC and double click the 'Kneesim' Icon on the desktop. This will open the knee simulator program and the machine will automatically initialise.

3. If the machine does not initialise, then either the guards are open or the air supply is turned off. Remedy this situation, and then press the green button under the monitor to initialise the machine.

4. In the menu bar, click 'Machine' then select 'Periodic Readings. This will open a window that contains real-time readouts from all the sensors on the machine. There is a drop-down box in which you can select the station number, and tabs for all the axes of load/displacement. (Axial Force, Tibial Rotation, Anterior/Posterior, and Flexion/Extension)

5. For displacement calibration of the AP axis we are only interested in the 'Disp ADC' and the 'Disp' readouts. The 'Disp ADC' readout displays the raw data from the LVDT and the 'Disp' is the displacement in mm which is calculated using the calibration constants.

   N.B. The LVDTs used in the Prosim knee simulator all have a calibrated range of approximately 25mm. This is less than the range of travel of the AP sledge. The LVDTs were positioned so that at the fully anterior position the AP sledge is just inside the maximum range of the LVDT (approximately equal to an ADC value of 29,500). Consequently, the LVDTs will reach their minimum value of minus 32,768 before the AP sledge reaches its most posterior position.

6. Take the 10mm slip gauge and place it between the anterior wall of the Abduction/Adduction cradle and the bearing cylinder mounted on the AP sledge. Record the Disp ADC value for this position. Add an additional slip gauge, then record the Disp ADC value again. Continue until the minimum ADC value of minus 32,768 is reached. Repeat for all stations.

7. Plot the displacement (x axis) vs the ADC value (y axis) and add a trend-line and also the equation of the line. If you are happy with the trend line in relation to the data points, record the absolute value of m for each station.

8. In the machine software, navigate to, 'Machine' then 'Set Calibration Constants'. Click on the AP tab and input each m value in the 'Disp per unit ADC count' box. Ensure that the 'Zero displacement offset' is set to zero. Click 'OK and repeat for all stations. Remember to save in order to keep these updated constants.

9. Return to the 'Periodic Readings' display. Insert the larger end of the AP calibration rod so that it is in contact with the anterior wall if the AA cradle and the bearing

cylinder mounted on the AP sledge. Record the value listed in the 'Disp'. Repeat for each station, remembering that there is a unique AP calibration rod for each station.

10. Navigate back to the Calibration constants display and in the 'Zero displacement offset' enter the inverse of the value obtained in the previous step and repeat for each station.

A.3 Components Schematics

A.3.1 Articulating Station Components

Schematics of all the components used in the setup of each of the articulating stations in the Prosim knee simulator are in this section.

- Femur mounting block
- Modified Prosim tibia base plate
- PE tibia mount
- PE tibia plug

RIGHT

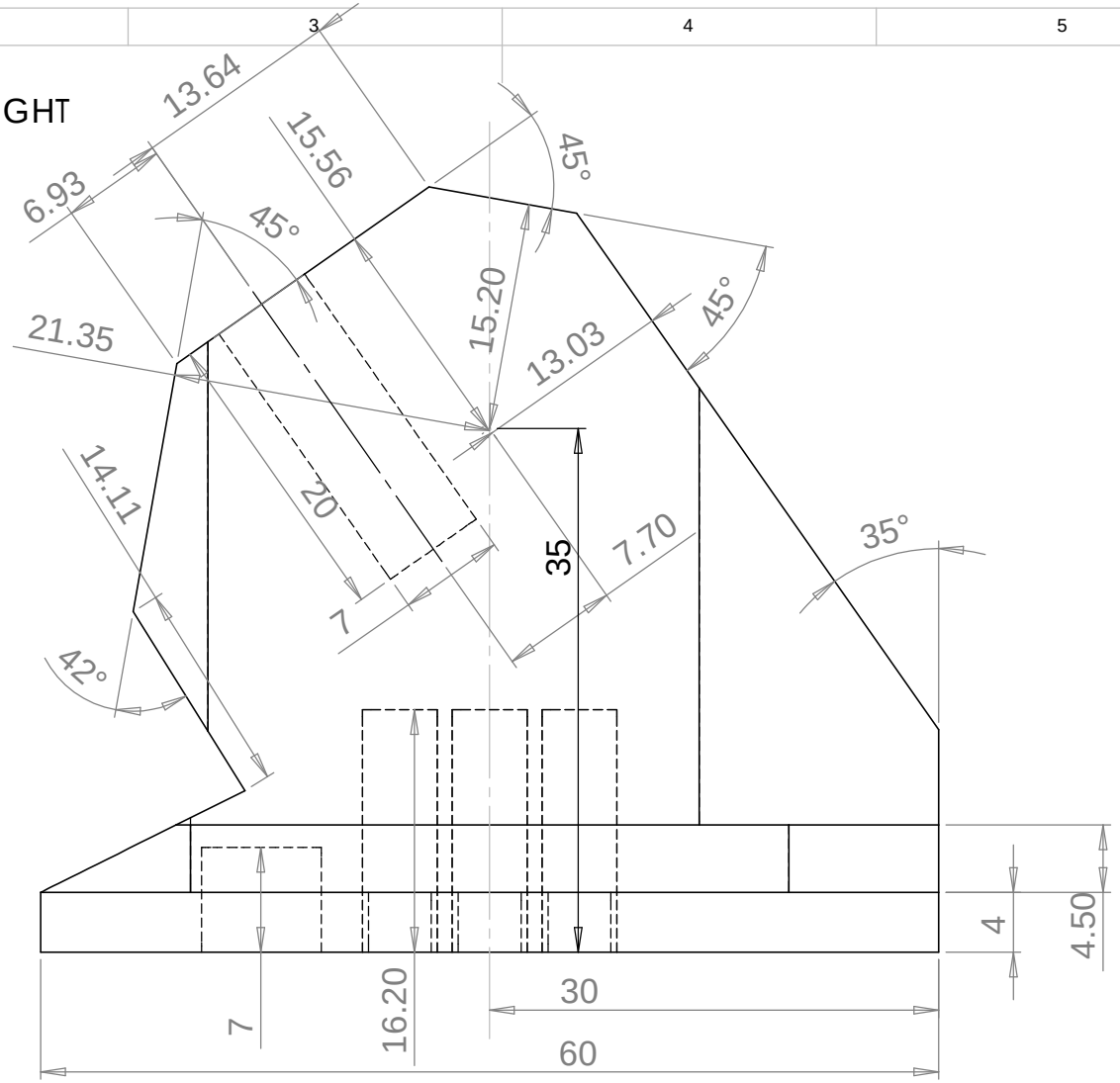

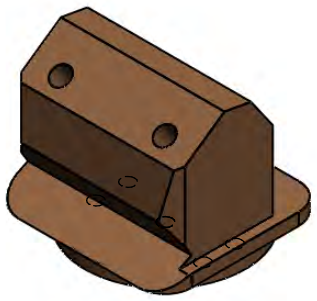

UNLESS OTHERWISE SPECIFIED: DIMENSIONS ARE IN MILLIMETERS SURFACE FINISH: TOLERANCES: LINEAR: ANGULAR:	FINISH:	DEBUR AND BREAK SHARP EDGES

	NAME	SIGNATURE	DATE
DRAWN			
CHK'D			
APPV'D			
MFG			
Q.A			

DO NOT SCALE DRAWING	REVISION
TITLE: Final Femoral Mounting Block	
MATERIAL:	DWG NO. A4
WEIGHT:	SCALE:1:1 SHEET 1 OF 2

BOTTOM

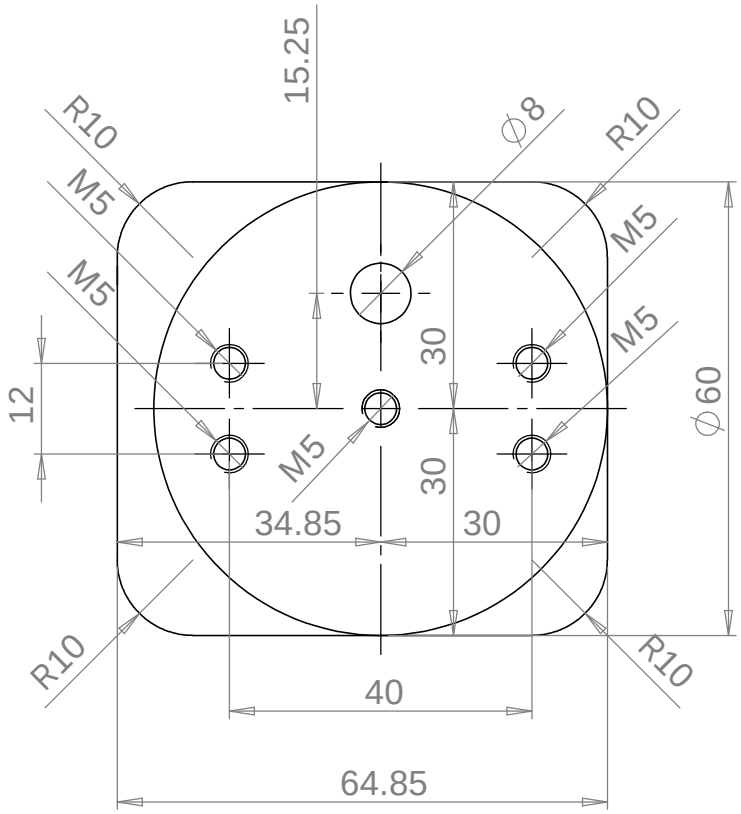

TOP

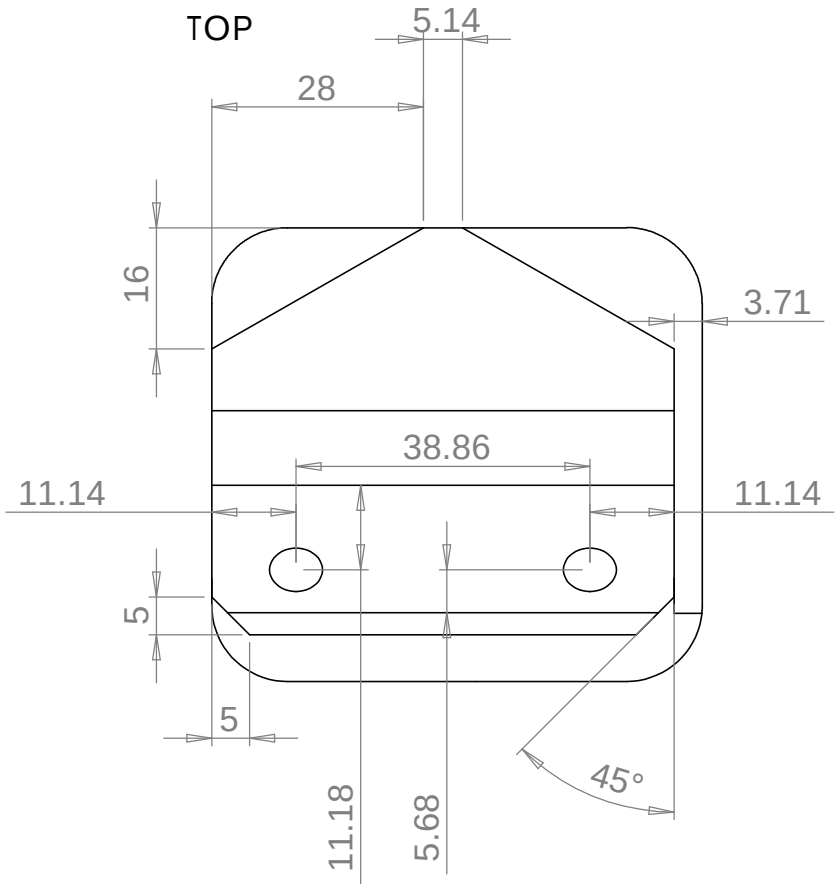

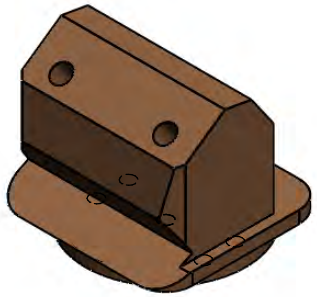

UNLESS OTHERWISE SPECIFIED: DIMENSIONS ARE IN MILLIMETERS SURFACE FINISH: TOLERANCES: LINEAR: ANGULAR:		FINISH:		DEBUR AND BREAK SHARP EDGES	DO NOT SCALE DRAWING	REVISION
	NAME	SIGNATURE	DATE		TITLE: Final Femoral Mounting Block	
DRAWN						
CHK'D						
APPV'D						
MFG						
Q.A				MATERIAL:	DWG NO.	A4
				WEIGHT:	SCALE:1:1	SHEET 2 OF 2

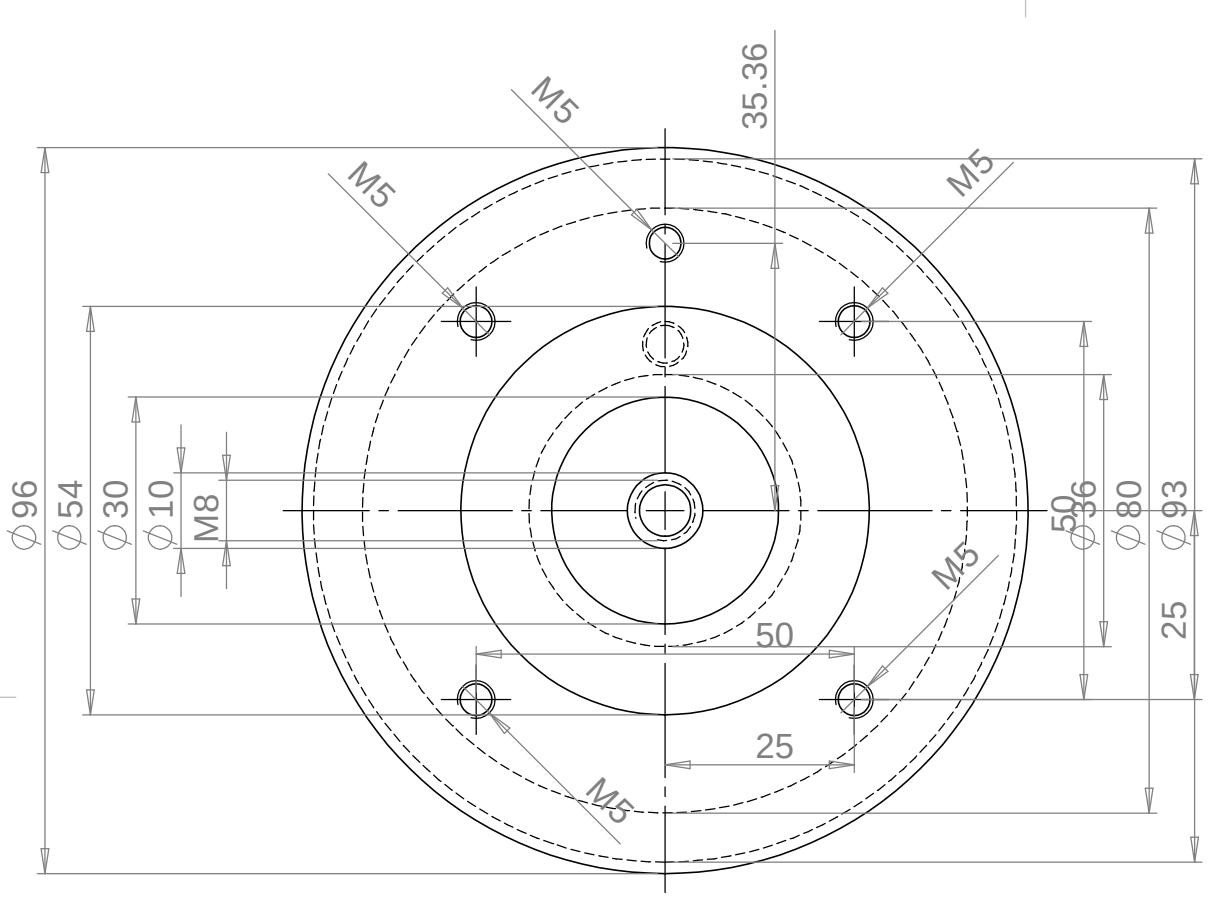

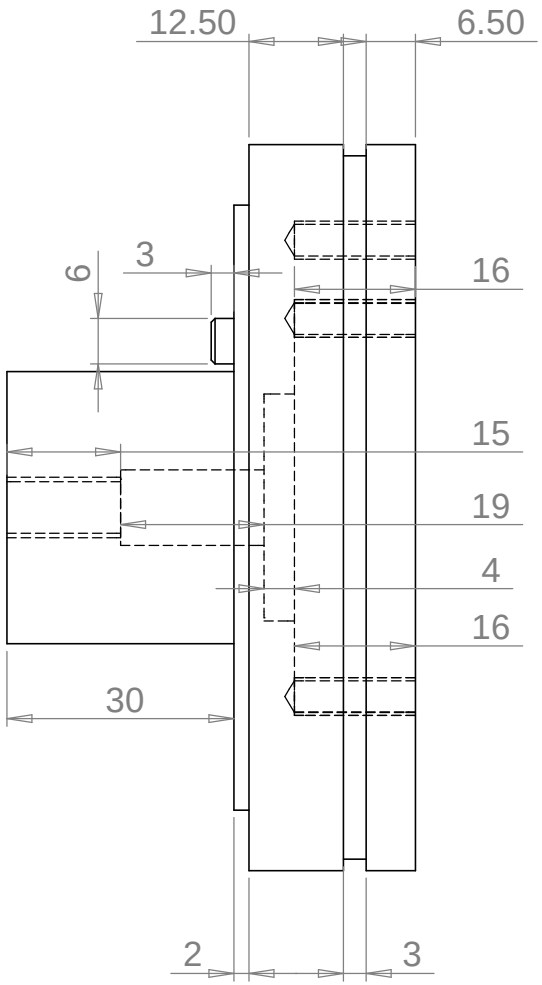

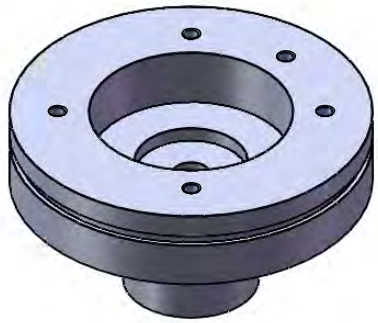

UNLESS OTHERWISE SPECIFIED: DIMENSIONS ARE IN MILLIMETERS SURFACE FINISH: TOLERANCES: LINEAR: ANGULAR:	FINISH:	DEBUR AND BREAK SHARP EDGES	DO NOT SCALE DRAWING / REVISION

	NAME	SIGNATURE	DATE
DRAWN			
CHK'D			
APPV'D			
MFG			
Q.A			

TITLE:

Tibial Base Plate Modified

MATERIAL:

DWG NO.

A4

WEIGHT:

SCALE:1:1

SHEET 1 OF 1

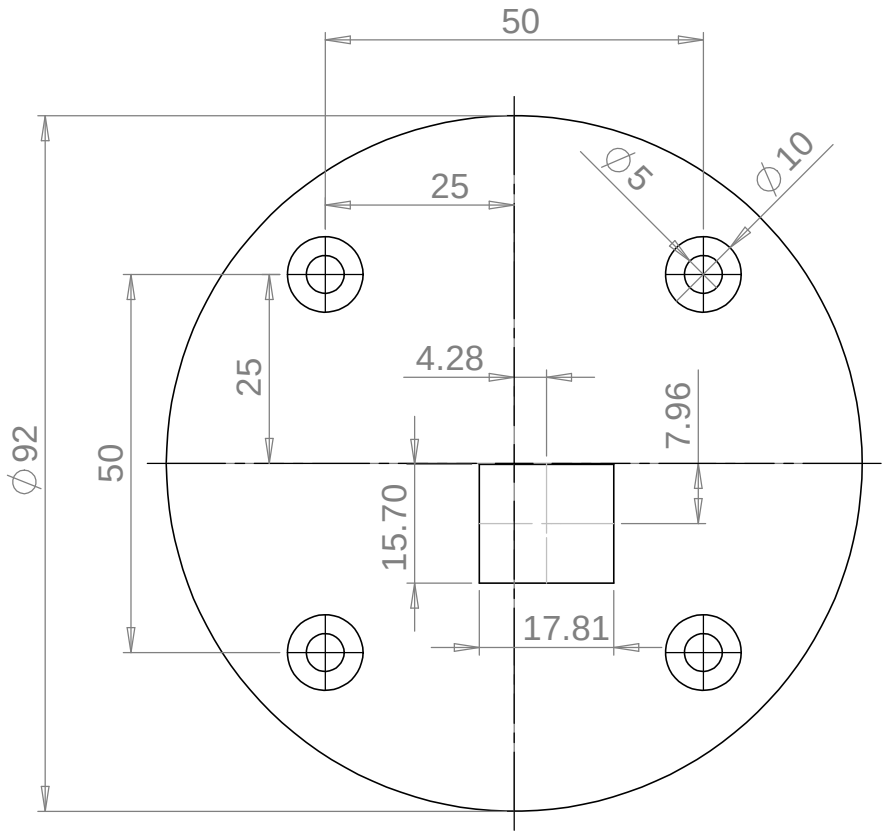

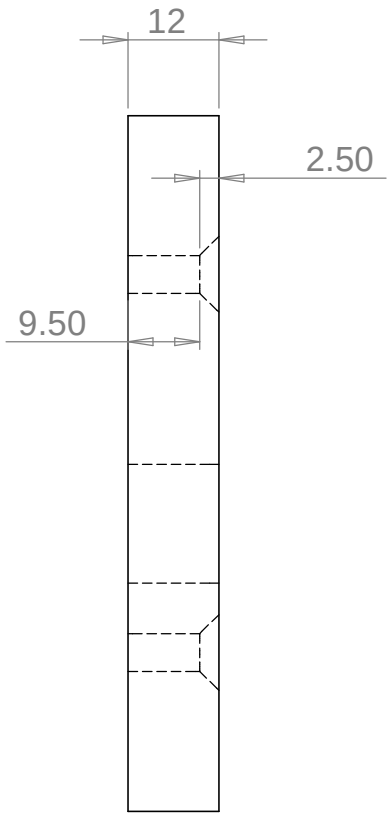

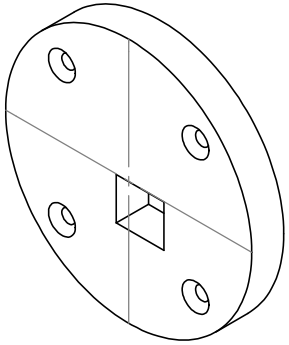

UNLESS OTHERWISE SPECIFIED: DIMENSIONS ARE IN MILLIMETERS SURFACE FINISH: TOLERANCES: LINEAR: ANGULAR:	FINISH:	DEBUR AND BREAK SHARP EDGES

	NAME	SIGNATURE	DATE
DRAWN			
CHK'D			
APPV'D			
MFG			
Q.A			

DO NOT SCALE DRAWING	REVISION
TITLE:	PE Tibial Mount
MATERIAL:	DWG NO. A4
WEIGHT:	SCALE:1:1 SHEET 1 OF 1

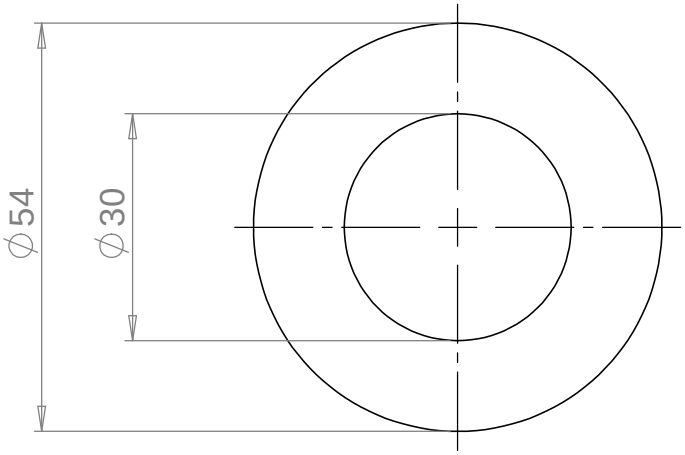

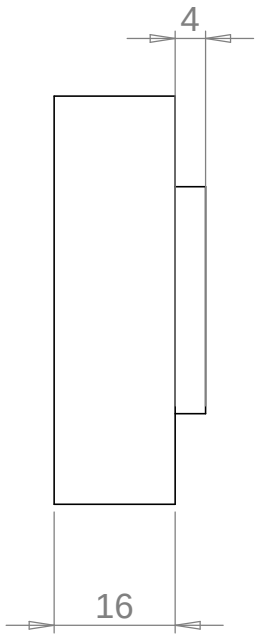

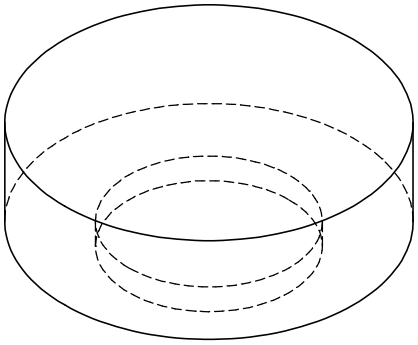

UNLESS OTHERWISE SPECIFIED:
DIMENSIONS ARE IN MILLIMETERS
SURFACE FINISH:
TOLERANCES:
LINEAR:
ANGULAR:

FINISH:

DEBUR AND BREAK SHARP EDGES

DO NOT SCALE DRAWING

REVISION

Martin Stanley

	NAME	SIGNATURE	DATE
DRAWN			
CHK'D			
APPV'D			
MFG			
Q.A			

TITLE:

Tibia PE Plug

MATERIAL:

High Density PE

DWG NO.

A4

WEIGHT:

SCALE:1:1

SHEET 1 OF 1

A.3.2 Thermocouple Component Schematics

Schematics of the modifications made to test components for the insertion of thermocouples are in this section.

- Modifications made to Vanguard femur
- Modifications made to Vanguard tibia
- Modifications made to the femur mount
- Modifications made to the tibia mount
- Modifications made to the Prosim tibia base plate

All holes 1.5mm diameter

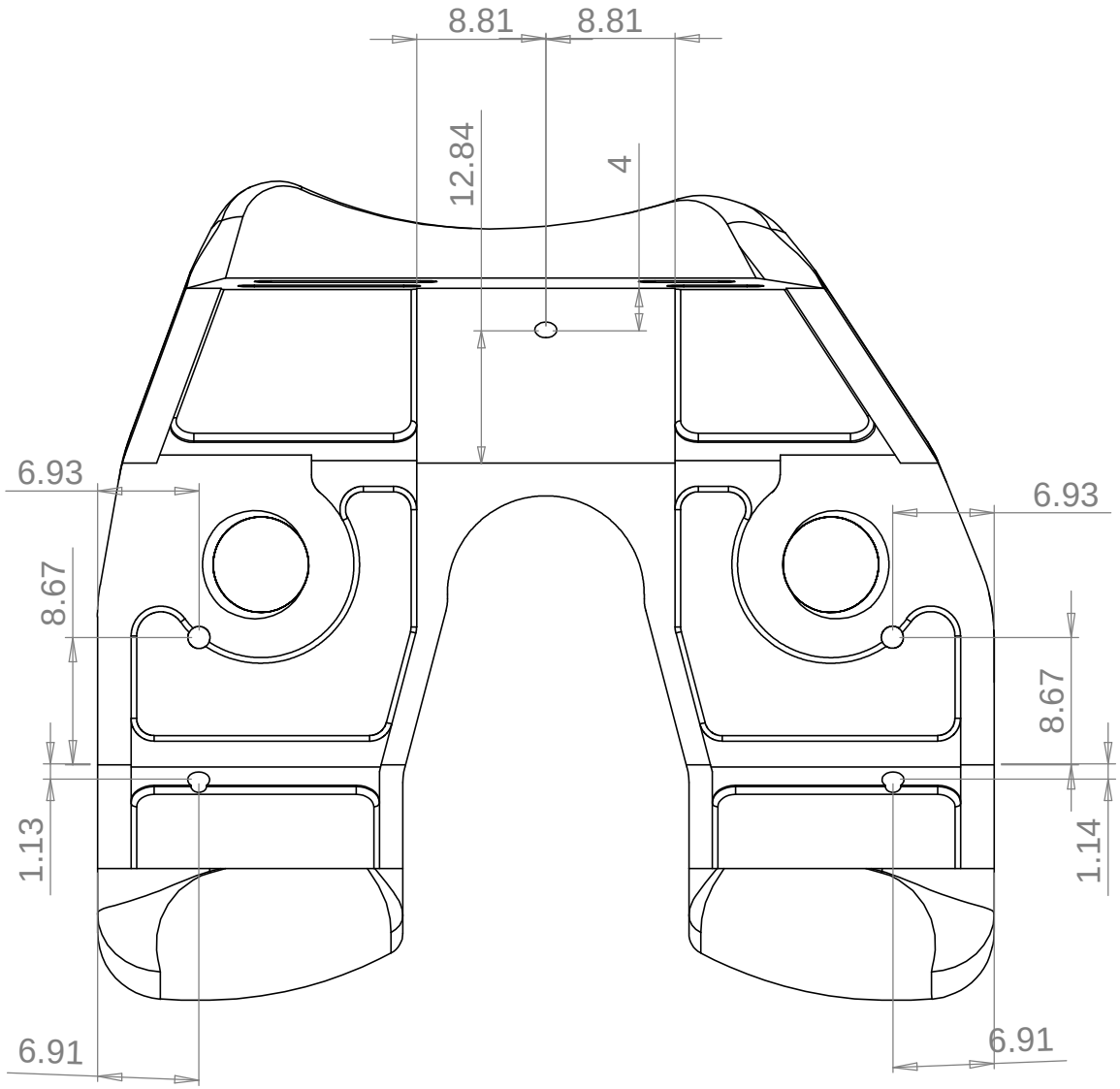

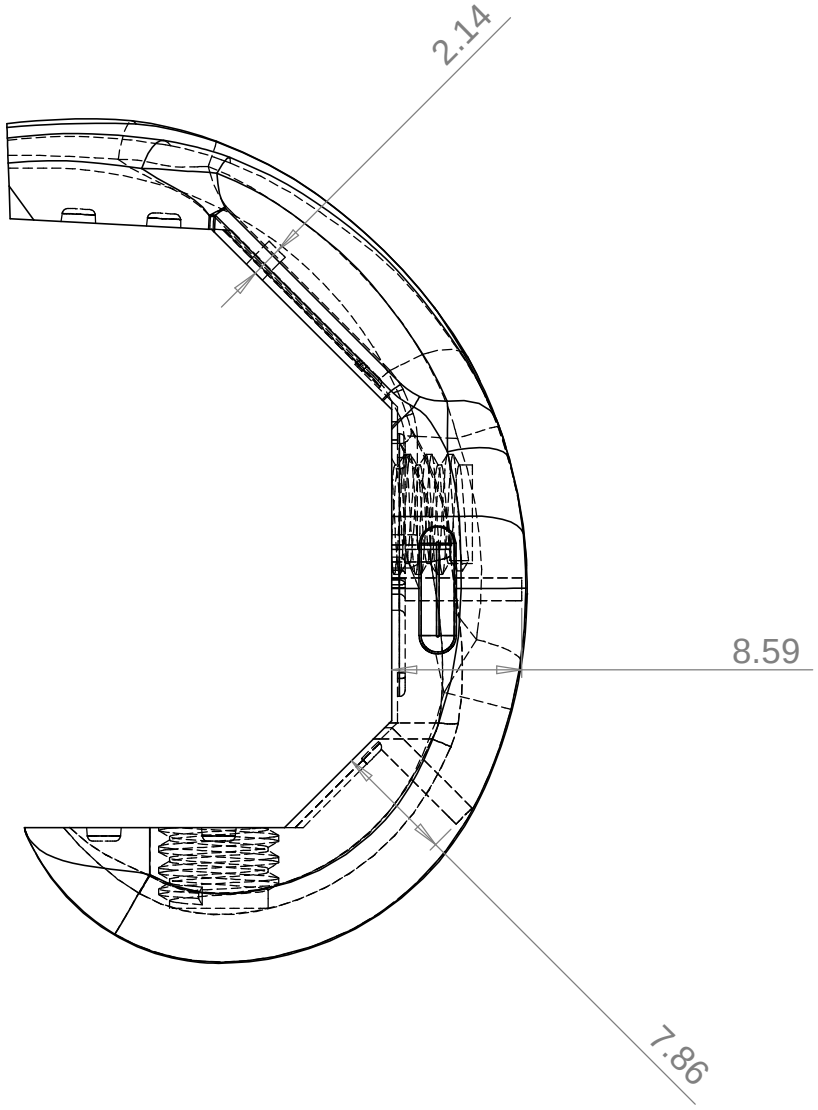

Martin Stanley	Femoral thermocouple locations and depths	Durham University School of Engineering Centre for Biomedical Engineering

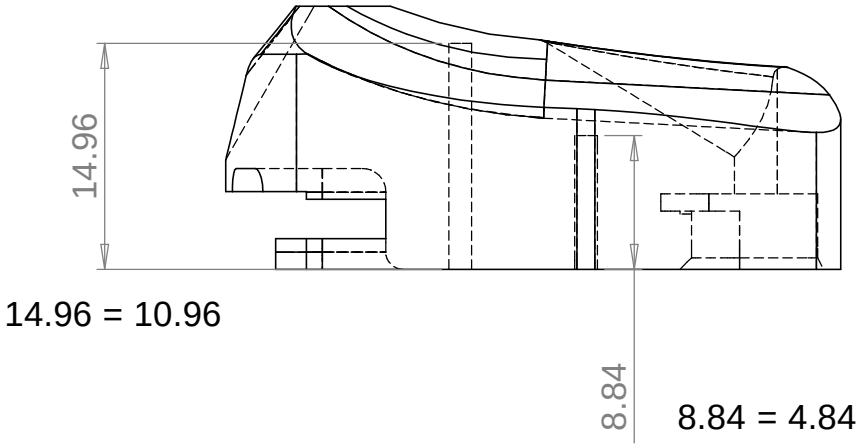

14.96 = 10.96

8.84 = 4.84

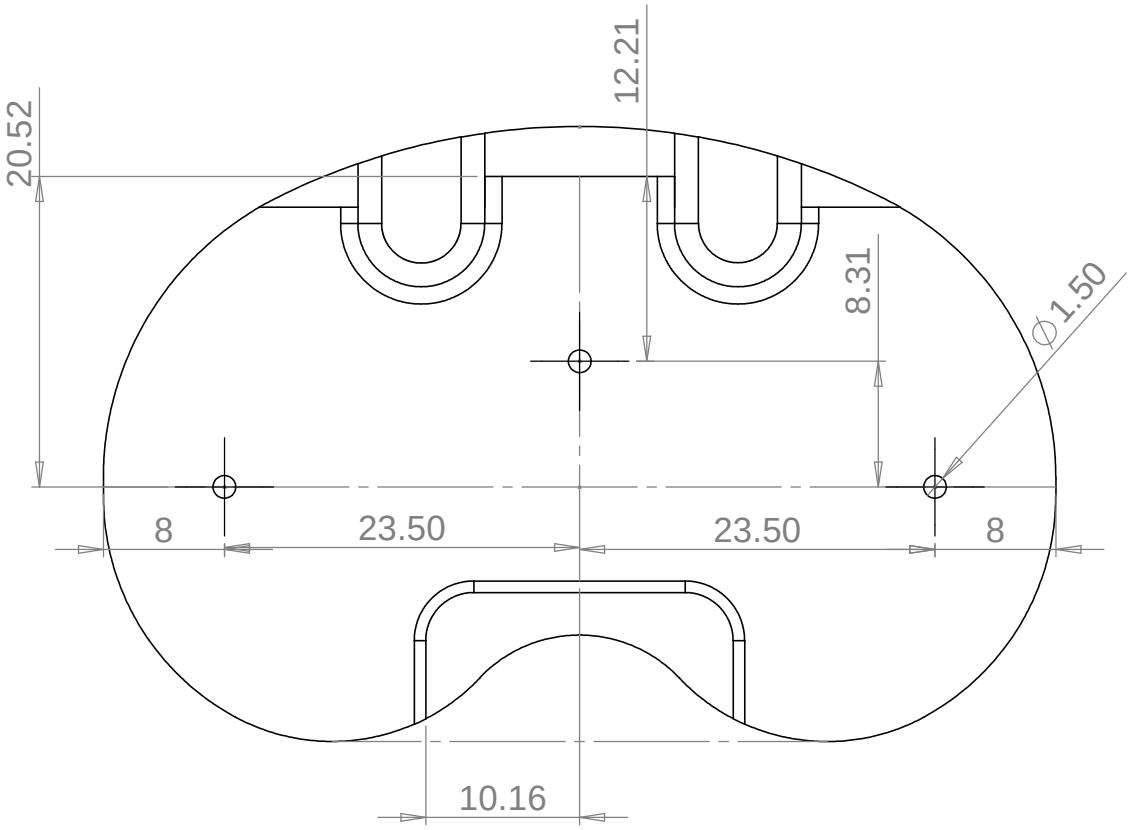

Remove 4mm from all depth measurements due to increased thickness of solidworks model over test sample

Martin Stanley	Tibial thermocouple locations and depths	Durham University School of Engineering Centre for Biomedical Engineering

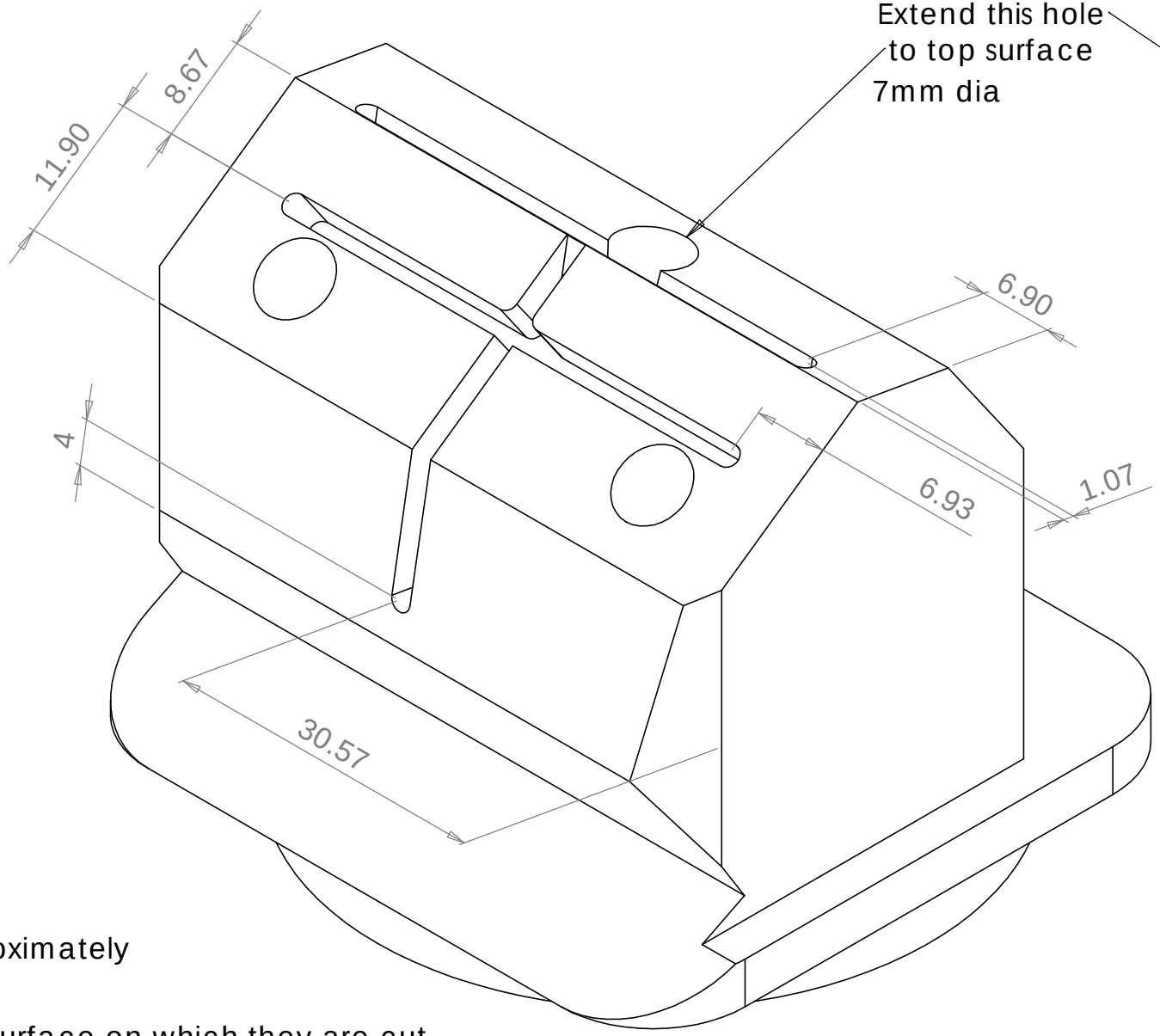

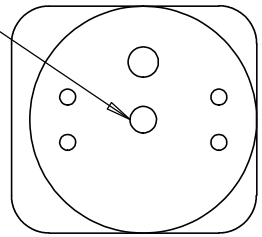

Bottom View

Channels are approximately
2mm wide
5mm deep
and normal to the surface on which they are cut

All dimensions are to
centres of radii

Martin Stanley	Thermo test femoral mount	Durham University School of Engineering Centre for Biomedical Engineering

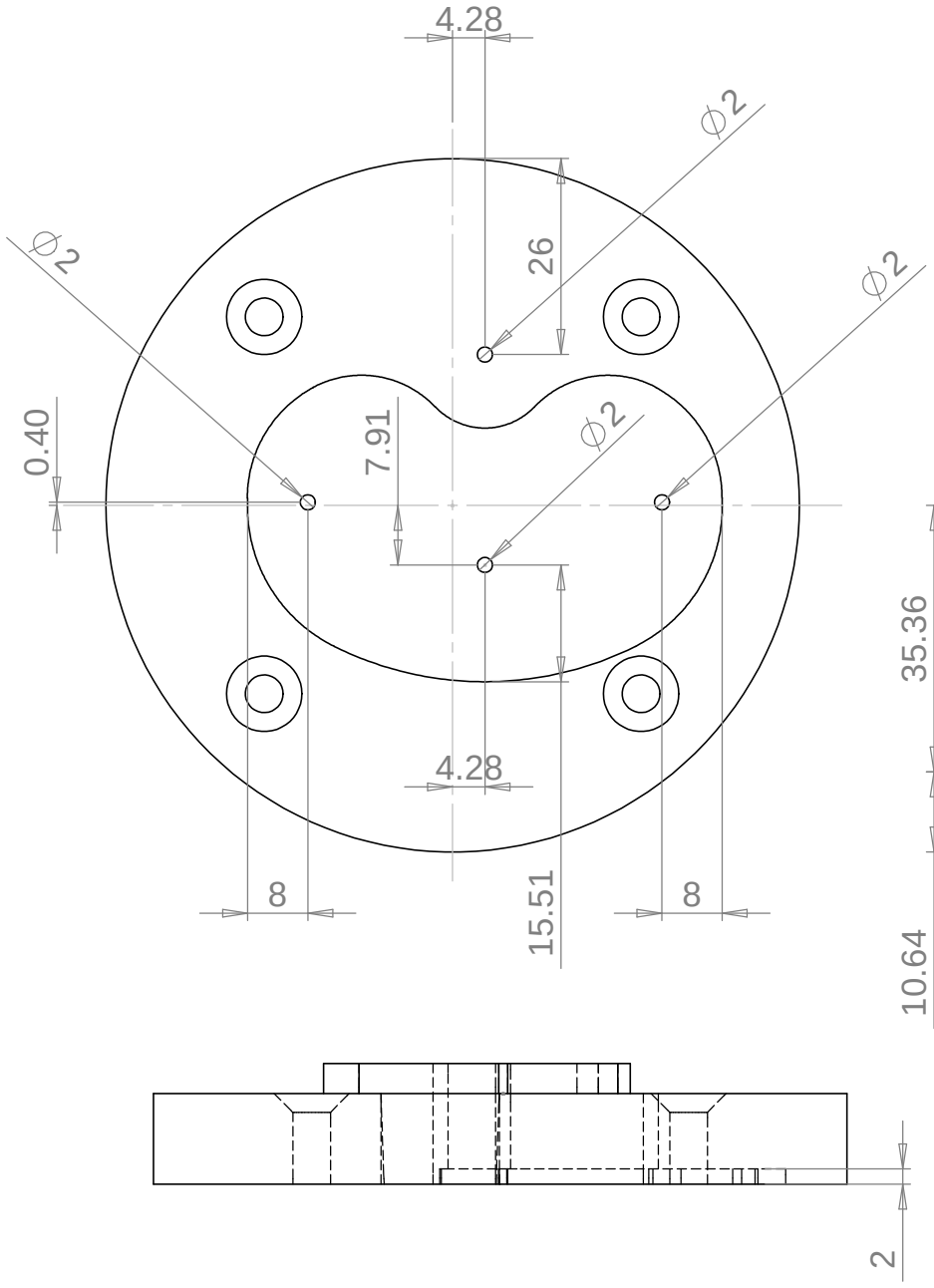

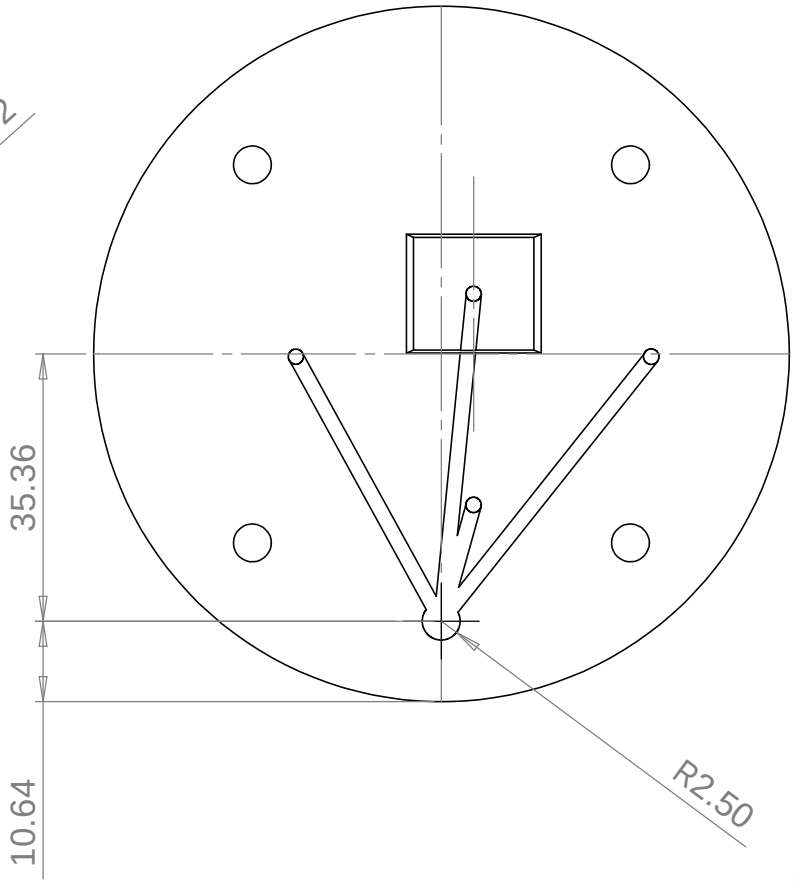

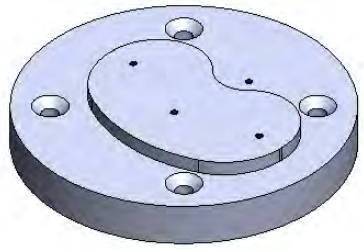

Martin Stanley

Durham University
School of Engineering
Centre for Biomedical Engineering

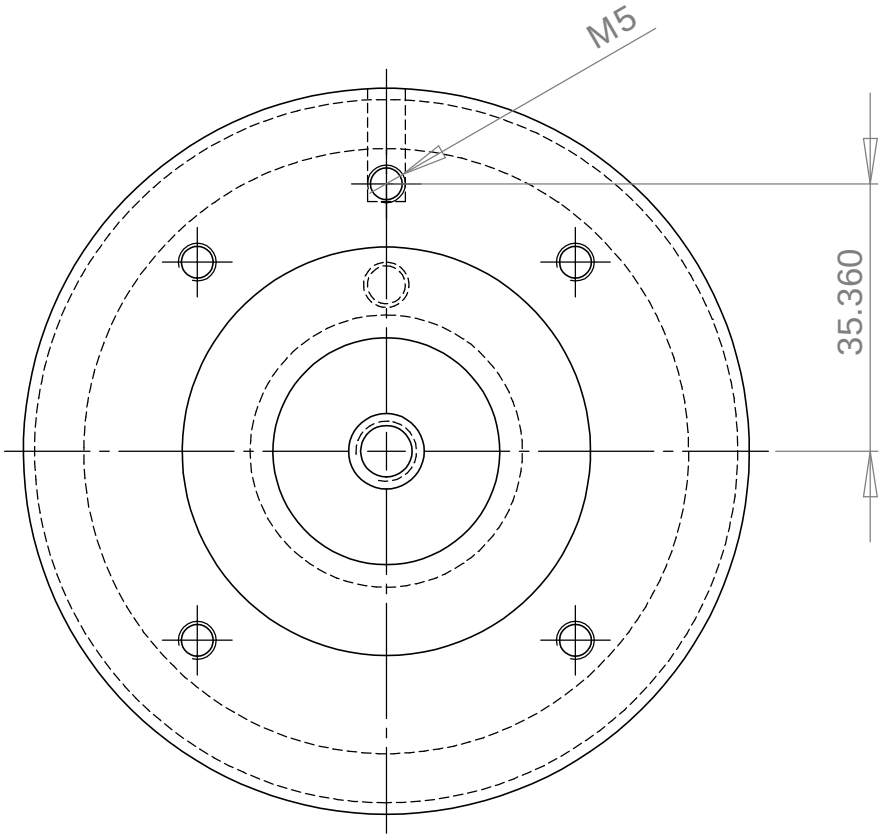

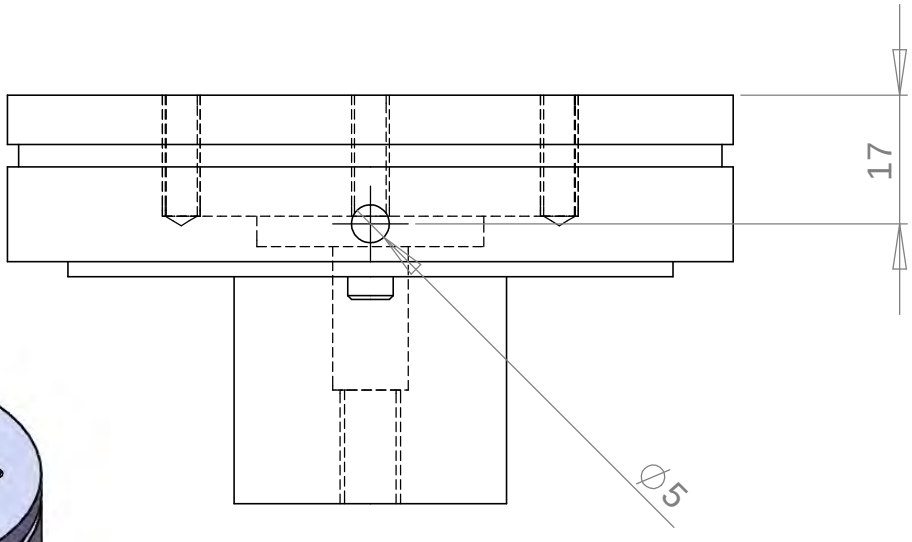

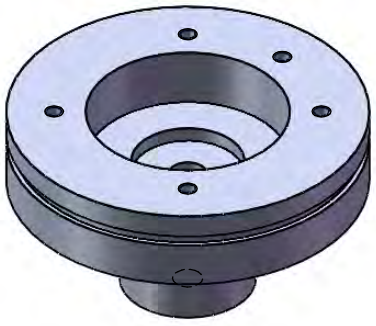

NEXT ASSY	USED ON
APPLICATION	

DIMENSIONS ARE IN INCHES
TOLERANCES:
FRACTIONAL ±
ANGULAR: MACH ± BEND ±
TWO PLACE DECIMAL ±
THREE PLACE DECIMAL ±

MATERIAL

FINISH

DO NOT SCALE DRAWING

	NAME	DATE
DRAWN		
CHECKED		
ENG APPR.		
MFG APPR.		
Q.A.		

COMMENTS:

SIZE	DWG. NO.	REV.
A	Tibial Mount Var. 1	
SCALE:1:2	WEIGHT:	SHEET 1 OF 1

A.3.3 Control Station Components

Schematics of all the components used in fabrication of the load soak control stations are presented in this section

- Control station femoral mounting block
- Control station femoral mounting plate
- Control station tibia PE mounting block
- Control station spacer
- Control station tibia mounting plate

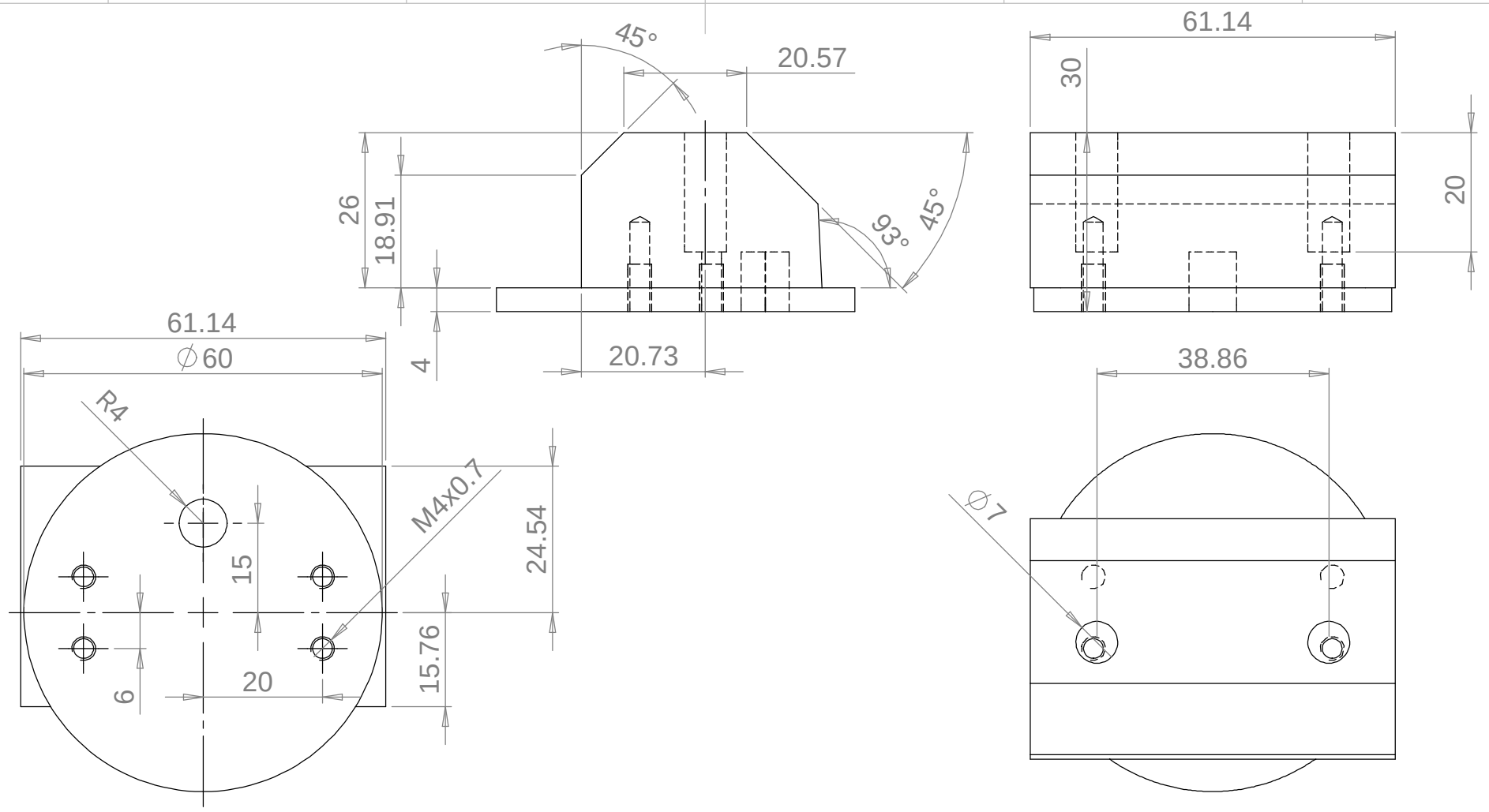

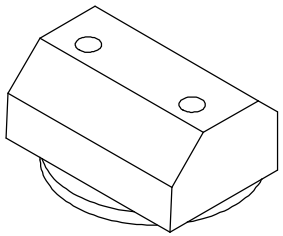

UNLESS OTHERWISE SPECIFIED: DIMENSIONS ARE IN MILLIMETERS SURFACE FINISH: TOLERANCES: LINEAR: ANGULAR:		FINISH:		DEBUR AND BREAK SHARP EDGES	DO NOT SCALE DRAWING	REVISION
					Quantity: 2	
	NAME	SIGNATURE	DATE		TITLE:	
DRAWN						
CHK'D						
APPV'D						
MFG						
Q.A				MATERIAL:	DWG NO.	A4
					CS Femoral Block	
				WEIGHT:	SCALE:1:1	SHEET 1 OF 1

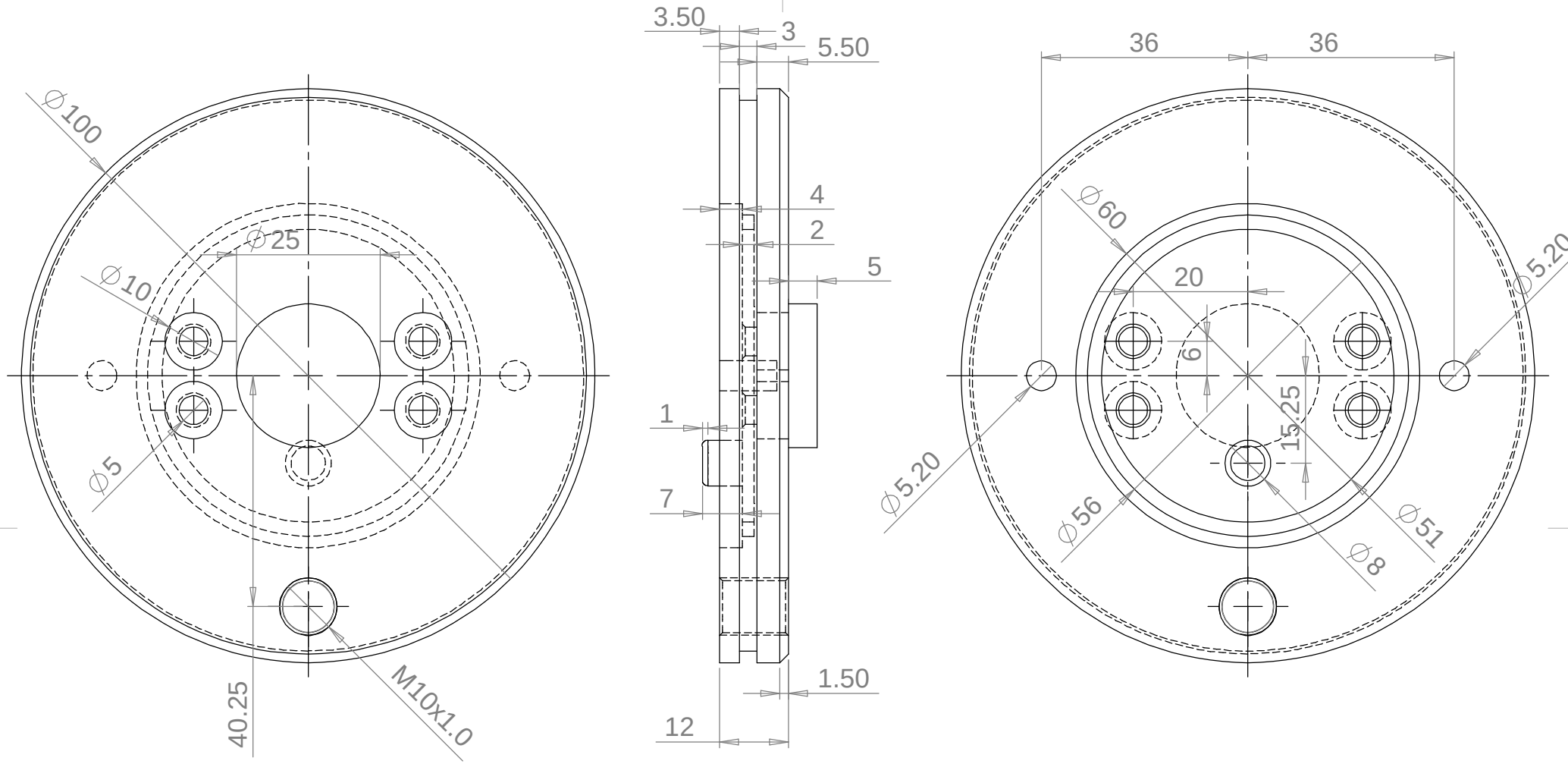

UNLESS OTHERWISE SPECIFIED: DIMENSIONS ARE IN MILLIMETERS SURFACE FINISH: TOLERANCES: LINEAR: ANGULAR:	FINISH:	DEBUR AND BREAK SHARP EDGES

	NAME	SIGNATURE	DATE
DRAWN			
CHK'D			
APPV'D			
MFG			
Q.A			

DO NOT SCALE DRAWING	REVISION
TITLE:	
MATERIAL:	DWG NO. A4
WEIGHT:	SCALE:1:2 SHEET 1 OF 1

CS Femur Mounting Plate

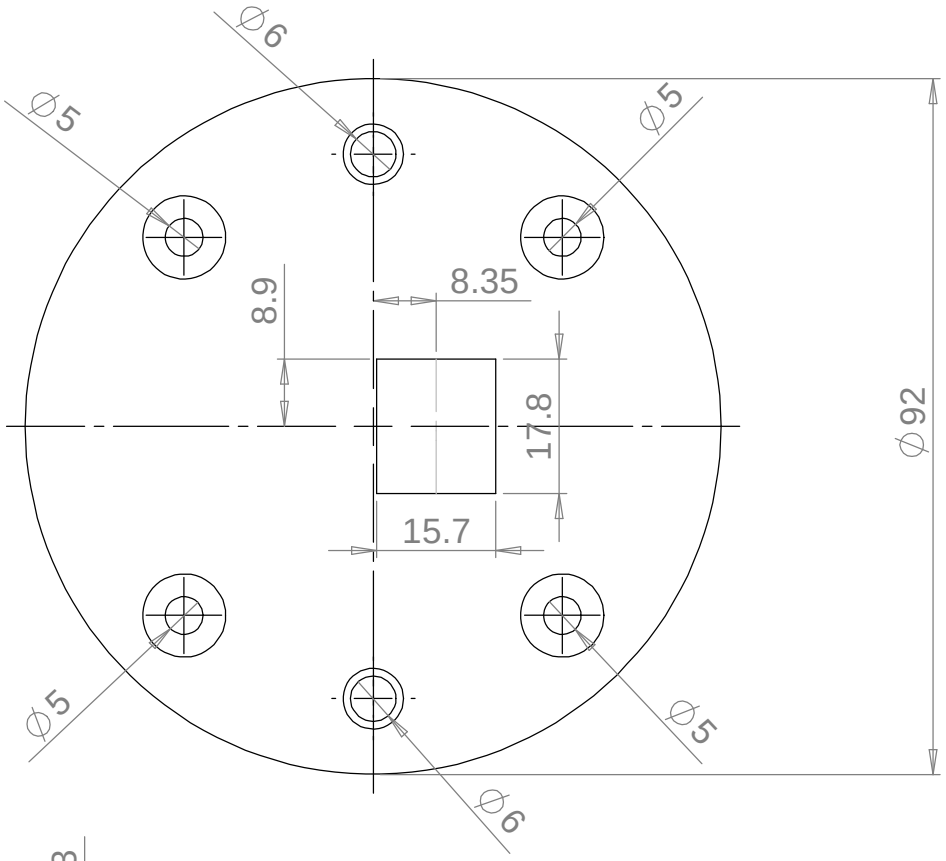

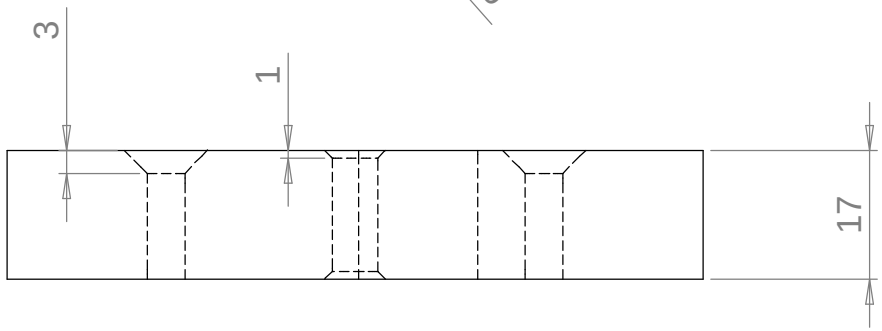

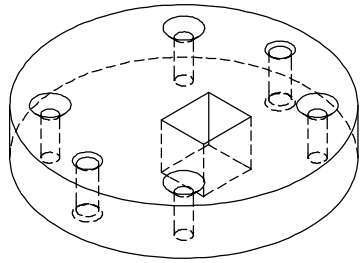

Quantity: 1

Material: Ultrahigh molecular weight Polyethylene

Martin Stanley	Ext: 42164	Vanguard CR Control Station - Tibial Base	Durham University School of Engineering Centre for Biomedical Engineering

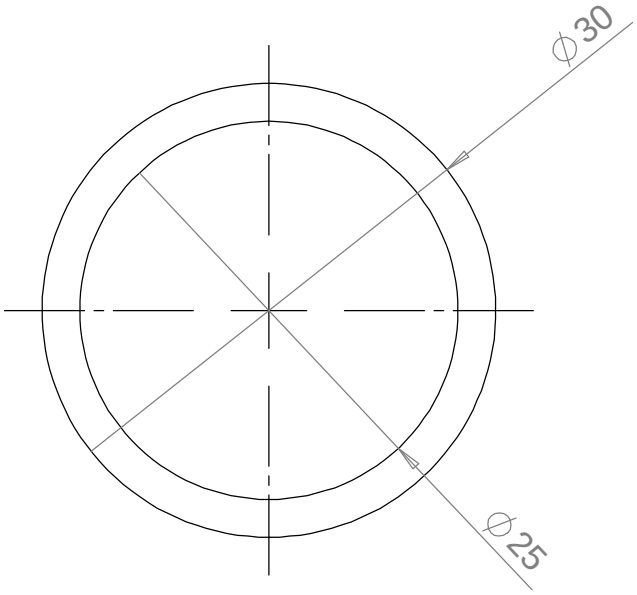

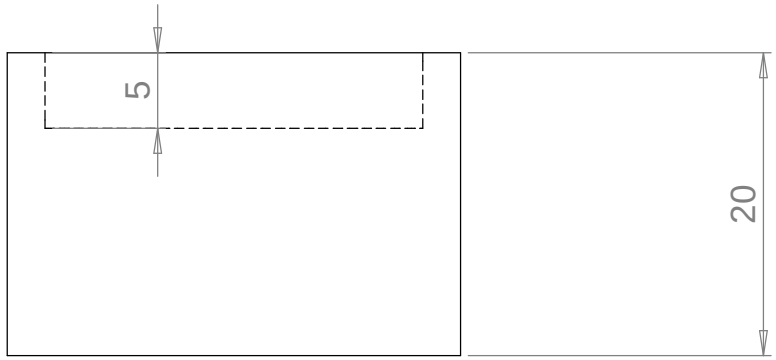

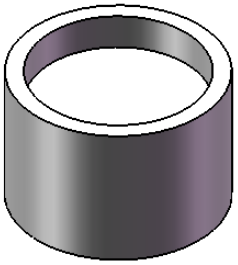

Martin Stanley	CS Spacer	Durham University School of Engineering Centre for Biomedical Engineering

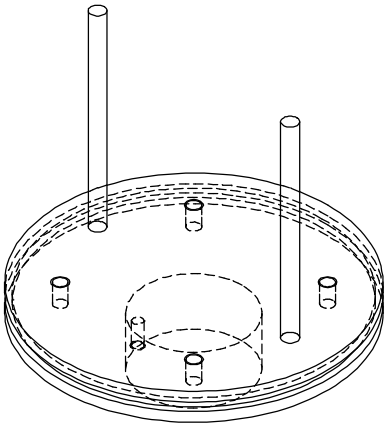

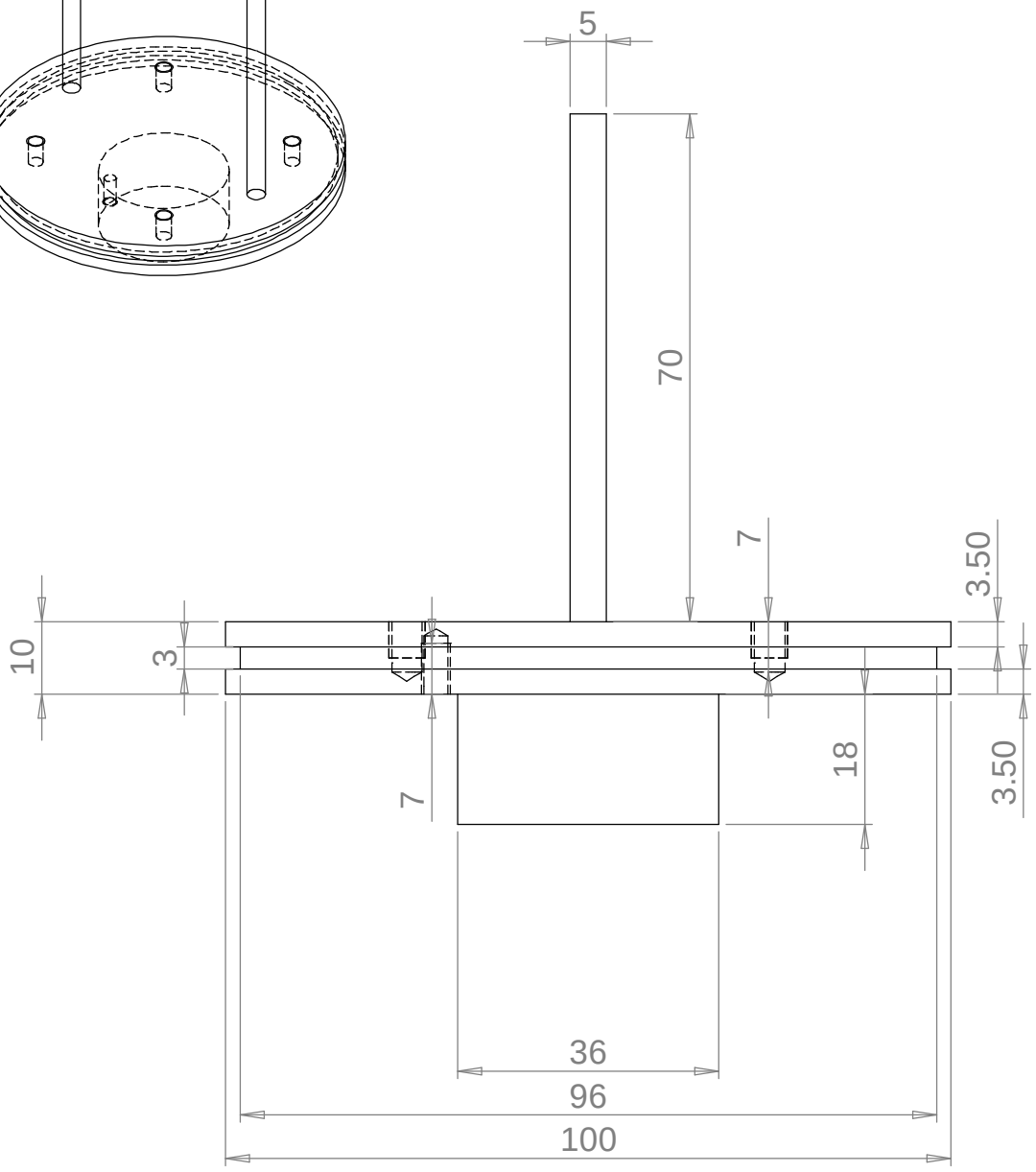

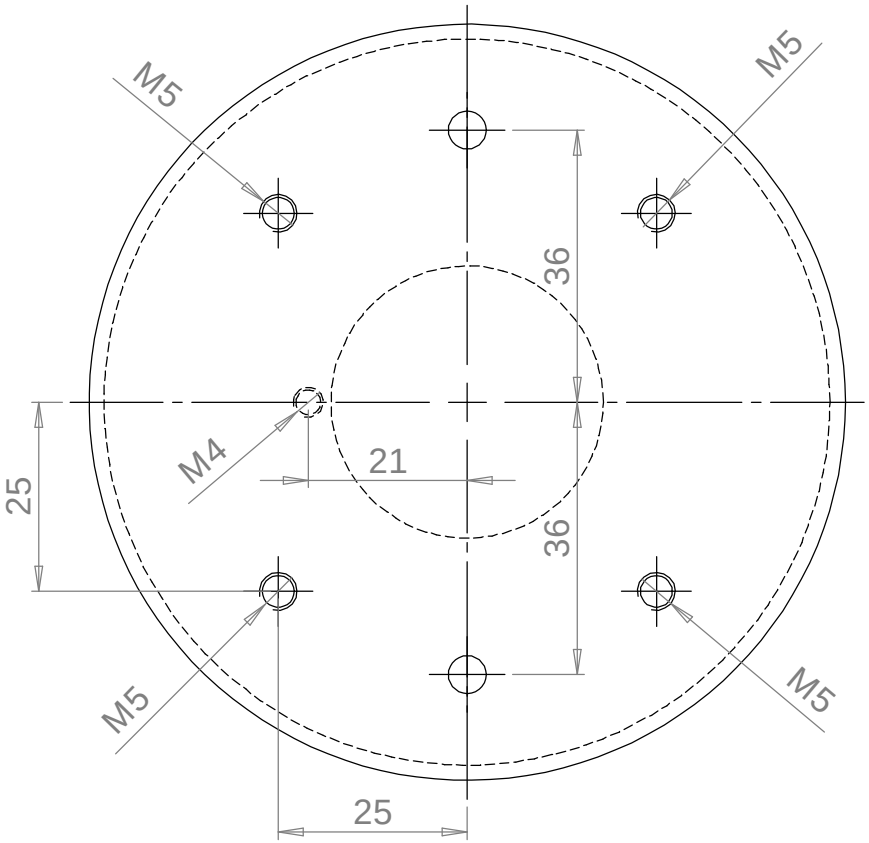

Martin Stanley	Ext 42164	Control Station Base	316 Stainless	Durham University School of Engineering Centre for Biomedical Engineering

A.3.4 Accelerated aging rig components

A parts list of the Swagelok components and schematics of the custom made components used in the manufacture of the accelerated aging rig are in this section.

Swagelok components

- SS-RL3S4-SC11 Stainless Steel low pressure release valve.
- SS-BVM4-SC11-SH-5389 Bleed valve
- SS-1KS4-A-SH-SC11 Inlet valve
- SS-400-3SC11 union tee piece
- SS-401-PCBLBQ Port connector
- SS-4-TA-1-4SC11 Tube fitting
- SS-810-1-4SC11 Female tube fitting
- PGI-100S-PG100-LARX-A Pressure gauge
- SS-QTM2A-B-400 Quick connect female
- SS-QTM2-S-400 Quick connect male

Custom components manufactured by TW Steam

- Pressure vessel lid.
- Pressure vessel base.
- Klingersil gasket.

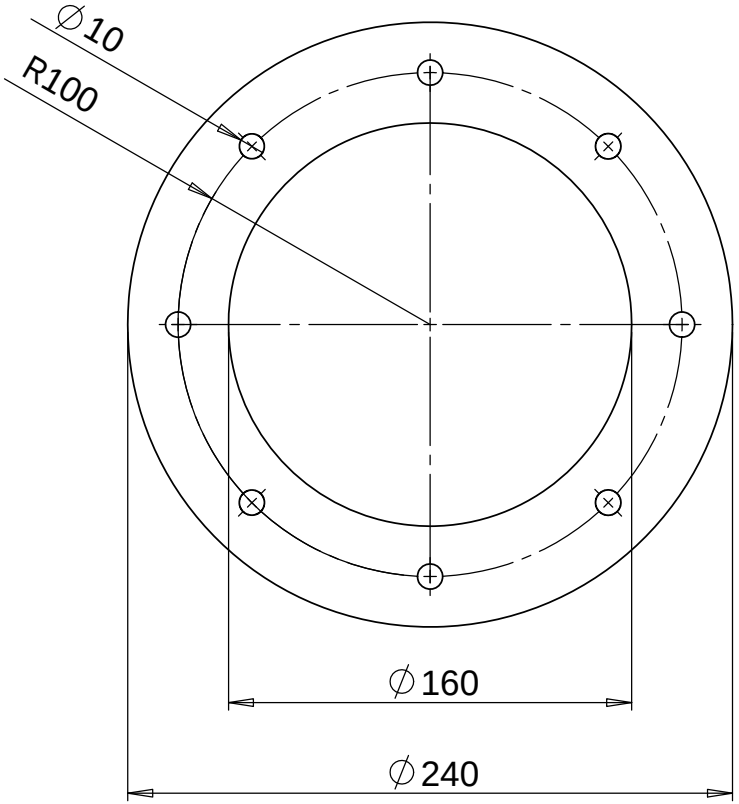

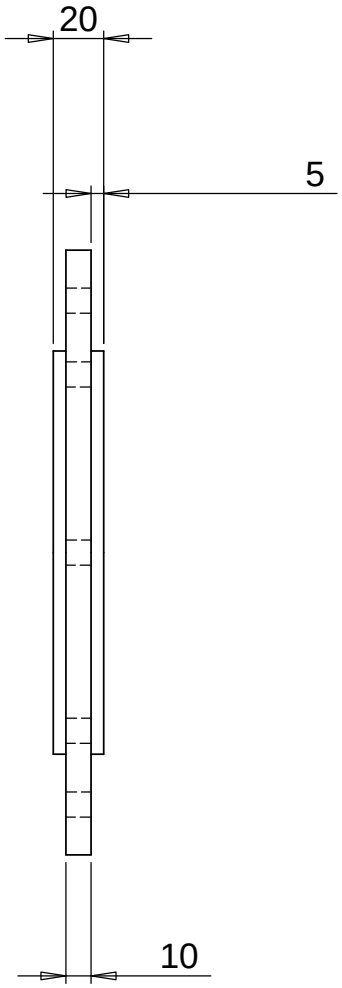

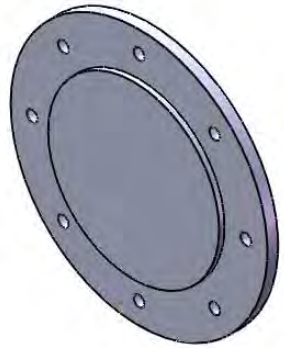

Martin Stanley	Scale 1:3	Durham University School of Engineering Centre for Biomedical Engineering

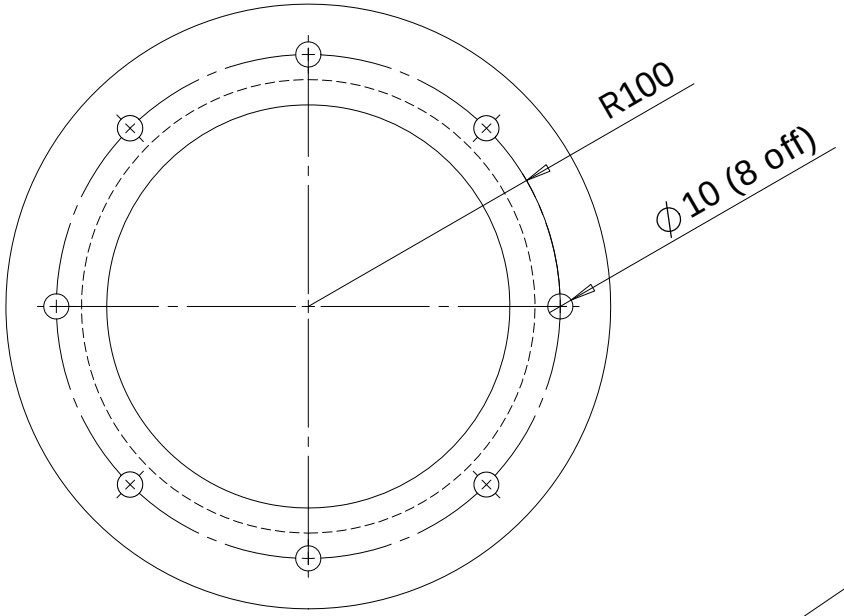

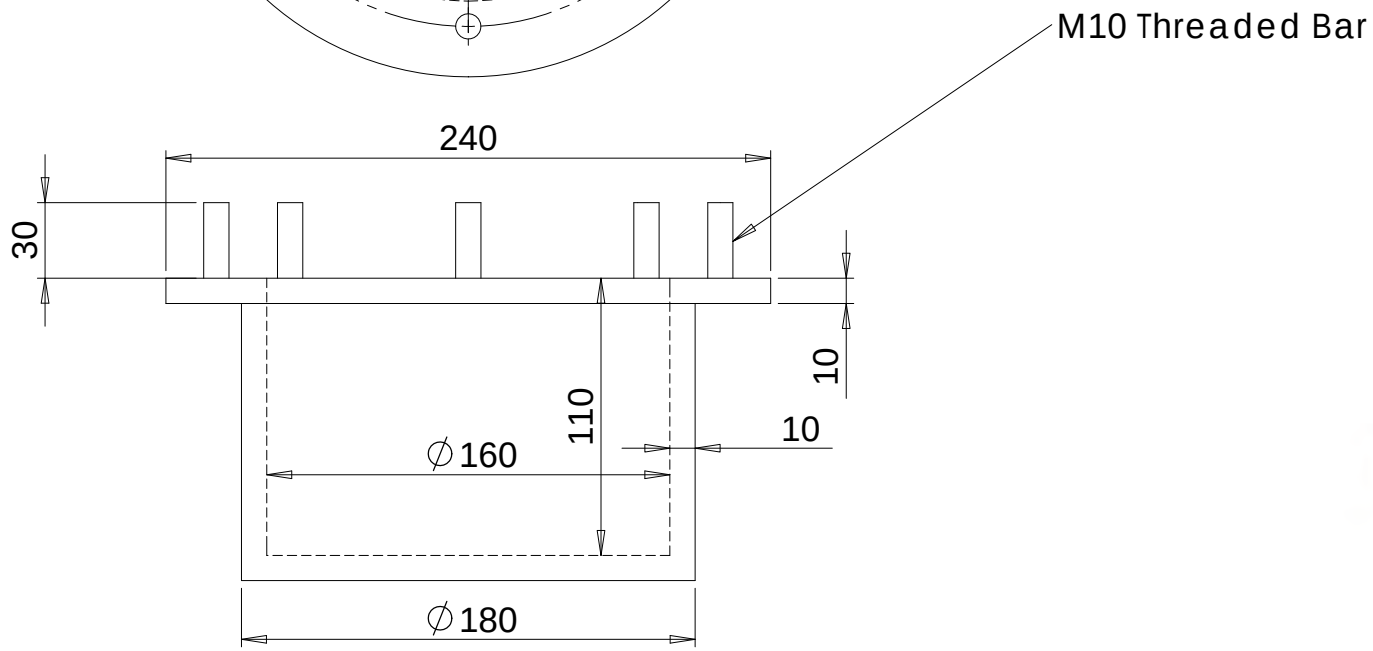

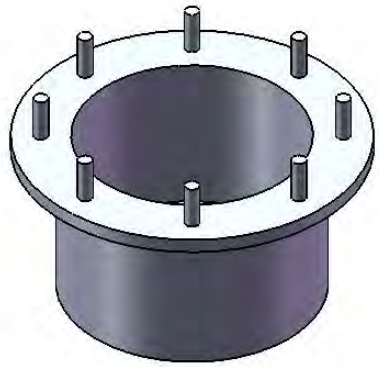

Martin Stanley	Scale 1:3	Durham University School of Engineering Centre for Biomedical Engineering

A.3.5 Additional components

Calibration components and any additional components manufactured are shown here.

- Vanguard CR Tibial Jig
- AP Calibration Rods

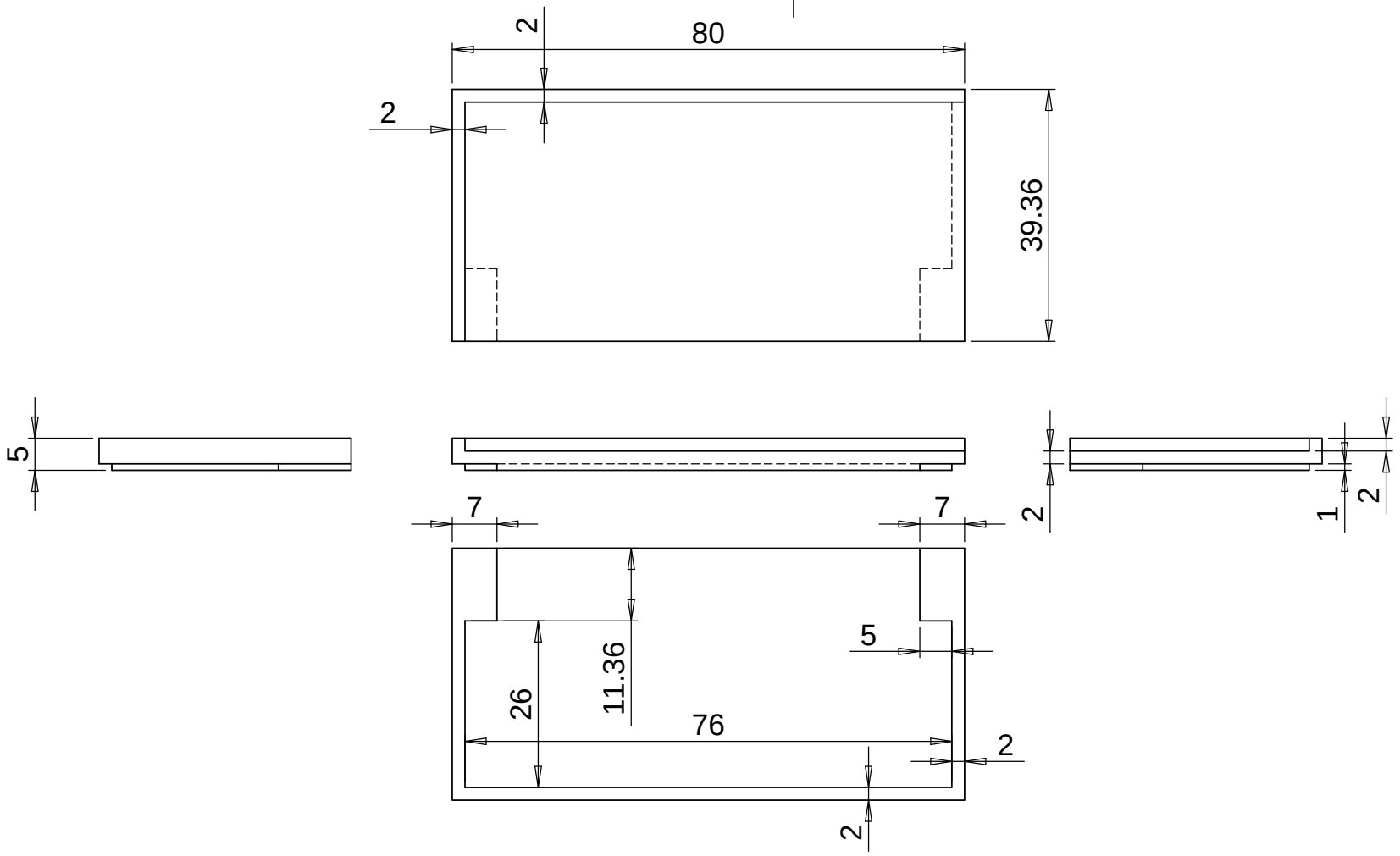

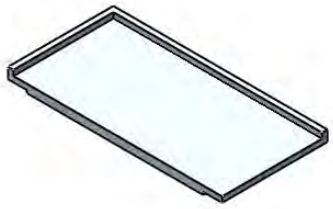

UNLESS OTHERWISE SPECIFIED: DIMENSIONS ARE IN MILLIMETERS SURFACE FINISH: TOLERANCES: LINEAR: ANGULAR:		FINISH:		DEBUR AND BREAK SHARP EDGES	DO NOT SCALE DRAWING	REVISION
	NAME	SIGNATURE	DATE		TITLE: Vanguard CR Tibia Jig	
DRAWN						
CHK'D						
APPV'D						
MFG						
Q.A				MATERIAL:	DWG NO.	A4
				WEIGHT:	SCALE:1:1	SHEET 1 OF 1

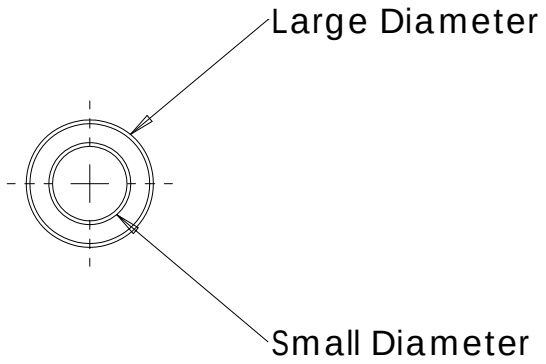

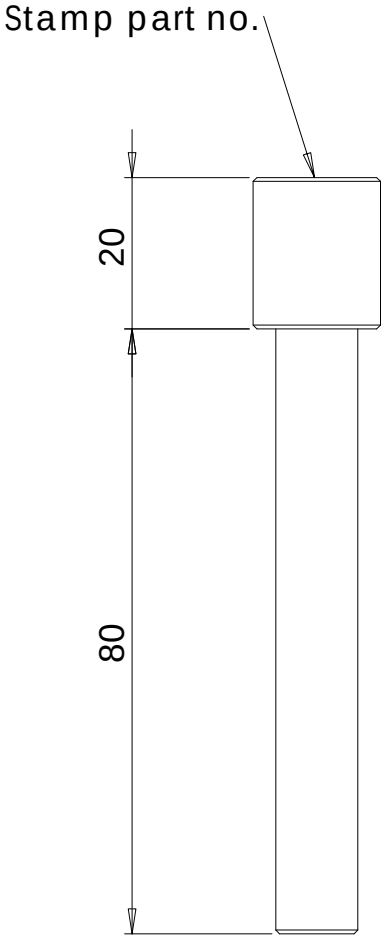

Part No.	Large Diameter	Small Diameter
0	16.85	10.85
1	16.18	10.18
2	16.59	10.59
3	16.38	10.38
4	17.05	11.05
5	16.45	10.45

NEXT ASSY	USED ON
APPLICATION	

DIMENSIONS ARE IN INCHES
TOLERANCES:
FRACTIONAL ±
ANGULAR: MACH ± BEND ±
TWO PLACE DECIMAL ±
THREE PLACE DECIMAL ±

MATERIAL

FINISH

DO NOT SCALE DRAWING

	NAME	DATE
DRAWN		
CHECKED		
ENG APPR.		
MFG APPR.		
Q.A.		

COMMENTS:

SIZE	DWG. NO.	REV.
A	AP Calibration Rod	
SCALE:1:1	WEIGHT:	SHEET 1 OF 1